603216

ONE PAGE OF ORIGINAL CONTAINS COLOR PLATES: ALL CFSTI REPRODUCTIONS WILL BE IN BLACK AND WHITE.

2 of 3

AD 603216

FINAL REPORT
Contract OCD-OS-62-232

197 p
hc ~ 5.00
mf ~ 1.00

LOCAL CIVIL DEFENSE SYSTEMS

A study of counterforce Defense Systems Methodology applied to Tucson, Arizona and environs.

OCD REVIEW NOTICE

This report has been reviewed in the Office of Civil Defense and approved for publication. Approval does not signify that the content necessarily reflects the views and policies of the Office of Civil Defense.

Office of Civil Defense
Department of Defense
The Pentagon
Washington 25, D. C.

4 June 1964
Engineering Research Laboratory
University of Arizona
Tucson, Arizona

ABSTRACT

This final report (Contract OCD-OS-62-232) presents procedures and methodologies necessary to evaluate local nuclear-attack hazards and applies results to target cities; specifically, Tucson, Arizona and environs are the subject of the pilot study.

The design concepts which have evolved from consideration of conceivable constraints (developed from the evaluations) are presented in general form. Particular concepts which appear to be most realistic, in light of economic factors, are described in greatest detail. Training requirements are outlined for the most desirable concept. Technical material in substantial detail is presented in the Appendix.

STAFF

The following persons, in addition to those referred to in context, have made a significant contribute to the study:

Howard P. Harrenstien, Ph.D
Morris W. Self, Ph.D
Ellery C. Green, MA
D. A. DaDeppo, Ph.D
George M. Sheets, LLB
Carol Rae

Don A. Linger, Ph.D
Ralph M. Richard, Ph.D
Robert L. Seale, Ph.D
Roy Post, Ph.D
T. L. Martin, Jr., Ph.D

Fred Bhannon
Jerome Q. Burns
H. A. Gillespie
Thomas Hughes
Edward A. Nowatski
S. Wayne Williams

B. Gail Buckmaster
Michael D. Callon
Richard H. Gunderson
Donald C. Lotham
L. Rolf Peterson

Stephen Bugay
Terrill C. Ewbank
Stanley D. Hansen
F. Dwayne Nielson
John R. Salmons

TABLE OF CONTENTS

SECTION I
INTRODUCTION

SECTION II
CONSTRAINTS FOR TYPICAL SITUATIONS

SECTION III
CONCEPTION AND EVALUATION

SECTION IV
TRAINING REQUIREMENTS

SECTION V
SUMMARY

LIST OF ILLUSTRATIONS

LIST OF ILLUSTRATIONS (continued)

SECTION I. INTRODUCTION

A. Scope of the Report

1. Requirement

This document is the final report on contract OCD-OS-62-232, which was awarded to the University of Arizona to conduct and administer, in consultation and cooperation with the United States Government, a pilot study of specified counterforce defense systems. The objective has been to develop procedures and methodologies for evaluating local hazards and to determine the potential civil defense countermeasures for cities closely associated with military targets. Tucson, Arizona, and its environs, is designated to be the subject of the pilot study.

The contractor, using data on targeting, weapons system parameters, and nuclear effects supplied by the Office of Civil Defense, proceeded to:

a. Define the attack consequences on the pilot study area and its environs including the interaction of the uses of multiple weapons, disturbed airflow effects and fallout climatology.

b. Develop a detailed set of plans for a variety of feasible shelter systems based on a cost-effectiveness analysis.

c. Identify the training requirements of the proposed protective systems.

2. Basic Approach

The contract was conducted in phases which corresponded closely to the following:

a. Targeting analysis
b. Pertinent surveys
c. Load predictions
d. Evaluations of surveys and loads on shelter requirements
e. Conception of feasible shelter systems
f. Evaluation of feasible systems
g. Cost-effectiveness analysis
h. Identification of training requirements

B. Arrangement of Report

The report is presented in two general divisions. The first is the main body of the report, which is generally non-technical. The second is the Appendix, which is technical in nature and which supports conclusions reached in the first division. The main body of the report is divided into five sections. Each of the sections, as well as the Appendix, has individual organization and usefulness as an entity alone and as part of the total report. The bulk of the material is devoted to exposition of scientific and engineering detail.

C. General Philosophy

It is psychologically desirable to hope and even believe that humanity and its national governments will not again resort to general war as a solution to international disagreements. Occasionally even the most cynical observer may be able to see a chink of light on this possibility. However, the historical record of relations between powerful nations casts a dark and imposing shadow over this optomistic, almost naive, outlook; and makes a "long-shot" gamble out of a living hope, the prevalence of which may lead to dying in despair. Failure to inform and protect the people may, by hindsight, appear to have been downright irresponsible when one considers present economic feasibility of protection vs the odds of a sudden attack. Both sides in the cold war have had occasion to rattle their "sword of Damocles." The odds are that history will repeat, and both sides are on record that any general war will be of thermonuclear character. It is a fact that the effects of these weapons of destruction are not beyond human comprehension. The threatened effects are, and always will be, subject to engineering analysis in relatively conventional terms.

Under the worst predictable nuclear attack circumstances on hard-target urban areas, many will survive the immediate blast, initial radiological, and thermal effects. There is no assurance, however, that these people can survive later effects without sheltering facilities. Therefore, elemental human compassion, and rational personal fear for self, family, nation, and humanity require that we provide for long-term survival of this group and improvement in their numbers. We can improve their initial numbers by adequate warning and training. We can improve their final numbers by proper construction of shelters and adequate training and direction. It is a virtual certainty that the vulnerable modern human who did survive immediately could not continue to survive alone (or in small numbers) for prolonged periods without the protective and other services which have become a vital necessity. Survival of small groups will depend largely on their makeup and in general, such survival is very low on the probability scale.

The prediction that some would survive is indicated by the pragmatic fact that an all-out attack, which would immediately kill every last unsheltered person, is not economically feasible or technically possible for any present or predictable enemy. We must not, therefore, remain or allow our neighbors to remain, completely vulnerable because of apathy or ignorance.

The attack forces are subject to reasonably, precise determination and analysis in terms which permit consideration in light of known vulnerable and protective factors. The present state of the art in targeting mathematics, using conservative tactical and strategic postulates (including a large element of "overkill" in any massed-raid type nuclear strike), yield workable predictions of maximum attack force both as to magnitude and location.(a) This data, together with the fact that technical advances in delivery system guidance have minimized the likelihood of "stray missiles", make survival predictions much more reliable and definitive.

Because of recent research efforts by agencies such as the Department of Defense, planning and preparation methods necessary to increase the rate of survival are likewise more advanced; and, what is more important, they provide a means whereby the immediate survivors can become long-term survivors. In most cases, the attack can be reduced to a monstrous inconvenience rather than a doomsday. It is true that a limited, and generally predictable geographic area around nuclear bursts may remain unprotected from close-in effects by presently feasible shelter systems. These areas are in the neighborhood of a radial mile or less in surface distance from the burst point of a surface burst of megaton size. For areas a mile or more from this burst point, modern methods of conservative engineering analysis and design can provide effective shelter, as far as probabilities of survival are concerned. Obviously, the probable effectiveness improves as the distance from the burst point increases.

Tucson, Arizona, is a target city which, consistent with a rational targeting analysis, may be subjected to the effects of nearby surface bursts of 10 megaton weapons which are aimed at each of the 18 nearby Titan missile sites, in addition to a possible 5 megaton attack on Davis-Monthan Air Force Base (a SAC base which is a relatively softer target located within two miles of the approximate center of population). The Tucson problem is considered a particularly difficult one in view of the weight and relative locations of predictable attack, and because of the fact that the usual urban facilities (such as underground transport or utility systems, storm sewers, etc.) are not present. The population is not as densely concentrated as it is in most urban areas, and yet the concentration is dense enough to require consideration of community-type shelter systems.

Scientific data, creative developmental research, and technical calculations which are included in this report, substantiate that a shelter system can be designed for Tucson which is economically feasible. It is noted that: 1) the strategic factors of location and magnitude of the nuclear-strike bursts are logically predictable for a given target or group of targets; 2) the relative magnitude of engineering loadings and their types are reasonably predictable for a given urban target area; 3) the worst existing situation of human vulnerability can presently be offered protection by use of flexible design in the conception and construction of shelter systems. It is likely that features of the plans for Tucson, Arizona, may be largely applicable to any target city.

It is noted that economic feasibility of any system is greatly enhanced by multi-purpose planning on a present and continuous basis. Conceivably, the purely shelter aspects of such a coordinated plan might well become the lesser cost of all items to be considered, in an ideally coordinated plan. In the final

(a) "Strategy For Survival," Martin-Latham, University of Arizona Press, Tucson, Arizona, 1963.

analysis, such a plan could pay its own way even if the attack should become less likely or even if shelter should become unnecessary. The multitude of shared-use methods which could be devised are only limited by the imagination and cooperative spirit of local planning agencies. No doubt the pragmatic political and economic considerations, which must be considered, will tend to minimize future fruitful realization; but speculation on the theoretical potential, is quite interesting.

The research, of which this document serves as a final report, is not concerned specifically with any single topic to the exclusion of all others. It is, however, an investigation of possible ways in which each effect may be considered in the ultimate conception of feasible shelter systems for target areas. The conception and subsequent evaluation of such systems represent the final step in the application of the fruits of research to the planned protection of population and related functions in an emergency. It is this type of research, that of systems evaluation, which is considered by the authors to be most urgently needed at the present time.

Each local problem is unique in many ways, but the instant study suggests solutions which will be worth consideration by any urban area which is threatened by the grand incidents of nuclear attack: initial effects and lingering fallout radiation. The study has suggested solutions to many facets of the general problem in which both active and passive constraints are considered. In the course of investigation and analysis, the staff has had occasion to consider the shelter design problem in more refined detail so as to apply techniques to the solution which may not have seemed apparent at earlier generalized levels of consideration.

SECTION II

CONSTRAINTS FOR TYPICAL SITUATIONS

A. General
B. Technical Constraints
    1. Targeting
    2. Loadings
        a. Overpressure
        b. Ground motion
        c. Initial nuclear radiation
        d. Thermal radiation
        e. Fallout radiation
    3. Surveys
        a. Population density
        b. Terrain and topography
        c. Water supply
        d. Waste disposal
        e. Location of schools, hospitals, etc.
        f. Existing shelter space
C. Non-Technical Constraints
    1. Psychological
    2. Survivor Characteristics
    3. Coordinated Shelter Plan

SUMMARY

This section of the report states the counterforce civil defense system problem in terms of constraints which must be considered as design criteria. The constraints are deliniated as technical and non-technical. The technical are generally those which readily permit numerical analysis; whereas the non-technical do not readily permit numerical analysis. An attempt is made to present the problem clearly and in enough detail to virtually dictate the solutions which follow in the next section.

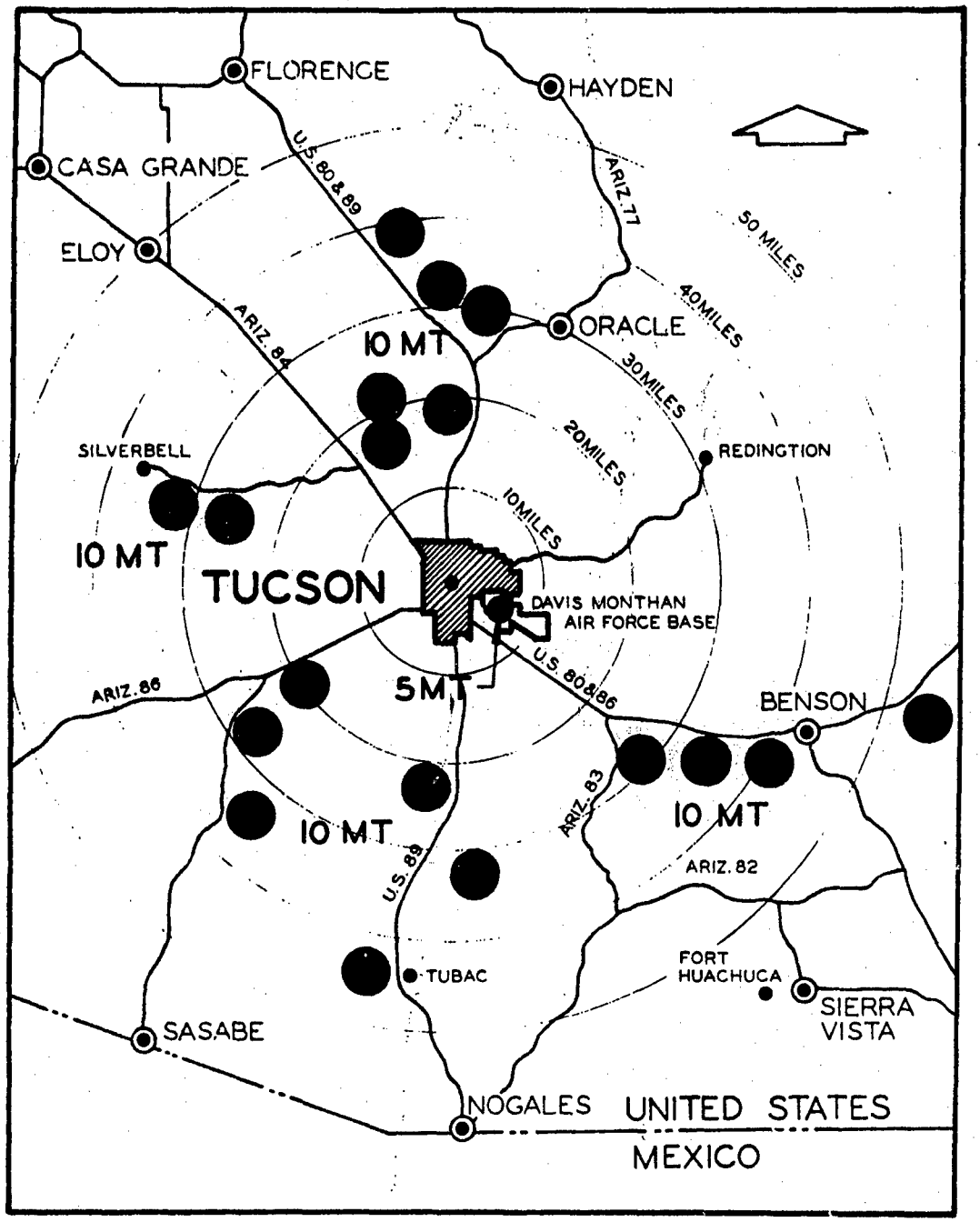

Figure 2-1. Target Locations

SECTION II. CONSTRAINTS FOR TYPICAL SITUATIONS

A. General

The creation of shelter systems for the protection of people in event of thermonuclear attack is a major element in the development and integration of a civil defense program. Although it is possible--from a technical standpoint--to design, construct, and equip reasonably adequate shelters, civil defense is a system complex which has many interdependent problem areas. Each of these impose constraints which mutually impinge as limitations on the whole as well as on each area of consideration. Therefore, the system approach is vital in order to maintain proper perspective. We begin by assessing the problem in terms of all the important constraints which are inherent in human as well as engineering and economic considerations.

Among other things, the ability of the enemy to mount his attack is a constraint. This constraint must be recognized as limited by economic factors, and in part, the character of our array of retaliatory weapons which this enemy must disable in order to protect himself. For example, a part of our retaliation system consists of hardened underground ballistic missile installations. The resistant character of these weapons (in their silos) will likely cause the enemy to plan to expend certain numbers of his weapons on each target complex. Furthermore, because of the immediate destructive capability of this portion of our retaliatory system, we may postulate that any attack will be such that the first lethal effects of blast, fire, and initial radiation will be largely confined to areas within 2-3 radial miles from such military installations. This sort of a possibility provides the basis from which numerical levels of constraint, in the form of weapons effects for these target areas, may be generated.

The damage and casualties that may be expected in urban areas associated with military targets may be caused by active constraints such as: blast, initial thermal and nuclear radiation, and radiation from fallout. The probable magnitudes of these effects can be predicted by methods similar to those presented in part B of the Appendix to this report. The magnitude and number of sources of these loadings can be predicted by methods similar to those presented in part A of the Appendix.

The items--things, people, and institutionally valuable entities which are to be protected are passive constraints and, therefore, must be surveyed and stated. The effects and the stated items then must be considered for their vulnerability in order to determine survivability. The predictions from this consideration form the input to an engineering analysis, which is necessary in order to design an adequate shelter system and recovery plan.

B. Technical Constraints

These constraints are those which in general, are subject to numerical determination before the event. They involve such general areas as targeting, loadings, and surveys.

1. Targeting

Procedures which may be used to develop numerical values of these constraints, were presented in the first quarterly progress report on contract OCD-OS-62-232. A brief presentation of this approach is found in part A of the Appendix to this report. The general procedure is given in the text, "Strategy For Survival" by Thomas L. Martin, Jr., published by the University of Arizona press.

The results of such a targeting analysis as applied to Tucson, are shown in Figure 2-1. They are generated in part A of the Appendix. It will be observed that the Tucson area may expect one 10 MT surface burst on each of the 18 Titan II sites which surround the city. In addition to this barrage, it is likely that the SAC base, Davis-Monthan Air Force Base, will receive a 5 MT surface burst. Obviously, these decisions are subject to some argument which stems largely from lethal radius and CEP assumptions. For purposes of this study, it is assumed that they are realistic and, in fact, correct.

2. Loadings

Before a discussion of these types of contraints, it is necessary to identify which types of loadings

are deemed pertinent. The following were considered most pertinent:

Overpressure
Ground motion
Initial nuclear radiation
Thermal radiation
Fallout radiation

The reader is referred to the latest addition of the "Effects of Nuclear Weapons" for a description and definition of these various effects.

a. Overpressure

For civil defense planning, it is necessary that probabilities be introduced when considering loadings such as overpressure. It is not economically feasible to consider the design of shelter systems for a magnitude of this constraint which is associated with a 100% reliability of this magnitude not being exceeded at the point in question. In other words, civil defense planners should never be forced to produce designs which are guaranteed to be absolutely, or 100% effective. It is much more realistic to consider overpressure constraints which are in the neighborhood of 90% reliable as far as their probability of occurrence is concerned. As an example of the reason for this decision, consider the curve shown in figure 2-2. This curve, which is typical, presents the probable upper limit on blast overpressure at a point 4.0 miles from a 5 megaton surface burst. Note that there is a 50% probability that the maximum overpressure will be 7 psi, or less at the point in question. There is an 80% probability that it will be 8.5 psi or less at this same point. The curve breaks rather sharply above the 90% level, thus it seems uneconomical and undesirable to consider design overpressures in excess of those required by a 90% probability of reliability analysis. The full set of curves, from which this typical one was taken, are included in part B of the Appendix.

Using curves similar to that in figure 2-2, contours may be drawn which indicate probable conservative design overpressures for all points surrounding a target. This process, applied to the Tucson situation, results in the overpressure contours shown in figure 2-3. This figure shows the overpressures that have a 90% chance of being conservative if Davis-Monthan receives a 5 MT surface burst. The weapon is assumed to be delivered by a system with a one mile CPE.* It will be observed that the effects of the 10 MT surface bursts on the Titan sites are also plotted on this figure. The only burst which has a noticeable effect on the map shown, is the one on the site immediately northwest of the city.

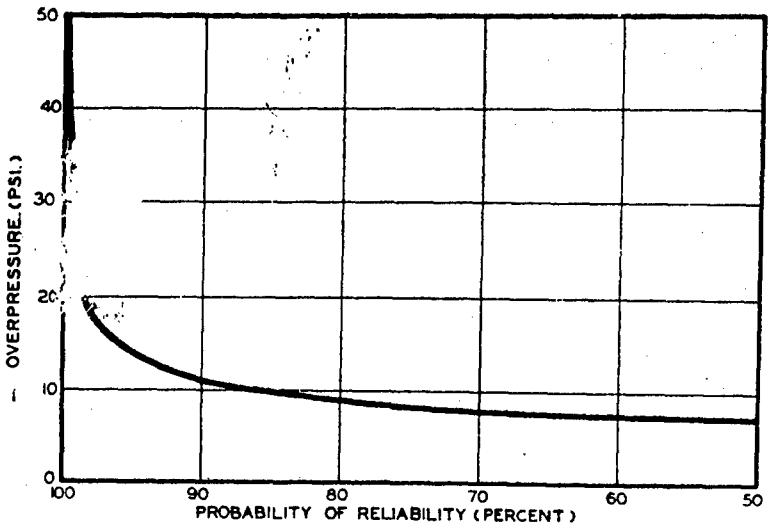

Figure 2-2. Design Effectiveness

*CPE is used in this context as a general term meaning circular probable error; it is often stated as CEP.

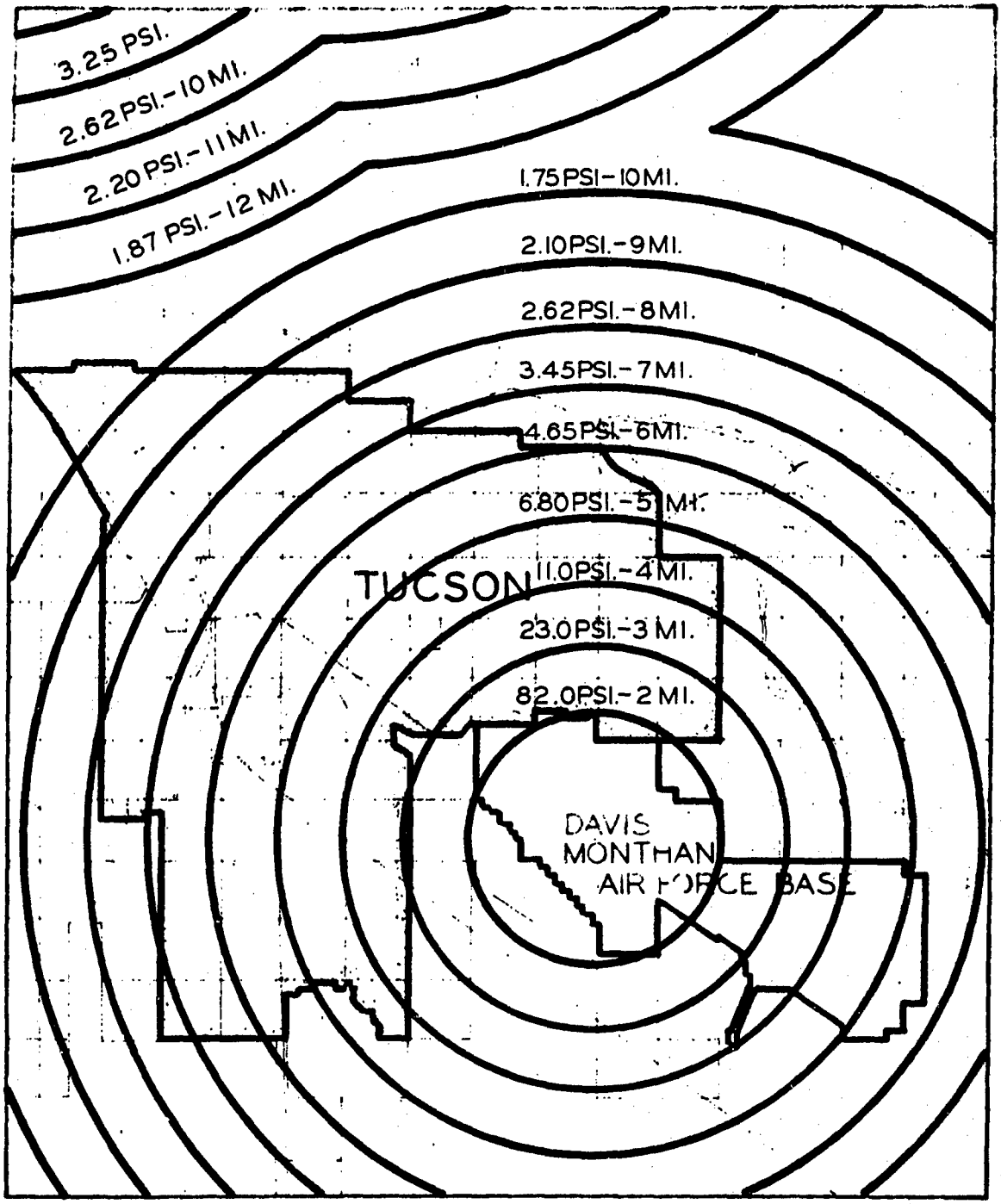

OVERPRESSURE FOR 90% PROBABILITY OF RELIABILITY FOR A 5 M.T. SURFACE BURST ON DAVIS MONTHAN AIR FORCE BASE AND A 10 M.T. SURFACE BURST AT THE TITAN SITES

Figure 2-3. Probability of Reliability Contours

b. Ground motion

These constraints are extremely difficult to predict with any great reliability. There are various methods in existence--each of which involves many simplifying assumptions as to the soil medium and its behavior under dynamic loadings of the intense magnitude associated with nuclear bursts. In the process of this phase of the current investigation, a computer program was developed which essentially uses the same approach as that presented in the Air Force Design Manual.(b) Inasmuch as this approach neglects the effects of the inertial resistance of the soil to the dynamically applied loading, values generated are likely upper bounds to the actual values. Part B of the Appendix discusses the specifics of this phase of the problem. Figures 2-4 through 2-6 respectively, present possible accelerations, velocities, and vertical displacements for the ground surface in and around Tucson.

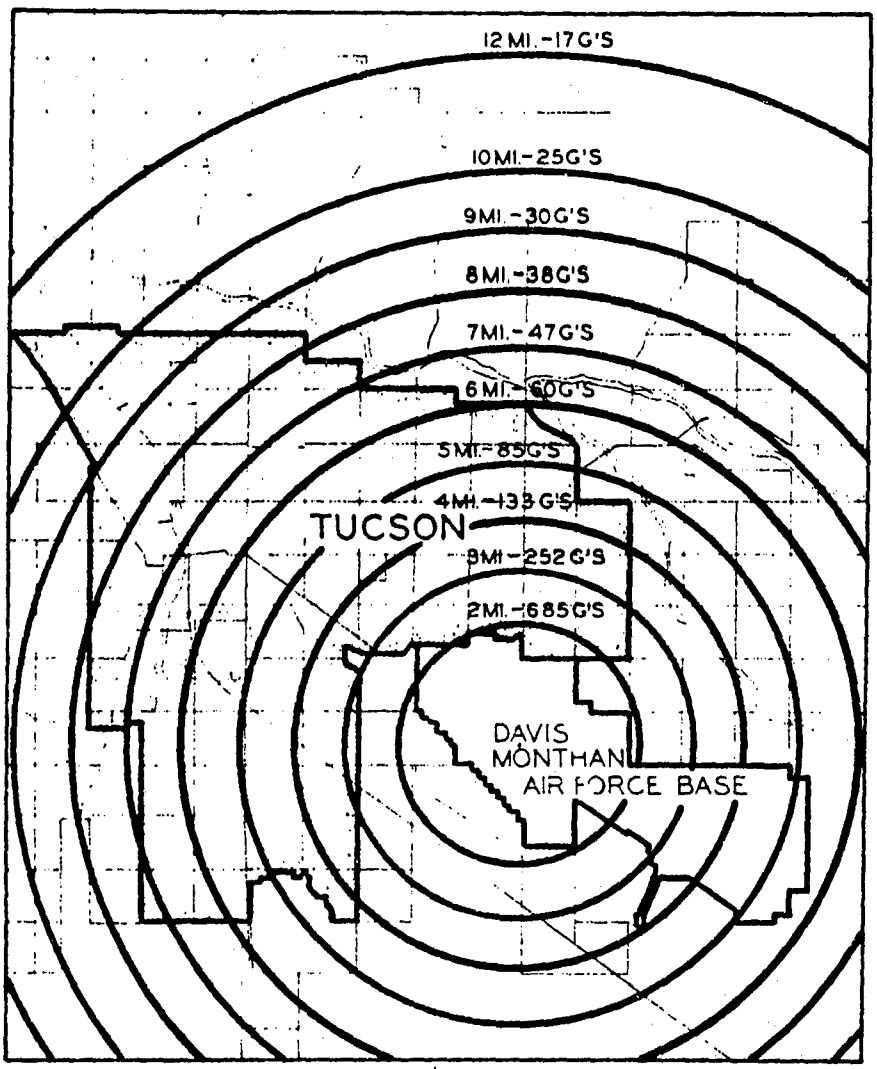

PREDICTED PEAK VERTICAL ACCELERATION OF GROUND SURFACE DUE TO A 5MT. OPTIMUM AIR BURST ON DAVIS MONTHAN AIR FORCE BASE

Figure 2-4. Peak Vertical Acceleration

(b) Air Force Design Manual, Principles and Practices For Design of Hardened Structures, AFSWC-TDR-62-138.

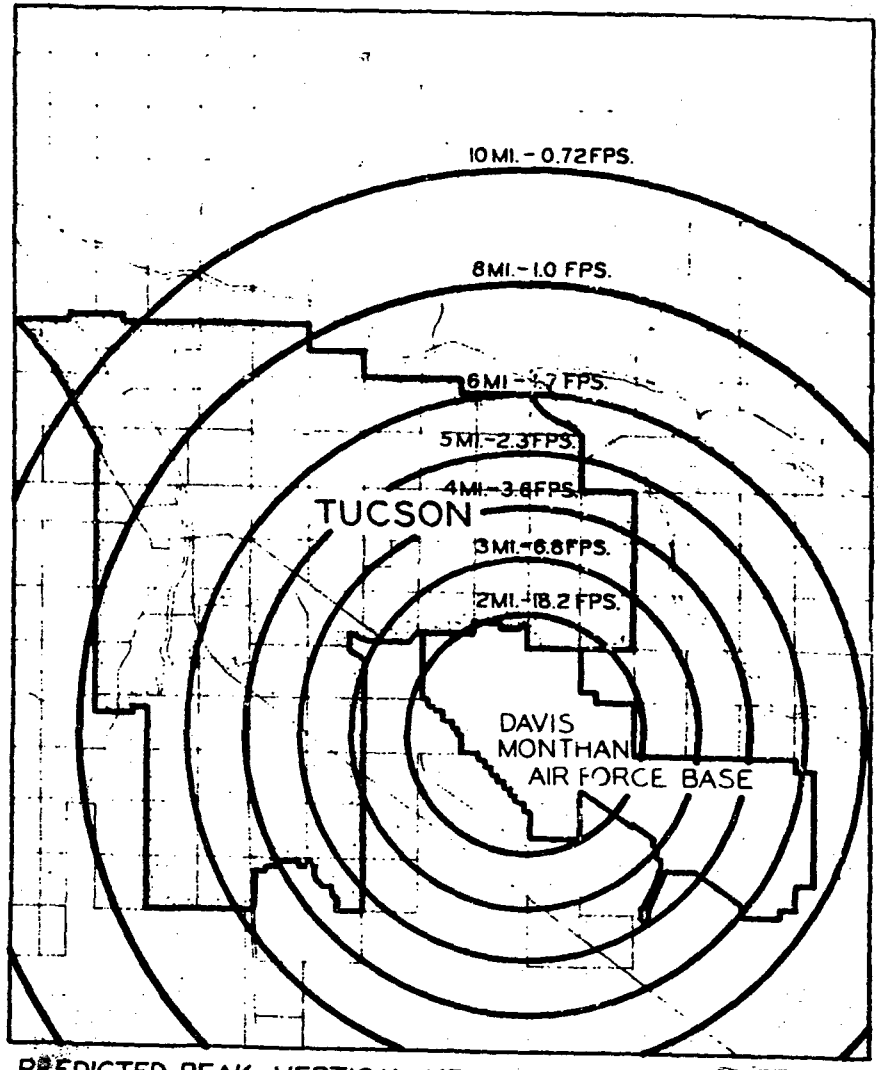

PREDICTED PEAK VERTICAL VELOCITY OF GROUND SURFACE DUE TO A 5MT. OPTIMUM AIR BURST ON DAVIS MONTHAN AIR FORCE BASE

Figure 2-5. Vertical Velocity

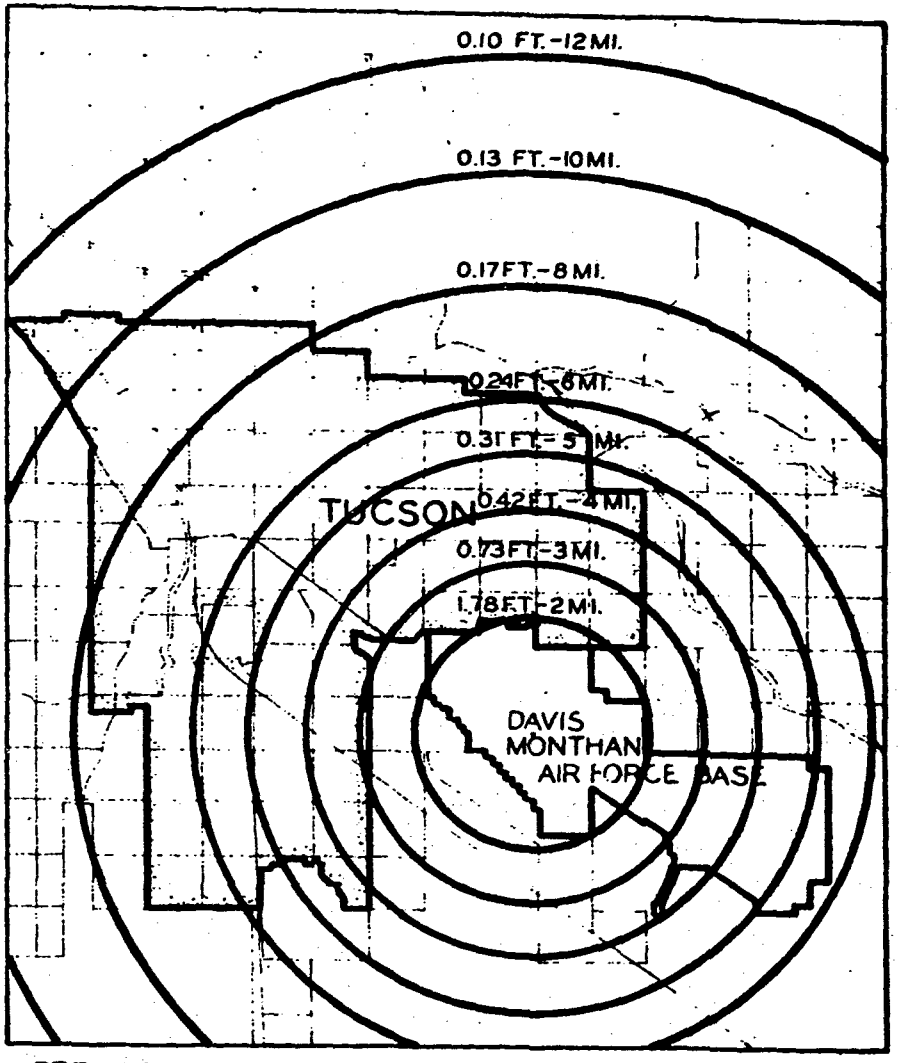

PREDICTED FINAL SURFACE DEFLECTION DUE TO A 5M.T. OPTIMUM AIR BURST ON DAVIS MONTHAN AIR FORCE BASE

Figure 2-6. Surface Deflection

c. Initial nuclear radiation

When consideration is given to close-in effects, as is necessary in the development of shelter systems for cities closely associated with military targets, it is appropriate to evaluate the constraint imposed by initial nuclear radiation. It is this active constraint which may cause certain materials in the immediate vicinity of the burst to later emit gamma radiation not unlike that from fallout itself.

The sources of radiation resulting from a nuclear burst include both neutrons and gamma rays. The initial reactions which emit this radiation take place within a fraction of a microsecond; some persist over long periods after the burst and are scattered or radiated, from atoms outside the bomb debris. In excess of 90% of both the neutrons and gamma rays are captured or absorbed within the bomb itself; even so, the remainder that escapes creates large doses outside the bomb. Further, gamma rays result from the capture of neutrons in nitrogen atoms in the air which give gamma ray emission about 13% of the time. These gamma rays have energies up to 10 mev and are more penetrating than the primary gamma rays resulting from the bomb burst itself. All of this form of activity is restricted to regions in the immediate vicinity of the burst and allow a radially symmetric definition. Part B of the Appendix presents technical predictions of this constraint phenomena. Figure 2-7 shows the total dose in rads which would be received in an unprotected environment at various points in the Tucson vicinity.

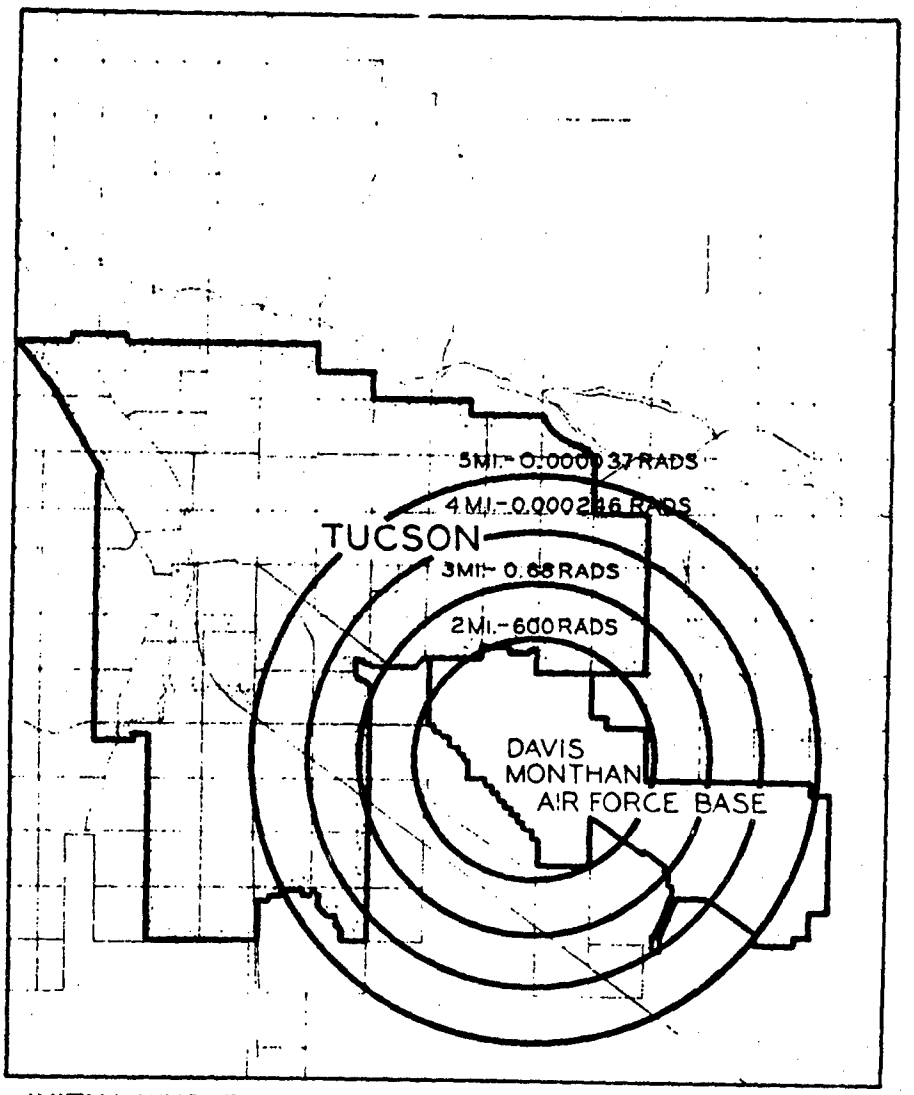

INITIAL WHOLE BODY NUCLEAR RADIATION FOR A 5 MT. OPTIMUM AIR BURST ON DAVIS MONTHAN AIR FORCE BASE

Figure 2-7. Initial Radiation Contours

d. Thermal radiation

In addition to overpressure and initial nuclear radiation, thermal radiation offers an imposing constraint on the system. The explosion of a nuclear weapon results in the creation of extremely high temperatures in the fireball. Since the amount of energy which is thermally radiated by a hot object varies as the fourth power of the temperature, a nuclear bomb radiates a proportionately large fraction of its energy production. This energy is called the thermal radiation. This energy is emitted in a pulse, the length of which depends on the size of the explosion. This pulse can be up to 30 seconds long for bombs in the megaton range. The intensity of the radiated energy decreases as an observer moves away from the burst. Typical levels are: for a 5 megaton bomb and 50 mile visibility, 3 calories per square centimeter at 30 miles, and 12 calories per square centimeter at 15 miles. Three calories per square centimeter is sufficient to ignite newspaper and dark rayon clothing, or burn exposed skin. A radiation level of 12 calories per square centimeter will ignite heavy paper, tree leaves, and cotton cloth. See Figure 2-8.

The exact results depend on the type of material, its thickness, the humidity of the air, the duration of the radiant pulse, and the density of the atmosphere. A layer of clouds, haze, smog, or smoke will act to shield the radiation in a manner analogous to this effect on visible light. The color of an object will also affect its response;

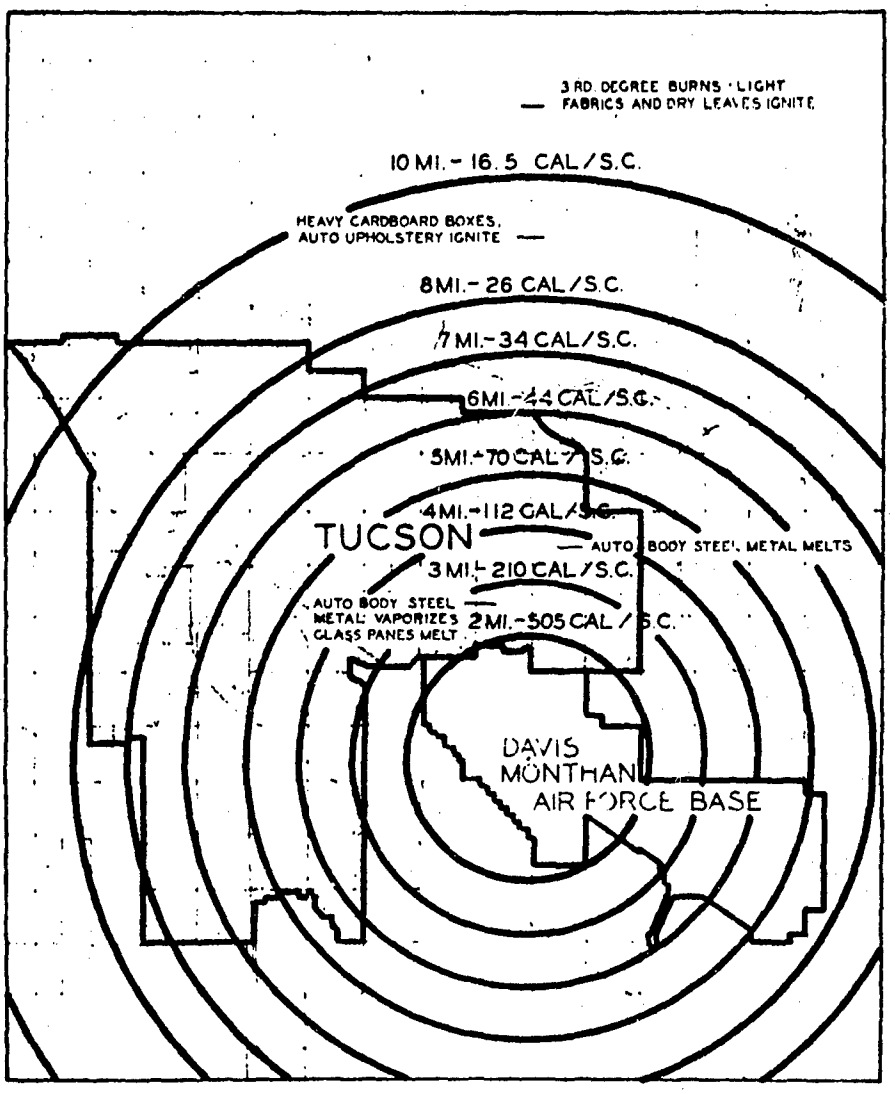

THERMAL RADIATION FROM A 5MT. OPTIMUM AIR BURST ON DAVIS MONTHAN AIR FORCE BASE

Figure 2-8. Thermal Radiation Contours

dark objects being more easily ignited than light colored ones. Thus, a painted frame house will be less likely to burn than an unpainted one. Plastic materials will tend to smoke and boil, but will not burn.

In any event, prolonged burning is not likely with most surfaces, rather they will tend to char and smoke, and then will snuff out as soon as the fireball cools. An exception would probably be dry wooded areas in which many small fires could become well developed during the 30 second life of the thermal radiation pulse.

Thermal radiation contours were generated for the Tucson case and are presented in figure 2-8. Methods that were used in predicting these values are contained in part B of the Appendix.

e. Fallout radiation

The last active constraint which is a direct effect of the nuclear burst is that of fallout radiation. The general nature of reliable predictions of the magnitude of this effect is well explained in Rand's publication, "Close-in Fallout" and James E. McDonald's treatment of the subject in the Journal of the Academy of Science, August, 1961. An adaptation of this approach is presented in part B of the Appendix to this report.

Because of the nature of interaction effects, it is unrealistic to attempt to plot precise fallout radiation contours in advance of the occurrence. It is, however, deemed sufficient to indicate that, as presented in the Appendix, one-hour dose rates may be expected in the vicinity of 10,000 to 100,000 r/hr. It is significant to note that there will be regions in which little fallout will be present. There also will be regions in which tremendous amounts will be deposited. Such regions generally defy reasonable predictions in spite of the intricacies of the analysis.

3. Surveys

Surveys are technical constraints, the magnitudes of which may be determined by collection of existing data from various readily available sources. Categories of these constraints considered pertinent to this study are:

Location of targets
Population density
Weather patterns
Terrain and topography
Water supply
Waste disposal
Soil characteristics
Existing shelter space
Location of schools, hospitals, etc.

The results of certain of these surveys are included with other material in various portions of this report. For example, the location of targets was presented in the targeting section of loadings. Weather patterns were considered in the material associated with fallout prediction. The soil characteristics are considered in the ground motion predictions. Therefore, this discussion will consider only the following survey results which are not presented elsewhere in this report:

Population density
Terrain and topography
Water supply
Waste disposal
Existing shelter space
Location of schools, hospitals, etc.

a. Population density

It is obviously necessary to locate the population if realistic decisions on sheltering are to be made. Because of the mobile nature of this population, exact predictions of the specific location of all persons at a given instant is not possible. Probabilities would indicate, however, that the location of these people would be bounded by the night-time distribution (perhaps the most dispersed) and by the noon-time distribution on the other end of the spectrum.

If the ultimate shelter system incorporates a degree of flexibility in its design, to the extent of allowing rapid adjustment in shelter assignment or protected motion after the attack, then this exact location of the population becomes less important.

For Tucson, the present population matrix is as shown in Figure 2-9. The future population situation in Tucson, one of the nation's fastest growing cities, is anyone's guess. For 1973, the best predictions that are available at the present time are indicated on Figure 2-10.

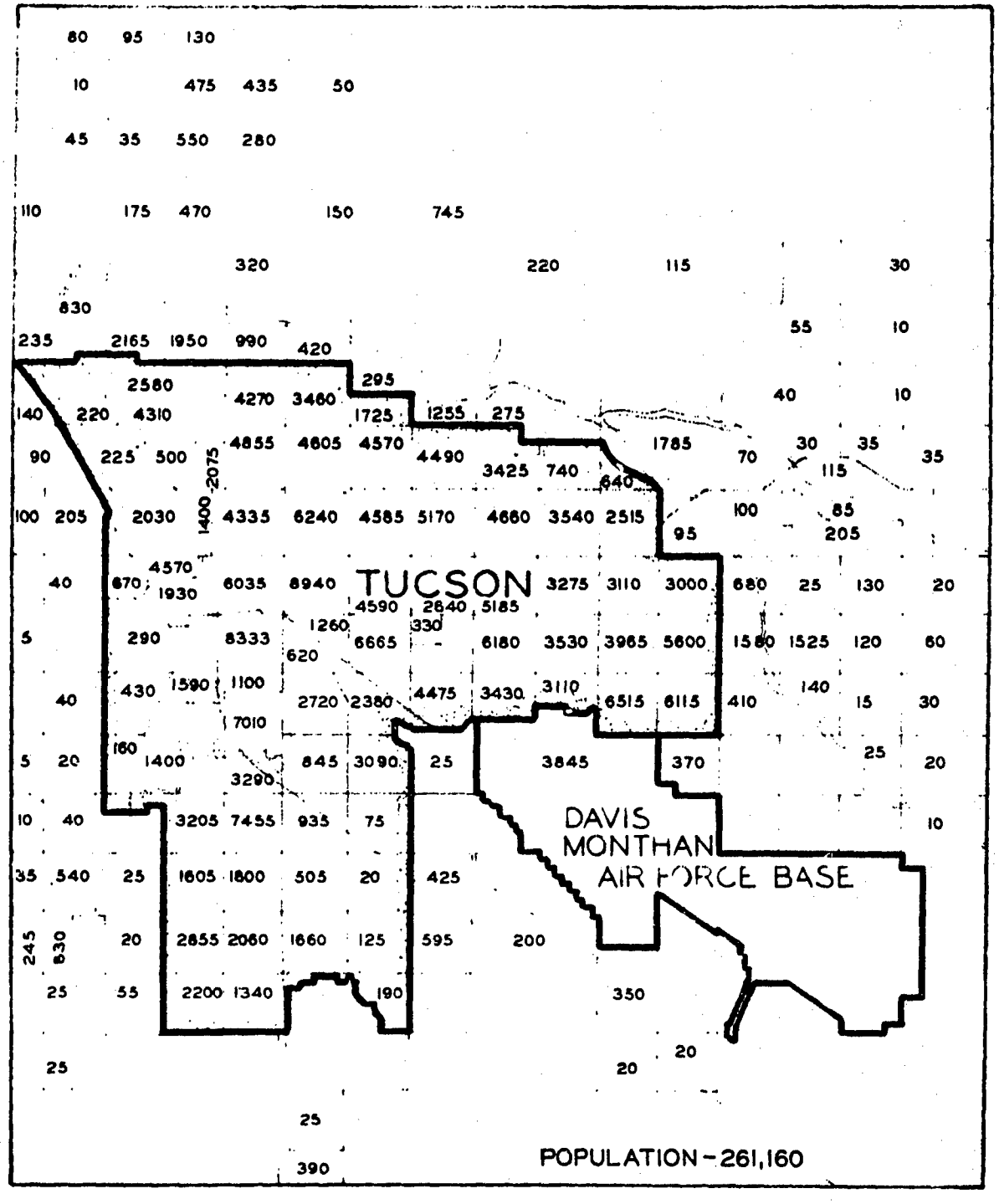

Figure 2-9. Population Density-1963

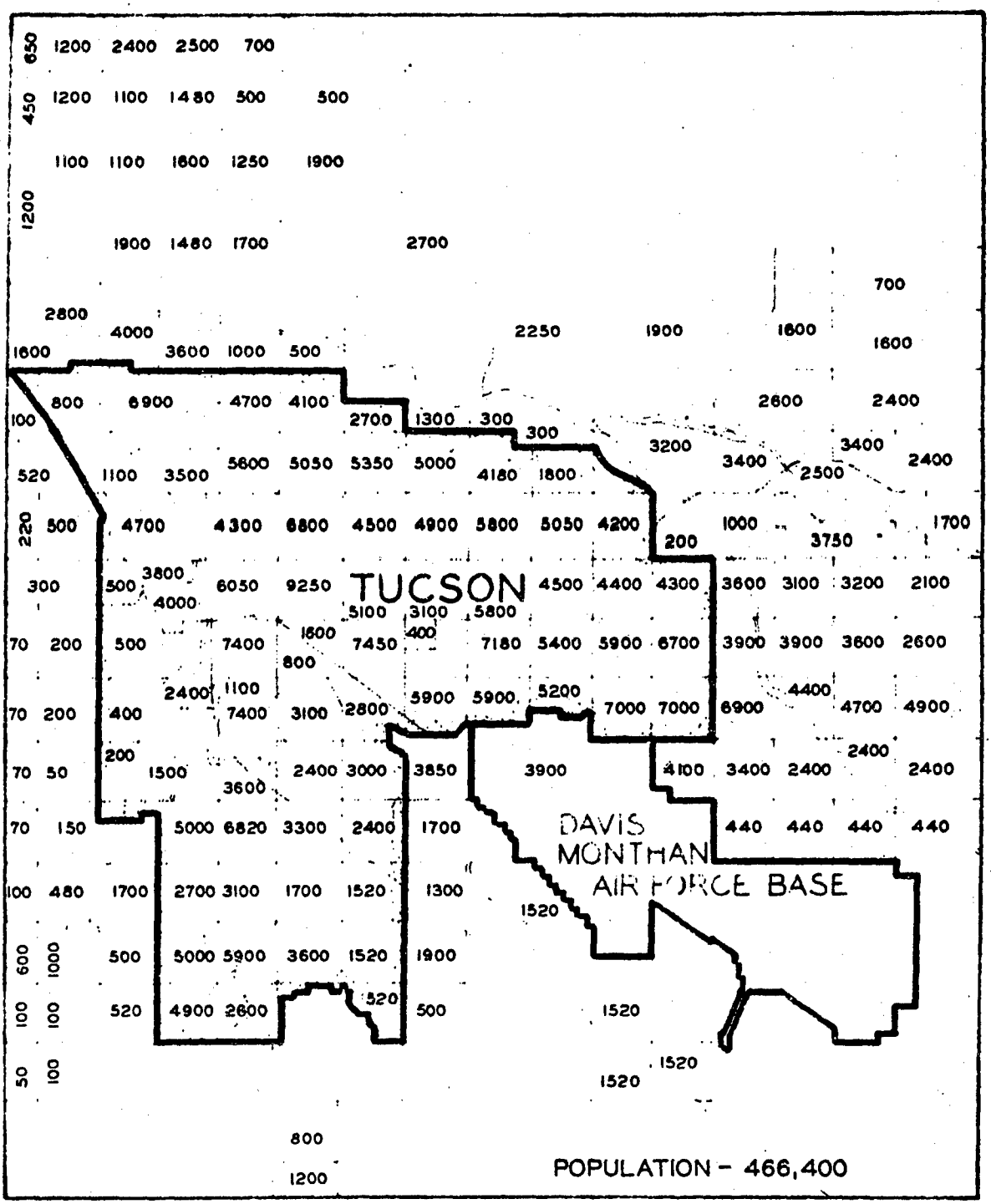

Figure 2-10. Predicted Population Density-1973

b. Terrain and topography

Terrain and topography affect the immediate levels of initial radiaton, thermal radiation, blast overpressures, fallout distribution (to some extent), and ground motion. Unfortunately, there is no direct rational quantitative procedure which permits the full evaluation of the extent of this effect on each active constraint cited.

The most obvious way in which such an item affects these constraints is qualitatively noticed by observing the direct shielding that hills and mountains offer to any effect which radiates linearly from the burst itself, i.e., thermal and initial nuclear radiation. The less obvious ways are those in which the surface irregularities attenuate magnitudes of blast overpressures, create irregular fallout deposition, and modify ground motions.

Contours which indicate some of the outstanding features of the mountainous terrain around Tucson are shown in Figure 2-11. Note the shielded "slot" from Tucson to Redington.

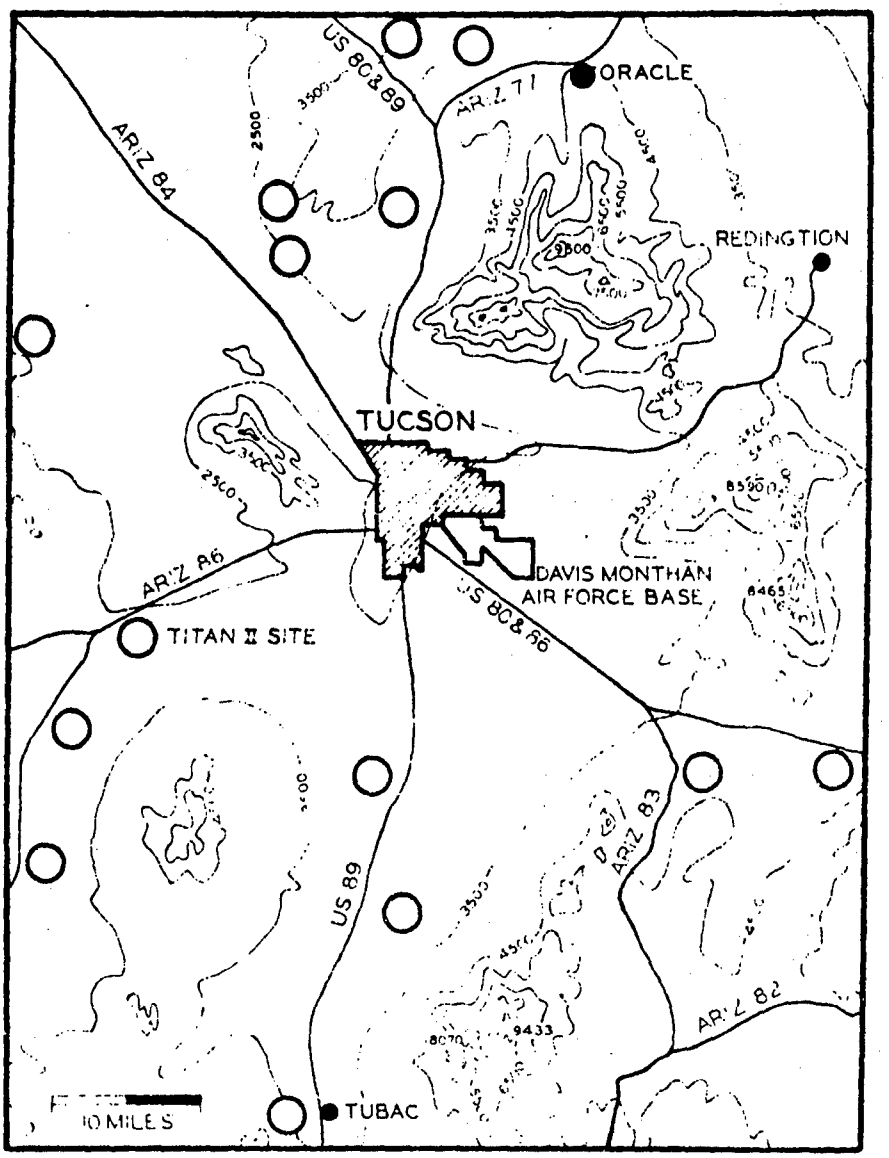

Figure 2-11. Terrain and Topography

c. Water supply

Adequate supplies of potable water are a necessary component of any shelter system. Because of the long-term sheltering requirements for target areas, and because of the possible heavy deposition of fallout in open reservoirs, an underground water source is most desirable.

These same long-term requirements preclude the possibility of providing this underground supply from simple storage tanks, because of the quantities of water that would ultimately be required. If decontamination is incorporated into the plan, large quantities of water in addition to that used for the life support system, may be required. It would thus seem that the most practical source of water for all of these applications would be from wells.

Tucson obtains all of its water from wells which, in general, will remain uncontaminated as far as fallout radiation is concerned. After a survey of several sources of available data for depth to ground water for the Tucson situation, it was found that the most accurate and desirable source was that obtained from the Department of Agricultural Engineering, the University of Arizona. Individual annual well records were examined and static water level elevations were compared to surface elevations at the well site. Well data for the entire Santa Cruz Valley were analyzed. With a map of well locations and their individual depths, a thirty-foot water-level contour was drawn. This information is presented as the shaded area on the map shown in Figure 2-12. The area prescribed as having a water table level of thirty-foot depth or less can be seen to border parts or all of Rillito, Agua Caliente, Tanque Verde, and Rincon creeks. In the past, water in this shaded region has not been particularly potable because of organic surface contamination but, in an emergency this region would provide large quantities of useable water at economical pumping heads.

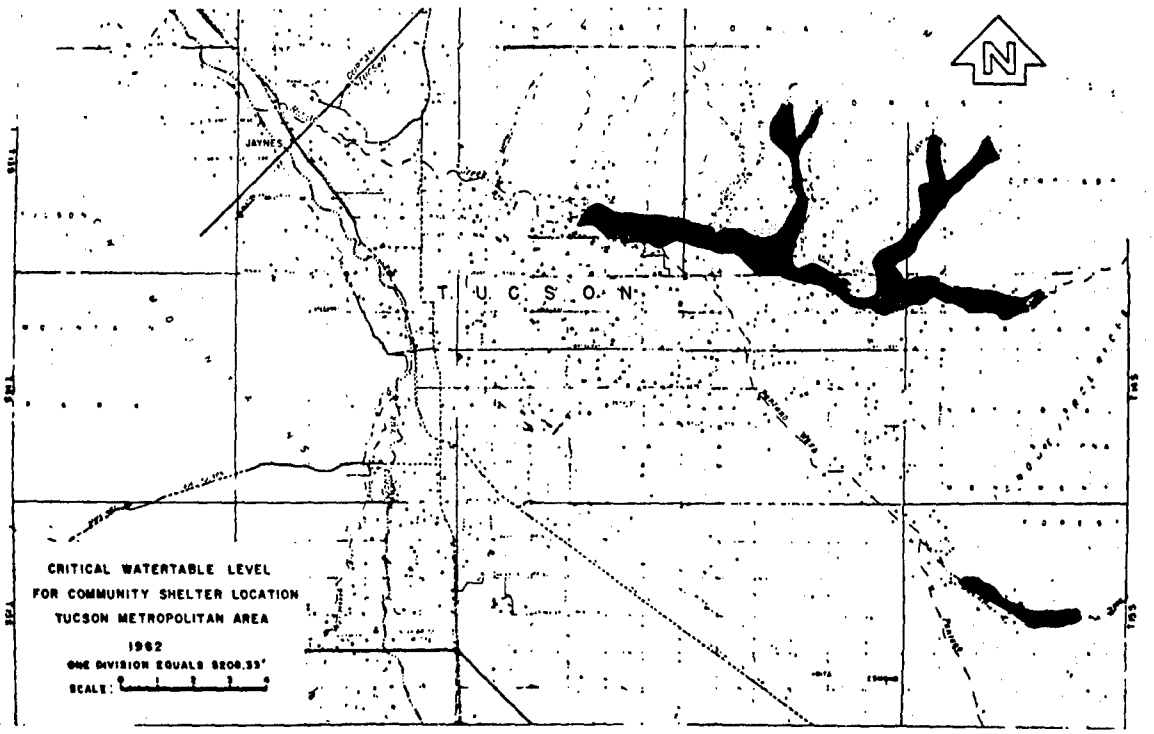

Figure 2-12. 30 Ft Water Table Contour

d. Waste disposal

The disposal of waste can be a minor problem if existing sanitary sewers remain intact. In general, this should be accomplished in regions where peak blast overpressures are under 15 psi. Pumping waste into these sewers will create surface problems at sewage points, but such problems are deemed relatively insignificant when considered in the light of the other particulars of the emergency situation.

It is further observed that a broken sanitary sewer will continue to function, but as a seepage bed, if sewage is pumped into it under pressure. For Tucson, it may be assumed that regions in which the peak blast overpressures are predicted to be less than 15 psi, generally in the northern part of the city, are those in which existing sanitary sewers may be used. In addition to this, useable data on the probable static overpressure resistance of all sewers in the immediate vicinity of schools are presented in table 2-1.

TABLE 2-1

SCHOOL	LOCATION	NEAREST SEWER LOCATION	SIZE (inches)	TYPE	Depth of Backfill COVER (feet)	Depth of Backfill LOAD (lb/ft)	Ultimate Allowable LOAD (lb/ft)	Ultimate Allowable OVERPRESSURE (psi)
(Sr. High)								
Catalina	3645 E. Pima	Palo Verde Blvd.	10	VCP*	8.5	1,150	2,200	12.1
Palo Verde	1302 S. Avenida Vega	22nd Street	10	VCP	8.4	1,130	2,200	9.3
Pueblo	3500 S. 12th Avenue	S. 12th Avenue	12	VCP	4.0	720	2,480	11.8
Rincon	422 N. Arcadia Blvd.	Swan Road	8	VCP	4.1	720	2,200	10.3
Tucson	400 N. 2nd Avenue	6th Street	8	VCP	9.3	1,180	2,200	8.2
(Jr. High)								
Doolen	2400 N. Country Club	N. Country Club	10	VCP	5.0	840	2,200	10.7
Mansfield	1300 E. 6th Street	7th Street	8	VCP	8.8	1,150	2,200	15.2
Naylor	1701 S. Columbus	S. Columbus	8	VCP	11.3	1,250	2,200	22.0
Roskruge	500 E. 6th Street	6th Street	8	VCP	9.3	1,180	2,200	8.2
Safford	300 S. 5th Avenue	13th Street	8	VCP	5.6	650	2,200	14.2
Spring	300 W. 2nd Street	Main Street	14	VCP	9.0	1,150	2,850	19.8
Townsend	2120 N. Beverly	Beverly	8	VCP	7.9	1,100	2,200	8.1
Utterback	3233 S. Pinal Vista	1st Alley west of Pinal Vista	8	VCP	5.1	840	2,200	10.7
Vail	5350 E. 16th Street	Craycroft Road	10	VCP	9.3	1,180	2,200	8.2
Wakefield	400 W. 44th Street	44th Street	12	VCP	11.3	1,250	2,480	50.0
(Elementary)								
Blenman	1600 N. Country Club	Bentley Avenue	8	VCP	8.2	1,100	2,200	14.7
Bonillas	4711 E. 16th Street	Swan Road	8	VCP	2.8	553	2,200	9.5
Borton	700 E. 22nd Street	22nd Street	8	VCP	6.7	1,080	2,200	13.9
Brown	1705 N. Sahuara	Waverly Street	6	VCP	5.7	910	2,200	8.3
Carillo	440 S. Main	Saman leGo Street	8	VCP	10.7	1,300	2,200	7.6
Cavett	2120 E. Naco Vista	Naco Vista	8	VCP	6.1	1,030	2,200	8.1
Corbett	5949 E. 29th Street	Sahuara Avenue	8	VCP	6.6	985	2,200	8.1
Cragin	2945 N. Tucson Blvd.	N. Tucson Blvd.	21	VCP	5.9	1,120	4,235	16.5
Davidson	3260 N. Alvernon	Ft. Lowell Road	8	VCP	7.2	1,030	2,200	8.1
Davis	500 W. St. Mary's Road	Main Street	30	CP *	10.3	4,150	4,450	2.4
Drachman	549 S. Convent	17th Street	8	VCP	5.8	913	2,200	8.3
Duffy	5145 E. 5th Street	Rosemont Blvd.	15	VCP	7.7	1,080	3,025	24.1
Fort Lowell	5151 E. Pima	Rosemont Blvd.	18	VCP	6.8	1,000	3,630	18.3
Govt. Hts.	150 W. Ajo Way	W. Ajo Way	8	VCP	6.7	1,000	2,200	8.3
Holladay	1110 E. 33rd Street	34th Street	8	VCP	5.9	936	2,200	11.9
Howell	401 N. Irving Avenue	Holmes Street	8	VCP	5.1	865	2,200	10.8
Howenstine	2131 E. Winsett Blvd.	E. 16th Street	6	VCP	Unavailable		2,200	
Hudlow	6900 E. 5th Street	E. 4th Street		VCP	Unavailable		2,200	
Hughes	700 N. Wilson Avenue	E. 4th Street	8	VCP	6.2	960	2,200	12.3
Jefferson Park	1701 E. Seneca	Warren Avenue	12	VCP	2.5	504	2,480	10.4
Keen	3538 E. Ellington Pl	Ellington Pl.	6	VCP	10.1	1,230	2,200	18.7
Kellond	6606 E. Lehigh Dr.	Lehigh Dr.	6	VCP	11.2	1,250	2,200	20.6
Lineweaver	461 S. Bryant Ave.	Columbus Blvd.	8	VCP	7.1	1,030	2,200	13.1
Lynn	1573 W. Ajo Way	Phoebe Avenue	4	CP	7.6	1,300	-----	50.0+
Manzo	1301 W. Ontario	St. Clair Street	8	VCP	5.0	840	2,200	8.4
Menlo Park	1100 W. Fresno	W. Fresno	8	VCP	6.3	960	2,200	8.3
Miles	1400 E. Broadway	12th Street	21	VCP	9.4	1,820	4,230	19.7

TABLE 2-I continued

SCHOOL	LOCATION	NEAREST SEWER LOCATION	SIZE (inches)	TYPE	Depth of Backfill COVER (feet)	LOAD (lb/ft)	Ultimate Allowable LOAD (lb/ft)	OVERPRESSURE (psi)
Mission View	2600 S. 8th Avenue	S. 8th Avenue	8	VCP	7.2	1,820	2,200	4.1
Myers	5000 E. Andrew	Rosemont Avenue	8	VCP	5.7	864	2,200	8.3
Ochoa	101 W. 25th Street	8th Avenue	12	VCP	7.8	1,080	2,480	10.1
Pueblo Gardens	2210 E. 33rd Street	Plumer Avenue	6	CP	7.1	1,820	2,200	4.1
Richey	2209 N. 15th Avenue	N. 15th Avenue	6	VCP	9.1	1,150	2,200	16.6
Roberts	4355 E. Calle Aurora	Columbus Blvd.	8	VCP	10.6	1,250	2,200	18.3
Robison	2745 E. 18th Street	Winsett Blvd.	8	VCP	5.9	938	2,200	11.8
Rogers	6000 E. 15th Street	Directly S. of school	8	VCP	11.1	1,270	2,200	20.2
Roosevelt	1201 N. 9th Avenue	Helen Street	8	VCP	10.2	1,230	2,200	17.7
Rose	800 W. Michigan Drive	15th Avenue	8	VCP	5.6	890	2,200	11.4
Sewell	425 N. Sahuora	Chantilly Drive	8	VCP	5.0	840	2,200	10.7
Tully	1701 W. El Rio Dr.	El Rio Dr.	6	VCP	6.9	1,030	2,200	12.7
Univ. Hts.	1201 N. Park Ave.	Mabel Street	8	VCP	10.0	1,250	2,200	19.4
Van Buskirk	725 E. Fair Street	Fair Street	8	VCP	2.2	432	2,200	8.8
Wheeler	1818 S. Aven. Del Sol	Calle Castor	8	VCP	8.4	1,130	2,200	14.9
Whitmore	5330 E. Glenn	Glenn	8	VCP	6.5	985	2,200	12.4
Wright	4311 E. Linden Street	Seneca Street	8	VCP	6.5	985	2,200	12.4
---	End District 1							
Laguna	5001 N. Shannon Road	Joynes Station Road	12	AC-240	11.0	1,250	3,300	44.5
Davis	4250 N. Romero Road	Romero Road	30	CP	16.0	2,800	4,460	22.6
Wetmore	701 W. Wetmore Road	Wetmore Road	24	CP	9.7	1,840	3,960	17.8
Catalina Foothills	E. River Road	Septic Tank						
Wrightstown	8950 E. Wrightstown Road	Septic Tank						
Tanque Verde	Tanque Verde Rd.	Septic Tank						
Fickett	7240 E. Calle Aurturo	Kolb Road	6	VCP	Unknown			
White	2315 W. Canada	Canada St.	8	VCP	5.6	840	2,200	11.8
Brichta	1501 N. Silverbell	Golden Hills Road	8	VCP	6.5	985	2,200	12.4
Dietz	1801 S. Turquoise	Vista Palma Drive	6	VCP	7.4	1,060	2,200	13.2
Liberty	5101 S. Liberty Ave.	S. Liberty Ave.	8	VCP	4.9	840	2,200	10.7
Mission Manor	Santa Clara and Santa Rosa	Santa Rosa Road	10	VCP	7.9	1,100	2,200	14.1
Sunnyside Sr.	1725 E. Bilby Rd.	Bilby Rd.	8	VCP	9.3	1,180	2,200	16.9
Sunnyside	250 E. Valencia Rd.	Valencia Rd.	12	VCP	8.2	1,100	2,475	18.4
Ranchitos	Ginter Road	Sears Blvd.	8	VCP	4.3	1,190	4,180	11
Flowing Wells	3725 N. Flowing Wells Rd.	Prince Road	27	CP	4.3	1,190	4,180	11
Frans	1456 W. Prince Rd.	Prince Road	27	CP	5.5	1,460	4,180	11.2
Harelson	826 W. Chapala Drive	Magee Road	6	VCP	4.4	768	2,860	14.8
Nash	515 W. Kelso	Tipton Drive	6	VCP	5.5	888	2,200	15.2
Keeling	435 E. Glenn	Los Altos Ave.	8	VCP	5.0	840	2,200	10.7
Amphi-Sr.	125 W. Yavapai Rd.	Oracle Rd.	15	VCP	11.3	1,270	3,010	40.3
Amphi-Jr.	315 E. Prince Road	Prince Road	27	CP	6.3	1,620	4,180	11.9
Prince	315 E. Prince Road	Prince Road	27	CP	6.3	1,620	4,180	11.9
Holaway	3500 N. Cherry	Prince Road	10	VCP	1.1	220	2,200	8.3

*VCP - vitreous clay pipe
*CP - clay pipe

e. Location of schools, hospitals, etc.

Location of schools, hospitals, governmental offices, and larger commercial centers are shown as entrances in illustrations which depict the buried conduit shelter system. Table 2-I presents locations of public schools by street address.

f. Existing shelter space

In general, no target area has, in existence, sufficient shelter space which may be classed as adequate to resist the levels of active constraints offered by the close-in effects of nuclear surface bursts. In fact, few areas have sufficient fallout shelter space with protection factors of 100, or better, much less blast and radiation resistant space with protection factors in the required millions.

A rather extensive fallout shelter survey was conducted for Tucson in connection with contract CDM-61-35. Quoting from the abstract to the report on this contract (1), "The survey clearly shows the total inadequacy of the existing shelter spaces to protect the population of Tucson from fallout which might be induced by nuclear action."

Tucson has approximately 2,100 spaces now in existence which may be classed as adequate for the expected levels of active constraint. This represents shelter space for less than 1% of the total population.

C. Non-Technical Constraints

1. Psychological

The effect of psychological factors on the development of a shelter system has historically been overshadowed in light of the problems which must be considered by the structural and mechanical engineer. This is unfortunate, however, because it is known that the shelter system must satisfy more than the physical necessities of protected man--it must elicit positive responses from those whom it protects. Therefore, it must consider such possible psychological constraints as: changes in mental state or response caused by individualized stimuli (warning method, personal observations, etc.); preservation of the system of social values; creation of a confidence factor or positive belief; and the need to disseminate information about the system and system purposes.

Ideally, the planner might wish to create a shelter system which would duplicate all the comforts and conveniences of the ordinary community. Obviously, this ideal must be compromised, in large measure, by the economic constraints. This then may become a source of psychological pressure on the people to be protected. They will probably need to learn to live with common facilities; and with much reduced personal privacy in a setting which may, at least temporarily, separate them from familiar people and occupations.

In addition to this, the mechanical problem may require that the shelter system be quite confined, even altogether underground, at least for early periods. Provision of attention-distracting or diverting elements should be considered in order to improve the anticipated outlook and personal compatibility during the possible longer-stay periods.

If travel times to shelter entrances are relatively long, the elements of individual panic will more likely be present at time of emergency, and trans-attack plans will be more complicated. Required warning times will, of course, be longer for more remote shelter entrances.

For prolonged shelter stay-times, the psychological factors in the shelter problem increase in rapid proportion. Only the most speculative answers are available for: thousands of law-abiding persons, for weeks in confining quarters, with the only occupation being survival. However, the planner must consider this problem, in terms of organization of in-shelter leadership and administration, in addition to protective physical design of the system.

The social system inherent in American culture seems to function best when the family unit is maintained intact. So it seems natural that any shelter system will be most effective if it can overcome the potential psychological constraints inherent in separating members of the family. It should consider means by which the family group can communicate, or ideally, remain in contact. Provision should be made to re-unite members of a family group who were not at home when the warning sounded. This need tends to conflict with the economic constraints in conventional shelter systems.

For the purpose of later recovery plans, which are of large import when considering attitudes of protected man, the system should promise to provide means which will allow him to cooperate in post-strike rescue evacuation, or recovery activities.

In the case of more prolonged stay times (caused by close-in, high-intensity fallout radiation) it may be expeditious to evacuate the mass of people to less contaminated areas. This may require protection of even such decontamination equipment as heavy earth moving equipment for use in creating clear landing strips for air-evacuation and in creating decontaminated areas in which temporary outdoor communities may be established.

2. Survivor Characteristics

An additional constraint is related to the makeup of the survivor group. It should be possible to predict statistically what percentage of the population in a given urban area must be survivors, as well as the things they will need, in order to preserve a viable economy. The shelter system must consider protection of the group and the things as a minimum, or it is only worth passing consideration. However, the notion that it is sufficient to provide merely a certain amount or number of spaces, regardless of who or what is protected, will not completely answer the problem. The system should provide for relatively certain preservation of most

vital skills, services, and records as well as more commonly understood provision for vital governmental officials and functions. Storage space must be provided for supplies and equipment which must be protected from blast and thermal damage.

The special provision which must be made for survival of skills in areas such as medical, sanitation, public utilities, transportation, education, construction, etc., must be given similar priority to that which we plan to provide for governmental functions. The entrance accessibility provided by the recommended shelter system should tend to fulfill this requirement without requiring major additional planning in physical design or trans-attack planning. Efficient use of relatively dead space in interconnecting devices and inexpensive extension areas would provide ample accessible storage space without prohibitive additional cost. The long-range outlook for survival of the existing economic pattern will bear a materially direct relationship to the acceptance and cooperation which the plan receives from existing influential economic entities. As an instance, the vital production records and operating policy records of large enterprises could be preserved, along with governmental records, to expedite recovery.

3. Coordinated Shelter Plan

A form of economic constraint is involved in the consideration of the need for a coordinated shelter plan. Ideally, a shelter plan which can be designed largely to also serve everyday community needs would be most acceptable. Therefore, the designer should consider coordinating new shelter construction with local community needs for heavy construction which might be compatible in a shared-use program.

Some examples of shared-use methods are suggested in very general reference, and without recourse to actual plans or stated needs: 1) the streets of most communities are burdened with the problem of transporting large masses of goods to outlying areas from central distribution points; 2) storm water runoff sewers are not adequate in most cities; 3) water supply methods constantly require improvement; 4) other overburdened utility and communication services provide additional examples of possible ways in which everyday community plans might be coordinated with a shelter plan to reduce the total burden on economic resources.

SECTION III

CONCEPTION AND EVALUATION

A. General
B. Conception of General Systems
    1. General Interest Concepts
        a. Fixed
        b. Movable
        c. Mixed
    2. Tucson Concepts - General
        a. Fixed
    3. Tucson Concepts - Movable
    4. Tucson Concepts - Mixed
        a. General
        b. System advantages
        c. Shared-use concepts
C. Cost-Effectiveness Evaluation
    1. Cost Alternatives
    2. Fixed Individual Shelter
        a. Culvert-type shelter
        b. Flat-plate roof type shelter
        c. Dished-roof type shelter
        d. Domed-roof type shelter
        e. Concrete-box type shelter
    3. Fixed Community Shelter Systems
        a. Flexible type (4,500 person capacity)
        b. Rigid type (1,000 person capacity)
    4. Multi-Purpose Buried Conduit System (Mixed)
    5. Cost-Effectiveness Analysis
    6. Summary
        a. System comparisons
        b. Multi-purpose cost sharing

SUMMARY

This section considers counterforce defense system concepts in general as well as specific context, and evaluates them in terms of Tucson constraints. The most feasible systems are further evaluated in terms of cost and cost-effectiveness. Tentative conclusions are drawn concerning the desirability of certain technically feasible systems.

SECTION III. CONCEPTION AND EVALUATION

A. General

It has long been apparent that nature demonstrates a survival of the fittest approach to the creative process. Briefly, this approach is based on conceiving a large, possibly infinite, number of solutions to a given problem; then to subject the solutions to the rigors of evaluation and testing in the naturally hostile environment. The solutions which survive tend to be best adapted to the natural constraints.

This study has followed a similar approach to conception of methodology leading to design of a system, or systems, which will serve to shelter urban population. Concepts which survived general theoretical analysis were subjected to evaluation in light of determined constraints related to those of a physical, sociological, and psychological nature.

The physical, social, and unavoidable political constraints have theoretically impinged on each concept and have, to a degree, defined each solution. The eventual generalization which is derived responds to the question: what are the most likely of possible physical solutions which provide realistic resistance to the nuclear hazards which confront the population of target cities?

B. Conception of General Systems

1. General Interest Concepts

In simplest form, all possible shelter concepts fall into three major categories. The first two of these generally may be considered fixed and movable in countermeasure character. The third is a mix of the first two, selecting components of each. The fixed solutions are those which involve little or no travel on the part of those who are protected. The solutions called movable would require the protected people to make an evacuation trip of either a pre, trans, or post-attack nature. The various possible solutions consistent with these categories are outlined as follows:

a. Fixed

(1) Eliminate war
(2) Eliminate targets
(3) Do nothing
(4) Anti-Ballistic Missile, plus fixed shelter systems
(5) Fixed individual home shelter system
(6) Fixed community shelter system

b. Movable

(1) Pre-attack evacuation

(a) Determined destination
(b) Undetermined destination

(2) Trans-attack evacuation

(a) Protected
(b) Unprotected

(3) Post-attack evacuation

(a) Protected
(b) Unprotected

c. Mixed

(1) Primary evacuation to secondary fixed shelters
(2) Primary fixed shelter occupation with secondary or emergency protected evacuation

2. Tucson Concepts - General

The above general interest concepts form the framework under which all Tucson concepts, both feasible and not feasible, may be originated. It is observed that shelter systems for target cities have severe levels of technical constraints imposed upon them which tend to immediately invalidate many otherwise feasible general concepts. A number of conceivable solutions and systems have received consideration in the course of the study to determine the best shelter system concept for Tucson. Distinct categories of solution are presented: fixed or not primarily active, in terms of system plan; those which primarily require travel (called movable); and systems predicated on a mix of both fixed and movable concepts.

a. Fixed

(1) Certain of the fixed considerations are interesting and even desirable alternatives for Tucson, but they will contribute but little to conception and design of pragmatic solutions.

On the desirability of eliminating war, as a solution, no doubt the highest level of policymaker can agree with the least informed, or most apprehensive, private citizen, that this solution is most desirable; however, even he finds that his best efforts do not entirely accomplish the purpose. The constraints, in the form of international disagreements, seem to be greater than present counterforce methodology can solve.

(2) It is assumed that the possibility of eliminating targets has obviously been given consideration at the highest level of defense planning and, therefore, must not be presently feasible for apparent tactical and economic reasons. Possibly this proposition may become more likely when the arsenal of deterrant weapons reaches proportions and efficiency which can permit at least relocation of some of the more critical military targets. The Tucson problem would be considerably simplified by moving the Titan sites from upwind locations southwest of the city to northern and northeastern sites, or by eliminating them entirely. (c)

(3) The suggestion that any active plan or fixed construction plan would be worse than doing nothing, has many adherents who argue that effectiveness is either not possible, or if a plan is effective to the purpose, it will increase world tension or create doubt in peoples minds about the adequacy of deterrant weapons systems. It is even suggested that world-wide fallout radiation will make the entire world untenable, therefore, why the bother? This study group--aware of the technical validity, or lack of it, in these arguments; aware of the heritage of positive resolution inherent in the historical nature of American temperment; and aware of the most recent evaluations of most probable enemy reaction---reject this concept as being contrary to the best interests and consensus of the people. It is not technically accurate to say that the world will become untenable due to fallout radioactivity. The effects of nuclear weapons are subject to reasonable evaluation in conventional terms. An additional fact is that civil defense systems are more likely to be additive to deterrant weapons systems, and to be considered such by the people, in general. Experience with the most likely nuclear enemy teaches that nuclear shelter counterforce methods would probably cause them to initiate the same kind of action, and might serve to encourage peaceful negotiation, even disarmament agreements. (d)

(4) The concept of an ABM (Anti-Ballistic Missile system) plus a fixed shelter system appears a most desirable solution although it may present a large economic constraint just short of actual costs of a conventional war. Most estimates of the cost of ABM systems alone have been in multiples of a billion dollars. The additional cost of adequate shelter construction would be a relatively small sum. The adequate shelter is presented here as an interim solution compatible with later ABM systems.

(c) James E. McDonald, Journal of Arizona Academy of Science, March, 1961.
(d) Anthony J. Wiener, Hudson Institute rpt on the "Civil Defense Controversy" in OCD Systems Evaluation Conference.

(5). Fixed Individual Shelters

(a) General

Individual or family-type shelters have their greatest usefulness in sparsely settled areas. They are not satisfactory in urban areas for many reasons (space requirements, psychological, social, cost, etc). Nevertheless, this type of shelter is in existence in limited numbers and should be investigated further to give balance to the overall feasibility evaluation studies which follow.

(b) Designs

Three distinct configurations of individual shelters were considered from the standpoint of effectiveness and cost considerations--the culvert type, the flat plate and dish types, and the dome type.

In order to make more direct comparison of individual shelter structures, minimum entrance configurations are assumed for all designs even though the accompanying drawings may show more elaborate entrances. These designs are predicated on protection against 60 psi overpressure, and an adequate shelter-space for 6-8 persons (commodius for a few less).

The culvert, as a shelter, has undergone perhaps the most extensive tests and theoretical investigation of any buried structure now being used. See figures 3-1 and 3-2. The efficiency of this type of structure in resisting blast effects is well established. Unfortunately, to our knowledge, the ends of these tubes have received little attention, largely because of the complex boundary conditions which develop at these points. It appears that the dished steel membrane supported by the formed T-shape shown is superior in performance and cost to any end plate that is presently available. Such an end detail will largely assure that the ends will in fact, be as strong as or stronger than, the culvert itself.

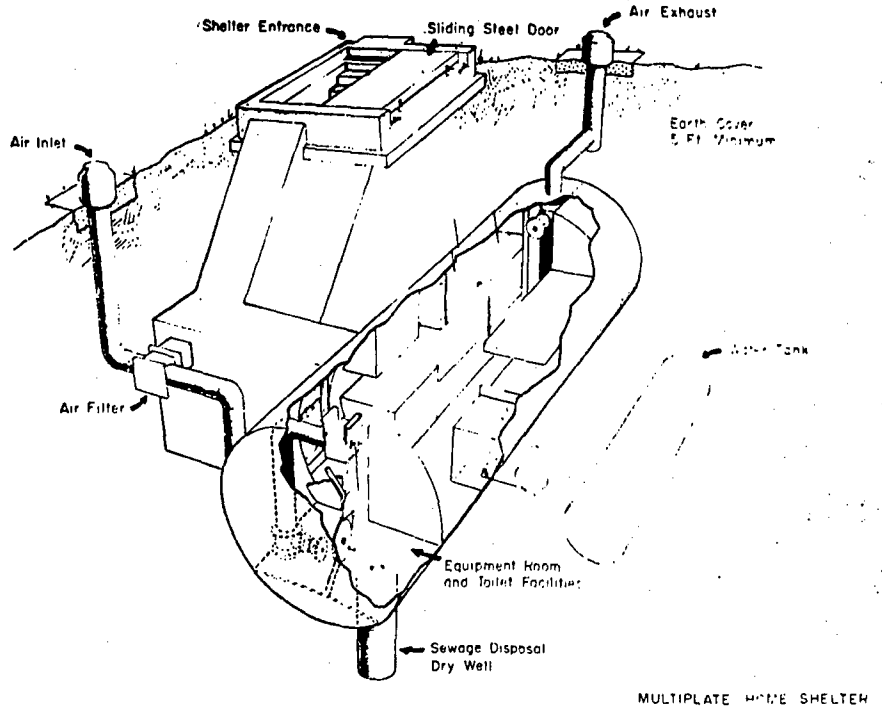

Figure 3-1. Culvert-Type Family Shelter

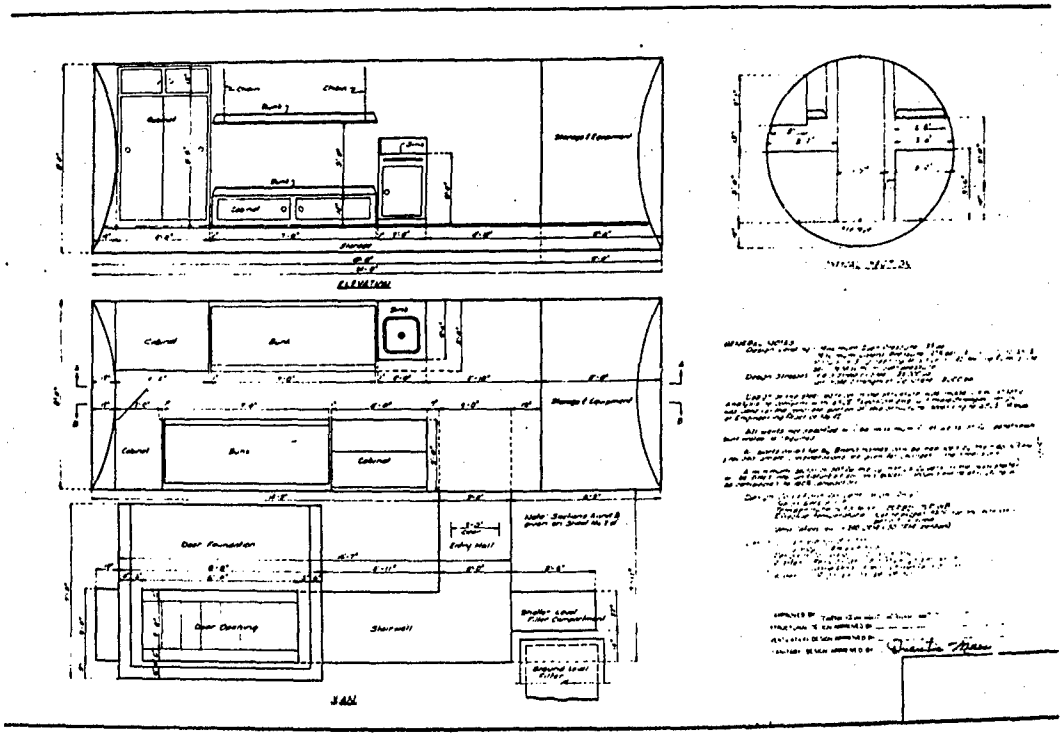

Figure 3-2. Plan and Elevation Details For a Culvert-Type Shelter

The flat plate type shelter is presented in figures 3-3 and 3-4. An alternate solution involving a steel membrane roof structure similar to that shown later in figure 3-10 is also considered. The steel membrane in ultimate capacity will support pressure and shock loadings far in excess of the reinforced concrete roof. The prime reason for this is that the concrete roof must resist load by developing structurally inefficient bending stresses, while the steel membrane supports its load in uniform yield-tension similar to the way in which a soap bubble contains its internal air pressure. It is in this configuration that the material is operating at its maximum efficiency.

The dome-type individual shelter is a special case of elliptical dome in which, under uniform pressure, the membrane hoop stresses are zero along the equator or junction with the vertial wall. See figures 3-5 and 3-6. By programming precise bending calculations on the IBM 650 computer, bending moments consistent with membrane displacements were determined. It is observed that this 3-inch thick concrete dome has the same initial capacity as the previously presented flat concrete plate and dished steel membrane. Domes of this type are presently being constructed by a Tucson firm. Their construction procedure consists of spraying "gunite" concrete over a domed fibreglass liner which remains in place as an energy-absorbing protective ceiling.

(6). Fixed Community Shelter

For densely settled urban areas subjected to close-in nuclear effects, the flexible community shelter system allows great improvement in cost-effectiveness over individual shelters. Because of the lack of existing efficient community shelter designs for close-in effects, a unique concept was developed for inclusion in this study at this point. The source of uniqueness relies on the development of a roof system, consisting of dished membranes resting on precast concrete column shapes. The structure conceived is composed almost exclusively of pre-formed shapes which, because of the multiplicity of use, may achieve the economies associated with mass production. Engineering drawings, model configurations, and calculations have been produced for this dished-membrane community blast shelter, however, these must be regarded as preliminary in nature. See figures 3-7 through 3-12.

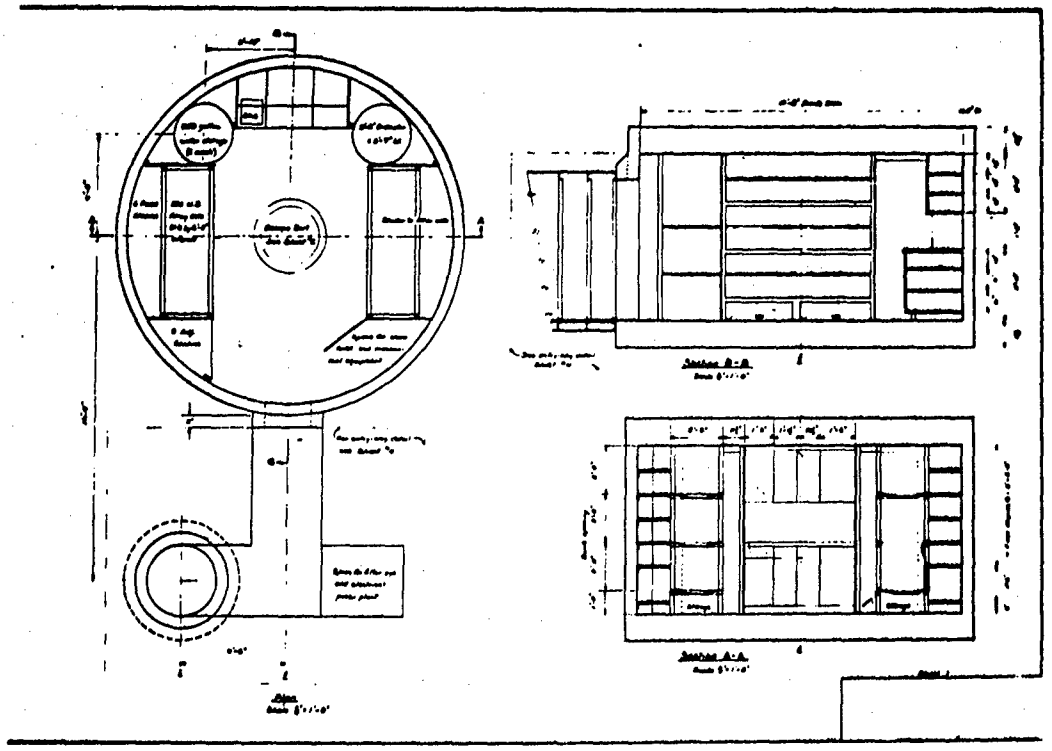

Figure 3-3. Plan of Family Shelter

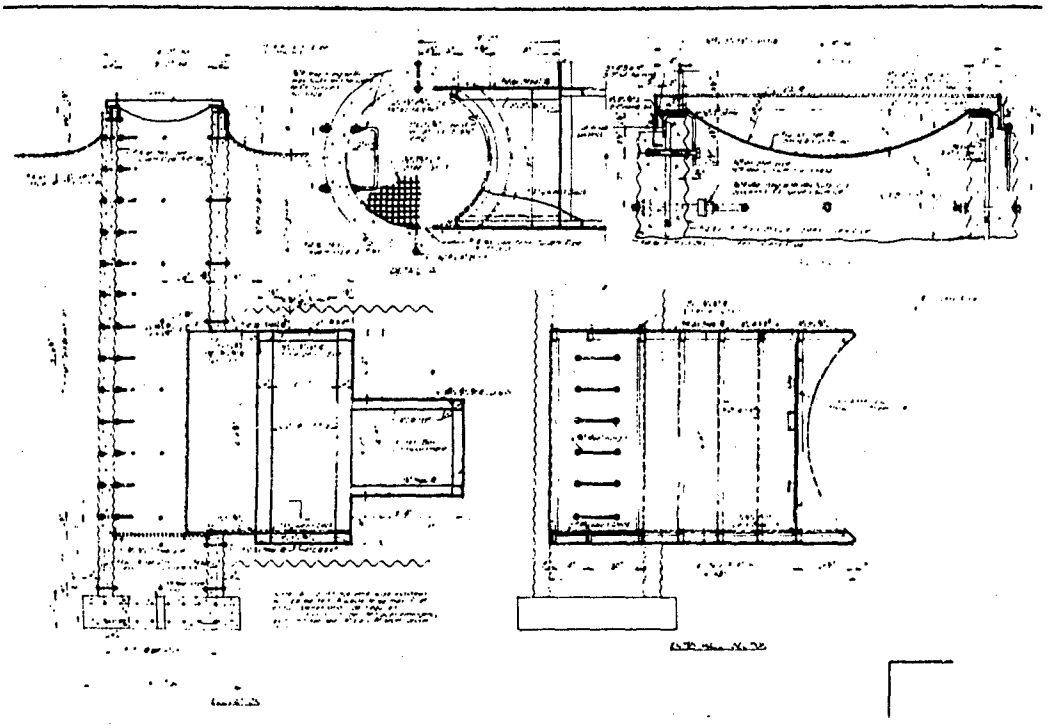

Figure 3-4. Vertical Entrance and Door Detail

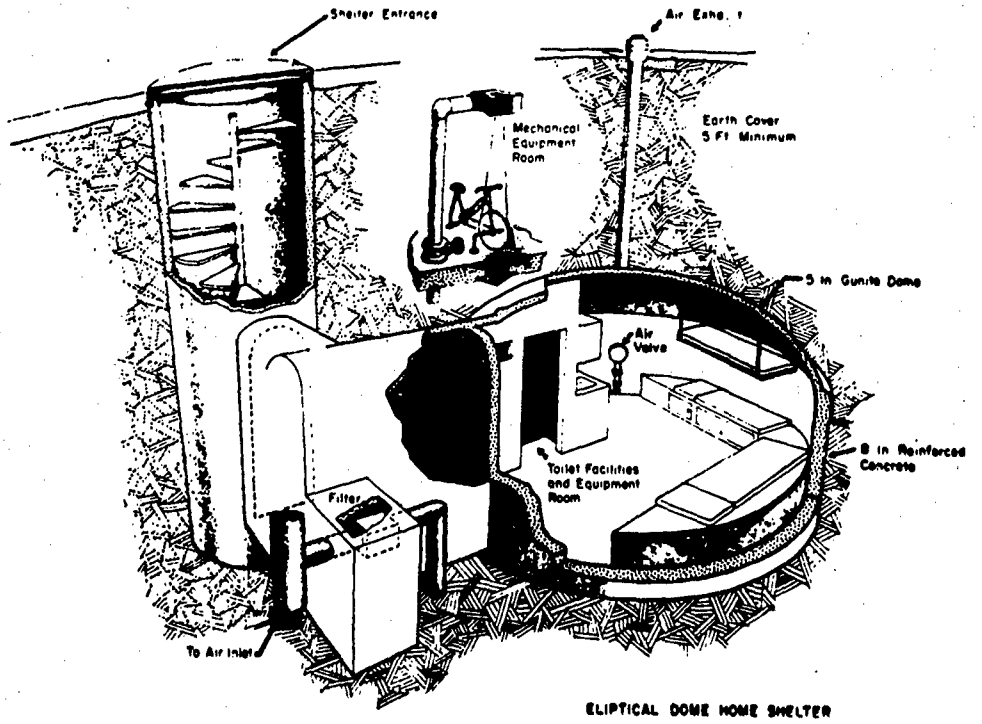

Figure 3-5. Dome-Type Family Shelter

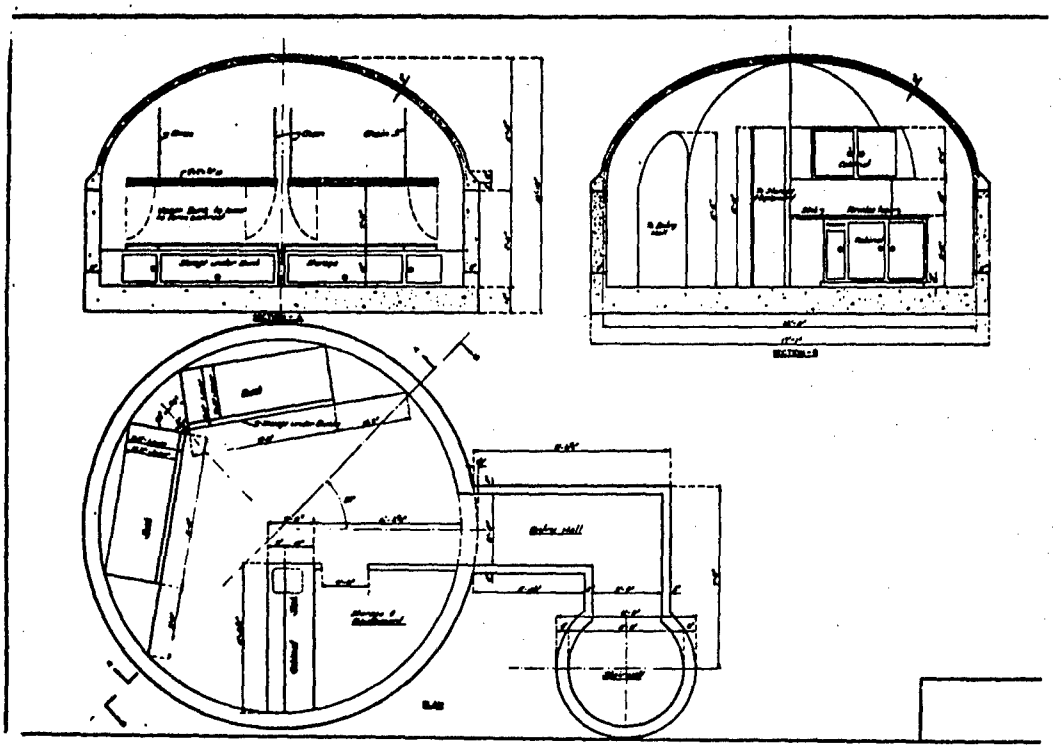

Figure 3-6. Floor and Elevation Sections for Dome-Type Family Shelter

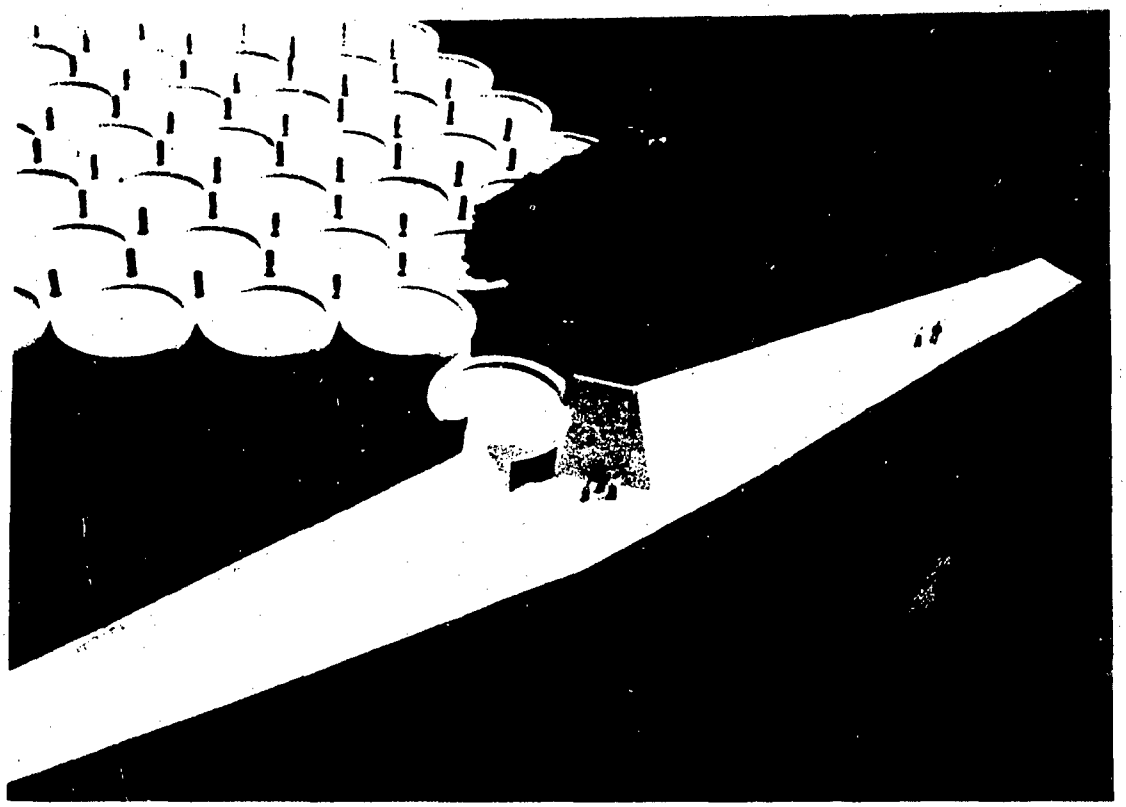

Figure 3-7. Entrance to Community Shelter

Figure 3-8. Precast Column--Forms All Interior Walls

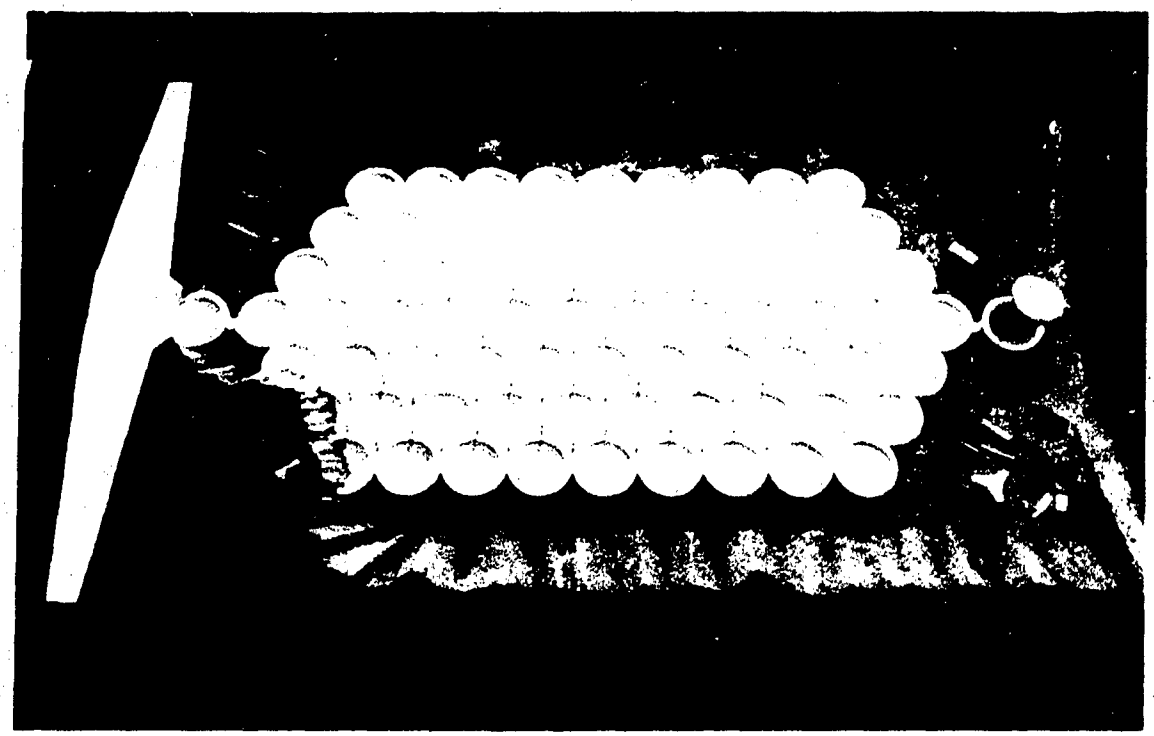

Figure 3-9. Community Shelter for 4,500 People

Figure 3-10. Cross-Section of Community Shelter Module

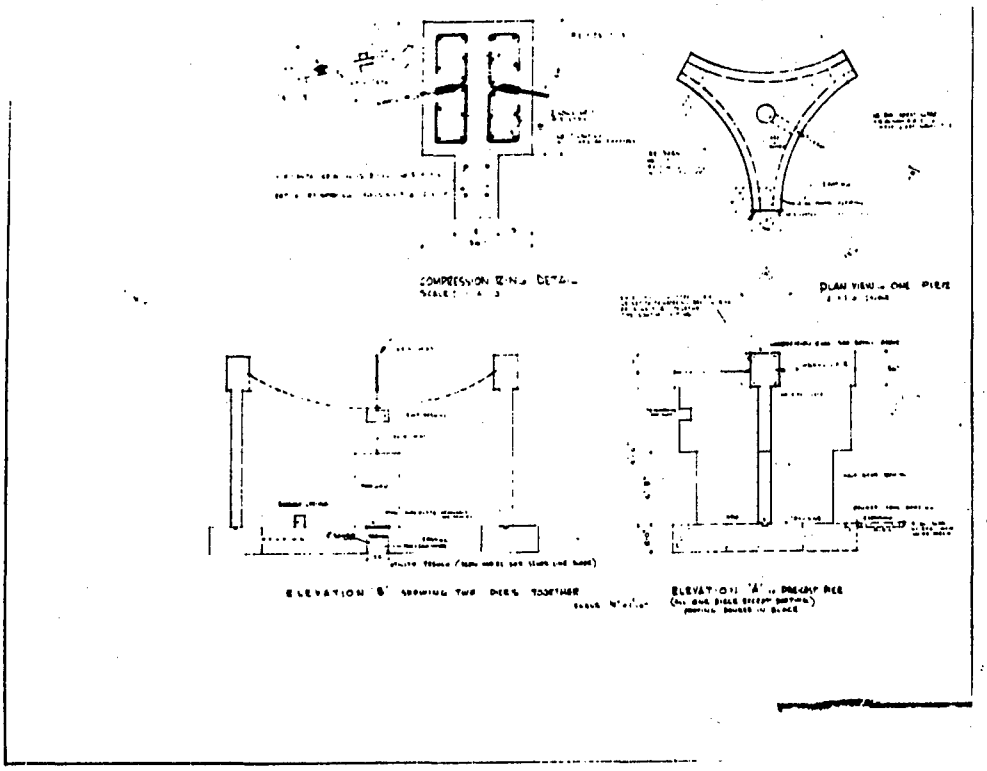

Figure 3-11. Precast Pier Detail For Community Shelter

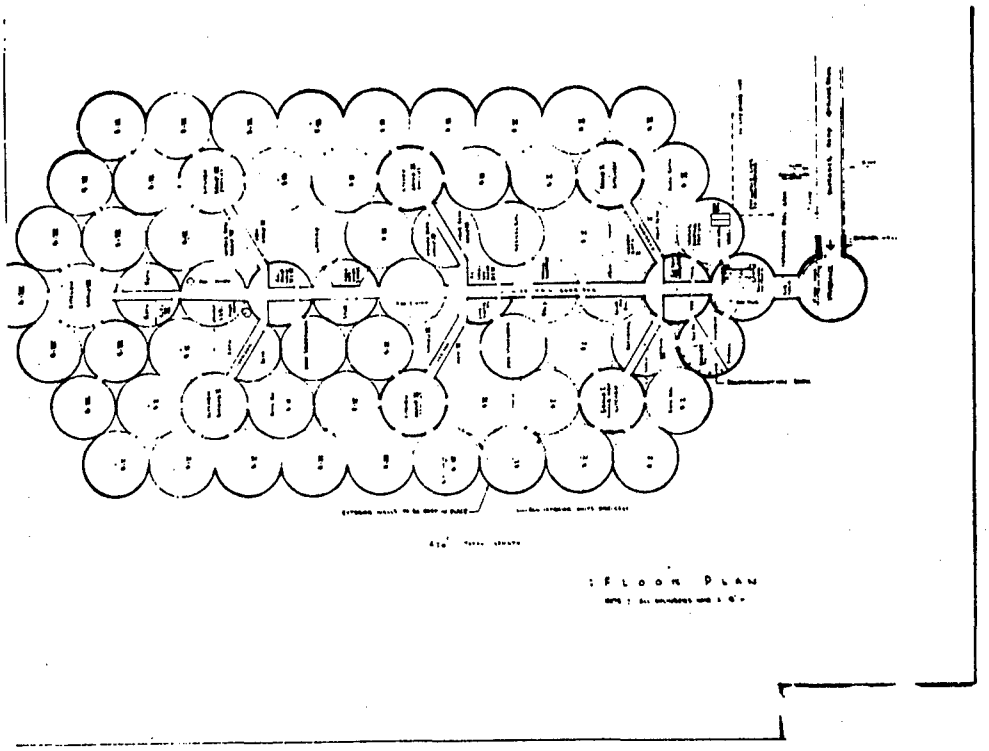

Figure 3-12. Air Conditioning Layout for Community Shelter

The architectural arrangement develops maximum use of floor space and divides the shelter population into individual groups of manageable size from the standpoint of control and logistic support. The need for group concept was recognized after a thorough study and evaluation of material on the subject of psychological and social adjustments in a shelter. Large numbers of persons can be accommodated in one structure by dividing the number of people into small groups whereby the circulating of people and material may be minimized.

The shelter is composed of seven groups of approximately 600 people. The sleeping and living accommodations surround a nucleus composed of the kitchen and bathrooms. Each group is independent from other groups. The only cross-traffic necessary is to reach the medical facilities, central library, supply distribution centers, and work areas. The management of the shelter is simplified by a system of individual group management monitored by the shelter's central control.

The shelter was designed for dynamic behavior using an ultimate strength theory and theoretical blast loadings consistent with a peak incident shock of 60 psi of a megaton range weapon.

A rigid reinforced concrete cell arrangement has also been conceived during the study period. It is presented in figure 3-13. Only the structural detail is shown. The concept has not been developed sufficiently to show further detail. It does, however, present a reasonable alternate approach to the risk-oriented sheltering philosophy.

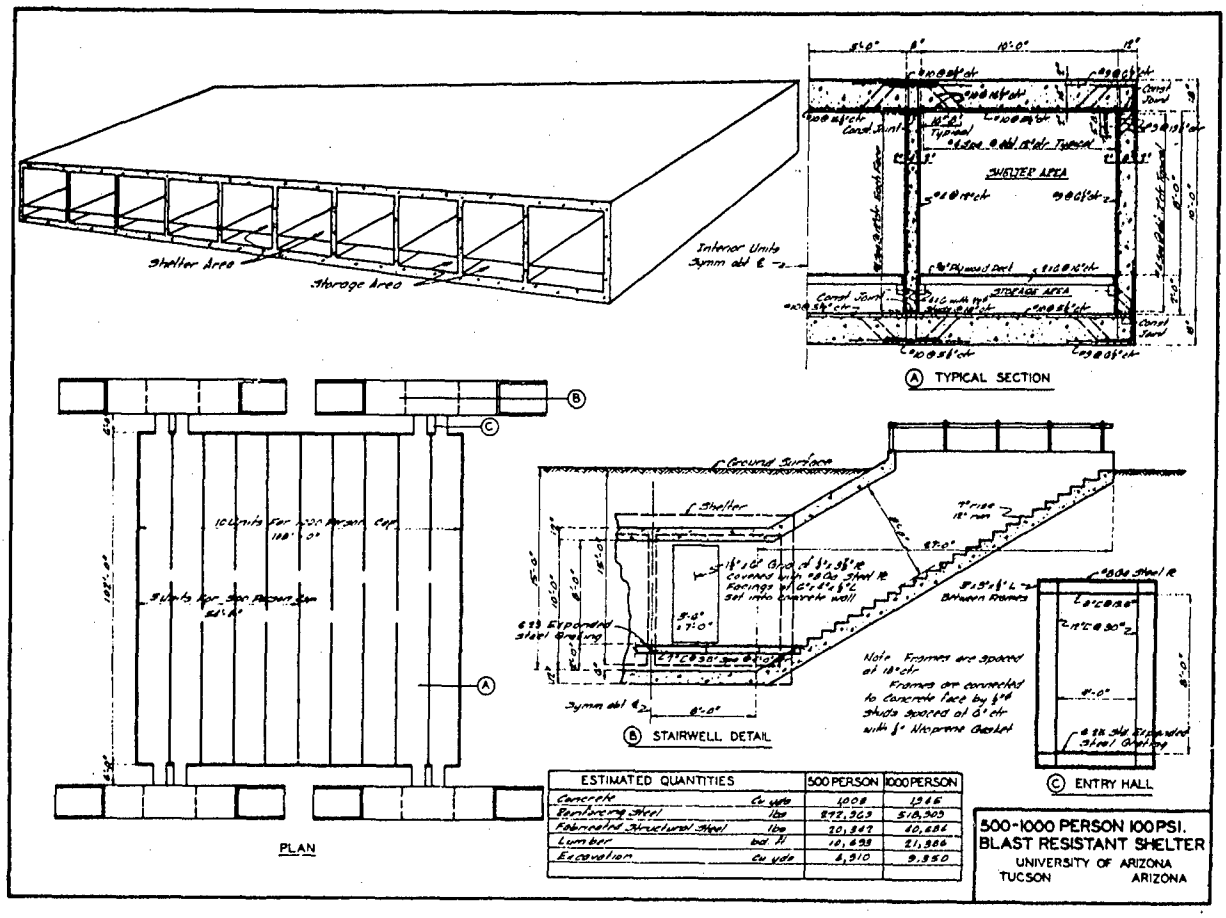

Figure 3-13. Reinforced Concrete, Community Shelter

3. Tucson Concept - Movable

Systems classified as movable are mainly categories of evacuation of people and things to less vulnerable locations. This methodology involves planning and scheduling transportation modes (and routing) as well as determining adequacy of destinations, or necessary improvments. In general, evacuation may be classified as pre-attack, trans-attack, or post-attack. In this immediate context, only the first two are considered as providing a nuclear effects counterforce system. Protected post-attack evacuation is included later as part of the mixed system.

Planning pre-attack evacuation would begin by considering whether or not specifically assigned destinations are possible or desirable. The plan should reflect this decision and go on to provide training in recognition of the procedures, and alternates, which individual persons or groups must follow to execute the plan. The plan should be regularly exercised to assure improvement of the plan and familiarity in the evacuee group. In the local case, lack of adequate destinations would probably preclude pre-attack evacuation even assuming adequate alerting time.

Plans for trans-attack evacuation are subject to all the constraints for pre-attack evacuation methodology, plus the requirement to determine whether evacuation will be protected or unprotected. This decision probably will depend largely on adequacy of warning times and,to a considerable extent, on vulnerability of egress routes or modes of transportation. In the local case, trans-attack evacuation would provide solutions for only a fortunate few who were particularly well equipped for, and adapted to, primitive survival. Most available evacuation routes and methods for Tucson would be denied evacuees by the fact that local military targets lie in close proximity along all existing highways and railways.

4. Tucson Concept - Mixed

a. General

A system which takes advantage of the best features of all methodologies is likely to provide the greatest effectiveness and, if it does not increase the cost factor materially in the process, will present the most desirable cost-effectiveness ratio. In the local case, such a system is both more effective and costs less, per shelter space, than any other adequate counterforce methodology. Protection factors are as good as, or better than, those given previously and costs are materially lower than those for usual community or family shelter systems.

The system consists mainly of a network of steel conduits buried under five feet of earth. Two sizes of conduit are recommended, 44.8 miles of 16'-7" pipe arch (Main Conduit), and 204 miles of 8' pipe as Secondary Conduit. (See figure 3-14.) The Main Conduit will permit limited vehicular traffic. Entrances would lead to extension conduits running at right angles from main artery conduits to schools, public buildings, and other locations as necessary to provide efficient access for present and predicted density of population. A means of protected egress, from the points which are hardest hit, is provided. The termination point of this egress should be located in such a way that water and supplies would be readily available. The region which, in our opinion, offers the most advantages as an immediate survival area is shown in figure 3-14, as the Survival Area. A plan view of a system of conduits which could provide the necessary underground passageways to this survival area is also shown. The conduits themselves would be the initial blast and early fallout shelters. Long-term fallout protection would be accomplished in the protected region. Decontamination capabilities would be an integral part of the fallout protection that is supplied in this region. In addition, decontaminated emergency landing fields and open living areas could be created here.

Conceptual isometric views of major system components are shown in figure 3-15. Much of the data and analysis presented as part of the previous systems (which pertains to flexible structures such as steel conduits, sloping entrances, pre-fabricated sections, and steel membrane roofs) will directly apply to aspects of this system.

b. System advantages

In terms of the mandatory design constraints, the buried conduit system offers a desirable solution. A most desirable feature is inherent in the distribution of population in-shelter. No new concentration of people is created so that the possibility of stray missiles, or deliberate targeting, will not readily create large numbers of casualties; this fact will more likely assure survivors in proportion to existing population. The

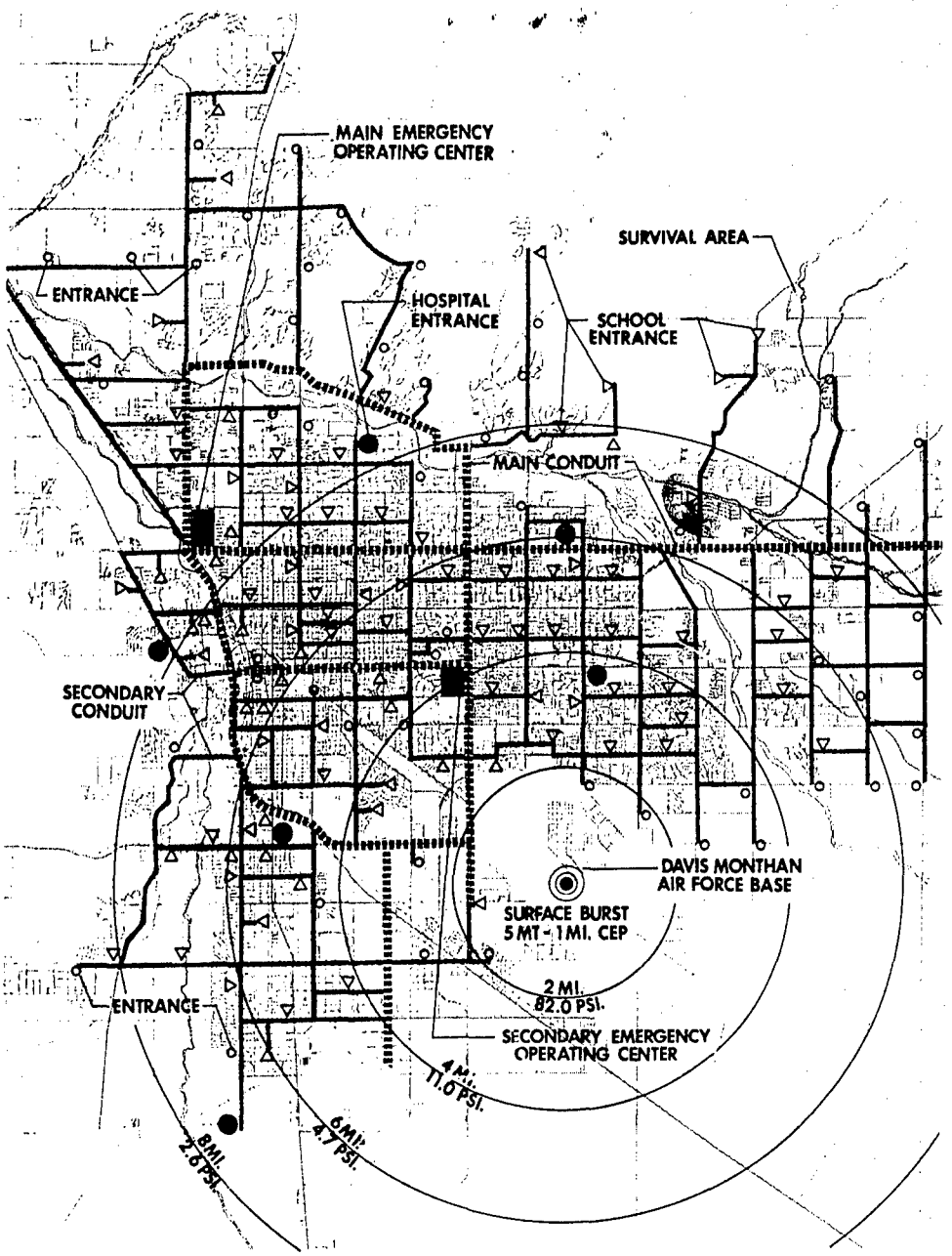

Figure 3-14. Plan View of Buried Conduit System for Tucson, Arizona

buried steel conduit, as a structure, has been subjected to extensive testing and use so that is has become a familiar medium for use against vertical overpressure. Ground motions in other directions will not rupture or separate the sections of steel conduits as readily as might be the case with more rigid structures; they will tend to stretch or compress to conform to stress and strain patterns, without breaking.

The protection offered against thermal and radiological hazards demonstrates a particularly desirable aspect of this system. Protection against the thermal and initial radiation pulses are in a one-million plus attenuation range which is adequate for even some of the most intense situations. However, intense fallout radiation effects demonstrate the system most favorably. Aside from the desirable attenuation factor, which remains important, this system permits coordinated monitoring and decontamination operations. Recovery operations will, therefore, be more meaningful because the whole community can operate as they

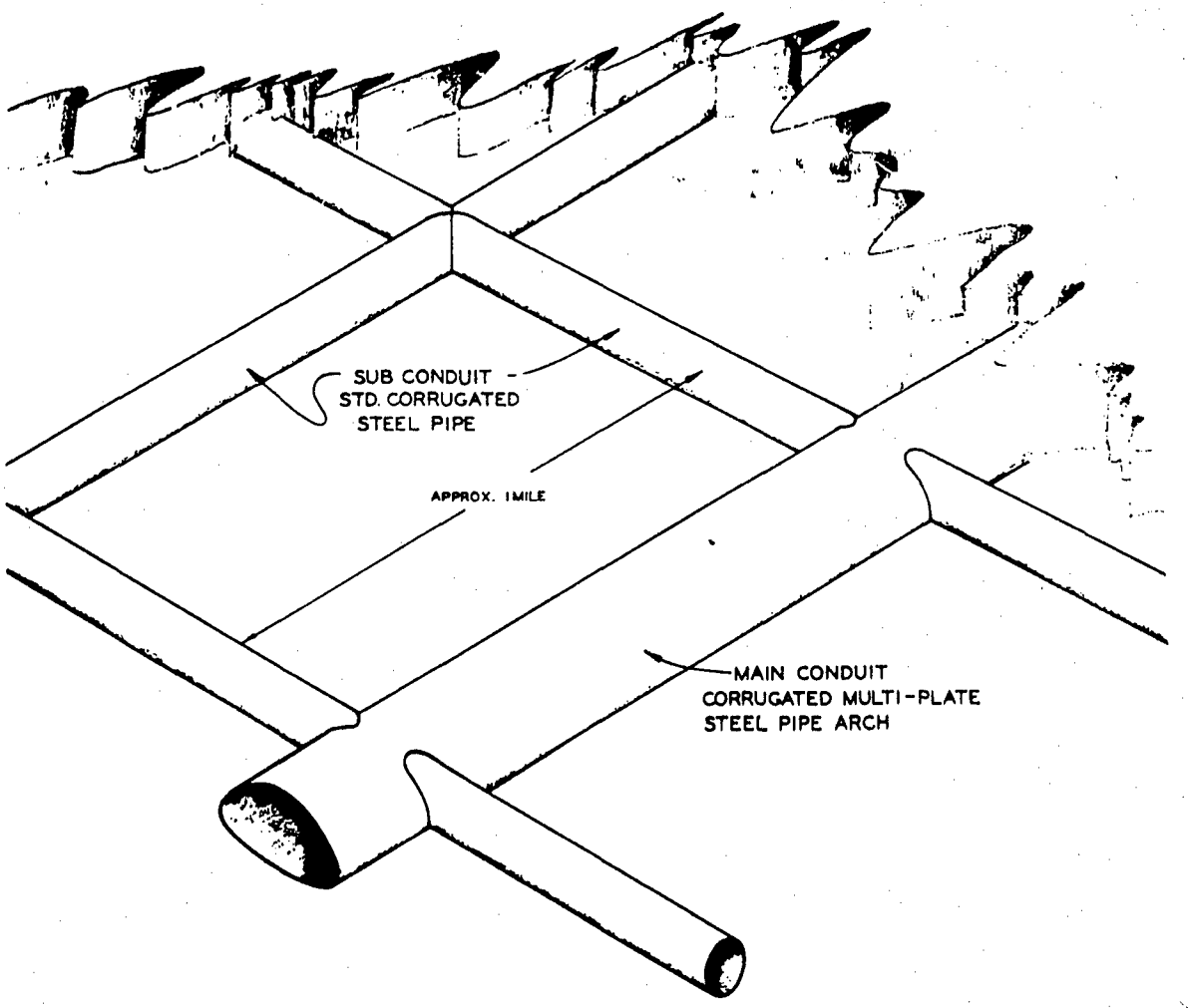

SCHEMATIC OF CONDUIT SYSTEM

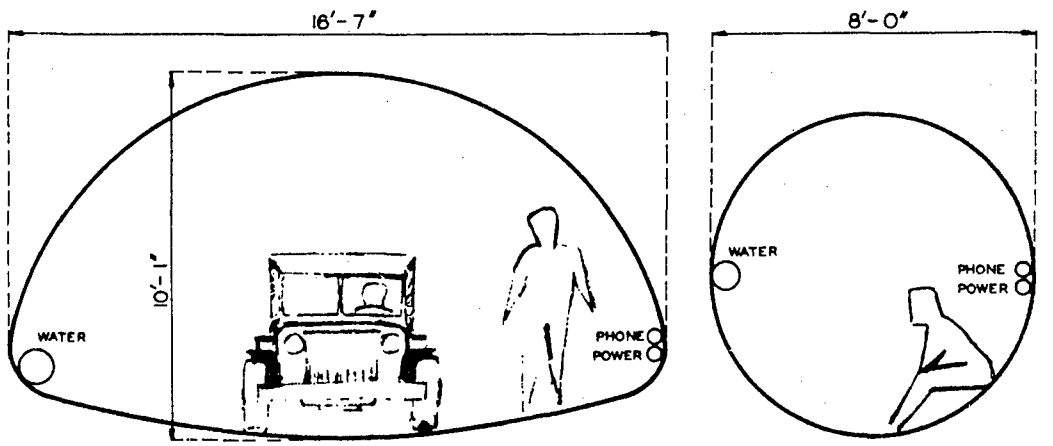

SECTION - MAIN CONDUIT

SECTION - SUB CONDUIT

Figure 3-15. Conceptual Views of Buried Conduit System

are most accustomed to acting; and with their chosen leadership instead of as isolated small groups. If local post-attack fallout radiation intensity indicates protracted periods of lethal radiation, the system makes it possible to carry out post-attack evacuation of the entire population through a single cleared escape route.

Many additional advantages are inherent in this system which are not likely for other systems. Most of the psychological objections to other buried systems are overcome by the fact that family groups, who were separated at warning time, can shortly be reunited. In-shelter administrative and control problems are diminished by the fact that existing authority figures can be in direct contact. Location of entrances at schools, hospitals, and other commercial or governmental centers tends to serve as the most efficient method by which the largest part of the population can enter the shelter in the shortest time. For business-day population distribution, this configuration is ideal; it also provides familiar, consistent entrance location patterns for other population distributions (holiday, weekend, etc.). Usually schools and hospital entrances will be near the center of night-population density, which is about the same distribution as that for weekends, holidays, and early evenings.

The system offers the additional value of providing shelter readily in terms of elapsed time after decision to construct. The conduits could be constructed in states which would permit useful shelter, on a crash basis, quite readily. As an instance, the main conduits conduits could be constructed first in order to serve the greater number of persons in the least amount of time. Next, the secondary conduits could be connected, in the most populous areas. At the same time, construction could progress on entrances and operating centers. Each phase of construction would be useful as basic shelter almost immediately as it would simply require excavation, emplacement of the conduit, backfill, and ventilation tubes. Details and refinement of construction would improve the system, but basic shelter can be available most readily since form-building, concrete-curing times, and complex foundations are not necessary in most of the construction phases.

The system also allows relatively inexpensive expansion into newly developed areas. The additional cost should be proportional to that ratio which the number of new persons to be served, bears to the total population; or even slightly less. Largely it will be a matter of adding enough conduit to reach into the area in point.

e. Shared-use advantages

The buried conduit system is ideally adaptable to multipurpose planning. Utility systems such as water, electricity, and telephone could install trucklines throughout the shelter system. In addition, inlets, outlets, and protection for mechanical equipment could be provided which would allow use as efficient storm drains. The most obvious purpose for shared-use techniques is to reduce the purely shelter costs; however, the benefit realized by the utility systems (and the community generally) would be substantial. Installation and maintenance accessability would be considerably improved, in the case of utility systems; they would also, of course, be less vulnerable to damage by nuclear weapons effects. The storm drains could represent the first stage of any overall storm damage or water conservation and control system.

In general, any shelter system will be more useful at the ultimate moment if it has not been completely idle during the interim period. Long-range prospective developments may well include high-speed underground transportation systems for distribution of goods and even commuter traffic.

C. Cost Effectiveness Evaluation

1. Cost Alternatives

For purposes of this evaluation, possible installation costs for various types of shelter systems are generated. The costs involved are those which pertain to the installation costs of each of the fixed shelter types and also to the mixed concept. No attempt has been made to approximate the costs of the movable systems.

2. Fixed Individual Shelters

a. Culvert-type shelter

Construction cost estimates for this type of shelter are developed as follows:

COST ESTIMATE - CULVERT TYPE SHELTER

STRUCTURAL ESTIMATE	Quantity	Unit	Unit Cost	Total Cost
EXCAVATION				
Excavation Backfill or removal from site	275	cu.yds.	2.25	$ 618.75
CONCRETE				
No forming				
Material (Concrete)	3.9	cu.yds.	14.00	54.60
Placement (Labor)	3.9	cu.yds.	5.00	19.50
REINFORCING STEEL Material and Labor	148	lbs.	0.25	37.00
FABRICATED STRUCTURAL STEEL Material and Labor	5,675	lbs.	1.00	5,625.00
CORRUGATED METAL PIPE	+10% Freight			
8' -#8 Ga. Multi-Plate	24	lin.ft.	52.26	1,254.24
4' -#14 Ga. Std.	15.5	lin.ft.	10.45	161.98
3' -#14 Ga. Std.	15.5	lin.ft.	7.69	119.20
2' -#14 Ga. Std.	12	lin.ft.	4.61	55.32
TIMBER 3/4" Plywood	108	sq.ft.	0.38	41.04
SEALER COAT Labor and Material	898	sq.ft.	0.20	179.60
TOTAL STRUCTURAL COST				8,166.23
MECHANICAL				2,500.00
SUPPLIES				1,150.00
TOTAL ESTIMATED COST				$ 11,816.23

The total of $11,816.23 compares with an independent contractors' estimate of $18,000. The figures above represent those which are most consistent with costs associated with mass production techniques. It is entirely possible that the estimate of $18,000 could be reduced, in this light by approximately 1/3, to the more realistic value, for this situation.

The total cost of a shelter system for Tucson which is composed exclusively of this type of shelter is estimated by considering the existing homes per person ratio and multiplying by the population, and then again by the cost per shelter value, as follows:

(Homes per person) x (Total persons) x (cost per home shelter) = Total Cost

(.321) (465,000) (11,816.23) = (149,500) (12,000) = $1,766,526,385

for 1973 population.

b. Flat-plate roof type shelter

Construction cost estimates for this type of shelter are developed as follows:

COST ESTIMATE - CIRCULAR FLAT PLATE TYPE SHELTER

STRUCTURAL ESTIMATE	Quantity	Unit	Unit Cost	Total Cost
EXCAVATION	366	cu.yds.	2.25	$ 923.50
CONCRETE				
Forming (Material and Labor)				
Walls	1565	sq.ft.	0.40	626.00
Overhead	201	sq.ft.	0.75	150.75
Material (Concrete)	38.9	cu.yds.	14.00	544.60
Placement (Labor)	38.9	cu.yds.	3.00	116.70
REINFORCING STEEL				
Material and Labor	7494	lbs.	0.25	1,872.50
FABRICATED STRUCTURAL STEEL				
Material and Labor	1574	lbs.	1.00	1,574.00
SEALER COAT				
Material and Labor	1000	sq.ft.	0.20	200.00
STRUCTURAL COST				6,008.05
MECHANICAL				
VENTILATION				
POWER				
SANITARY				2,500.00
SUPPLIES				
HOTEL PACKAGE				
MEDICAL PACKAGE				1,150.00
TOTAL ESTIMATED COST				$ 9,658.05

The total of $9,685.05 results in an overall system cost of 149,500 x $9,685.05 = $1,443,878,475 for Tucson.

d. Domed-roof type home shelter

Construction cost estimates for this type of shelter are developed as follows:

COST ESTIMATE - DOME TYPE SHELTER

STRUCTURAL ESTIMATE	Quantity	Unit	Unit Cost	Total Cost
EXCAVATION	365	cu.yds.	2.25	$ 921.25
CONCRETE				
Forming (Material and Labor)				
Walls	1273	sq.ft.	0.40	509.21
Overhead	438	sq.ft.	1.00	438.00
Material (Concrete)	28.5	cu.yds.	14.00	399.00
Placement (Labor)	28.5	cu.yds.	3.00	85.50
REINFORCING STEEL Material and Labor	4487	lbs.	0.25	1,123.50
FABRICATED STRUCTURAL STEEL Material and Labor	1550	lbs.	1.00	1,550.00
SEALER COAT Material and Labor	1074	sq.ft.	0.20	214.80
STRUCTURAL COST				5,241.26
MECHANICAL				
VENTILATION				
POWER				2,500.00
SANITARY				
SUPPLIES				
HOTEL PACKAGE				1,150.00
MEDICAL PACKAGE				
TOTAL ESTIMATED COST				$ 8,891.26

The total of $8,891.26 results in an overall system cost of 149,500 x $8,891.26 = $1,329,243,370 for Tucson.

e. Concrete box type shelter

Construction cost estimates for this type of shelter (for 30 psi) are developed as follows:

COST ESTIMATE - BOX TYPE SHELTER

STRUCTURAL ESTIMATE	Quantity	Unit	Unit Cost	Total Cost
EXCAVATION	260	cu.yds.	2.25	$ 585.00
CONCRETE				
Forming (Material and Labor)				
Walls	1265	sq.ft.	0.40	506.00
Overhead	137	sq.ft.	0.75	102.75
Material (Concrete)	24.4	cu.yds.	14.00	341.60
Placement (Labor)	24.4	cu.yds.	3.00	73.20
REINFORCING STEEL				
Material and Labor	3691	lbs.	0.25	922.50
FABRICATED STRUCTURAL STEEL				
Material and Labor	771	lbs.	1.00	771.00
SEALER COAT				
Material and Labor	770	sq.ft.	0.20	154.00
STRUCTURAL COST				3,456.05
MECHANICAL				
VENTILATION				
POWER				
SANITARY				1,800.00
SUPPLIES				
HOTEL PACKAGE				
MEDICAL PACKAGE				882.00
TOTAL ESTIMATED COST				$ 6,138.05

The total cost of $6,138.05 results in an overall system cost of 149,500 x $6,138.05 = $917,638,475 for Tucson.

3. Fixed Community Shelter Systems

a. Flexible type (4,500 person capacity)

Construction cost estimates for this type of shelter are developed as follows:

COST ESTIMATE - FLEXIBLE COMMUNITY SHELTER

STRUCTURAL ESTIMATE	Quantity	Unit	Unit Cost	Total Cost
EXCAVATION				
Excavation	64,870	cu.yds.	1.94	$ 106,330.00
Fill under slabs	700	cu.yds.	2.00	1,400.00
CONCRETE				
Forming (Material and Labor) Walls	184,971	sq.ft.	0.38	70,270.00
Material (Concrete)	9,149	cu.yds.	12.25	112,056.00
Placement (Labor)	9,149	cu.yds.	1.32	12,083.00
Slabs (Material and Finish)	60,842	sq.ft.	0.50	30,421.00
Gunite (Material and Labor)	42	cu.yds.	55.00	2,310.00
REINFORCING STEEL Material and Labor	1,319,787	lbs.	0.25	329,947.00
FABRICATED STRUCTURAL STEEL Material and Labor	1,038,277	lbs.	0.10	103,828.00
MISCELLANEOUS				
Plumbing, Pipes, Well casings, Doors, etc.				74,250.00
SEALER COAT Material and Labor	71,300	sq.ft.	0.10	7,130.00
STRUCTURAL COST				849,848.00
MECHANICAL				
VENTILATION AND HEATING				183,897.00
POWER PACKAGE				75,474.00
CONTROL PACKAGE				18,000.00
SUPPLIES				
MEDICAL PACKAGE				11,900.00
HOTEL PACKAGE				288,000.00
TOTAL ESTIMATED COST PER UNIT				$ 288,000.00

The total of $1,427,119 multiplied by 113.83, the number of units required for Tucson population, yields $162,448,956 as the total system price.

b. Rigid type (1,000 person capacity)

A rigid concrete cell arrangement designed for 1,000 persons. Construction costs are developed as follows:

COST ESTIMATE - 1000 PERSON - 100 PSI SHELTER

STRUCTURAL ESTIMATE	Quantity	Unit	Unit Cost	Total Cost
EXCAVATION				
Excavation Backfill or removal from site	7,730	cu.yds.	1.85	$ 14,300.50
CONCRETE				
Forming (Material and Labor)				
Top Slab	10,000	sq.ft.	0.50	5,000.00
Walls	27,798	sq.ft.	0.38	10,563.24
Material (Concrete)	1,636	cu.yds.	12.25	20,041.00
Placement (Labor)	1,636	cu.yds.	1.35	2,045.00
REINFORCING STEEL (Material and Labor)	426,509	lbs.	0.11	46,915.99
TIMBER				
2x6 and 4x6	13,885	bd.ft.	0.30	4,165.50
3/4" Plywood	10,000	sq.ft.	0.38	3,800.00
SEALER COAT (Material and Labor)	16,860	sq.ft.	0.10	1,686.00
ENTRY 100 psi - Double Entry (p.48)	4	Each	10,697.22	42,788.88
TOTAL ESTIMATED COST				$ 151,306.11

The total of $151,306.11 as the total system structural cost exclusive of mechanical and service costs which are estimated at $129,032.25 for each shelter. Total shelter cost per unit therefore becomes $280,338.36. When multiplied by 465 (number of shelter units necessary for Tucson), total system cost becomes $130,357,340.

4. Multi-Purpose Buried Conduit System

Construction cost estimates for this system are developed as follows:

COST ESTIMATE - BURIED CONDUIT SYSTEM

CONDUIT	Quantity	Unit	Unit Cost	Total Cost
EXCAVATION (Includes replacement of paving)				
8' Diameter Pipe	6,695,473	cu.yds.	3.00	$ 20,086,419.00
16' -7" Span Pipe Arch	2,814,874	cu.yds.	3.00	8,444,622.00
CORRUGATED PIPE (30% reduction due to volume)				
8' Diameter #8 Ga. Std. Pipe	1,078,176	ft.	32.61	35,159,319.00
16' -7" Span - #5 Ga. Pipe Arch	236,544	ft.	68.63	16,233,015.00
MECHANICAL				
Ventilation and Sanitary	1,078,176	ft.	17.64	19,019,025.00
SUPPLIES				
Hotel and Medical Package	465,000	Persons	47.00	21,855,000.00
ENTRANCES				
HOSPITAL ENTRY	4	Units	21,394.00	85,576.00
SCHOOL ENTRY	79	Units	20,136.00	1,590,744.00
INDEPENDENT ENTRY	54	Units	10,068.00	543,672.00
MAIN OPERATION CENTER				
COMMUNICATION SYSTEM TRANSPORTATION SYSTEM MAIN POWER SYSTEM	1	Unit	750,000.00	750,000.00
SECONDARY OPERATION CENTER	1	Unit	400,000.00	400,000.00
TOTAL ESTIMATED SYSTEM COST				$ 124,167,392.00

The total cost $124,167,392 represents total system cost, including mechanical and service costs. The multi-purpose uses which may be realized, will tend to reduce the purely shelter system costs.

5. Cost-Effectiveness Analysis

Cost-effectiveness ratio evaluations are somewhat nebulous in nature because of the problems of defining a suitable parameter or parameters which may be associated with these evaluations. One possible parameter which might be used for this purpose is the cost-effectiveness ratio. The cost-effectiveness ratio may be defined as that quantity which results when the total cost of a system is divided by a number which represents the total effectiveness of the system. The shelter system which has the lowest cost-effectiveness ratio associated with it is then among the most desirable.

Unfortunately, the true cost-effectiveness ratio for any given system is difficult to isolate. This ratio may be minimized, however, even though it is not isolated. The cost-effectiveness ratio may be considered to be a function of individual ratios, each pertaining to different phases of cost for certain types of effectiveness. That is:

$$\frac{C}{E} = F\left(\frac{C}{E_{po}}, \frac{C}{E_\gamma}, \frac{C}{E_t}, \frac{C}{E_{ne}}, \frac{C}{E_l} \cdots \frac{C}{E_i}\right)$$

where:

$\frac{C}{E}$ = Total cost-effectiveness ratio

$\frac{C}{E_{po}}$ = Cost-effectiveness ratio of system against overpressure

$\frac{C}{E_\gamma}$ = Cost-effectiveness ratio of system against gamma radiation

$\frac{C}{E_t}$ = Cost-effectiveness ratio of system against thermal radiation

$\frac{C}{E_{ne}}$ = Cost-effectiveness ratio of system against initial radiation

$\frac{C}{E_l}$ = Cost-effectiveness ratio of system with respect to location

$\frac{C}{E_i}$ = Cost-effectiveness ratio of system with respect to the i^{th} condition

The function "F" is undoubtedly quite complex and may even be mathematically undefinable. However, by rational deductions, it is possible to be slightly more specific about the true nature of this function. It is known that any increase in cost of any component of the system with effectiveness constant will increase the cost of the whole, and hence the cost-effectiveness ratio of the system. It is also known that any increase in effectiveness of a component of the system which might be obtained at little or no increase in cost will tend to increase the total effectiveness and hence reduce the cost-effectiveness ratio of the system.

From these observations, it is then possible to say that:

$$F\left(\frac{C}{E_{po}}, \frac{C}{E_\gamma}, \frac{C}{E_t}, \frac{C}{E_{ne}}, \frac{C}{E_l} \cdots \frac{C}{E_l}\right) =$$

$$F\left(\left|\frac{C}{E_{po}}\right|^{C_1}, \left|\frac{C}{E_\gamma}\right|^{C_2}, \left|\frac{C}{E_t}\right|^{C_3}, \left|\frac{C}{E_{ne}}\right|^{C_4}, \left|\frac{C}{E_l}\right|^{C_5} \cdots \left|\frac{C}{E_i}\right|^{C_i}\right)$$

where $C_1, C_2, C_3, C_4, C_5 \ldots C_i$ are all positive.

A sufficient condition for F to be a minimum, and hence $\frac{C}{E}$ for the total system, is that each $\frac{C}{E_i}$ ratio be a minimum. Unfortunately, because of the interdependency of the various $\frac{C}{E}$ ratios, it is not possible to show that this condition is both necessary and sufficient.

As an example of the determination of the cost-effectiveness ratio for a given component of the system, consider the ratio $\frac{C}{E_{po}}$. It is recalled that this ratio represents the cost of resisting overpressure divided by a number E_{po} which represents the total effectiveness of this resistance. It is observed that:

$$\frac{C}{E_{po}} = F_{po}\left(\frac{C}{E_{st}}, \frac{C}{E_{bv}}, \frac{C}{E_{dc}} \ldots \frac{C}{E_h}\right)$$

where:

$\frac{C}{E_{st}}$ = Structural cost-effectiveness ratio to resist overpressure

$\frac{C}{E_{bv}}$ = Blast value cost-effectiveness ratio to resist overpressure

$\frac{C}{E_{dc}}$ = Door closure cost-effectiveness ratio to resist overpressure

$\frac{C}{E_h}$ = H^{th} type cost-effectiveness ratio to resist overpressure

As before with the function "F", the function F_{po} is difficult to determine. The same deductions apply, however, that is:

$$F_{po}\left(\frac{C}{E_{st}}, \frac{C}{E_{bv}}, \frac{C}{E_{dc}} \ldots \frac{C}{E_h}\right) = F_{po}\left(\left|\frac{C}{E_{st}}\right|^{d_1}, \left|\frac{C}{E_{bv}}\right|^{d_2}, \left|\frac{C}{E_{dc}}\right|^{d_3} \ldots \left|\frac{C}{E_h}\right|^{d_h}\right)$$

where: $d_1 . d_2 . d_3 \ldots d_h$ are all positive.

Because of the nature of the variables involved in this function, it is deduced that they are each independent. That is $\frac{C}{E_{st}}$ is independent of $\frac{C}{E_{bv}}$ and $\frac{C}{E_{dc}}$ and $\frac{C}{E_h}$. It may then be said that:

$$\frac{C}{E_{po}} = \sum_{k=1}^{h} A_k \left|\frac{C_k}{E_k}\right|^{d_k}$$

where: k_1 = st
k_2 = bv
k_3 = dc
.
.
.
k_h = h

To minimize $\frac{C}{E_{po}}$ it is now both necessary and sufficient that each term of the equation be minimized. As an example of the way in which $A_k \left|\frac{C_k}{E_k}\right|^{dk}$, where k = 1 may be minimized, consider the following:

$$A_k \left|\frac{C_k}{E_k}\right|^{d_k} = A_{st} \left|\frac{C_{st}}{E_{st}}\right|^{d_{st}} \qquad k = 1$$

Observation indicates that this quantity will be a minimum for that type of structure for which $\frac{C_{st}}{E_{st}}$ is a direct function of $\frac{C}{E_{ep}}$ and $\frac{C}{E_{gm}}$ where:

$\frac{C}{E_{ep}}$ Cost-effectiveness ratio of a structure for resisting an effective pressure

$\frac{C}{E_{gm}}$ Cost-effectiveness ratio of a structure for resisting ground motion

To minimize $\frac{C}{E_{ep}}$, consider the case of a buried structure subjected to an effective soil-structure interaction pressure of P_o. One may choose from a wide variety of structural forms ranging from rigid to flexible. The table below shows potential cost versus overpressure curves for 4 different basic types of structural systems. Curves can be drawn to represent the relative merits of the structural systems as overpressure versus relative cost and overpressure versus cost-effectiveness. The cost-effectiveness ratio for each point on each curve is defined as being the level of cost divided by the level of overpressure for that point. In other words, it is the ordinate divided by the abcissa. Graphically, it is the slope of a line drawn from the origin to the specific point on the curve in question. (See figures 3-16 and 3-17.)

The table lists the magnitude of cost-effectiveness ratios for various overpressures. These ratios are obtained by taking the various ordinates and dividing by the respective abcissas.

$\frac{C}{E_p}$ ($/sq. ft of shelter)

OVERPRESSURE	CONCRETE BOX	CONCRETE CULVERT	MEMBRANE ROOF-TYPE	STEEL CULVERT
10	0.838	0.318	0.536	0.845
20	0.546	0.243	0.342	0.429
30	0.430	0.145	0.242	0.290
40	0.370	0.1128	0.183	0.221
50	0.327	0.0955	0.161	0.179
60	0.299	0.0834	0.1353	0.152
70	0.278	0.0767	0.1202	0.131
80	0.263	0.0721	0.1060	0.1190
90	0.251	0.0685	0.0950	0.1032
100	0.2425	0.0650	0.0876	0.0947

It is now possible to evaluate the relative effectiveness of a given structural type with respect to a given overpressure. Those types which yield minimums should be used as components of feasible shelter systems.

Cost-effectiveness ratios $\frac{C}{E_{gm}}$ are less determinable because of lack of sufficient research studies on the effects of ground motions on buried structures. Intuitively, however, it may be observed that flexible structures will survive with greater effectiveness and for less cost.

The procedures and methodologies for minimizing the cost-effectiveness ratio are now defined. It must be observed that those shelter systems which have low cost-effectiveness ratios are only members of a set of such systems. That is, within the domain of all shelter systems, there exists a set of systems, S, which have associated with them a minimum cost-effectiveness ratio. The most feasible of this set is that system for which the absolute cost is a minimum. Until such time as sufficient research data supports the methodical calculation and verification of such as absolute minimum it is necessary to rely heavily on the abilities of specialists, to make judgement decisions as to the attainment of this condition. Such decisions were made in the selection of feasible shelter systems for Tucson.

The important fact involved in the preceding discussion is that a shelter system cannot be considered absolutely feasible unless the cost-effectiveness ratios of each of its components is minimized either independently or collectively. In short, low-cost maximum effectiveness components must be used.

As an interesting sidelight to the cost-effectiveness ratio concept, consider the value of this ratio if any one of the ratios which serve to define it should be associated with a failure. That is, if the structure fails under effective overpressure, then $\frac{C}{E_{ep}} \longrightarrow \infty$ because $E_{ep} \longrightarrow 0$. It then follows, because of the nature of the functional relationship, "F", that $\frac{C}{E}$ for the system $\longrightarrow \infty$. This, of course, is anything but a minimum.

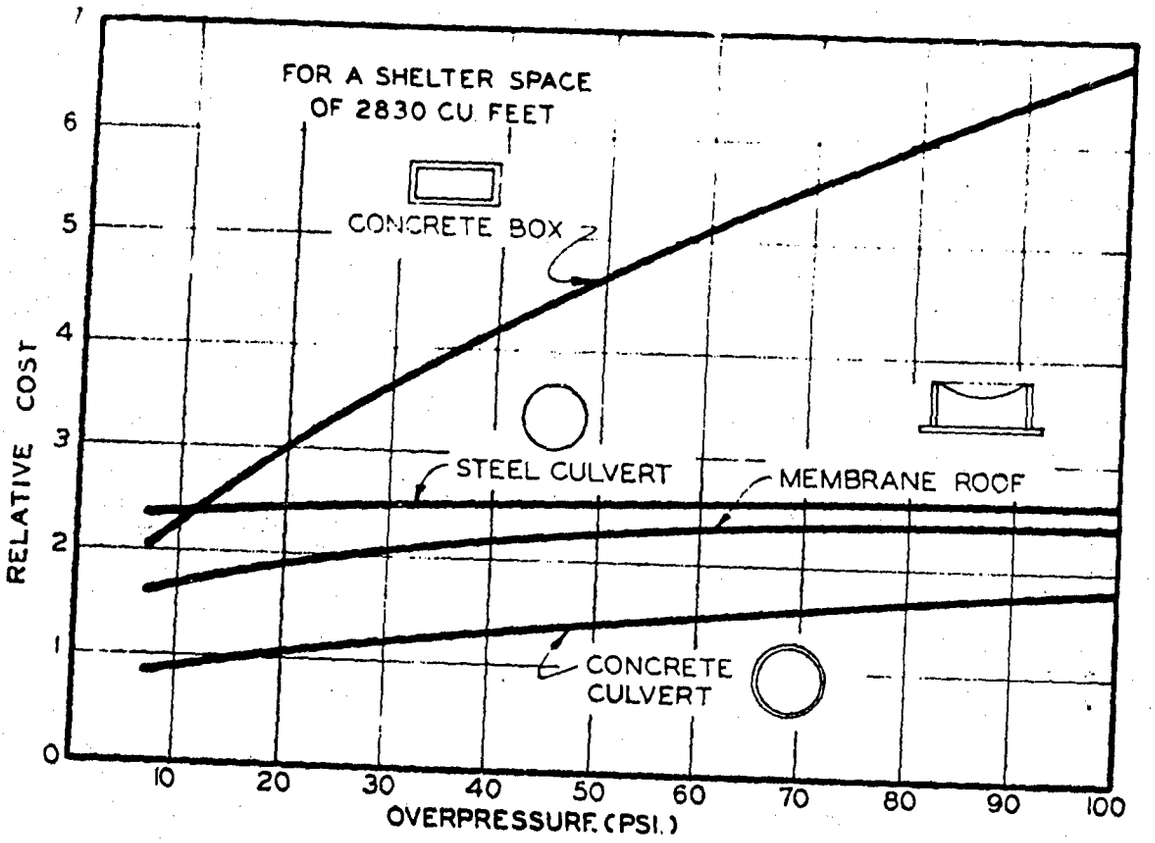

Figure 3-16. Relative Cost vs Overpressure

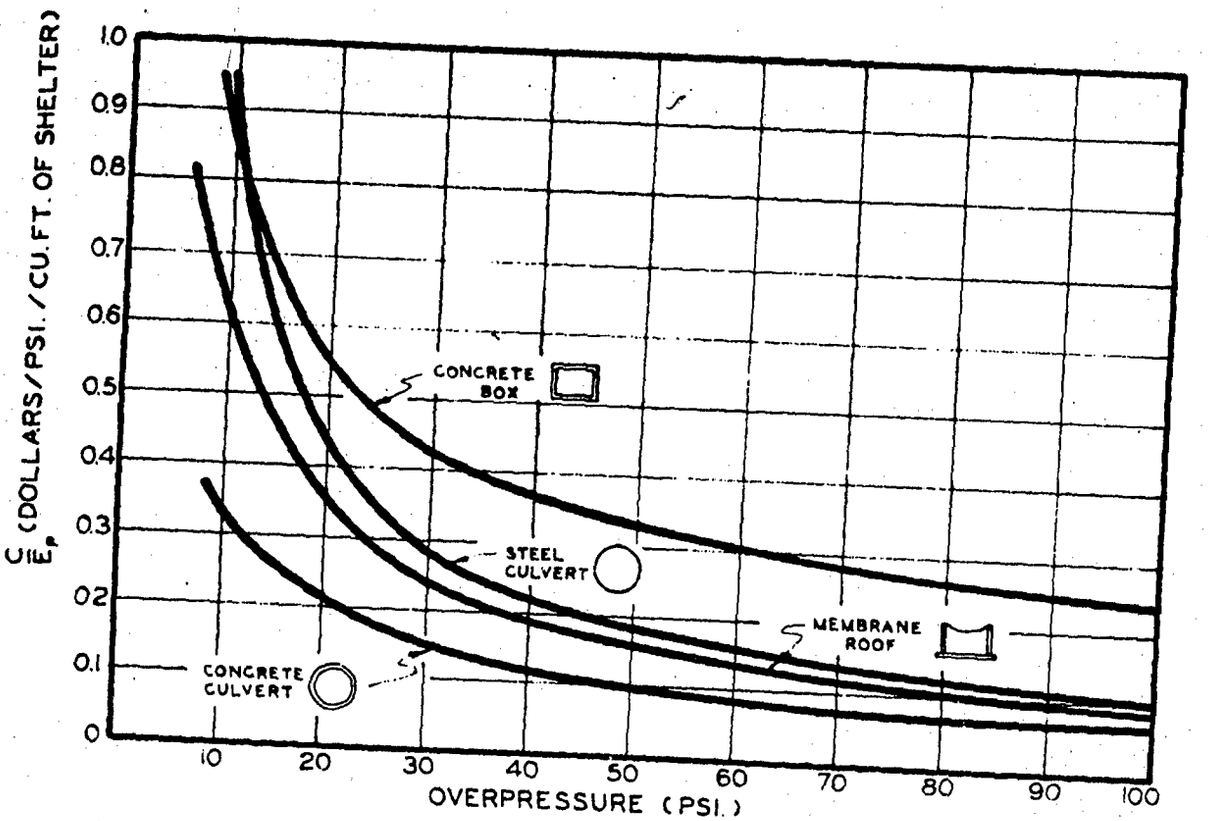

Figure 3-17. Cost Effectiveness vs Overpressure

6. Summary

a. Systems Comparison

The preceding material has presented the cost of various shelter systems and a method by which cost-effectiveness can be determined. Each system or concept has special merit depending upon the prospective hostile conditions. One aspect of cost-effectiveness should be considered with respect to any system. That is, what is the cost per survivor? If all other factors are in equilibrium, then cost per survivor will determine which is the most desirable system.

The following table presents the total cost and cost-per-survivor for each type of shelter system subjected to detailed consideration in the course of study.

SHELTER TYPE	Unit Cost	Total Units (1973 Pop.)	Total Cost	Cost Per Person
CULVERT (individual)	11,816.23	149,500	1,766,526,385	$ 3,820.48
FLAT PLATE ROOF	9,658.05	149,500	1,443,878,475	3,105.11
DOMED ROOF	8,891.26	149,500	1,329,243,370	2,858.58
DISHED ROOF	10,902.60	149,500	1,629,938,700	3,505.24
CONCRETE BOX (30 psi)	6,138.05	149,500	917,638,475	1,973.41
RIGID COMMUNITY	280,338.36	465	130,357,340	280.33
FLEXIBLE COMMUNITY	1,427,119.00	113,83	162,448,956	349.35
BURIED CONDUIT		1	24,167,372	267.02

b. Multi-Purpose Cost Sharing

For most shelter systems, it is difficult to imagine multi-purpose or shared-use concepts which are workable. Exception, of course, must be made for the many new structures which are being designed with build-in shelter space. However, the buried conduit system presented herein does offer many possibilities for shared-use. Conceivably a major part of the cost could be amortized in this manner. If one considers the value to utility systems and minimum present value of a storm sewer system, material reductions from overall system cost should readily be realized.

SECTION IV. TRAINING REQUIREMENTS

A. Introduction

If we begin by considering a common problem in a single community, the training requirements are largely dictated by the type of shelter systems. The requirement may vary widely from the most extensive requirement represented by total reliance on individual shelters to the minimum which would be required by mass shelter systems.

In an individual shelter program, each shelter must have a person who is trained to use radiation measuring devices and is knowledgeable in at least elemental decontamination methods and procedures. The communication, rescue, first aid, and numerous other survival information areas that would be duplicated for each shelter, make the training problem a quite substantial economic consideration. The training requirement in a mass-shelter system will be greatly reduced by the simple fact that larger groups can be guided and protected, for most of the usual purposes, by a single trained person.

In outline form, the following specific training would be necessary to initiate and retain effectiveness of the buried conduit shelter system. The skills acquired during this training plus other existing skills, for all persons who will use the shelter system, should be placed on punch cards along with the persons shelter space assignment and local mailing address to be used to locate and contract additional specific talent when it is required.

B. For the General Public:

1. Leaflets or Cards

   a. Shelter entrances
   b. General space assignments
   c. Warning method
   d. What authority to obey
   e. Sources of information
   f. Sources of direction

2. Publicity in Public Media

   a. Newspaper articles
   b. Radio and TV programs

C. For Public Officials, Police, and Firemen

1. Familiarization Courses Keyed to Individual Duties

   a. Shelter management
   b. Nuclear effects monitoring
   c. Decontamination methods
   d. Possible alternatives to recovery or evacuation plans

2. Specific Detailed Training Programs

   a. Rescue operations
   b. Internal utility systems
   c. In-shelter communication systems operation
   d. Damage control
   e. Radiation monitoring

D. For Technical Volunteers

1. Familiarization courses updating particular technical skills to nuclear effects criteria
2. Specific detailed training on particular technical operations aspects of the system
3. Specific training for sub-systems periodic maintenance

E. Training for Scientific, Medical, and Legal Advisors

1. Familiarization lectures covering physical configuration
2. Familiarization lectures covering in-shelter and recovery plans
3. Periodic conferences with responsible officials

F. School, Hospital, Church, and Service Club Groups

1. Volunteer manning of community health and welfare functions
2. Monitoring and assistance to children, handicapped, and injured
3. Organize and staff volunteer first aid stations
4. Man kitchens and food distribution points
5. Staff information centers

SECTION V. SUMMARY

A. Introduction

This final report on contract OCD-OS-62-232 represents the findings made in the course of a pilot study which developed procedures and methodologies for evaluating potential local hazards from a nuclear attack. The procedures are applied to the particular hostile environment to determine potential civil defense countermeasures for cities closely associated with military targets. The specific subject of the study was Tucson, Arizona, and environs.

Systems, which have evolved, consider the attitudes and sensibilities of protected man as well as sound scientific and engineering criteria for structures which will shield him from the hazards.

B. Constraints

In order to clearly consider the problem of civil defense in the instant type of setting, it has been postulated in terms of constraints. These constraints are further categorized as technical and non-technical; the technical constraints being those subject to numerical analysis. The remaining constraints are then considered according to the manner in which they will most likely impinge on the system. Nuclear effects, as with all other effects, are more or less hazardous at a specific location depending upon magnitude, proximity, and direction of the source. Therefore, the targeting analysis is presented early in the report.

From the targeting analysis, a set of numerical engineering-loading determinants are derived specifically for the environs of the source. These raw loadings and the results of a probability of reliability analysis, which is also developed from the targeting analysis, are extrapolated to produce reasonably accurate predictions of the types of hostile-environmental hazards which the system must confront.

C. Design Evaluation

Design concepts, evolved to satisfy local constraints, were then subjected to cost-effectiveness analysis as a part of early determination of feasibility. Those systems which provided the necessary protection at the lowest cost were investigated further in terms of the acceptability they would enjoy in the minds of the protected people. The systems which remained feasible are reported in greatest detail.

Multiple-use system concepts are considered most feasible, and a particularly desirable form of this concept is presented as the multiple-use buried conduit system. This form would provide protection for the whole community in one continuous shelter system; and, at the same time, would be of value to the community in numerous other respects. Also, this system would cost substantially less, per person, than the other systems; especially considering the structural strengths required to provide protection against the extreme hazards potentially presented to target cities such as Tucson, Arizona.

D. Training Requirements

In order to fully appreciate the hazards and, therefore, necessary precautions which must be taken; a high percentage of the protected population must be given involved training if more conventional shelter methods are pursued. The report outlines the training necessary to make the recommended system effective from this standpoint. It becomes readily apparent that this training is substantially less than would be necessary, as an instance, if individual shelters comprised the entire system.

Contract OCD-OS-62-232

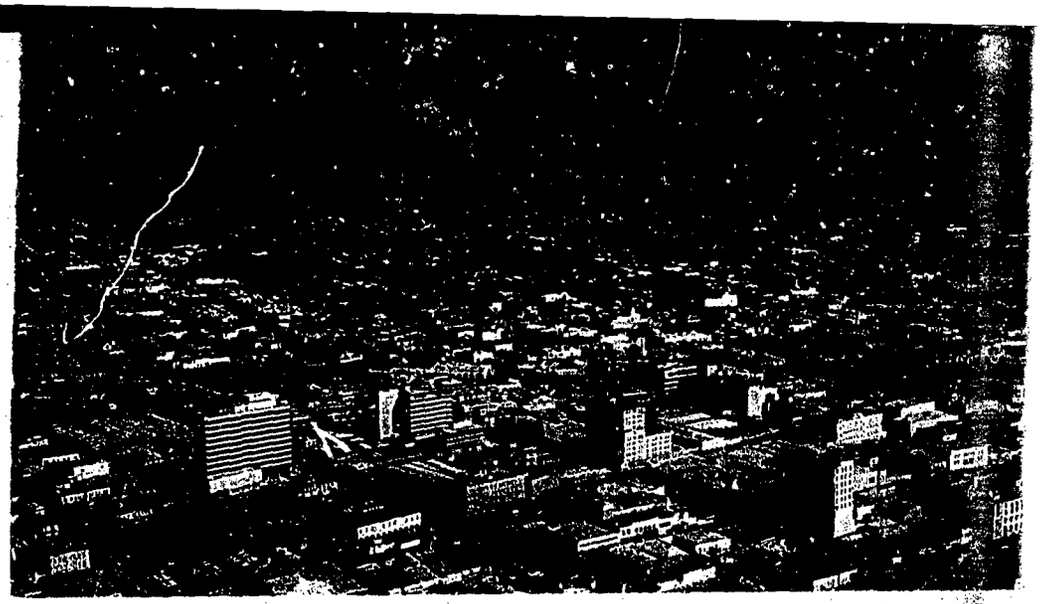

APPENDIX

LOCAL CIVIL DEFENSE SYSTEMS

APPENDIX - PART A
MATHEMATICS OF TARGETING

LIST OF ILLUSTRATIONS

PART A

THE MATHEMATICS OF TARGETING

A. General

This part of the Appendix presents, in detail, the initial effort of the study--the targeting problem, and the resulting civil defense hazards created for cities associated with retaliatory military complexes. It is assumed that the reader is familiar with the general characteristics of nuclear weapons and their effects.

The analysis of the general targeting consideration presented here is an adaptation of work performed independently of this contract (and prior to its receipt) by Thomas L. Martin, Jr. (a)The original material from which this adaptation has been made has been published.(b) The authors of this report are grateful for the opportunity to make use of these derivations and computations.

B. The Mathematics of Single Target Attacks

First consider the basic ingredients in the firing problem against a single point target, such as a hardened missile site. The problem and the various terms required in its description are shown in schematic form in figure A-1.

This shows a point target and the impact point of an attacking weapon. The lethal zone surrounding the impact point is the area of total destruction created by the attacking weapon. In other words, if the lethal zone encompasses the point target, the target is destroyed. If, however, the target is outside the lethal zone, the target is relatively unaffected and survives. The firing problem against a single point target then reduces to a calculation of the number of weapons of a given lethal radius necessary to achieve some specified mathematical probability of a hit.

The calculation of this radius turns out to be a more complicated derivation than it may appear initially. Consider for example, a small target at a particular point. Now suppose that several thousand carefully aimed missiles are released against this target. In this case it developes that all of the weapons, each equally well aimed, do not hit the target. Instead, the impact points are distributed over a wide area surrounding the target. The results always appear as shown approximately in figure A-2.

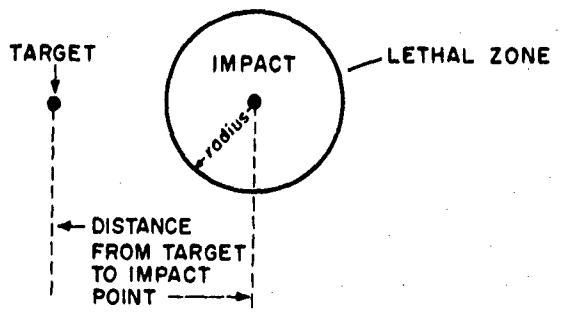

Figure A-1. Targeting, Schematic Diagram

Figure A-2. Impact Points

(a) Thomas L. Martin, Jr., formerly, Dean of Engineering, The University of Arizona, Tucson, Arizona, now Dean of Engineering, University of Florida, Gainsville, Florida.
(b) "Strategy For Survival," by T. L. Martin, Jr., and Donald Latham, The University of Arizona Press, Tucson, Arizona, 1963.

Note the distribution of the weapons impact points in figure A-2. Clearly, there are more near the target than are far away. Yet, some impact points miss the target by wide margins. These variations in the location of the impact points of equally well aimed weapons result from variations in the guidance system of the rocket, inconsistencies in rocket propulsion, and numerous other reasons. If a graph showing the density of impact points as a function of the distance, r, from the target is made, the result always (c) takes the general form shown in figure A-3, which is known as a normal distribution curve for the circular case. This curve is described (d) by the following equation:

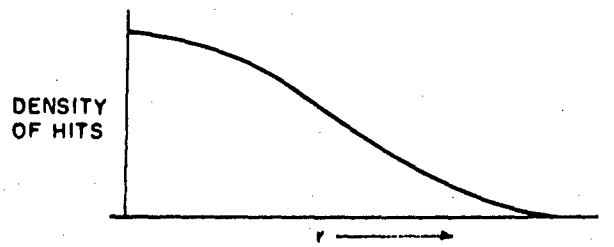

Figure A-3. Normal Distribution Curve

$$\text{probability density} = \frac{r}{\sigma^2} e^{-\frac{1}{2}\left(\frac{r}{\sigma}\right)^2}$$

where the various terms are defined as follows:

r = distance measured from the target
e = natural, or napierian base = 2.718 . . .
σ = standard deviation

The standard deviation, σ, will be eliminated from this equation later and a new term introduced.

Under most circumstances, interest is not centered upon the probability density, but on the more understandable factor of simple probability, in particular, the probability of a hit against the target.

It can be shown (e) that the probability P_1 of a hit with a single weapon is given by the following equation:

$$P_1 = 1 - e^{-\frac{1}{2}\left(\frac{L}{\sigma}\right)^2} \qquad (A.1)$$

The only new term introduced here is the lethal radius which is denoted by L. From a rudimentary knowledge of probability it is clear from equation (A.1) that the probability Q_1 of a miss by a distance of r miles or more is:

$$Q_1 = 1 - P_1 = e^{-\frac{1}{2}\left(\frac{L}{\sigma}\right)^2} \qquad (A.2)$$

Finally, the probability P_n of a hit through directing n different weapons against a single point target is:

$$P_n = 1 - (1 - P_1)^n \qquad (A.3)$$

where:

n = number of weapons fired
P_1 = probability of a hit with one weapon
P_n = probability of a hit with n weapons

Emphasis in many targeting studies falls upon the calculation of the number of weapons, n, that must be directed against a target to achieve a specified probability of a hit. This calculation is comparatively simple.

The necessary equation is derived by solving equation (A.3) for n. The result is:

$$n = \frac{\ln (1-P_n)}{\ln (1-P_1)} \qquad (A.4)$$

where the logarithms may be taken to the natural base, e, or to the base 10.

Practical calculations with these four formulas are possible only when some physical meaning is attached to all of the mathematical symbols. Practically all of these identifications have been made. For example:

P_1 = probability of a hit with one weapon
P_n = probability of a hit with n weapons
n = number of weapons fired
L = lethal radius in miles

(c) This distribution results from the assumption of equal errors in both range and deflection and this is not true for all weapon systems. It is close enough, however, for most targeting studies in civil defense planning.
(d) G. A. Korn, T. M. Korn, "Mathematical Handbook for Scientists and Engineers", McGraw-Hill, New York, 1961, p. 569.
(e) P. M. Morse, G. E. Kimball, "Methods of Operations Research", Technology Press, John Wiley and Sons, N. Y., 1st Ed., 1951, p.113.

r = distance from impact point to target in miles
Q = probability of a miss

The only term that has not been described in targeting analysis terms is, σ, the standard deviation. This term is related to the accuracy of the missile firing as shown below.

Weapon accuracy is expressed in terms of the circular probable error, which is abbreviated CPE, or circle of equal probability, which is abbreviated CEP, rather than in terms of the standard deviation σ. The CPE (or CEP) is the radius of a circle about the target which encloses exactly half, or 50%, of the impact points in figure A-2. When missile accuracy is specified as 1 mile or 2 miles, it means that the circular probable error is 1 mile or 2 miles; that is, 50% of the bombs dropped or the missiles fired land within 1 mile or 2 miles of the target. CPE will be used herein to designate the general concept of error probability.

The standard deviation σ is related to the circular probable error by a constant factor of 0.849 so that $\sigma = 0.849$ CPE. This factor is determined by setting P_1 equal to 0.50 and L equal to CPE in equation (A.1) and solving for σ in terms of CPE. Hence, the probability P_1 of a hit with a single weapon against a single point target can be written in terms of the lethal radius L and circular probable error CEP as:

$$P_1 = 1 - e^{-0.693 \left(\frac{L}{CPE}\right)^2} \qquad (A.5)$$

and the probability Q_1 of a miss is quite clearly:

$$Q_1 = 1 - P_1 = e^{-0.693 \left(\frac{L}{CPE}\right)^2} \qquad (A.6)$$

With these probabilities in this form, the equation for P_n and n are unchanged.

The circular probable error for Russian rocketry is believed to be approximately 2 miles, though improving rapidly and significantly. In particular, in 1962, Russian rocketry was usually credited with a circular probable error somewhere between about 1 and 2 miles. In the period covering 1964 and 1965 it is believed that this will improve to about 1 mile. The United States presently (1964) claims 1/2 to 1 mile circular probable errors for its missiles and it therefore seems reasonable for civil defense planning to assume that the Russians have approximately the same accuracy. Table A-1 lists probabilities for CPE's of 1/2, 1, and 2 miles.

C. A Numerical Example

The formulas developed in the preceding discussion provide the basis for particular and detailed targeting studies. Although these equations are quite simple, the concepts may be unfamiliar. An illustrative example may help to unify the subject.

Consider firing a rocket which has an accuracy corresponding to a circular probable error of 2 miles. In addition, assume that it carries a thermonuclear warhead with a yield which provides a lethal radius of 0.65 miles. The assumed situation requires that the symbols in the preceding formulas have the following values:

$L = 0.65$ miles
$CPE = 2$ miles

The probability of P_1 of a hit with a single missile is calculated from equation (A.5). Substitution of the above values in this equation results in:

$$P_1 = 0.254$$

Thus, the probability of a hit is 25.4%, corresponding to about 1 chance out of 4 tries that there will be a destructive hit.

Similarly, using equation (A.6), the probability Q_1 of a miss is found to be:

$$Q_1 = 0.746$$

Note that the sum of the hit probability and the miss probability is 1, or certainty. This simply means that the chances are 100% that the missile will either hit or miss.

TABLE A-1

PROBABILITY OF A HIT AGAINST A SINGLE POINT TARGET BY A SINGLE WEAPON

Lethal Radius L in Miles	Probability of a Hit in Percent		
	1/2 mile CPE	1 mile CPE	2 miles CPE
.50	50	16	4
.75	79	32	9
1.00	94	50	16
1.50	99.8	79	32
2.00	over 99.99	94	50
2.50	almost 100	98	66
3.00	almost 100	99.8	79
4.00	almost 100	over 99.99	94

The calculation above showed that there is about 1 chance in 4 of a hit with a single missile. One might be inclined to assume then that the firing of 4 missiles would certainly produce a hit, that is, the probability P_4 would be 100%, however, this is not true. In equation (A.3), let:

$n = 4$
$P_1 = 0.254$ = probability of a hit with 1 missile

Then P_4 is found to be: $P_4 = 0.691$

This hit probability of 69.1% is much less than the 100% that intuitive guessing may have suggested. This discrepancy underscores the advantage of a rigorous mathematical analysis in preventing the analyst from arriving at erroneous but seemingly logical conclusions.

Suppose, however, it is necessary to know how many of these particular rockets must be fired against the target to create an 80% probability of a hit. Equation (A.4) is now used with:

$P_1 = 0.254$
$P_n = 0.80$

and the value of n is computed to be: $n = 5.5$, which rounds off to 6 in whole numbers.

Hence, six missiles of 2 mile CPE and 0.65 mile lethal radius must be fired against the target to have an 80% probability of scoring a hit. Table A.2 lists typical results for the multiple firing problem.

TABLE A-2

PROBABILITY OF A HIT AGAINST A SINGLE POINT TARGET BY FIRING SEVERAL WEAPONS

Probability of a hit with 1 weapon in percent	Probability of a hit in percent by firing several weapons			
	2 weapons fired	3 weapons fired	4 weapons fired	5 weapons fired
4	7.6	12	15	18
9	17	25	31	37
16	29	41	50	58
32	54	69	79	85
50	75	88	94	98
66	88	96	99	99+
79	96	99	99+	99+
94	99+	99+	99+	99+
98	99+	99+	99+	99+

Later in this report, calculations of this sort are used to compute the probable number and size of weapons to be used against missile sites, air bases, and cities. Before doing this, the mathematics of targeting will be applied to the miss distance problem.

D. The Miss Distance Problem

Earlier, in equation (A.6), the formula for the probability Q_1 that a weapon will miss the target by a distance exceeding the lethal radius L was given. If L is replaced by r, the equation then specifies the probability, Q_1, that the weapon will miss the aiming point by a distance of r miles or more. The result is:

$$Q_1 = e^{-0.693 \left(\frac{r}{CPE} \right)^2} \qquad (A.7)$$

This probability may be calculated for any specified circular probable error CPE and miss distance, r. Some typical results are given in Table (A.3).

TABLE A-3 .

PROBABILITY THAT A WEAPON WILL MISS THE AIMING POINT

Miss Distance in Miles	Percent probability of a miss	
	2 Mile CPE	1 Mile CPE
2	50	6.2
3	21	0.2
4	6.3	less than 0.01
5	1.3	less than 0.01
6	0.2	virtually zero

Table A-3 shows that the probability that a weapon will miss the aiming point by 5 miles or more is only 1.3%, or about one chance in about 77, when the circular probable error is two miles. When the weapon accuracy is improved to correspond to a circular probable error of one mile, the chances of a miss by a distance of only three miles or more is only 0.2%, or about one chance in 500. While there is always some chance that a weapon will miss the aiming point by a large distance, the probability is very small.

E. The Mathematics of Many-Target Attacks

Up to this point the discussion has treated single firing problems, that is, firings against one target at a time. Now, every single target which requires separate aiming constitutes a separate firing problem and is known as a ballistically independent target. Thus, the preceding discussion could have been called, the mathematics of attacking ballistically independent targets.

There is a mathematical method which provides some insight into the many target problem. Indeed, without this mathematics there is no way to assess the many delicate nuances of tactical plans and their consequences. Let:

x = number of ballistically independent targets which must be attacked
y = number of hits desired
P_n = probability of a hit against each of the x ballistically independent targets.

This probability P_n of a hit against each target may result from an attack with one weapon, following equation (A.5), or with n weapons, using equation (A.3). It only matters that P_n is the probability of a hit against a single, ballistically independent, target.

Now assume that the attacker can adjust this hit probability P_n at will. This is a good assumption as seen from the numerical example given earlier. Further assume that the attacker adjusts this probability P_n so that it has the same value for every single attack against each target. Then, the overall probability P_{xy} of making at least y hits out of x targets, where the probability of hitting each target P_n, is: (f)

$$P_{xy} = \sum_{j=y}^{j=x} \frac{x!}{j!(x-j)!} P_n^j (1-P_n)^{x-j} \qquad (A.8)$$

Where, for convenience in reference, define again these various terms as follows:

x = number of independent targets
y = number of hits
P_n = probability of a hit against one target
P_{xy} = overall probability of hitting at least y targets
j = integer having values starting with y and proceeding one digit at a time up to x
! = denotes a factorial quantity; for example: $5! = (5)(4)(3)(2)(1) = 120$

Consider a hypothetical attack against our 42 Strategic Air Command bomber bases. Suppose that the enemy strategists would like to hit at least 40 of these bases to limit our retaliatory strike and thereby minimize damage to themselves. Finally, assume that the enemy wants to be rather certain of accomplishing this, in view of the consequences of failure, and they set a 95% probability of success as necessary to their plans. They must now determine the hit probability P_n necessary against each of the 42 ballistically independent targets to produce a 95% probability of hitting at least 40 of these SAC bases.

Therefore, the mathematical symbols in equation (A.8) now have the following particular values for this assumed, hypothetical, attack:

$P_{xy} = 0.95$
$x = 42$
$y = 40$

The mathematical problem reduces to a calculation of P_n. When these numbers are substituted into equation (A.8) the result is:

$$0.95 = 861\ P_n^{40}(1-P_n)^2 + 42\ P_n^{41}(1-P_n) + P_n^{42} \qquad (A.9)$$

This equation can be solved by trial and error. That is, assume a value for P_n, substitute this into equation (A.9) and see if the equation is satisfied. This procedure eventually yields the following answer: $P_n = 0.98$. Thus, the hit probability required against each individual SAC bomber base must be 98% to achieve an overall probability of 95% of hitting at least 40 of the 42 bases.

The enemy must next determine the number of weapons required to mount this attack, and to determine whether they possess the resources necessary to carry out the strike with the assurances of success they demand. The first step in this calculation is the computation of the probability P_1 of a hit with one weapon against a single target. This probability is given in terms of the lethal radius L and circular probable error CPE in equation (A.5) as:

$$P_1 = 1 - e^{-0.693\left(\frac{L}{CPE}\right)^2}$$

Next, the number of weapons n required to attack each base to give a probability P_n of a hit, when each weapon has a hit probability of P_1, is given by equation (A.4) as:

$$n = \frac{\ln(1-P_n)}{\ln(1-P_1)}$$

Then, the total number N of weapons required for the whole attack against all x targets is: $N = xn = 42\ n$.
This number is then compared against the inventory of available weapons and the feasibility of the attack may be estimated.

With the aid of combinatorial probabilities it is clear that attack planning is perfectly straight forward when the real uncertainties have been assumed out of existence.

It would be incorrect to think that these calculations are simple; they are straight forward, but not simple. The preceding illustration treated a mere 42 point attack. Yet we know that any potential attacker must necessarily consider something much closer to a 1,000 point attack.

The routine mechanics of calculating 1,000 point attacks are extremely time consuming and the type of calculation customarily handled by large scale, electronic digital computers or by various approximation techniques. With the cooperation of the Numerical Analysis Laboratory of The University of Arizona, equation (A.8) was approximated and a series of solutions were computed for various assumed attack conditions. The results of this computation are compiled in Tables A-4 and A-5 .

The great advantages of this mathematical approach is the precise way in which it pinpoints the assumptions necessary in any postulated attack plan.

F. Analysis of the Many-Point Attack Data

Consider first the use of Table A-2 , for example. Assume a hypothetical attack pattern against 600 targets with the requirement that at least 550 be destroyed with an overall success probability of 90%. In symbolic form then, $x = 600$, $y = 550$, and $P_{xy} = 0.90$. From Table (A.4) the value for P_n is found to be 0.93. That is, the probability of hitting each of the 600 targets must be 93% to have an overall probability of 90% of hitting at least 550 of the 600 targets. Similar values can be worked out for various other assumed attack patterns.

(f) Korn and Korn, op, cit., Sec. 18.2-1 to 18.2-5.

TABLE A-4

LARGE SCALE (400 to 1,000) MANY-POINT ATTACK DATA

P_n = Probability Required For a Hit on a Single Target (Given in the x column)

P_{xy}	y	x = 400	y	x = 600	y	x = 800	y	x = 1000
0.85	300	0.77	500	0.85	650	0.83	850	0.86
	350	0.89	550	0.93	700	0.89	900	0.91
	375	0.95	575	0.97	750	0.95	950	0.96
0.90	300	0.78	500	0.85	650	0.83	850	0.86
	350	0.89	550	0.93	700	0.89	900	0.91
	375	0.95	575	0.97	750	0.95	950	0.96
0.95	300	0.78	500	0.86	650	0.83	850	0.87
	350	0.90	550	0.94	700	0.89	900	0.92
	375	0.96	575	0.97	750	0.95	950	0.96

TABLE A-5

SMALL SCALE (40 to 100) MANY-POINT ATTACK DATA

P_n = Probability Required For a Hit on a Single Target (Given in the x column)

P_{xy}	y	x = 42	y	x = 60	y	x = 80	y	x = 100
0.70	27	0.67	45	0.77	65	0.83	85	0.86
	32	0.78	50	0.85	70	0.89	90	0.91
	37	0.89	55	0.92	75	0.94	95	0.95
	40	0.95	58	0.97	78	0.98	98	0.98
0.80	27	0.69	45	0.79	65	0.84	85	0.88
	32	0.80	50	0.86	70	0.90	90	0.92
	37	0.91	55	0.94	75	0.95	95	0.96
	40	0.96	58	0.97	78	0.98	98	0.99
0.90	27	0.72	45	0.81	65	0.86	85	0.89
	32	0.83	50	0.88	70	0.91	90	0.93
	37	0.92	55	0.95	75	0.96	95	0.97
	40	0.97	58	0.98	78	0.99	98	0.99
0.95	27	0.74	45	0.83	65	0.87	85	0.90
	32	0.85	50	0.89	70	0.93	90	0.94
	37	0.94	55	0.96	75	0.97	95	0.97
	40	0.98	58	0.99	78	0.99	98	0.99

Both tables reveal an important characteristic of the mathematics, though it is somewhat more evident in Table A-4 . Assume any value for x and y and then note the values for P_n for each value of P_{xy}. For example, take x = 600 and y = 500. Then:

$P_n = 0.85$ when $P_{xy} = 0.85$
$P_n = 0.85$ when $P_{xy} = 0.90$
$P_n = 0.86$ when $P_{xy} = 0.95$

In other words, the overall probability of success P_{xy} in hitting at least y of the x targets has very little effect on the single target hit probability P_n. This is true only for large values of x and y and when P_{xy} begins to approach 1.

Now consider the data slightly differently. Assume any value for x and P_{xy} and then note the values for P_n for each value of y. For example, take x = 600 and $P_{xy} = 0.85$. Then:

$P_n = 0.85$ for y = 500
$P_n = 0.93$ for y = 550
$P_n = 0.97$ for y = 575

In short, the single target hit probability P_n is quite sensitive to changes in the number of targets that must be hit.

These observations may be interpreted to mean that attack planning is much more crutially dependent upon the number of targets that must be hit than it is upon the overall probability of success. In other words, in the targeting studies which follow, greater care must be exercised in the selection of the value for y than is required in assigning a value to P_{xy}.

The importance of this conclusion should be more apparent after tracing through the analyses that follow.

G. Targeting Hardened Missile Sites

The term hardening is used to designate the process whereby a structure is deliberately strengthened to withstand some specified amount of weapon effect, usually in terms of blast overpressure. Most missile sites within the continental United States are hardened to withstand blast overpressures of either 25 psi, 100 psi, or 300 psi, depending upon the particular missile installation. In theory, missile silos hardened

to these levels could withstand these blast overpressures from a nearby nuclear explosion and survive in workable condition.

Hardened missile silos are point targets and each missile in its launching silo is ballistically independent of all other silos. Therefore, all of the mathematical formulas discussed up to this point can now be used for targeting studies of hardened missile sites.

As a first step, the number of ballistically independent targets to be used in the analysis must be specified. This is the factor x which appears in equation (A.8). Assume that x = 1000 because this number corresponds very closely to the expected American inventory of operational missiles in 1965. Next, try to estimate the number of misses the enemy may believe they can tolerate. The enemy will virtually be required to assume that nearly every one of our missiles that they miss will eventually land in enemy territory. When these weapons are added to those delivered by surviving bombers of the Strategic Air Command, from carrier-based nuclear bombers, and from Polaris submarines, it is clear that the enemy cannot afford very many misses in any target category. Arbitrarily, now assume that they will want to hit at least 950 of the 1000 targets, leaving no more than 50 available to the United States for retaliation. Thus, the factor y appearing in equation (A.8) has a value of 950.

This might seem to be a rather large number of surviving U. S. missiles, but it also looks like a high percentage of hits. Our Atlas and Titan missiles carry warheads of about 7 megatons while the Minuteman lifts something less than 1 megaton. Moreover, the Minuteman will outnumber the Atlas and Titan missiles by nearly 4 to 1 in 1965. So, as a crude guess, if 50 missiles survive there should be about 40 Minutemen and about 10 Atlas or Titans. The total megatonnage then delivered by these forces would then be about 110 megatons. This would create considerable destruction, but possibly not so great that it could not be considered "acceptable", all factors taken into account.

Next, the probability Pxy of success which the enemy feels must be attached to this strike must be estimated. In other words, what assurances of success do they consider the minimum to warrant the risk of failure. Based upon the discussion in the preceding section, and rather arbitrarily, assume that the enemy could not accept an overall probability Pxy of success of less than about 90 percent. Anything less could be catastrophic while anything more might require an excessive expenditure of attacking missiles.

Thus, to sum up the basis for the targeting against missile sites:

x = 1000 = number of target points
y = 950 = minimum number of hits
Pxy = 0.90 = overall probability of success

Table A-4 shows that these assumed targeting conditions require a hit probability Pn of 0.96 for the attack against each of the 1000 missile sites.

Before proceeding further, consider the fact that this point in the analysis was reached with very little factual support--it has been accomplished by arbitrary assumptions. Certain readers may object to some of these assumptions on various grounds, including access to better information. However, the study was in enough detail so that other computations may be made, by any reader, if better information is available.

A first guess at a possible value for Pn has been made. The number of missiles required for an attack against each target may now be determined. The necessary relationship is given by equation (A.4). That is:

$$n = \frac{\ln(1-P_n)}{\ln(1-P_1)} \qquad (A.11)$$

where P_1 = probability of a hit against a target with a single missile. This probability P_1 was given previously in equation (A.5) as:

$$P_1 = 1 - e^{-0.693\left(\frac{L}{CPE}\right)^2}$$

By re-arranging the terms in this equation, it may be written:

$$\ln(1-P_1) = -0.693\left(\frac{L}{CPE}\right)^2 \qquad (A.12)$$

Substituting this result into equation (A.11), the number of missiles required for an attack against a single target can be determined, that is:

$$n = 1\,\frac{\ln(1-P_n)}{0.693}\left(\frac{CPE}{L}\right)^2 \qquad (A.13)$$

This result can now be specialized, to the particular attack pattern theorized, by replacing Pn with its computed value of 0.96, and then computing ln(1-Pn). The final result is:

$$n = 4.65\left(\frac{CPE}{L}\right)^2 \qquad (A.14)$$

where n, in this case, is the number of missiles required to give a probability Pn of 0.96 of hitting the target. For ease of calculation the equation has been expressed in terms of the lethal radius L and CPE.

Equation (A.14) may be specialized to the cases of particular and representative missile accuracies by inserting approximate values for the CPE. This procedure leads to the following very compact formulas:

$n(CPE = 1/2\ mile) = 1.16/L^2$ (A.15)
$n(CPE = 1\ mile) = 4.65/L^2$ (A.16)
$n(CPE = 2\ miles) = 18.6/L^2$ (A.17)

These formulas simplify calculations to be made in a few moments.

The calculation cannot be completed until proper values are available for the lethal radius L for different degrees of hardening and weapon yield. The lethal radius is the one remaining unknown in these formulas.

The lethal radius is defined as the distance from ground zero to the point where the blast overpressure is large enough to cause destruction of the target. Assume that these destructive overpressures are as follows:

(1) for 25 psi hardening - destruction by 30 psi
(2) for 100 psi hardening - destruction by 120 psi
(3) for 300 psi hardening - destruction by 350 psi

These are assumptions unsupported by factual knowledge of structural safety factors used in the construction of missile silos.

The lethal radii corresponding to these pressure levels for nuclear weapons of different yield are given in Table A-6 .

Surface bursts have been assumed in all cases because, at these high overpressure levels of 30, 120, and 350 psi, the lethal radii of surface bursts exceeds that of air bursts. In short, in this application, surface bursts represent a more economical usage of nuclear weapons.

There is a possibility of using bursts below the surface of the ground against highly hardened targets. Although information on this subject is limited, it does indicate that such explosions create much stronger ground shocks and larger craters than surface bursts of equal yield.

Substituting these lethal radii into equations (A.15) through (A.17) and assuming a hit probability Pn of 0.96, the number, n, of missiles required to hit each target may be determined. The results are given in Table A-7 for three different, but representative, CPE's.

Certain conclusions are obvious from this table. For example, it is very clear that it is a near impossibility to plan a rational attack against 300 psi hardened targets, with 1 megaton warheads, carried by missiles with an accuracy of 2 miles. Each such attack would require 91 missiles and the cost would be extremely high. Conversely, there is no reason to use a 50 megaton weapon with a 1/2 mile CPE against a 25 psi hardened target. Table A-7 shows that a single 0.5 megaton weapon would do the job just as well. Clearly, tabular data of this form are vital in detailed targeting studies.

An attack in a period when the United States will have about 1000 hardened missiles in place has been postulated. In this period Russian missile accuracy should be quite close to the 1/2 mile CPE category. Thus, reference to table A-7 shows that the most likely weapons to be used against United States hardened missile sites are the following:

(1) against 25 psi hardening - 1.0 megaton
(2) against 100 psi hardening - 5 megatons
(3) against 300 psi hardening - 10-20 megatons

TABLE A-6

THE LETHAL RADII OF NUCLEAR WEAPONS
AGAINST HARDENED TARGET - SURFACE BURST

Bomb Yield Megatons	Lethal radius L in miles 25 psi hardening 30 psi contour	100 psi hardening 120 psi contour	300 psi hardening 350 psi contour
0.5	.88	.46	.30
1	1.11	.59	.38
2	1.39	.74	.48
5	1.87	1.01	.65
10	2.39	1.29	.82
20	3.00	1.60	1.03
50	4.12	2.24	1.40
100	5.19	2.81	1.77

TABLE A-7

NUMBER (g) OF MISSILES REQUIRED TO GIVE A PERCENT
PROBABILITY OF A HIT AGAINST HARDENED TARGETS

Bomb Yield in	n = number of missiles required 25 psi hardening			100 psi hardening			300 psi hardening		
Megatons	2 mile CPE	1 mile CPE	1/2 mile CPE	2 mile CPE	1 mile CPE	1/2 mile CPE	2 mile CPE	1 mile CPE	1/2 mile CPE
0.5	24	6	2	88	22	5	200	51	13
1	15	4	1	54	13	3	129	32	8
2	10	2	1	34	9	2	81	20	5
5	5	1	1	18	5	1	44	11	3
10	3	1	1	12	3	1	28	7	2
20	2	1	1	7	2	1	18	4	1
50	1	1	1	4	1	1	10	2	1
100	1	1	1	2	1	1	6	1	1

Because of the many uncertainties which underlie this analysis, particularly the 1/2 mile figure assumed for the CPE, the results computed should be interpreted to be first approximations which can and should be refined as additional information becomes available. In particular, it is probably best to say:

0.5 to 1 megaton against 25 psi hardening
5 to 7 megatons against 100 psi hardening
10 to 20 megatons against 300 psi hardening

In view of the above analysis, a 10 megaton surface burst is postulated for the 300 psi hardened, Titan II missile sites.

(g) Rounded off to the nearest whole number; 0.5 rounded off to the next largest whole number.

H. Targeting Air Bases

There are more than 100 cities in the United States located near major bases of the Strategic Air Command and Air Defense Command. Hence, an estimate of the probable nuclear weapons which might be used against air bases is information of vital concern to several million United States citizens.

In military parlance, air bases are soft targets, meaning that all of the buildings and parked aircraft are extremely vulnerable to the effects of air blast. It has been noted that tests in Nevada indicate that complete destruction of aircraft occurs at peak overpressures in the vicinity of five pounds per square inch. In addition, the light industrial type buildings and residential construction characteristic of Air Force bases are damaged very severely, or destroyed completely, by blast overpressures of 5 psi. Thus, in general, the weapon to be used against an air base is selected to create at least 5 psi of blast overpressure over the entire working area of the air base.

Most of our air bases have an alert city to house the flying personnel who are maintained on an alert status. These alert cities are buried in the ground and hardened to resist the effects of air blast overpressure. It is estimated that these structures are hardened to withstand about 25 psi overpressure.

With this degree of hardening, these alert cities could survive close to the ground zero point of an air burst of a nuclear weapon, however, they would very likely collapse under the increased overpressure and ground shock created by a surface burst. The alert cities are usually very near the alert aircraft and are correspondingly quite close to the aiming point or expected ground zero.

Fuel and nuclear weapons are probably stored in hardened structures with hardening estimated at 25 psi. This hardening may be in an intrinsic characteristic of the storage structure, such as cylindrical tanks, or it may be by special design. Moreover, because of the characteristics of modern aircraft, the runway is hardened and should withstand blast overpressures well in excess of 25 psi. In effect then, the modern Air Force base appears likely to be targeted as a soft target with some hardened components.

Because nearly all air bases contain some hardened elements, some analysts(h) have developed their targeting on the assumption that the entire base must be treated as a 25 psi hardened target. However, it is felt here that this is an overly pessimistic approach which leads to prediction of an excessively heavy megaton attack. The air base can be killed with much less weapon yield than this sort of calculation suggests.

It would be feasible to plan an attack against an air base using either an air burst or a surface burst. The surface burst, however, provides the superior tactics because this burst creates massive quantities of local fallout. The extremely intense layer of radioactivity laid down by this fallout would be so severe that it would immobilize the air base for a long period of time. The high levels of radiation intensity resulting from a surface burst would require the surviving base personnel to remain sheltered. Thus, for some time the base could not be used for further prosecution of the war even though the runways, stored bombs, and fuel might be undamaged. It is not necessary, therefore, to totally destroy all hardened components; it is only necessary to destroy the fragile exposed aircraft by blast overpressure and then to render the air base unusable because of intense radioactive fallout.

These dual objectives are met very readily through the use of a surface burst with the yield chosen to create a blast overpressure of 5 psi over the entire area of the base. There is an additional benefit accruing from this weapon choice: the overpressures near ground zero are very much greater for a surface burst than for an air burst exploded at optimum height to maximize the 5 psi contour. Because the hardened alert city is quite near the expected ground zero point, there is a good chance that it would be destroyed by a surface burst whereas it might survive an air burst which maximizes the area covered by the 5 psi pressure contour. The bonus to the enemy in this case is that trained crew members, who might otherwise survive, are prevented from continuing hostilities at a later date with other facilities.

Often an attack against air bases is theorized upon the assumption that the runways must be cratered by a surface burst to keep the United States from re-using the field. However, local fallout from a surface burst will be so great that the field will not be usable in any case, even if the runway is intact. Additionally, a simple mathematical analysis of the targeting of an area as small as a runway shows that an extremely large number of missiles would be required, in terms of the additional benefits accruing to the attacker. Besides, there are at least 400 civilian runways that would also have to be cratered. Thus, cratering of the runways is not an important factor in targeting air bases.

Moreover, if runway cratering does become an important factor in the later phases of such a war, it could be quite readily achieved by a bomber attack with a comparatively low yield weapon. Such a mopping up action could be carried through during the period when the air base is still immobilized by fallout. Thus, we are not considering this aspect of tactics in our targeting study because it is felt to be a minor consideration relative to other factors.

Generally speaking, the important target area of a typical United States bomber base will not exceed about 12 to 13 square miles. This corresponds to the area enclosed by a circle about two miles in radius. A typical case is shown in figure A-4. This shows Davis-Monthan AFB, which is a B-47 base of the Strategic Air Command located near Tucson, Arizona. Note that the air base is enclosed by a circle two miles in radius.(i)

Of course, because of local differences in terrain and air base layout, there will be minor variations in shape and size of the bases. These variations should not be very great and would not generally alter seriously the targeting analysis given here.

Fighter-interceptor bases of the Air Defense Command would probably be somewhat smaller than the bomber bases. But once again, the difference is not significant in comparison with the many other uncertainties involved in these calculations. Moreover, many of these fighter-interceptor squadrons are based on the same field as the bombers of the Strategic Air Command.

Thus, it is assumed here for the purposes of these calculations that the target area of Air Force bases corresponds to that area enclosed by a circle two miles in radius. The aiming point on each air base is taken to be the center of the principal runway or runways.

(h) See for example, E. D. Callahan, L. Rosenblum, J. D. Kaplan, D. R. Batten, "The Probable Fallout Threat Over the Continental United States", Report No. TC-B 60-12, Dec. 1, 1960, Contract CDM-SR-59-33, ASTIA Doc. No. 256 072L, p. 21.
(i) See Targeting Analysis

The bomb yield is then computed so that it creates a blast overpressure of at least 5 psi everywhere within the target area circle which has a radius of two miles.

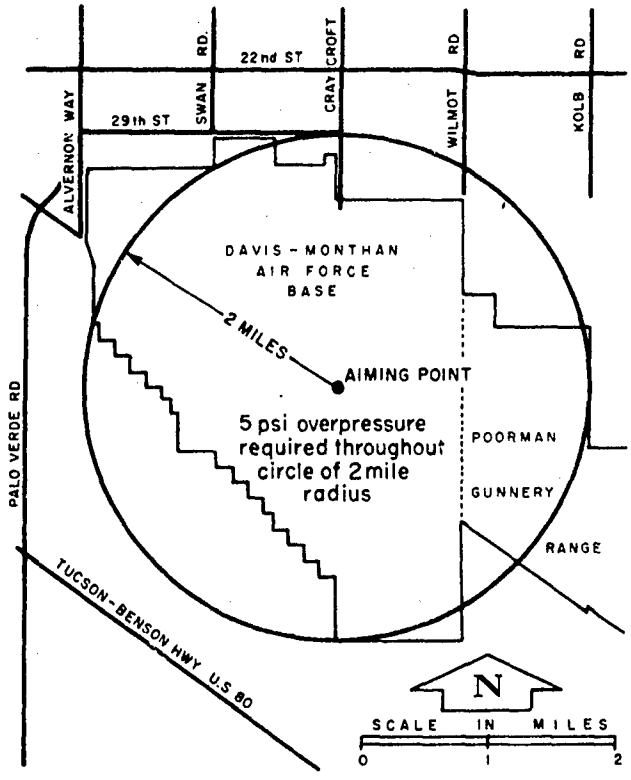

Figure A-4. Targeting, Davis Monthan AFB

1. Targeting SAC Bases

It is obvious that no one knows how effective the Russian air defense is and, as a result, how many misses they could tolerate in their first strike against the bases of SAC. Somewhat arbitrarily it is assumed that the Russian air defense can deal effectively with the aircraft from five SAC bomber bases in the United States. In other words, the assumption made here is that the Russians cannot afford to miss more than five SAC bomber bases in the continental United States.

It will also be assumed that the Russians require an overall probability Pxy of 95 percent that their misses will not exceed this number. In other words, it is assumed that the Russians want 95 chances out of 100 that their attack will succeed. They are willing to take a small risk, 1 out of 20, that they might fail.

If there are 42 SAC bomber bases to be attacked, then the values which should be assigned to the various mathematical symbols are:

$x = 42$
$y = 37$
$Pxy = 95$

Then, reference to Table A-5 , in a preceding section, shows that these conditions require a hit probability Pn of 94 percent for each separate air base attack. It will develop later that this probability Pn of a hit is easily achieved by a single missile. Therefore, Pn should be replaced by P_1 where P_1 has a value of 94 percent.

Now, consider the meaning of this probability P_1. Because the problem is now centered about an area target rather than a point target, the mathematics require a slightly different interpretation from that used previously. For the case of an area target, equation (A.5) must be re-written as:

$$P_1 = 1 - e^{-0.693 \left(\frac{R}{CPE} \right)^2} \qquad (A.18)$$

P_1 is interpreted to be the probability that the weapon will land within the area enclosed by a circle of radius, R, drawn about the aiming point as center.

The sketch in figure A-5 helps to illustrate this concept. Two concentric circles, drawn about the aiming point as center, are shown. The target area corresponds to that region enclosed by the outer circle which has a radius of two miles in the case of an air base. The purpose of the attacking weapon is to produce 5 psi of blast overpressure within this target area thereby causing total target destruction. The inner circle of radius R shown in figure A-5, defines the area within which there is probability P_1 that the weapon will strike.

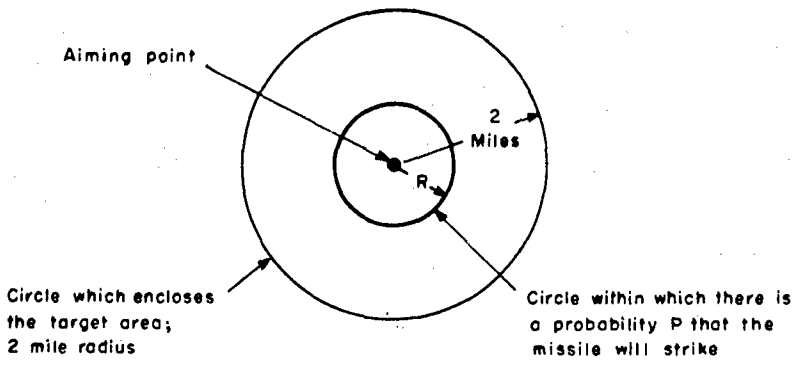

Figure A-5. Error Probability Contours

The weapon could strike anywhere within this circle of radius R, though it is more likely to fall nearer the aiming point than nearer the boundary of the circle. Nevertheless, it is reasonable to expect the enemy to plan conservatively and to assume an unfavorable impact location. From his point of view, such an unfavorable possibility corresponds to an impact point on the rim of the circle of radius,R. This is shown in figure A-6. Under these conditions, total destruction can be created throughout the entire target area only if the lethal radius of the weapon is equal to (2 + R), as shown. Hence: $L = 2 + R$ miles

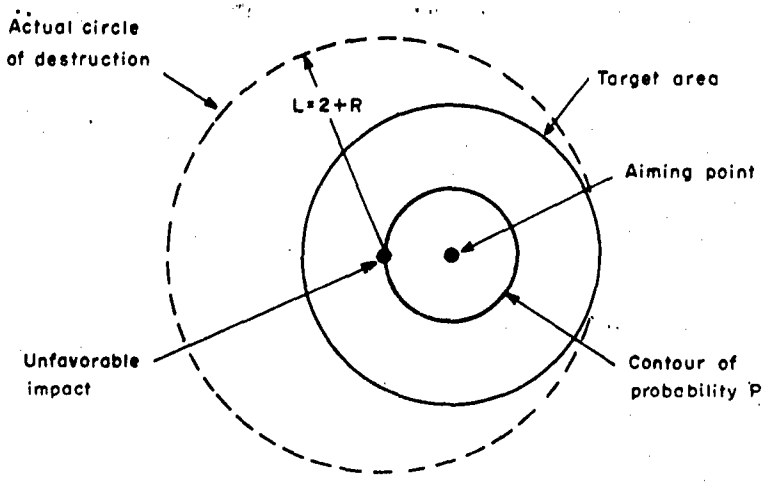

Figure A-6. Impact and Destruction Contours

The factor R can be computed directly from equation (1.18) to be:

$$R = CPE - \frac{\ln(1-P_1)}{0.693} \qquad (A.19)$$

Earlier it was found that the probability P_1 of a hit might reasonably be taken to be 0.94. Approximately then:

$$R = (2.02)CPE \qquad (A.20)$$

and the required lethal radius L for an attack against each bomber base of the Strategic Command is:

$$L = 2 + 2.02\ CPE \qquad (A.21)$$

The lethal radius computed according to equation (A.21) has a substantial overkill factor. This arises from the unfavorable impact location assumed in figure A-6 which, as a result, requires a quite large lethal radius compared to the target radius. In reality, the chances are better that the weapon will land much nearer the aiming point. If such occurs, then total destruction is created over a larger area than the target area. This constitutes the overkill. It is concluded, therefore, that weapon yields computed from equation (A.21) are quite realistic, and provide a basis for conservative civil defense planning.

The required lethal radius, computed from equation (A.21) for different circular probable errors, is found to have the following values:

Circular Probable Error	Corresponding Required Lethal Radius
2 miles	10.08
1 mile	4.02
1/2 mile	3.01

These required lethal radii are compared with the lethal radii available from nuclear weapons of various yields. These available radii are summarized (j) in table A-10 .

From a comparison of the available lethal radii given in table A-10 with the required lethal radii summarized earlier, it is clear that complete air base destruction is achieved by either an air burst or a surface burst. Something in the range of 2 to 5 megatons would do the job with the overkill margin dependent upon the circular probable error.

However, for the reasons set forth earlier, it is believed that a surface burst provides the best tactics even though this reduces the lethal radius somewhat below that obtained from an air burst of the same yield. The reduction is not large and is certainly offset by the bonus of local fallout which accompanies the surface burst.

Thus, all factors considered, it is believed that the most likely attack against bomber bases of SAC will consist of a 2 to 5 megaton surface burst delivered by missile. In particular, a 5 megaton surface burst is postulated for Davis-Monthan AFB.

2. Targeting ADC Bases

The Air Defense Command (ADC) operates a number of different kinds of bases. Nearly all of these bases are soft targets comparable to the bomber bases of SAC. Such bases would be targeted in precisely the same manner as was used for the bomber bases.

The targeting of these soft bases of ADC follows the same general pattern as that used earlier for the bomber bases of the SAC. The only important difference arises in the assumptions which must be made by the enemy; that is, how many of these soft bases can they miss in the initial attack without the survivors interfering seriously with the follow-on bomber attack?

TABLE A-10

LETHAL RADII (5 psi contour) OF NUCLEAR WEAPONS AGAINST AIR BASES

Bomb Yield megatons	Lethal radius L in miles	
	Air Burst	Surface Burst
0.5	3.45	2.19
1	4.32	2.76
2	5.41	3.45
5	7.4	4.7
10	9.3	5.9
20	11.8	7.5

Attempts to answer this question are obviously fraught with uncertainties. Unclassified information available concerning anticipated attack plans and weapons is inadequate to support any attempt at an authoritative answer. So, once again, as in the targeting of bomber bases, there is no recourse except to use the little data available to make an informed estimate. It is understood of course, that readers with better information can probably refine these calculations.

First, it must be recognized that destruction of bases of the ADC is not as crucial to the enemy as is the destruction of the SAC bomber bases. The reason is obvious: bases of ADC do not have the resources to retaliate against the enemy homeland; they can only blunt the effectiveness of the bomber attack. Stated somewhat differently, these bases constitute a force of attrition against enemy air attack; but they do not pose any direct threat to the enemy. Thus, relative to an attack on our SAC bomber bases, an attack on the soft bases of ADC can: operate at a lower level of destruction, and at a lower probability of success and still meet minimum requirements for a satisfactory attack.

Arbitrarily, and with no more justification than that given, it is assumed here that the enemy will seek to destroy all but ten of our soft bases within the continental United States. It is further assumed that there are 42 bases in all and that the Russians will require an 80 percent probability of success for their attack. Thus, it has been assumed that:

$x = 42$
$y = 32$
$Pxy = 0.80$

Then, from table A-5 given earlier, one finds that the enemy must have a hit probability P_1 of 80 percent against each of the soft bases of ADC.

At first glance it might appear that the assumptions have sim[illegible] attack very considerably since there are 43 fighter-interceptor bases and 6 Bomarc bases, and more are under construction. [illegible]ss assumed that the total number of soft bases was only 42. This apparent discrepancy in the total arises because many fighter-[illegible]tor groups are located on SAC bomber bases and would be accounted for in that targeting analysis. All factors considered, the ass[illegible]ue of 42 target bases seems reasonably conservative.

Now with the hit probability P_1 known to be about 80 perc[illegible], this value can be used in equations (A.19) and (A.21) to compute the lethal radius, L, required for an attack against the soft bases [illegible] ADC. The result is: $L = 2 + 1.53\ CPE$ (A.22)
Then, assuming a surface burst for the same reasons set forth earlier, from table A-10 one finds that this lethal radius can be supplied by a weapon with a yield of between about 1 and 5 megatons. Depending upon the assumed value for the attacker's circular probable error, 2 megatons represents a reasonable compromise value.

(j) From the Lovelace Bomb Effects Computer

I. Targeting Cities

Cities are area targets similar to air bases. Because cities are area targets, the general principles of targeting developed for use on air bases can be applied.

The lethal overpressure for use against cities is usually assumed to be 5 psi. Such a pressure would assure complete residential destruction and fairly complete destruction of much stronger commerical and industrial buildings. In addition, serious structural damage results from blast overpressures of 3 and 4 psi and these levels extend many miles beyond the 5 psi contour.

Thus, cities may be targeted by calculating the weapon yield required to generate a blast overpressure of 5 psi over the metropolitan area of the city. This area of blast destruction, however, is essentially circular in shape, and since very few cities have this configuration, a more thorough targeting analysis would require that each city be examined separately. In this case, the bomb yield would be selected to produce an overpressure of 5 psi over a distance equal to 1/2 the largest dimension of the metropolitan shaped cities. In such cases several weapons would be used to develop a blast pattern of the required shape and size.

Furthermore, it seems most probable that air bursts would be used against cities. Compared to a surface burst of the same yield, an air burst creates damaging overpressures of 5 psi, and lower, over a somewhat larger area. Moreover, air bursts are much more efficient than surface bursts in starting fires. Though the air burst lacks the fallout created by the surface burst, the other two advantages more than offset this deficiency. In any case, ample fallout will be produced by the hundreds of surface bursts used against other kinds of targets. This fallout will be sufficient to immobilize the population in shelters and to kill the unsheltered. Thus, an air burst will create all of the damage the enemy could wish for.

The proper weapon for use against a given city is then selected, as a first approximation, from the data in table A-II. This is done by matching, nearly as possible, the lethal area of the weapon to an arbitrary shape factor times the metropolitan area of the city. Or, for large or irregular cities, multiple weapons may be used to create the necessary pattern of blast. This may require drawing circles of blast, of the proper lethal radii, over a map of the city. This is where local talent can play a really significant role in refining these estimates.

I. Summary

This treatment has briefly covered the mathematical development of the targeting analysis which was used to arrive at a range of weapon sizes that could be expected to be employed against retaliatory military complexes such as Davis-Monthan AFB and the Titan II silos in and near Tucson. In addition, the data has been presented in a general form that will allow the use of these results on other target systems.

TABLE A-II

THE LETHAL RADII AND AREAS OF NUCLEAR
WEAPONS AGAINST CITIES - 5 PSI CONTOUR - AIR BURST (k)

Bomb Yield Megatons	Lethal radius (miles) 5 psi - contour	Lethal area, sq. miles area inside 5 psi contour
0.5	3.45	37.5
1	4.32	58.6
2	5.41	93
5	7.4	172
10	9.3	272
20	11.8	438

On the basis of the preceding detailed analysis, a 10 megaton surface burst for each of the Titan II sites and a 5 megaton surface burst for Davis-Monthan AFB is postulated and used as a basis for prediction of the nuclear weapon effects to which Tucson may be subjected.

(k) Lovelace Computer

APPENDIX - PART B
STRUCTURAL LOADINGS

LIST OF ILLUSTRATIONS

LIST OF ILLUSTRATIONS (continued)

PART B

STRUCTURAL LOADINGS

A. Introduction

Design of counterforce nuclear effects shelter systems requires use of the best available data on loadings, the mandatory engineering design criteria. In the field of modern shelter design, the loadings criteria are in the process of development. The available data are often of the most general nature. The material in this part of the Appendix was developed as an outgrowth of targeting studies, and in order to provide more particular inputs to the design concepts.

The reliability and cost of a shelter system is directly related to the accuracy with which loadings are determined. A concept of probability of reliability is helpful in this context.

B. Probability of Reliability (a)

This part of the Appendix presents the results of calculations of probability of reliability that a hardened structure that is located in the proximity of a nuclear burst will experience certain magnitudes of effects. These curves can be very useful in estimating the degree of hardness required by a shelter system for a given overall probability of survival.

The hardness of the shelter to be constructed at each location depends upon the probability of the shelter sustaining a given weapon effect from the assumed attack and the total amount of funds available for the shelter program. The relation between weapon effects and the probability of shelter reliability can most readily be approached by recalling that a Gaussian (normal) distribution of hits about an aiming point was used in the target analysis. The distribution is shown graphically in figure B-1. The cells in the interior of the figure are cells of equal probability; that is, the probability (0.001) of a hit in cell A is the same as the probability in cell B. The outermost cells have lesser probability values as indicated. The scale of the diagram is in CEP's and hence, may be used for any delivery system for which the CEP* is known.

The relation between weapon effects and the probability of the shelter sustaining a given weapon effect can best be illustrated by the following example:

Assumed weapon: 5-megaton surface burst on Davis-Monthan AFB.
CEP: 1 mile.
Distance of shelter from assumed aiming point: 3-1/4 miles.
Desired: The probability of sustaining different levels of overpressure.

In the CEP units of figure B-1, the distance between the aiming point and the shelter is plotted. The circles of radii of overpressures associated with a 5-megaton burst on Davis-Monthan AFB are drawn as an overlay on the cells of equal probability with the shelter as center. The cells of probability within a given circle represent the probability of a hit which will apply that pressure to the shelter. Thus, the probability of sustaining an overpressure of 100 psi or more is:

3	cells	0.001	0.003000
4-1/2	cells	0.00025	0.001125
2	cells	0.00010	0.000200
		TOTAL	0.004325

i.e., a shelter designed for 100 psi has a 99.5% of survival. Similarly, the probabilities associated with other overpressure values may be found in Table B-1.

TABLE B-1

Overpressure	Probability of Sustaining Overpressure	Probability of Not Sustaining Overpressure
50 psi	0.01248	0.9875
60 psi	0.00985	0.9902
100 psi	0.004325	0.9957
150 psi	0.00245	0.9975
200 psi	0.00113	0.9988

These data are plotted in figure B-2. It is apparent from the curve that for small increases in survival probability the shelter hardness increases rapidly and 100% is statistically unobtainable.

For a 50% increase in shelter hardness, there is approximately a 20 to 25% increase in shelter construction cost based on comparing existing shelter designs. Hardness must consider not only the blast effects but also the thermal, and initial nuclear radiation, weapon effects.

(a) The data in this section are based on work presented in the document NAVDOCKS P-81, "Personal Shelters and Protective Construction," Sept. 1961, Department of the Navy, Bureau of Yards and Docks, Washington, D. C.
*The term CPE (Circular Probable Error) is used elsewhere in this report to denote the same concept.

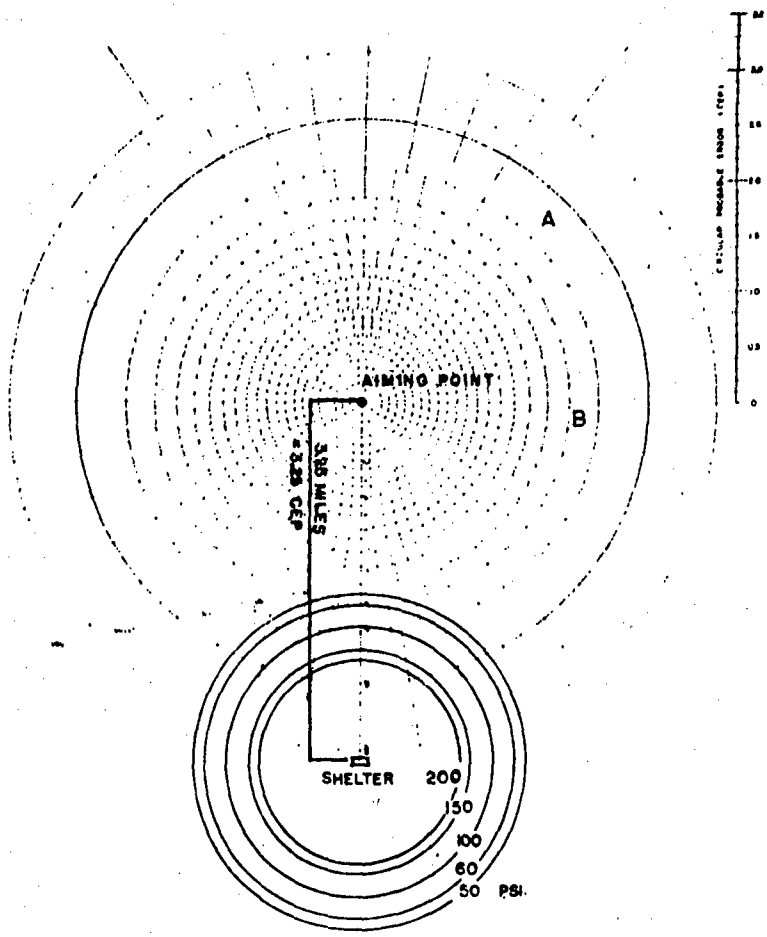

Graphical Solution For Determining The Probability That

A Shelter Would Sustain Given Overpressures

Figure B-1. Cells of Equal Probability

Table B-2 shows the relation between shelter design hardness for a 99.0% survival probability and the radial distance from the target aiming point, while Table B-3 shows the shelter hardness required for a 99.9% survival probability. Within the 75 psi overpressure contour the difference in required hardness is extremely pronounced.

TABLE B-2

MINIMUM DISTANCE BETWEEN AIMING POINT AND SHELTER FOR
A 99.0% PROBABILITY OF NOT SUSTAINING A GIVEN OVERPRESSURE

Overpressure (psi)	Radii Distance From Aiming Point (miles)
300	2.5
200	2.6
150	2.70
100	2.85
75	3.00
50	3.3
25	3.9
10	5.1
5	6.7

TABLE B-3

MINIMUM DISTANCE BETWEEN AIMING POINT AND SHELTER FOR A 99.9% PROBABILITY OF NOT SUSTAINING A GIVEN OVERPRESSURE

Overpressure (psi)	Radii Distance From Aiming Point (miles)
500	3.0
300	3.2
200	3.3
150	3.4
100	3.6
75	3.7
50	4.0
25	4.6
10	5.8
5	7.0

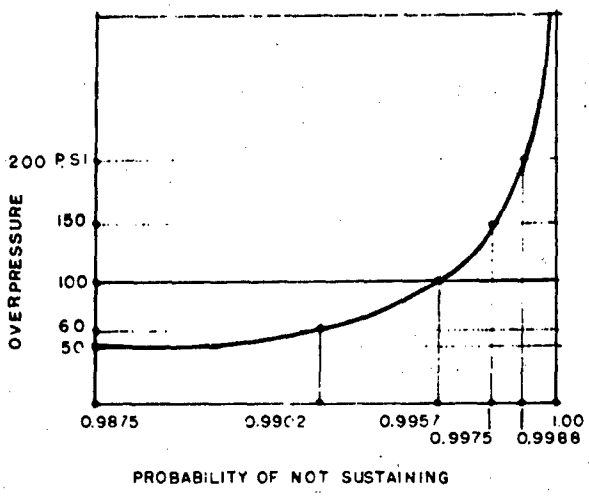

Figure B-2. Probability of Not Sustaining Given Overpressures

To continue this analysis and present a series of curves applicable for a variety of weapon yields and CEPs, calculations were made for 2 MT, 5 MT, 10 MT, and 20 MT, both air and surface bursts, for 1/2 mile, 1 mile and 2 mile CEP. These data form the basis for estimating the relative hardness of a shelter system for a variety of attack patterns and weapon yields. These curves can be scaled to other weapon yields and to other CEPs.

The curve labeled "absolute" on each graph corresponds to the overpressure versus distance for a direct hit. It may be noted that the breaking point appears to be at about 98% for all curves and that to design for any point above this level would result in a rapid increase in cost of the shelter system.

Using these graphs (figures B-3 through B-8), it is possible to select the probable maximum overpressure that would be observed at a given point with varying degrees of reliability. Consider figure B-5, a point 5 miles from a 5 MT air burst subject to a CPE of one mile, there is an 80% chance that the maximum overpressure will be less than 11.2 psi. At this same point, there is a 90% chance that it will be less than 12.6 psi, etc. Note that an overpressure of 28 psi is necessary before the probability increases to 99.9%. It does not appear to be feasible to select probabilities of reliability of design overpressures in a risk-oriented approach that are much greater than 90%. Note also, that the 0% chance curve lies reasonably close to the 80% curve.

As further justification for the 90% conclusion, consider figure B-2. This is a curve which shows the typical way in which magnitude of the design overpressure, for a specific point, varies with the probability that this value will not be exceeded. The 90% level seems to be the point at which greater reliability becomes very costly as far as magnitude of overpressure is concerned.

These graphs of overpressure versus distance have been used to construct maps of Tucson and its environs. These show the probable safe design overpressures for all points in the Tucson area if Tucson is subjected to an attack corresponding to a 5 MT air burst at Davis Monthan and a 20 MT surface burst at each of the 18 Titan II bases. An arbitrary CPE of 1.0 mile was used for each target. A separate presentation has been plotted for each of the following probabilities of reliability: 80%, 95%, 99%, 99.9%. (See figures B-9 through B-12). It is felt that any conservative risk-oriented study that is made of the Tucson problem will have a need for these charts.

This approach may be used for any city or assumed target area, but is dependent on the development of a reasonable targeting analysis for the specific area. For example, for Tucson soil conditions, in order to provide protective shelters for 96% of the area within an overpressure circle of 2 psi (outside of which blast shelters would not be necessary), one would design to 40 psi and an induced vertical soil displacement of about 10 inches.

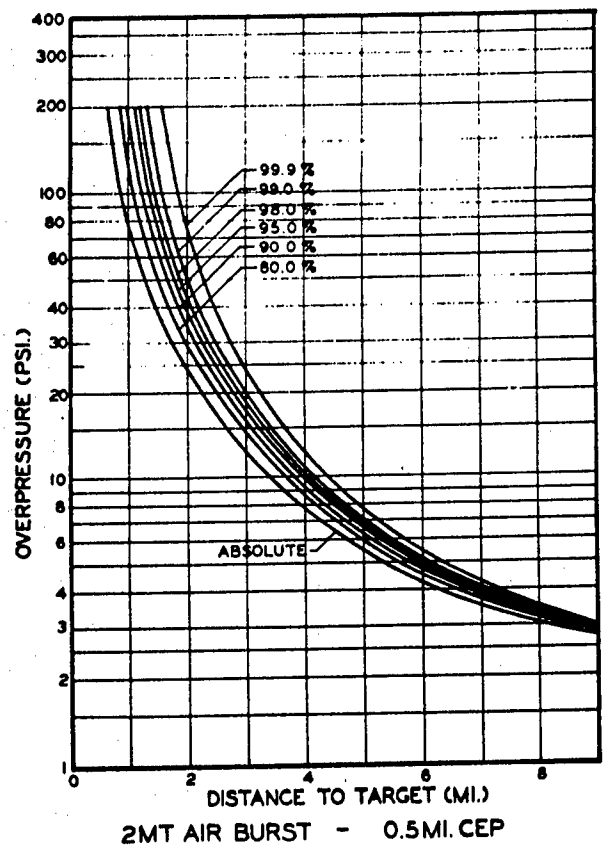

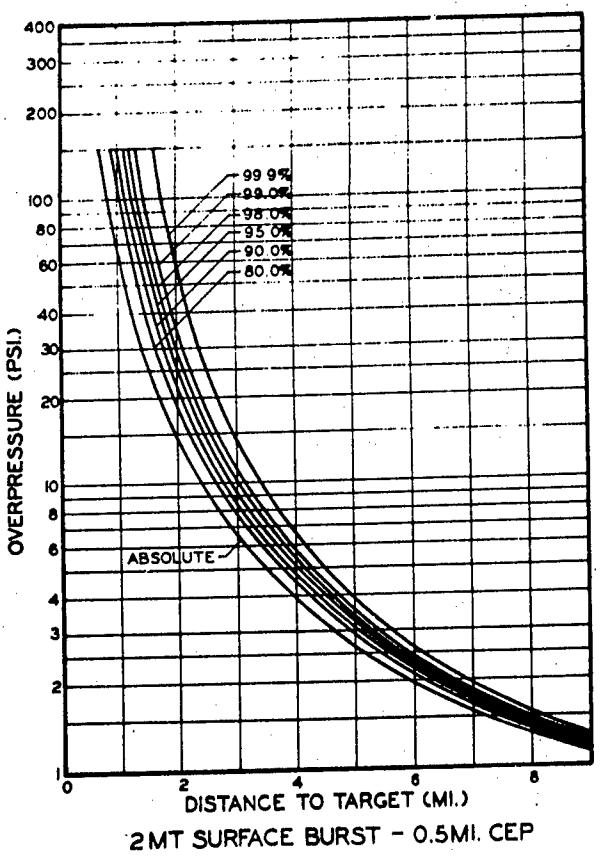

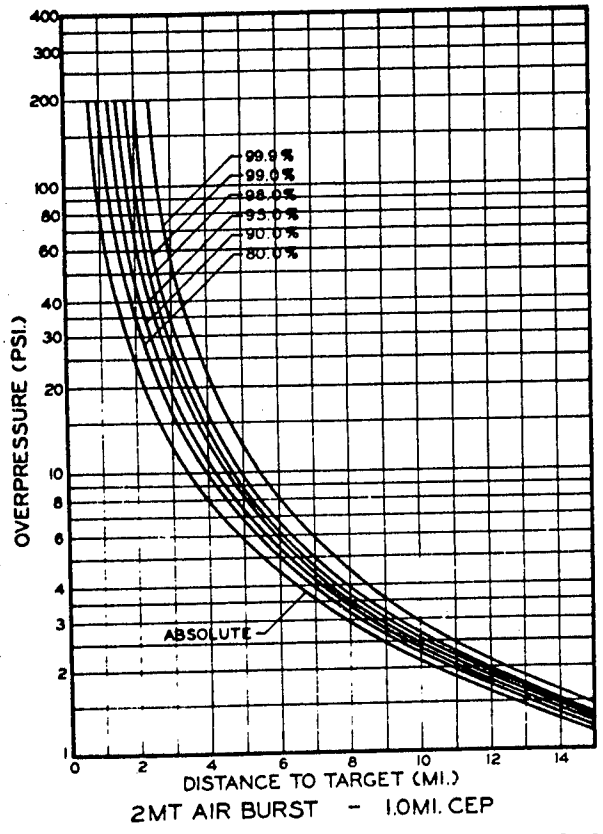

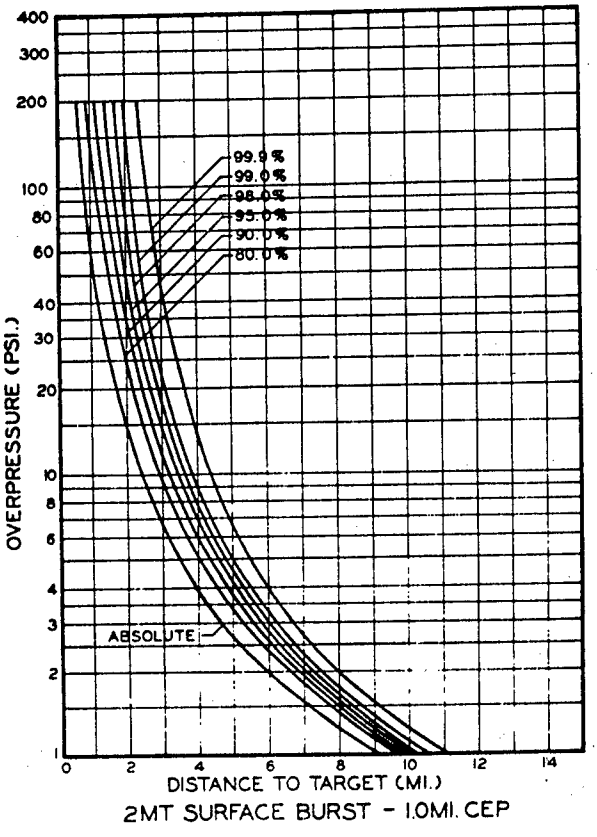

Figure B-3. Probability of Reliability, Chart I

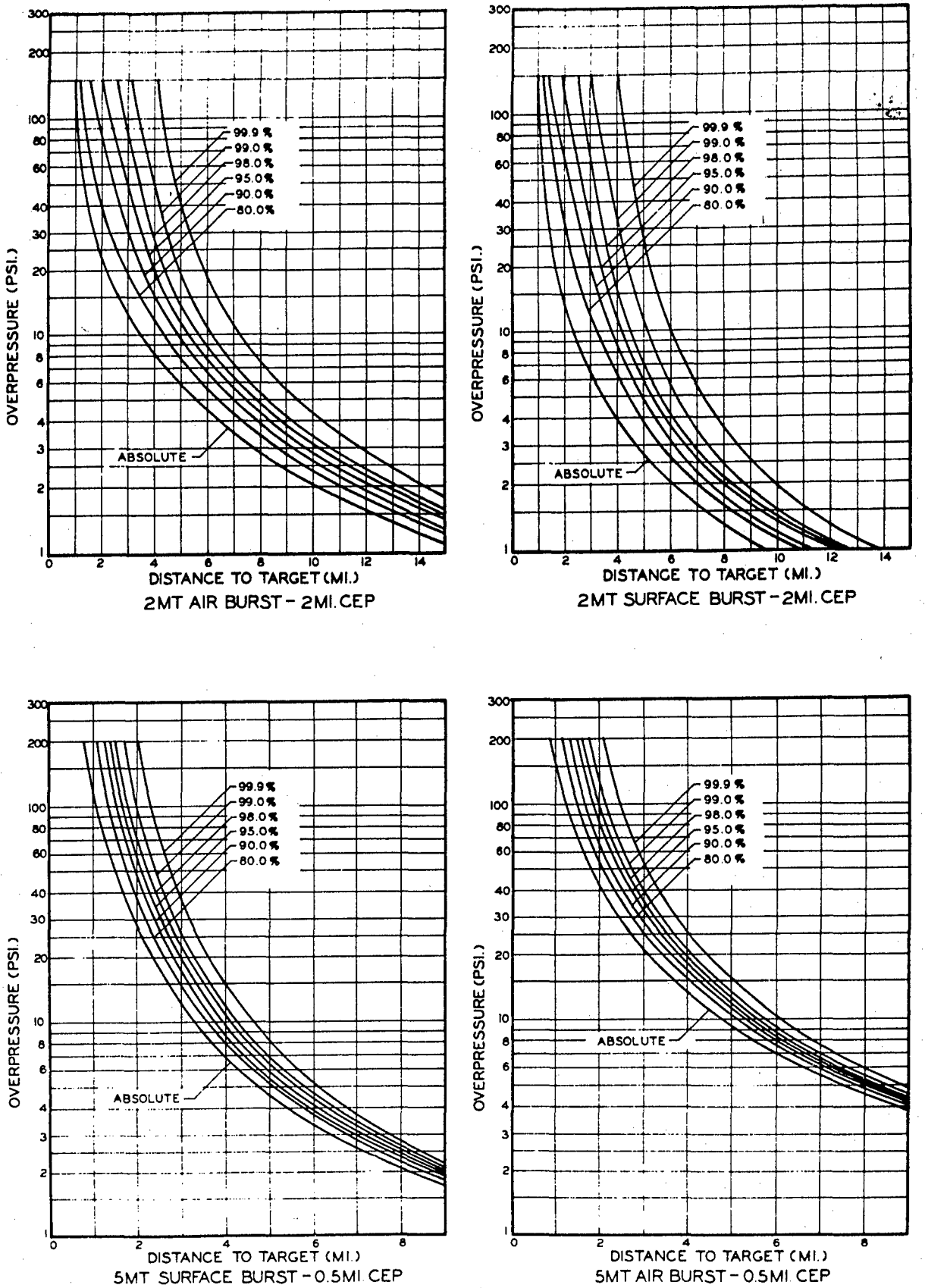

Figure B-4. Probability of Reliability, Chart 2

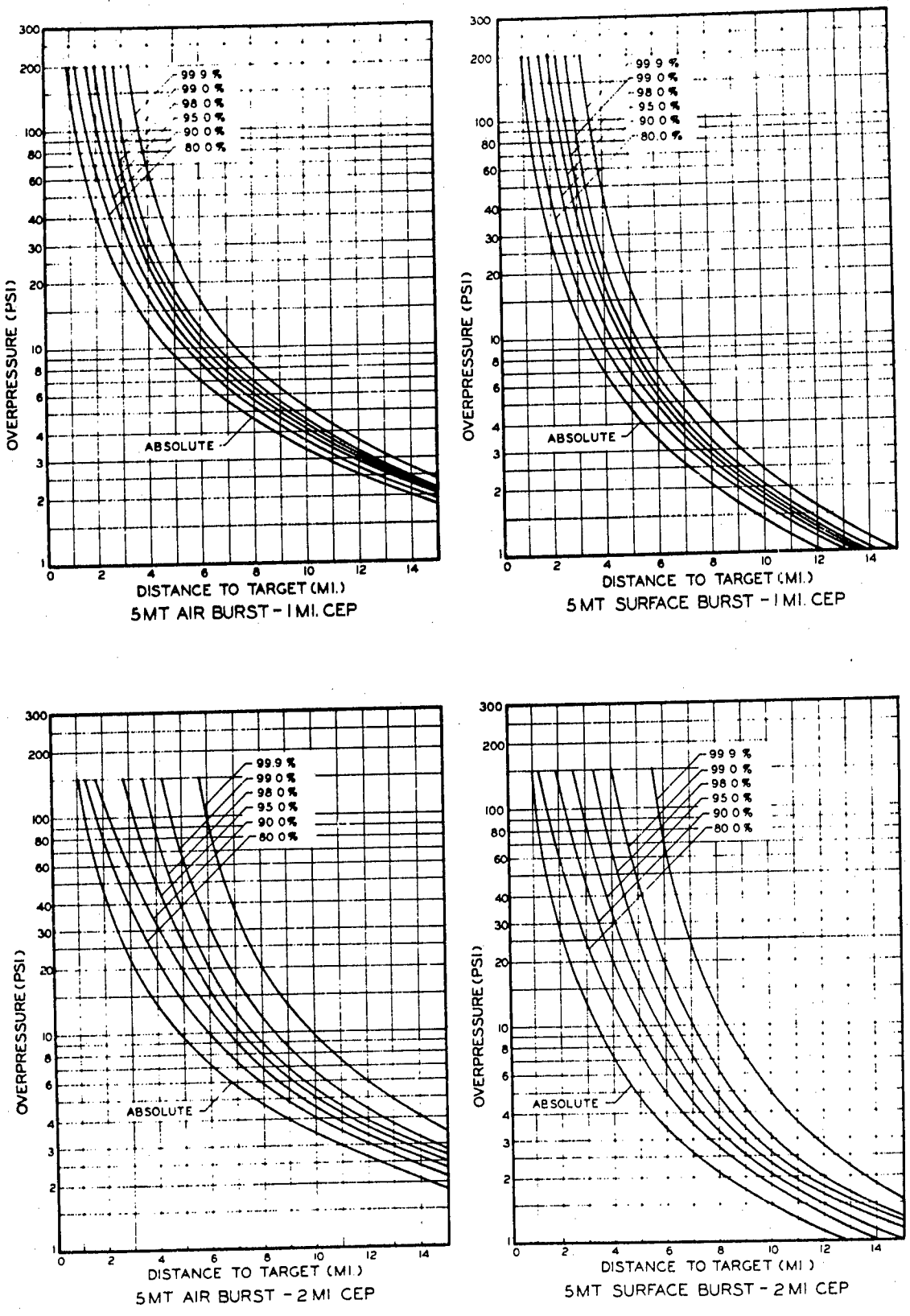

Figure B-5. Probability of Reliability, Chart 3

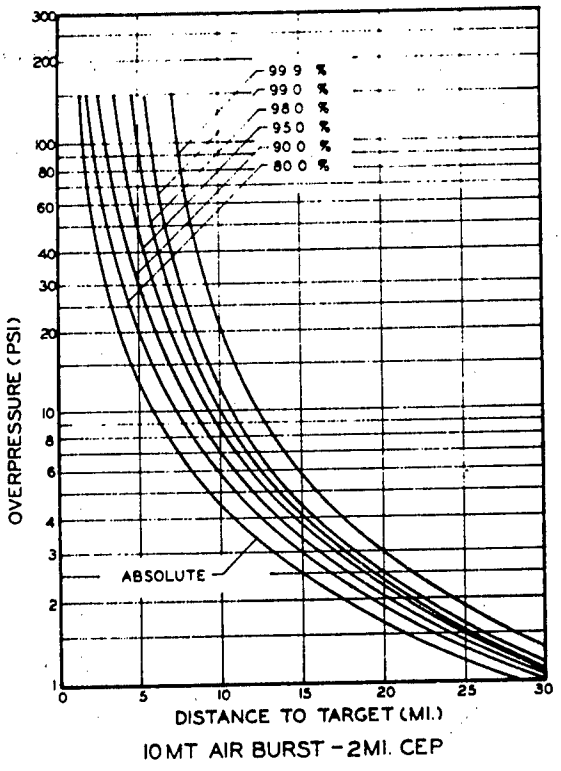

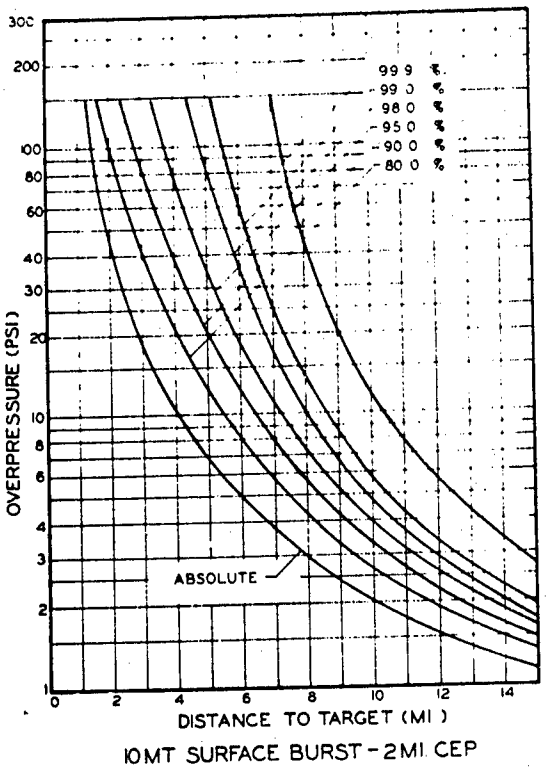

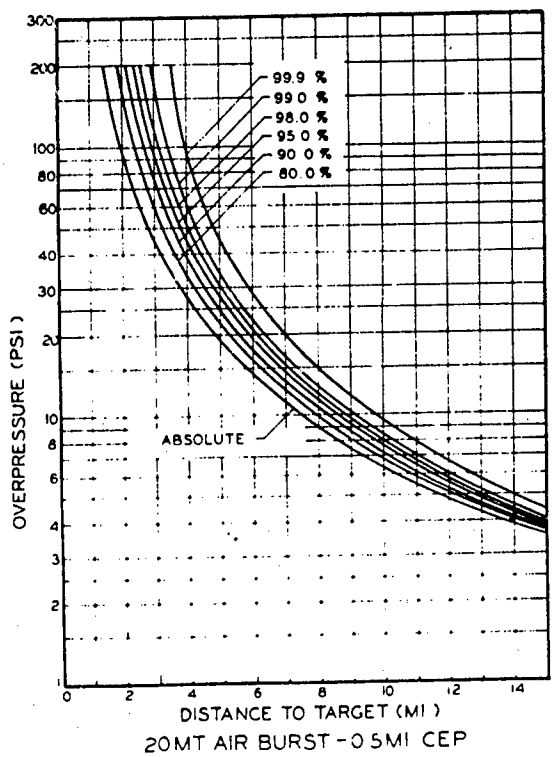

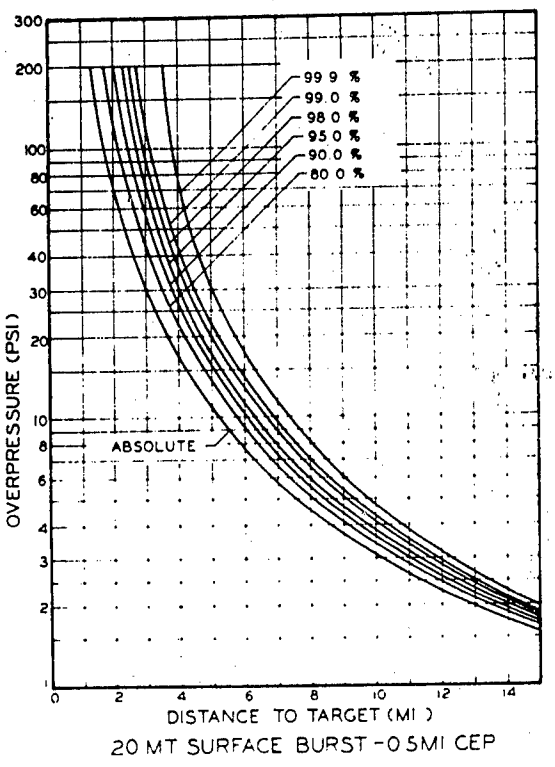

Figure B-6. Probability of Reliability, Chart 4

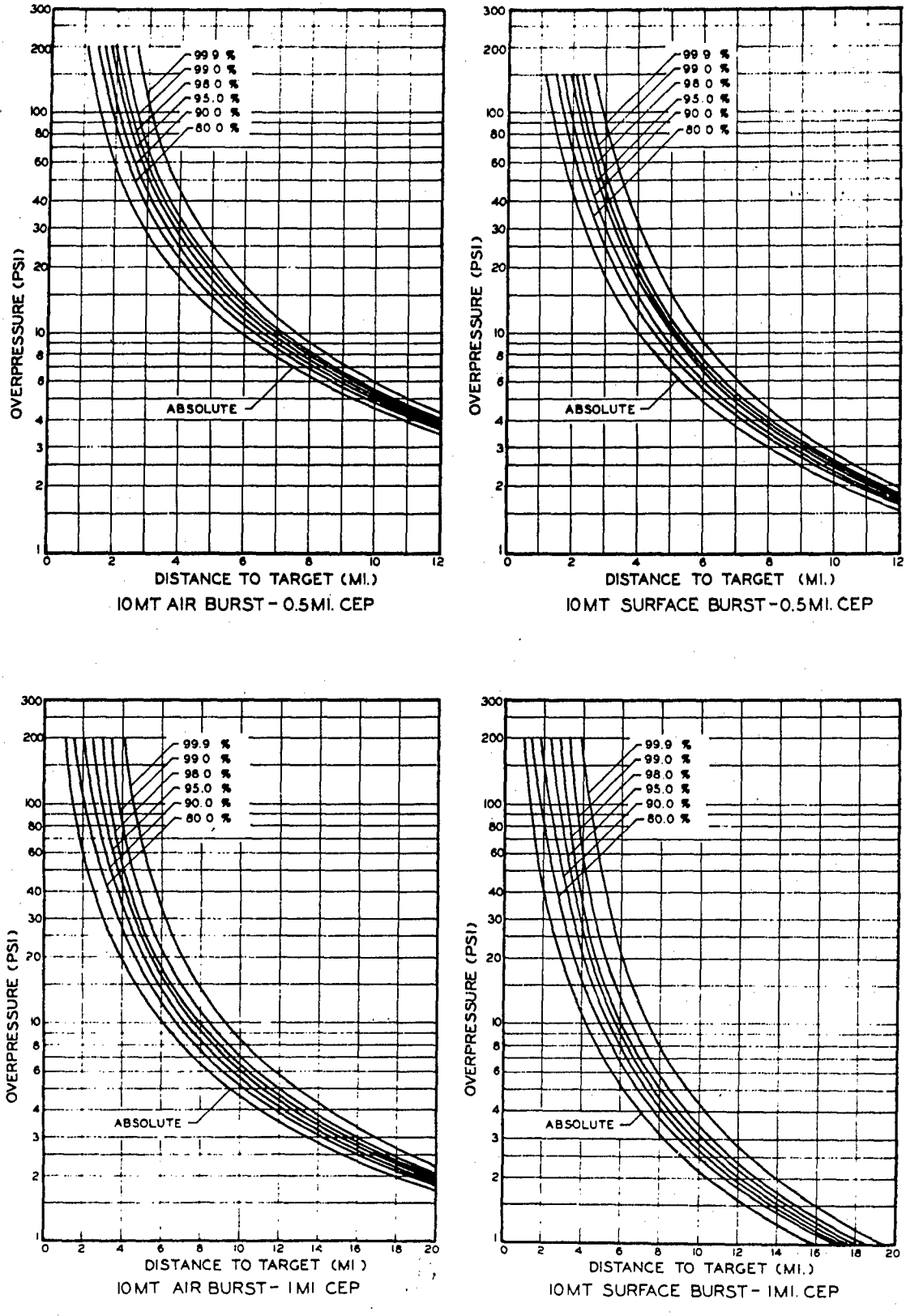

Figure B-7. Probability of Reliability, Chart 5

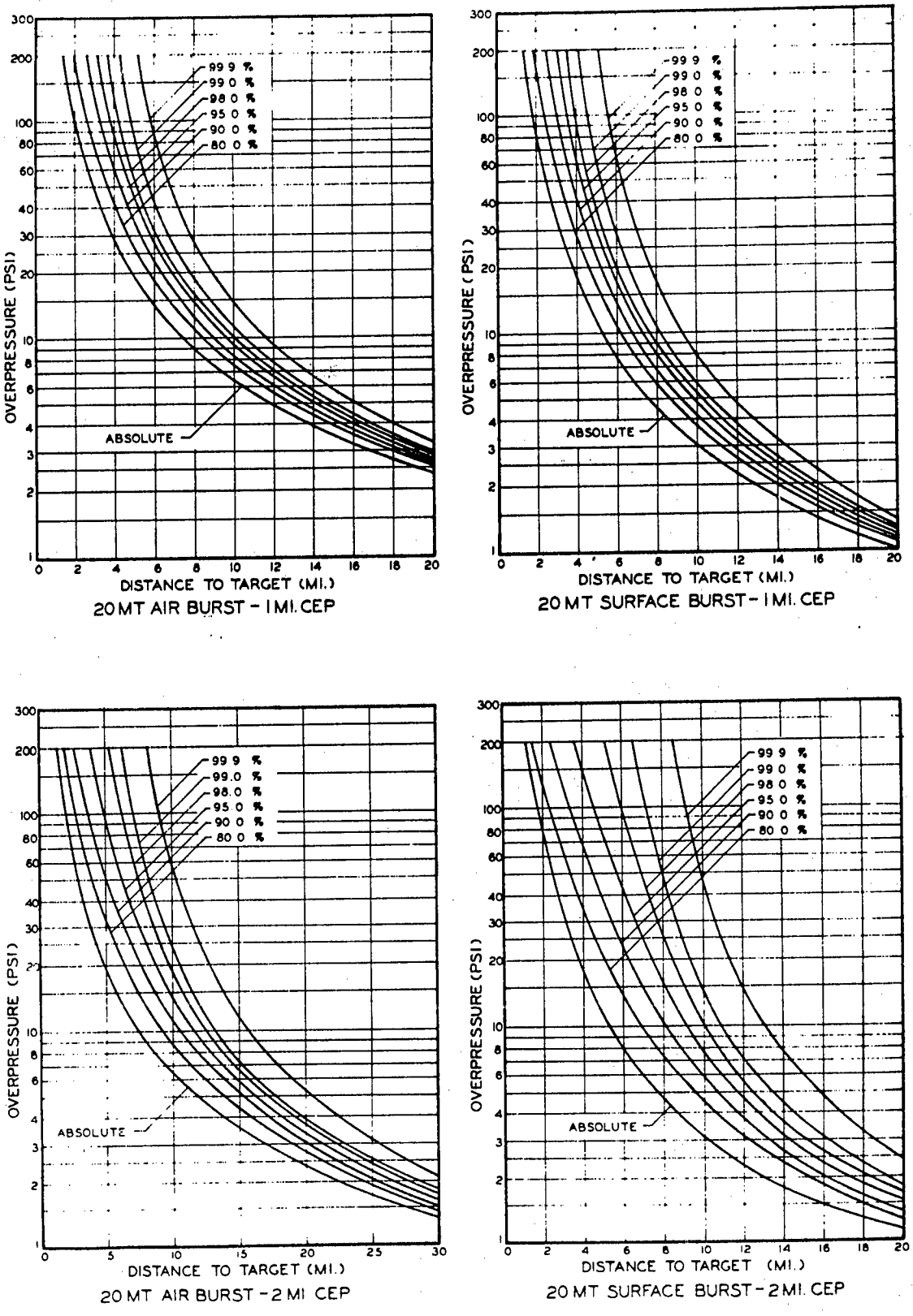

Figure B-8. Probability of Reliability, Chart 6

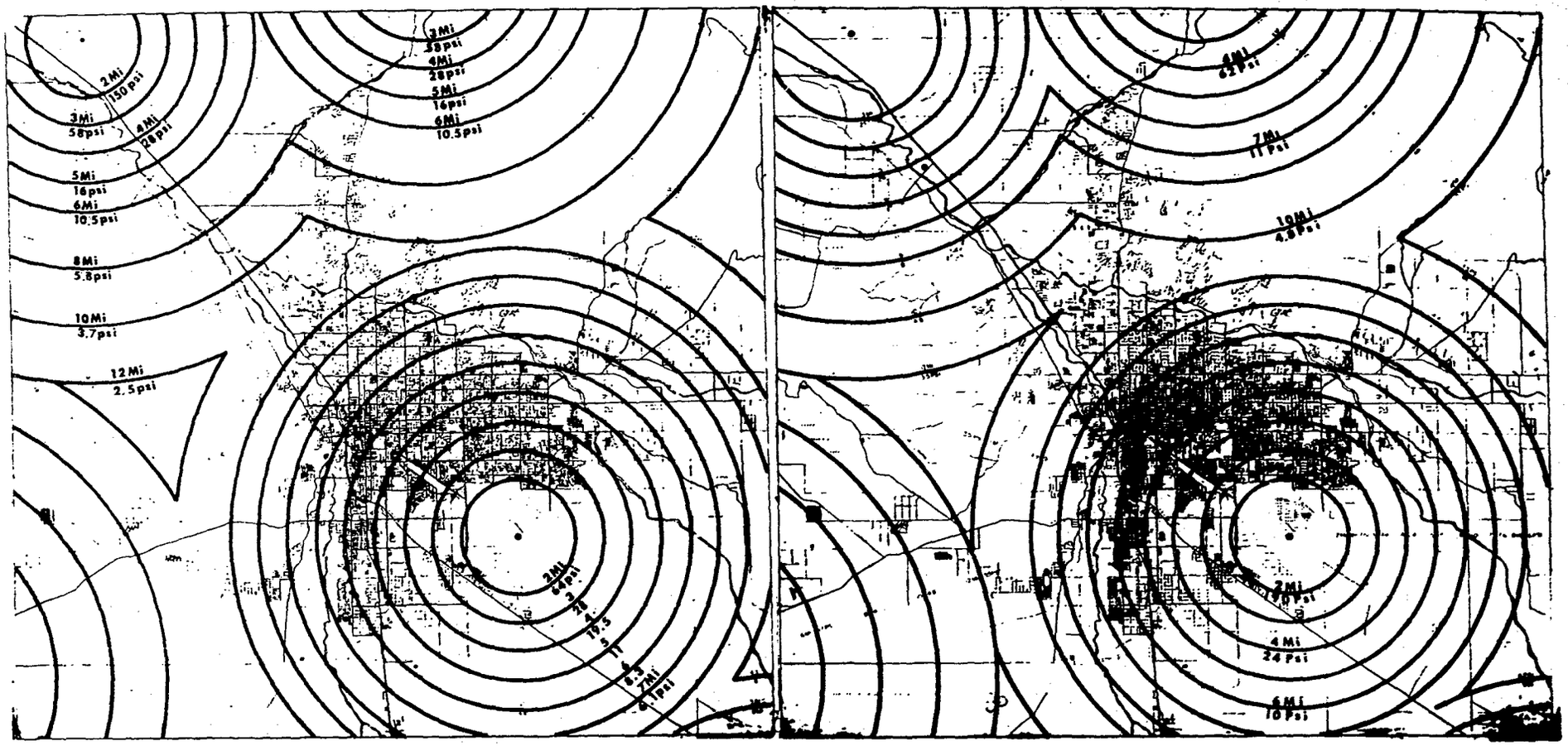

Figure B-9. Contours For 80% Probability of Reliability

Figure B-10. Contours For 95% Probability of Reliability

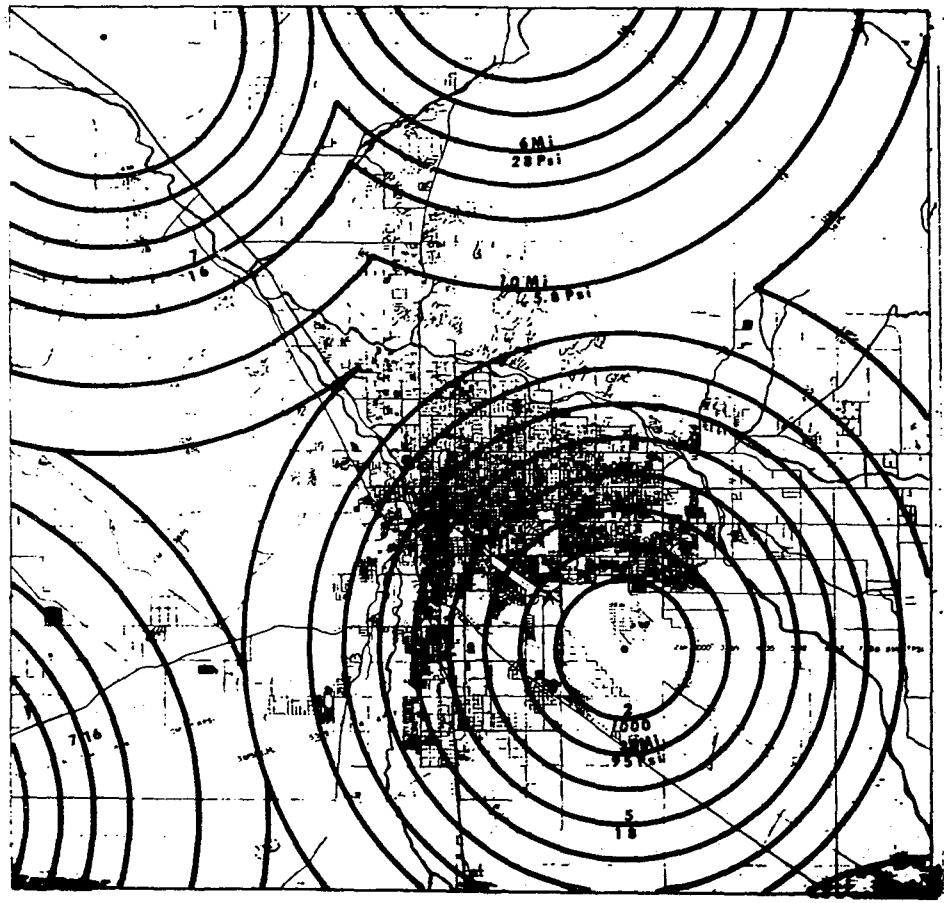

Figure B-11. Contours For 99% Probability of Reliability

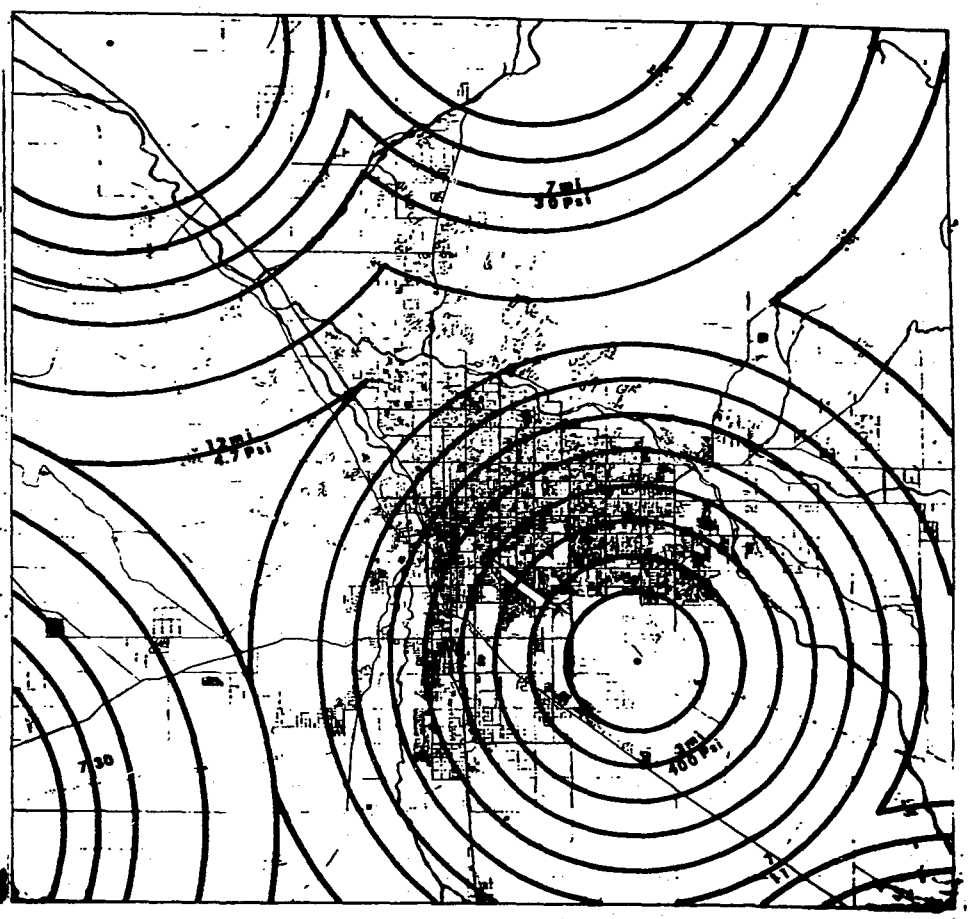

Figure B-12. Contours For 99.9% Probability of Reliability

C. Free-Field Ground Displacements, and Soil Structure Interaction

1. Introduction

In general, the discussion of free-field ground displacements (that is the displacements which ignore the effects of structures) due to a nuclear detonation, is limited to those displacements induced by air-blast loading. Therefore, displacements very close to ground zero are precluded in these analyses in as much as "near the crater" the ground disolacement results largely from the direct conversion of thermo-nuclear energy into mechanical energy.(b)

From the work that has been done, it seems that the problem of determining air-induced free-field ground displacements is in fact, a dual problem, both facets of which rely heavily upon assumptions to avoid impossible analytical complexities. Before a solution of the actual displacement problem can be attempted, the problem of the influence of soil properties upon the response of the soil to dynamic loading must be solved. Here it is generally felt that "the most significant soil property that influences strained modulus of deformation, and the selection of the proper value of this modulus is essential to a reliable prediction of the ground displacement."(c) Unfortunately, a constant-valued constrained modulus cannot be assigned to each soil type, since the value of the constrained modulus is itself effected by a large number of factors both intrinsic and extrinsic to the soil type. Intrinsic conditions such as water content, Atterberg Limits, degree of saturation, Poisson's Ratio, etc., as well as extrinsic conditions such as overburden pressures, lateral constraints, rate of loading, etc., make an accurate determination of the constrained modulus a very delicate problem. Laboratory procedures have been set up which attempt a solution to this problem, however these procedures are based upon assumptions which sharply define the limitations of the results obtained. A complete description of the typical laboratory procedure for the determination of a "selected modulus" is available in the AFDM pp. 4-12 to 4-26. (d)

After a satisfactory solution has been obtained to the first facet of the air-induced free-field ground displacement problem, that of the soil properties, the formulation of the assumptions necessary to approach the problem of actually computing displacements may be undertaken. Every researcher admits that his procedure, as it now stands, possesses inherent weaknesses. (e) This is due to the fact that our knowledge of the subject is at present so inadequate that we are compelled to make assumptions which we know misrepresent actual conditions. For example:

1. Stress attenuation with depth is based solely on theoretical considerations of spatial dispersion.
2. Linearization of the subsurface stress profile results from the assumption that the initial pulse stress front travels with a velocity equal to the seismic velocity, and that the peak stress front travels with a velocity which is a function of the constrained modulus.
3. Horizontal displacements are either entirely ignored or computed on the assumption that the entire pressure wave travels through a given stratum at constant velocity and inclination. In this case even the sense of direction of the horizontal displacement must be assumed since so little is known about it.
4. Neglect of the effect of variation in shape of the subsurface stress wave.
5. Neglectof the effect of high frequency components, reflection and Rayleigh waves.

These are a compilation of what one author (f) considers the weakening assumptions of his treatment of the problem. Other authors add or subtract from this list. However, nowhere does there exist enough information for predicting free-field ground displacements due to air-blast loading, or to allow the effect of these assumptions to be evaluated. It is, therefore, one objective of this study to set up a computer program using an IBM 7072-1401 computer system to analyze the effects of the various pertinent parameters on ground displacements. In general, the approach used by Wilson and Sibley and the resulting AFDM procedure will be employed. It is hoped that when the effects of our assumptions upon ground displacement predictions are analyzed, we will be able to incorporate parameters in the program which will eliminate the necessity of making the initial assumptions. In the meantime, we will continue the present approach to the problem; program it for the computer, and use it to predict ground displacements that can be expected in the Tucson area.

2. Ground Motion and Soil Structure Interaction

a. Introduction

Before the formal presentation of the analysis and program, it is deemed appropriate to include some background information on the geological structure of the Tucson soil environment. This information is obviously not all included in the theoretical analyses which are later developed, but pertinent quantitive values are referenced and used where necessary.

b. Tucson Soil Environment (g)

The desert region of the Southwest is characterized by isolated mountain ranges rising abruptly from low valleys or plains--the ranges generally occupy less area than do the intervening valleys. In southern Arizona the valley floors step up from near sea level to 2000 feet or more in elevation, and the ranges may rise to over 7000 feet.

Desert and steppe-type climates predominate--climate is controlled more by elevation than it is by latitude. Both climate types are characterized by a lack of precipitation, the former more so than the latter. Practically all the rain that falls in the region evaporates; runoff or recharge generally occurs only during the wettest period. Water table levels are generally being depressed. Vegetation is restricted and consists mainly of creosote bush, cacti and sage brush on the deserts, and mesquite, pinon juniper and various types of grass on the steppes.

Precipitation varies from about 3 inches on the warm deserts to about 12 inches on the steppes. Most of this falls in the summer or winter, with only rare late or early storms in other seasons. Summer thunderstorms, often accompanied by hail, often occur as cloudbursts sending torrents of water streaming down the mountains onto the surrounding valley floors filling washes and gullies and doing considerable damage. Rates of fall may exceed four inches per hour.

(b) "Ground Displacements From Air-Blast Loading," by Stanley D. Wilson and Earl A. Sibley, Journal of Soil Mechanics and Foundation Division, Proc ASCE, Vol. 88, No. SM6, Dec. 1962, p.3.
(c) Ibid p. 5. (Also refer to the Air Force Design Manual, Technical Documentary Report Number AFSWC-TDR-62-138, Dec. 1962, p.4-12).
(d) Ibid pp. 18-21.
(e) Ibid p. 29 (Also refer to AFDM p. 4-28.)
(f) Ibid
(g) W. C. Lacy, Professor of Geology, College of Mines, University of Arizona, Tucson, Arizona (Bibliography on page B-14)

The intermontane basins extend to unknown depths and are filled with a combination of lake deposits, alluvial fan and floodplain deposits. Although the basins have generally been aggrading at a rapid rate, periods of deposition have been interspersed with short periods of erosion--leaving a complex pattern of erosional and depositional features difficult to unravel from well drillers' logs. Basin fill can generally be considered to have accumulated rapidly in a water deficient climate, and to be normally loaded--this commonly results in the formation of low density soils.

Separating the deep intermontane basins from the ranges are gently sloping fan-capped pediment surfaces, the width of which may reflect the age of the range, the resistance of the rocks to erosion, and rainfall conditions in the range.

(1) Geomorphology and Character of Basin Fill

Tucson, Arizona lies within a basin bounded by the Catalina Mountains on the north, the Rincon Mountains on the east, and the Tucson Mountains on the west. (Figure B-13) It is situated on the toe of a large alluvial fan complex 30 miles long and 13 miles across the toe, extending from Mountain View to the confluence of the Santa Cruz River and Rillito Creek. It rises from 2200 feet at the confluence to 3200 feet at Mountain View, and has been formed largely by the outwash of Pantano Wash capping and reworking alluvium derived from the Catalina-Rincon Ranges. (Figures B-13 through B-16 follow the Bibliography on the next page.)

Drillers' records from water wells in the Tucson Basin have been variously interpreted by Kidwai (1957), Maddox (1960), and Streitz (1962) and correlated with sieve analyses; see figure B-14.

Maddox recognized a low permeability zone in the basin which had been channeled and capped with unconsolidated gravels in the Rillito Creek area. Streitz found this change in permeability of basin fill materials to represent an extensive angular unconformity with low topographic relief lying beneath the alluvial fan materials. Clay and silt inate above. A deep well south of Tucson encountered a "sticky clay" at a depth of 200 feet, and continued in the formation for some 1200 feet. No soil tests were run on this material, but a sample of the core delivered to the writer underwent shrinkage of 30% upon air drying.

Smith (1934) recognized a variation in soil types in the Tucson area resulting from a series of terraces developed by erosion and incomplete filling. He designated these, from oldest to youngest; see figure B-15: the University Terrace, the Cemetery Bench, the Jaynes Bench, and the Bottomlands. Each of these terraces is characterized by variations in soil types and geomorphic characteristics, and the writer believes that these are related to local changes in the drainage system and sources of alluvial material.

The University Terrace is characterized by low rolling hills with approximately 100 feet relief with a northwest trend. The soil consists of poorly sorted gravel, weakly cemented, usually with a hard caliche layer at or very near the surface. It has a seismic velocity of 1000 to 1500 feet per second. Rock fragments within the gravel are largely composed of granite gneiss with occasional Paleozoic quartzite and limestone fragments that appear to have been derived from the Catalina-Rincon Ranges. There is no accurate means of determining the depth of erosion that has taken place in these gravels but consolidation curves suggest little precompression, and it appears that little more than the soil layer has been stripped exposing the caliche zone at the surface.

Surrounding erosional remnants of the older University Terrace is a plain of low ridges of the Cemetery Bench at a level 30 to 60 feet below the older terrace. The soil consists of normally loaded clay and silt to depths of 100 feet or more. In place specific gravity measurements reveal densities of 85 to 90 pounds per cubic foot. Seismic velocities range from 500 to 800 feet per second. Soft caliche may be present in thicknesses in excess of 50 feet beneath soil cover. The writer suggests that this silty material was derived largely from the erosion of Tertiary lake bed deposits located in the basin between the Santa Rita Mountains, the Empire Mountains and the Whetstone Mountains following capture of this drainage by Pantano Wash. Development of bad-land topography in the clay and silt-rich lake beds of this area attest to some sort of erosional rejuvination.

The Jaynes Bench, some 30 feet below the Cemetery Bench, follows the present drainage as a flat bench with narrow gullies. It consists of silty material with soft limy subsoil grading into caliche in the area south of Tucson.

The Bottomlands are confined to the floodplains and consist of sand, gravel,and silt generally without the limy subsoil.

(2) Caliche Distribution

The presence of caliche layers at or near the surface of the ground and the nature of this layer is of concern to the contractor, the city planner, and the individual home owner since it influences foundation conditions, the ease of excavation, and landscaping, and, incidentally, shelter building.

Details of caliche distribution through the Tucson area have not been worked out, but preliminary observations by Streitz (1962) (figure B-15) from well logs indicates a consistent pattern with an absence of caliche in the floodplain areas and a general thickening around the toe of the Tucson fan to the south and southwest. In areas underlain by the University Terrace the caliche is hard and dense and frequently occurs at the ground surface. Lime analyses of individual layers exceeds 90% $CaCo_3$ (Breazeale and Smith, 1930). In the Cemetery and Jaynes Benches the caliche occurs at depths beneath a soil cover and is a spongey, limy subsoil. It appears that on the University Terrace the soil has been stripped by erosion exposing the caliche layer to weathering and reworking.

There is no evidence to indicate that the formation of caliche in the Tucson area has resulted in either a "jacking up" of the surface, or that solution has resulted in subsidence.

Damon, Long and Sigalov (1963) have found a general tendency for a decrease in the percentage of modern carbon in caliche with depth, indicating an upward growth of the layers during its formation. They concur with Breazeale and Smith (1930) in the opinion that the caliche has formed at the bottom of the capillary zone and represents lime carried down by percolating waters. The floodplain areas were subject to too much downward flushing to accumulate a caliche layer.

(3) Decline of Water Table

The subsurface water level in the Tucson area has been systematically recorded since 1916 by the University of Arizona Agricultural Station (Schwalen and Shaw, 1957). The water table ranges from about 30 feet to 300 feet below the land surface, but slopes generally to the northwest at approximately 20 feet per mile with the direction of flow parallel to the axis of the Tucson alluvial fan. There has been a gradual decline in the water table since 1916, at an accelerated rate since 1946 corresponding with an increased rate of water consumption. This has resulted in a conical depression of the water surface in the area of the city, (figure B-16) reaching a maximum

of approximately 60 feet since 1916, and 50 feet since 1947. The aquifer materials belong to the later more permeable gravels comprising the bulk of the alluvial fan, but the water table is rapidly approaching the low permeability lake beds below the erosion surface. See figure B-14.

(4) Basin Subsidence

U. S. Coast and Geodetic leveling data shows that many basin areas in the Southwest are undergoing subsidence, though insufficient stations have been established and maintained to determine the shape of these subsiding areas. In the Tucson basin subsidence between the years 1907 and 1952 totaled 4-1/2 inches; to the north of the vicinity of Picacho subsidence between 1905 and 1960 totaled 3.6 feet and prominent earth fissures have developed. These were described by Peterson (1962) who was able to correlate basin subsidence with depression of the water table in the Picacho area, and the location of the earth fissures with the step from shallow pediment cover to deep basin fill. Similar earth cracks were reported from near Casa Grande by Pashley (1961).

In the Tucson area rather limited leveling data indicates that subsidence is general throughout the valley and is not limited to the area of ground water table depression, but it reaches its maximum in the area underlain by the cone of water table depression.

Causes of the subsidence generally appear to be consolidation of basin sediments, accelerated by ground water withdrawal. The evidence for movement is supplemented by observations of differential movement around the margin of the deep basin fill. Where differential movement is appreciable earth cracks and transverse gullies develop, and where the movement is minor it is reflected in the cracking of walls and foundations of houses and commercial buildings.

Bibliography for Tucson Soil Environment

Breazeale, J. F. and Smith, H. V. (1930); Caliche in Arizona; University of Arizona Agricultural Experiment Station, Bull. No. 131.

Damon, P. E., Long, Austin and Sigalov, J. J. (1963); Arizona Radiocarbon Dates, IV; University of Arizona Geochronology Contribution, No. 60.

Kidwai, Z. U. (1957); the Relationship of Groundwater to Alluvium in the Tucson Area, Arizona; University of Arizona Masters Thesis.

Lofgren, B. E. (1960); Near Surface Land Subsidence in Western San Joaquin Valley, California; Jour. of Geophysical Research, vol. 65, no. 3, p. 1053-1062.

Maddox, G. E. (1960); Subsurface Geology along Northwest Rillito Creek; University of Arizona Masters Thesis.

Pashley, E. F. Jr. (1961); Subsidence Cracks in Alluvium near Casa Grande; Arizona Geological Society Digest, vol. IV, p. 96-102.

Platt, W. S. (1963); Land-surface Subsidence in the Tucson Area; University of Arizona Masters Thesis.

Smith, G. E. P. (1938); The Physiography of Arizona Valleys and the Occurrence of Groundwater; University of Arizona Department of Agricultural Engineering, Tech. Bull. 77, p. 45-91.

Streitz, Robert (1962); Subsurface Stratigraphy and Hydrology of the Rillito Creek-Tanque Verde Wash Area, Tucson, Arizona; University of Arizona Masters Thesis.

Voelger, L. (1953); Cenozoic Deposits in the Southern Foothills of the Santa Catalina Mountains near Tucson, Arizona; University of Arizona Masters Thesis.

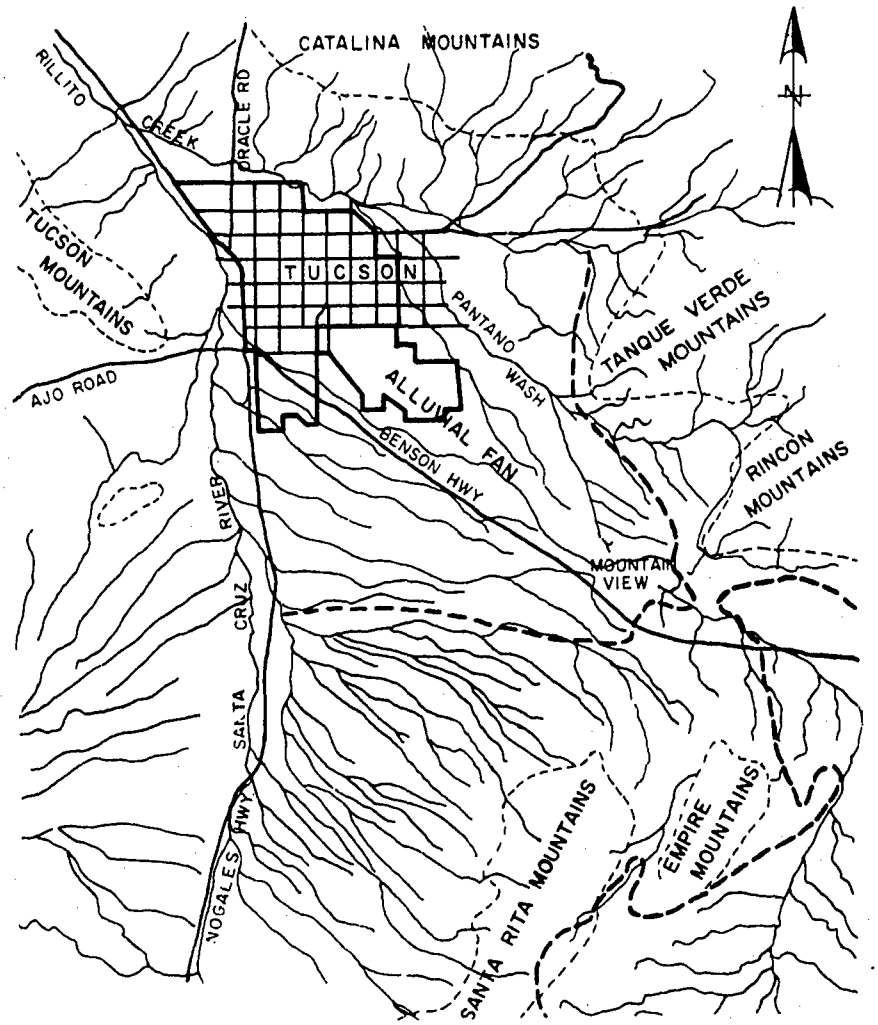

Figure B-13. Tucson area drainage pattern

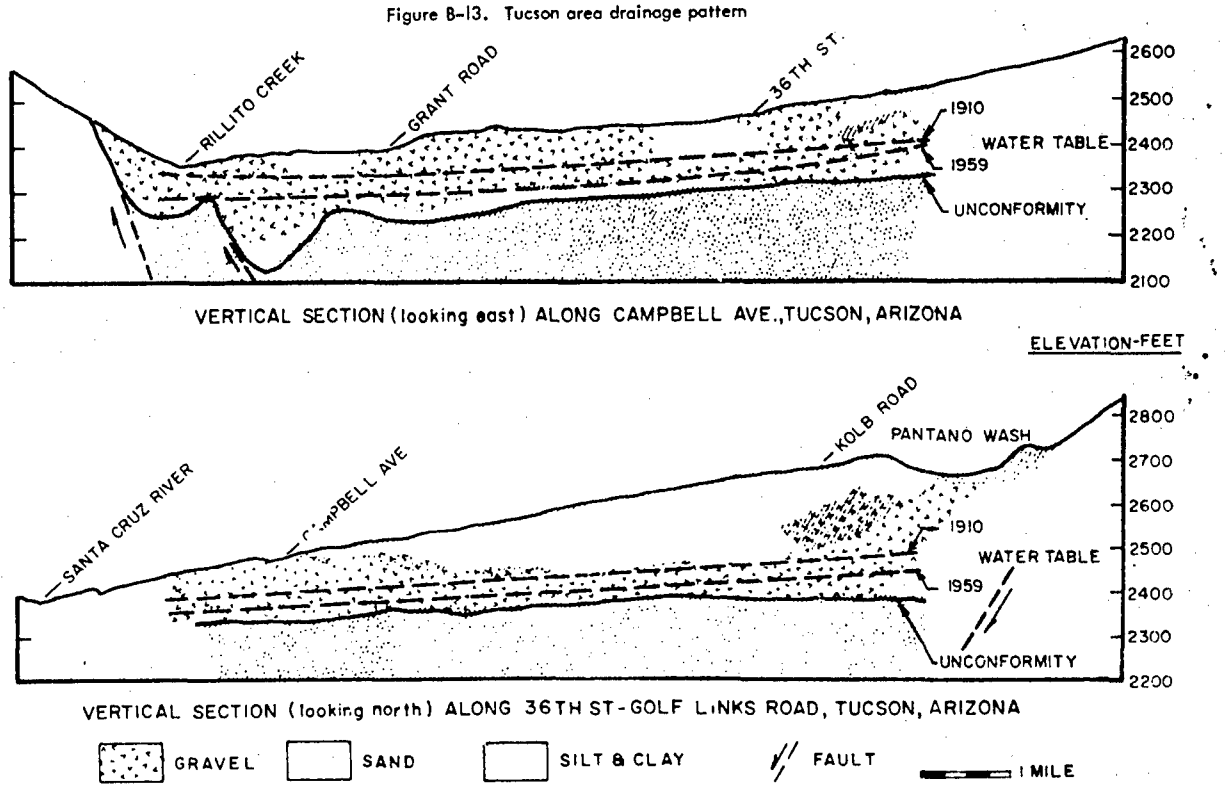

Figure B-14. Sample -- Tucson soil consistency

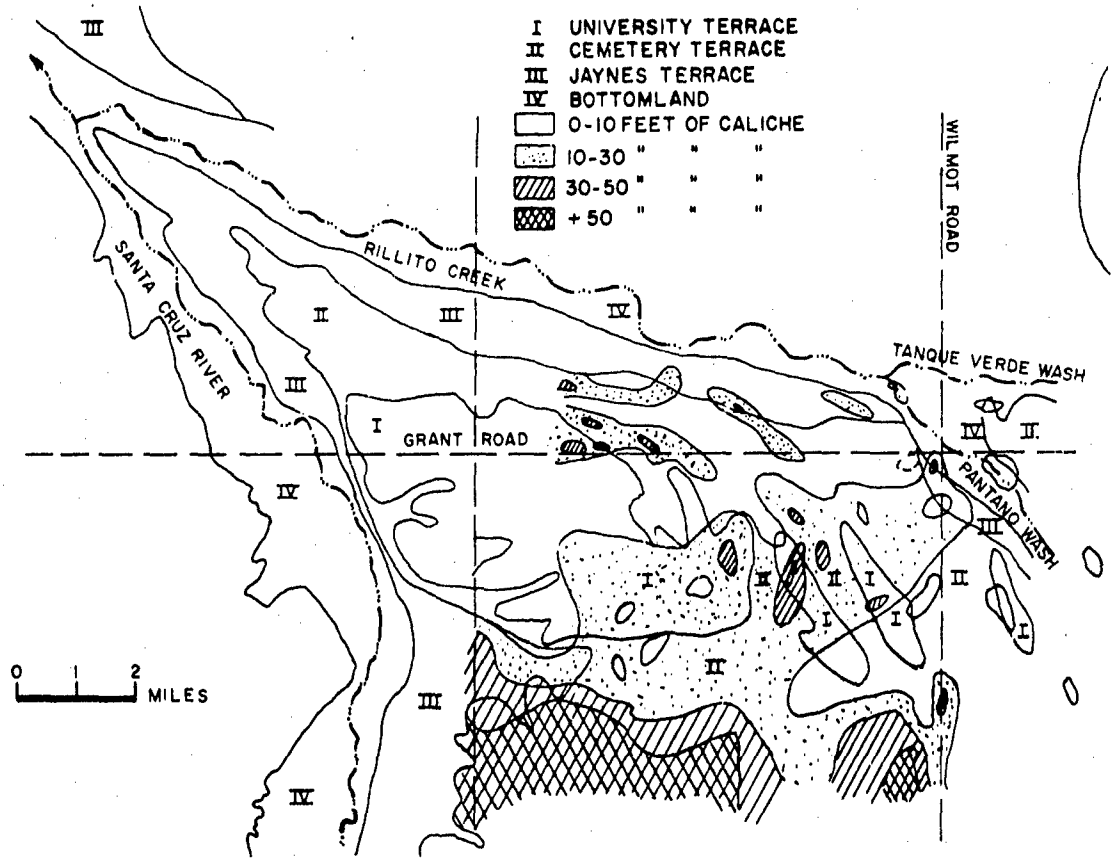

Figure B-15. Relations between physiographic divisions and caliche distribution

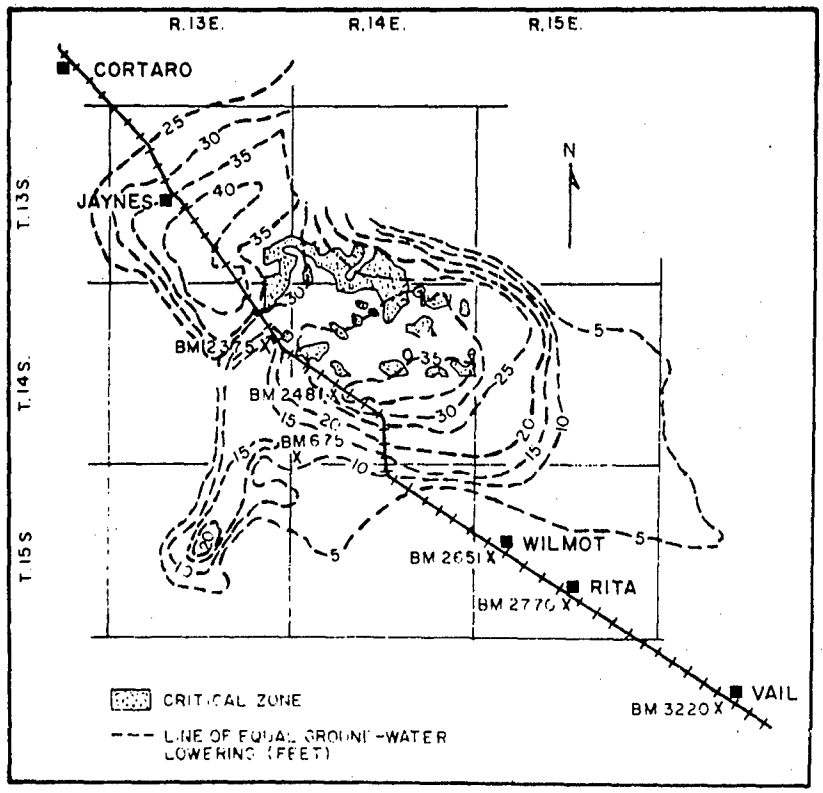

Figure B-16. Ground-water lowering in Tucson basin 1947-1959

c. Ground Waves

In a consideration of the effects of shock waves on a buried structure, an understanding of the modes of wave propagation through soil is essential. Basically, there are two types of wave motion that must be considered.

(1) Body waves. These are waves that occur below the surface and can be further classified as:

(a) Dilitational Wave. The propagation of this type body wave is through the compression and rarification of the soil particles along the axis of the shock path. Characteristic of this type wave is the movement of the soil particles in the direction of wave propagation. The dilitational body wave is described in figure B-17.

(b) Shear Wave. The propagation of this type body wave results in motion of the soil particles normal to the axis of the shock path. This wave form and particle motion is shown in figure B-17.

(2) Surface waves. These are waves that occur, as the name implies, on the surface. Surface waves are classified as:

(a) Love Wave (could be called a surface shear wave). The propagation of this type surface wave results in the lateral displacement of soil particles normal to the axis of the shock path in the plane of the surface. This wave configuration is shown in figure B-17.

(b) Rayleigh Wave. The propagation of this type surface wave results in a lateral displacement of the soil particles normal to the surface plane, similar to that of ocean waves. The displacement of the soil particles normal to the axis of the shock path is an elliptical motion. Figure B-17 also shows the Rayleigh Wave configuration.

d. Relationship of Ground Waves to Ground Motion

A contribution to both air induced and directly-transmitted ground motion due to nuclear explosion is made by the various body waves shown in figure B-17. In general, the velocity of wave propagation in an elastic medium is given by:

$$C = \sqrt{\frac{\text{ELASTIC CONSTANT}}{\text{MASS DENSITY}}}$$

e. The Dilitational Wave

To express the velocity of propagation of a dilitational wave in terms of these parameters, let us consider a cube of "elastic soil" subject to the stress and strains shown in figure B-18.

The relationships shown in figure B-18 can be written by superposition of three individual uniaxial loading conditions.

$$e_x = \frac{S_x}{E}$$

$$e_x = \frac{S_y}{E}$$

$$e_x = \frac{S_z}{E}$$

The solution of these equations for the stresses yield the relationships shown at the bottom of figure B-18.

The motion characteristics of a dilitational wave propagating in the z direction is defined by the following conditions:

$$e_x = e_y = 0$$

$$e_z = 0$$

which yield:

$$S = \frac{E(1-\mu)}{(1-2\mu)(1+\mu)} e_z$$

or the stress-strain ratio and hence the elastic constant is:

$$\frac{E(1-\mu)}{(1-2\mu)(1+\mu)}$$

$$\text{velocity of the dilitational wave} = \sqrt{\frac{E(1-\mu)}{(1-2\mu)(1+\mu)\rho}}$$

f. The Shear Wave

The motion characteristic of a shear wave propagating in the z direction is defined by the following elastic condition:

$$\frac{\text{Shear Stress}}{\text{Shear Strain}} = G = \frac{E}{2(1+\mu)}$$

from which it follows that velocity of shear wave $= \sqrt{\frac{E}{2(1+\mu)\rho}}$

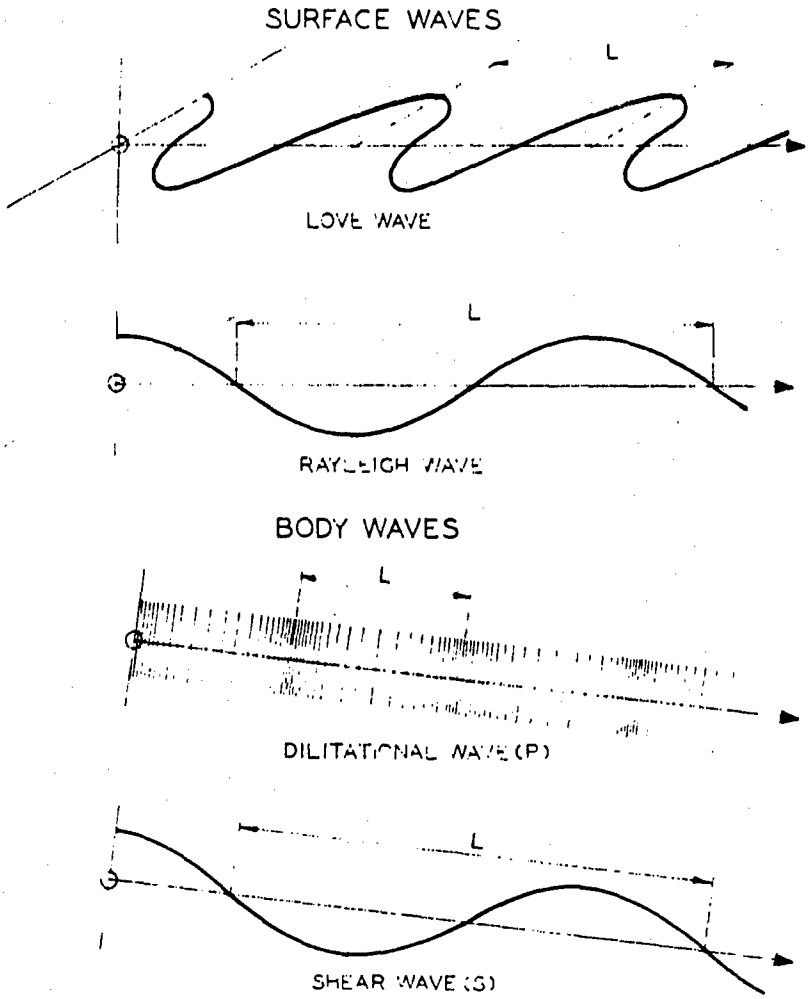

Figure B-17. Types of Waves

g. Modulus of Elasticity

It is apparent from the previous relationships, used to define the velocity of pressure waves in a soil mass, that the elastic constants of soil are of utmost importance. Since soil is not an elastic medium, but instead is a "locking" medium, and because it will be necessary to idealize this property of soil; an additional discussion of the elastic properties of soil will be presented.

The analysis of stress and strain in an isotropic, elastic, homogeneous medium shows these two parameters to be related through the modulus of elasticity. For steel, the classic example, this relationship is shown by the familiar stress-strain curve where the slope of the line in the elastic portion of the curve is the Modulus of Elasticity and the shaded area is a measure of the rebound or absorbed energy (figure B-19).

For soil there is no such "elastic portion" to the stress-strain curve even though in the usual analysis of earth shock, soil is considered an isotropic elastic, homogeneous material. The stress-strain curve for a typical soil takes the configuration shown in figure B-20.

In this figure we notice that there is no constant modulus on what we might consider the "elastic portion" of the curve. We also note that for the same amount of strain, the rebound or absorbed energy for soil is far less than that for steel as is the total energy or toughness. And, since soil is so nonhomogeneous, it is probable that there are certain soil characteristic properties which modify the modulus of elasticity of the soil. Figures B-21 and B-22 illustrate the effect of water content on the modulus of two soil types. Figure B-21 shows results obtained experimentally by D. D. Barkan, and Figure B-22 shows the results of a theoretical study.

From these considerations it becomes apparent that for soil, the modulus of elasticity must be experimentally obtained for the specific soil conditions and load characteristics used. The following sections will deal with the methods presently available for evaluating the necessary elastic properties of soil. The "constrained" modulus of elasticity will be the first property discussed since the velocity of the compression wave through the soil is dependent upon it.

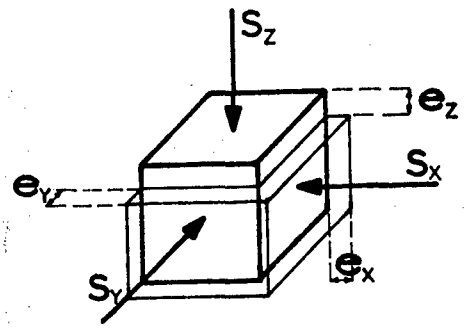

$$e_x = \frac{1}{E}\left[S_x - \mu\,(S_y + S_z)\right]$$
$$e_y = \frac{1}{E}\left[S_y - \mu\,(S_x + S_z)\right]$$
$$e_z = \frac{1}{E}\left[S_z - \mu\,(S_x + S_y)\right]$$

The solution of the equations for the stresses yields the following:

$$S_x = \frac{E}{(1-2\mu)(1+\mu)}\left[(1-\mu)\,e_x + \mu\,(e_y + e_z)\right]$$
$$S_y = \frac{E}{(1-2\mu)(1+\mu)}\left[(1-\mu)\,e_y + \mu\,(e_x + e_z)\right]$$
$$S_z = \frac{E}{(1-2\mu)(1+\mu)}\left[(1-\mu)\,e_z + \mu\,(e_x + e_y)\right]$$

Figure B-18. Stress-Strain Relationship

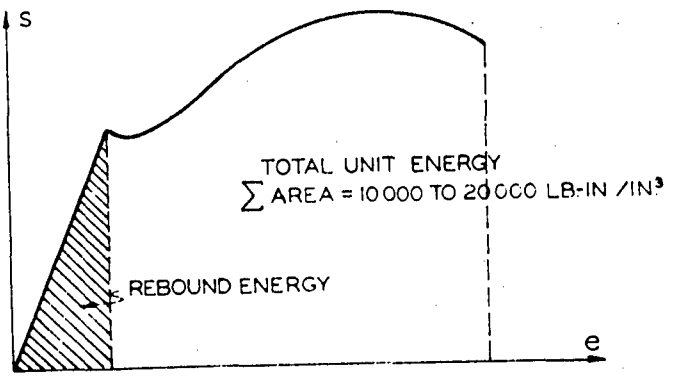

Figure B-19. Stress-Strain Diagram

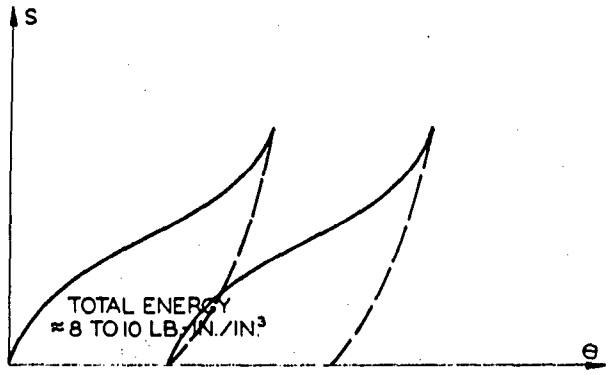

Figure B-20. Stress-Strain, Typical Soil

h. Determination of the Constrained Modulus

Since several soil phenomena (e.g. sample disturbance, preload, lateral confinement, saturation...) effect the elastic constant of soil, the approach is to define an upper and lower bound for the elastic constant. Then, depending upon the stress level expected, which in turn depends upon the above mentioned soil phenomena, certain ranges of the elastic modulus will be chosen which best fit the situation.

Thus, the immediate problem is to define the upper and lower bounds of M for any given soil type. This is accomplished by performing two tests:

(1) Seismic. This test will yield the upper bound of M. It entails setting off a subsurface charge and measuring the seismic velocity. This value v_s is then set equal to $\sqrt{\frac{M}{g}}$. Once the in situ density of the soil has been determined, the equation $v_s = \sqrt{\frac{M}{g}}$ can be solved for M. If the soil is uniform, this value will be constant; if the soil is layered, M will vary as a step function with depth.

(2) Static. This test will yield the lower bound of M. This test can be performed by any of the three methods listed below:

(a) Unconfined Compression Test. This test will in general, yield the results shown in figure B-21.

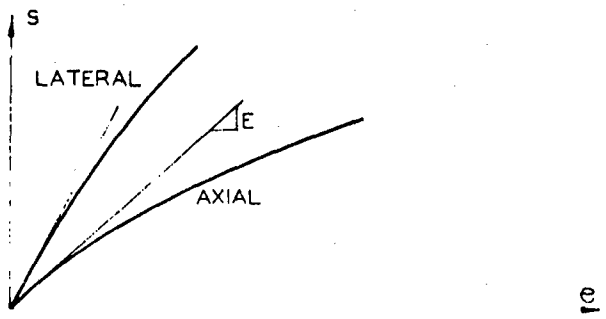

Figure B-21. Compression Test Curves

The ratio of the initial or lateral tangent modulus to the axial tangent modulus will determine Poisson's Ratio, (μ). From this one can compute $M = \frac{E(1-\mu)}{(1-2\mu)(1+\mu)}$. Some authors consider a reasonable value of M to be two or three times the initial tangent modulus.

(b) Triaxial Test. Results of this test, tempered by the confining pressure effects, will take a similar form. The effect of the lateral pressure will be to increase the modulus of elasticity. Figure B-22 shows a typical effect of the confining lateral pressure on the initial tangent modulus of a clayey silt. Some investigators suggest that a reasonable value for the constrained modulus can be obtained by doubling the value obtained from the triaxial test.

(c) Confined Compression Test. This test is run with a consolidometer. The slope of the stress-strain curve in this case is a direct determination of M. Such results, however, should be interpreted with a great deal of care for the soil phenomena previously mentioned have a pronounced effect in this case. The best procedure would be to use the results of this test in conjunction with either the triaxial or unconfined compression test results.

Once the seismic and static results have been obtained, a composite graph of depth vs M is made to define the desired ranges of M. Figure B-22 illustrates a typical relationship between depth and the constrained modulus M.

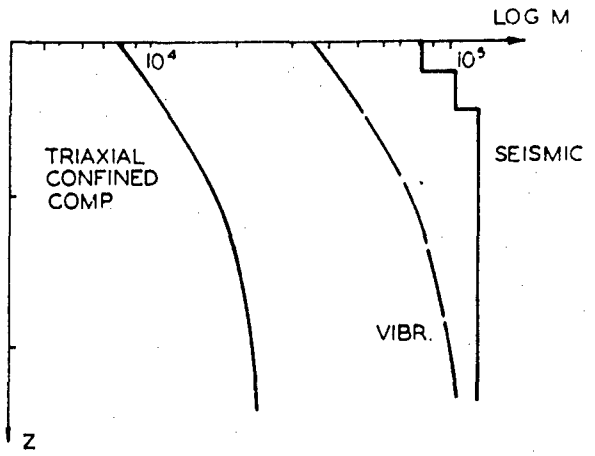

Figure B-22. Triaxial Confined Compression

In order to better define the selected modulus curve as it approaches the upper bound, another test can be run. This is the vibration test and is performed by taking a cylinder of soil (which may or may not be subjected to a confining pressure) and then propagating dilitational waves in the specimen until resonant frequency is obtained. Then shear waves are applied until resonant frequency is found. The former procedure yields a value ($E = C \omega f_d^2$) , Young's Modulus, while the latter procedure yields ($G = B \omega f_s^2$), Shear Modulus. These two values are used to compute Poisson's ratio which in turn is used to compute the constrained modulus (M). See figures B-23 and B-24.

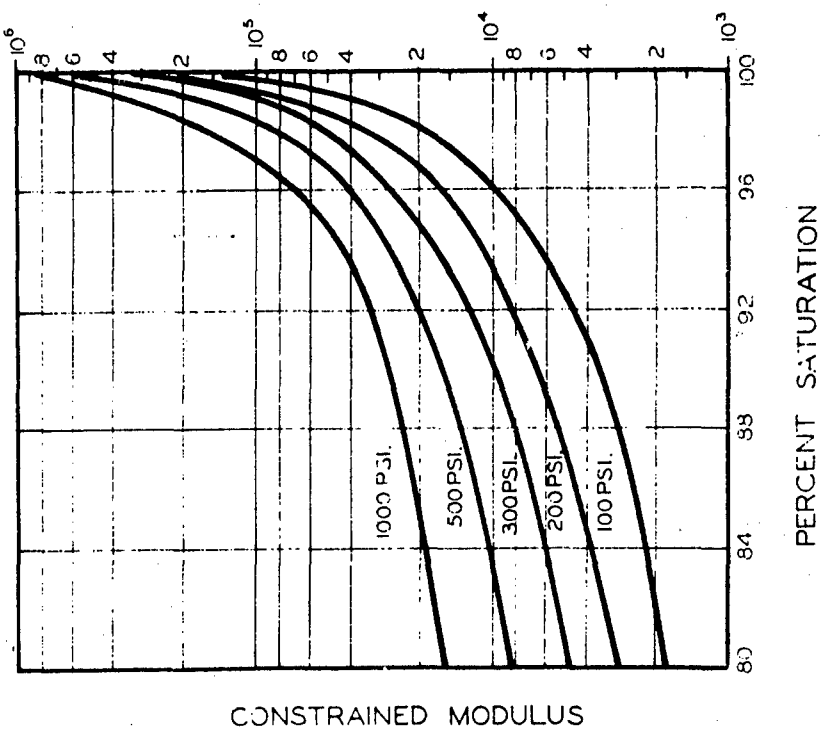

Figure B-23. Constrained Modulus Saturation

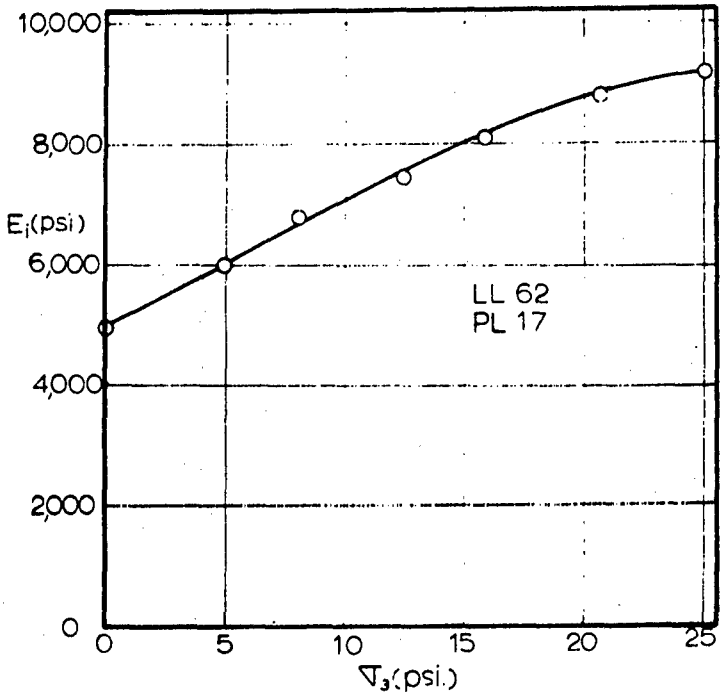

Figure B-24. Modulus of Elasticity vs Lateral Pressure

Listed below are typical values for seismic velocity, Young's Modulus and Poisson's Ratio for a number of various soil types. When specific test data are unavailable, the values may be used for preliminary computions, however they should not be used in lieu of such test data.

TABLE B-I

Soil	E (psi)		μ	
Good Granite	4.5×10^6	8.3×10^6	.15	.24
Bad Granite	1×10^6	2×10^6		
Limestone	3×10^6	7×10^6	.16	.23
Sandstone	2×10^6	4×10^6		
Dense Sand-Gravel	15×10^3	30×10^3		
Dense Sand	7×10^3	12×10^3	.3	.35
Loose Sand	1.5×10^3	3×10^3		
Hard Clay	1×10^3	2×10^3		
Semi-Plastic Clay	600	1200	.4	.45
Liquid Plastic Clay	200	600		
Liquid Clay	75	500		

The evaluation of the constrained modulus M is the most important step with respect to the dynamic loading problem, for it has a direct effect upon soil displacement as well as shock wave velocity computations. This will be shown in a later section.

i. Soil Pressures

As pointed out previously, the range of constraint modulus (M) to be used in a given situation depends upon the stress level expected at each depth under consideration. It is, therefore, necessary to study the theoretical distribution of stress and the modifications necessary for the applications to Soil Medium. The classical equations of Boussinesq are shown in figure B-25, with the usual simplification applied to the equations for stress in the x and y directions.

Referring to the figure, it is seen that for $x = y = 0$, the stress in the z direction directly under the load varies inversely as the square of the depth. The foregoing discussion treats the surface loads as instantaneous static loads. To evaluate the variation of subsurface stress with time, since the magnitude of nuclear blast overpressures are a function of time, we need only to integrate Boussinesq's equations over the varying distributed surface loading.

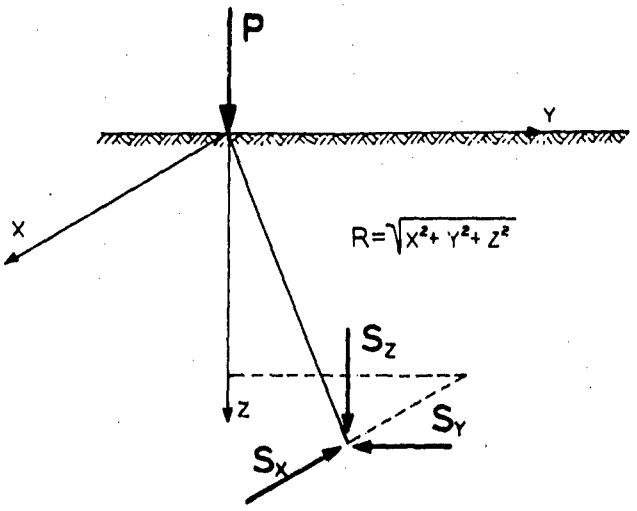

$$S_z = \frac{3Pz^3}{2\pi R^5}$$

$$S_x = \frac{P}{2\pi}\left[\frac{3x^2z}{R^5} - (1-2\mu)\left(\frac{x^2-y^2}{R(x^2+y^2)(R+z)} + \frac{y^2z}{R^3(x^2+y^2)}\right)\right]$$

$$S = \frac{P}{2\pi}\left[\frac{3y^2z}{R^5} - (1-2\mu)\left(\frac{y^2-x^2}{R(x^2+y^2)(R+z)} \quad \frac{x^2z}{R^3(x^2+y^2)}\right)\right]$$

For $\mu = \frac{1}{2}$

$$S_x = \frac{3Px^2y}{2\pi R^5} \qquad S_y = \frac{3Py^2x}{2\pi R^5}$$

Figure B-25. Boussinesq Equation

Figure B-26 indicates the vertical stress distributions in a soil due to a uniform surface pressure. This figure shows the variation in distribution of pressure with depth and also with radial distance from the center of the loaded area. The two tenths (0.2) isobar, or line of equal stress is also shown in this figure.

With these notions of stress distributions in mind, we can now proceed to a discussion of the relationship between the horizontal and vertical pressures resulting from a pressure wave.

Having analyzed the three-dimensional characteristic of stresses and strains, apply these stress-strain conditions to a dilitational wave propagating in one dimension only, with no lateral strains resulting in the other two directions. This brief analysis can then be used to determine a relationship between the magnitude of the longitudinal pressure wave and the induced lateral pressure resulting from the pressure wave. From three dimensional analysis, $e_x = \frac{1}{E}\left[S_x - \mu\,(S_y + S_z)\right]$

But if the wave travels in the z direction only, then:

$e_x = e_y = 0$ $\qquad S_x = S_y = S_{lateral}$ $\qquad S_z = S_{axial}$

Therefore, $S_{lateral}(1-\mu) - \mu S_{axial} = 0$ $\qquad$ or $\qquad \frac{S_{lateral}}{S_{axial}} = \frac{\mu}{1-\mu} = K$

This is the relationship obtained between Poisson's Ratio and K from a three dimensional stress approach. This value of K is used to relate the lateral induced stress to the axial pressure wave by: $S_{lateral} = K\,S_{axial}$

This elasticity approach should be kept in mind so that it can be compared with the typical Mohr envelope analysis. The use of an experimentally obtained Mohr envelope to determine the relationship between axial and lateral pressures is a classical approach and assumes incipient motion. This approach also can include the effects of the various experimentally obtained soil properties on the axial and lateral pressure relationship.

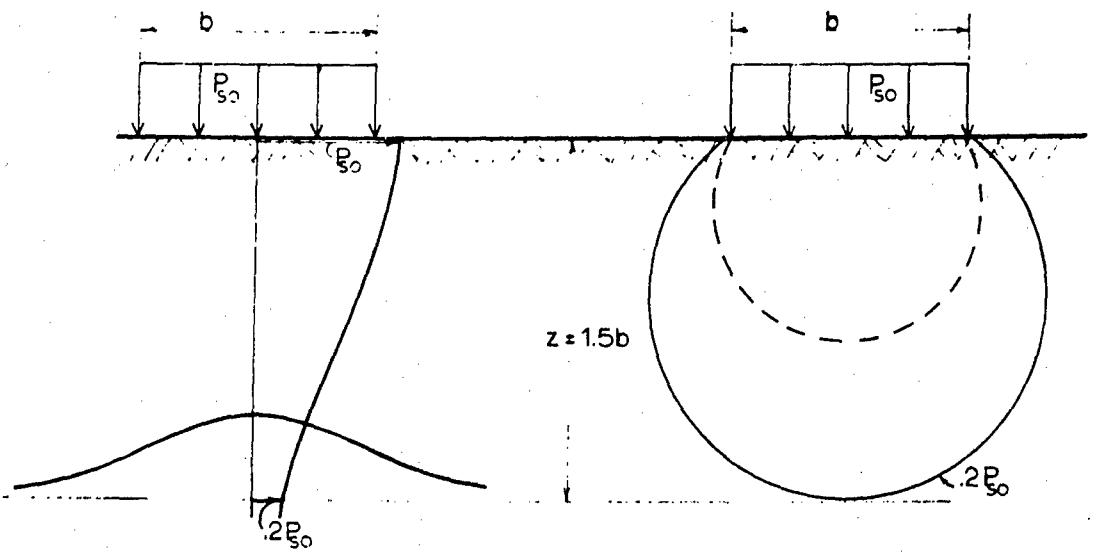

Figure B-26. Vertical Pressure Distribution

When the lateral strains are induced as shown (on the left) in figure B-27, the resulting horizontal pressure is related to the applied vertical pressure by the relationship $S_h/S_v = \frac{1-\sin\phi}{1+\sin\phi}$. This is known as the "active condition."

When inward strains occur, as shown (on the right) in figure B-27 by the action of the horizontal pressure, the resulting relationship is: $S_h/S_v = \frac{1+\sin\phi}{1-\sin\phi}$. This is known as the "passive condition."

A K value of unity indicates hydrostatic action. This topic can be treated from this aspect and relate K to the static angle of internal friction of a soil--rather than to Poisson's Ratio (μ). Consider Mohr's Circle of Stresses for a cohensionless soil as shown at the bottom of figure B-28. The relationship between the principal stresses is easily obtained and is shown beneath the figure. This is, of course, the active coefficient Ka which was discussed above. To derive this relationship, the triangle bounded by the envelope, the x-axis, and the radius yields:

$$\sin\phi = \frac{\frac{S_1 - S_2}{2}}{\frac{S_1 + S_2}{2}}$$

$$S_1(\sin\phi - 1) = -S_2(1+\sin\phi); \quad \frac{S_1}{S_2} = \frac{1+\sin\phi}{1-\sin\phi}$$

but, $$K = \frac{\sigma_{lateral}}{\sigma_{axial}} = \frac{S_2}{S_1} = \frac{1-\sin\phi}{1+\sin\phi}$$

On reconsideration of the elasticity relationships shown in figure B-18, a two dimensional field can be considered and the equations reduce to:

$$e_x = \frac{1}{E}(S_x - S_z)$$

Thus, if the dilitational wave travels in the horizontal direction only, we see that:

$$e_x = 0$$

$$S_x = S_{lateral}$$

$$S_z = S_{axial}$$

from which, $$0 = \frac{1}{E}(S_{lateral} - \mu S_{axial})$$

or $$\frac{S_{lateral}}{S_{axial}} = \mu$$

The difference between the two dimensional analysis and the three dimensional analysis is shown in figure B-28. With this background we can not approach the problem of soil displacements, velocities and accelerations.

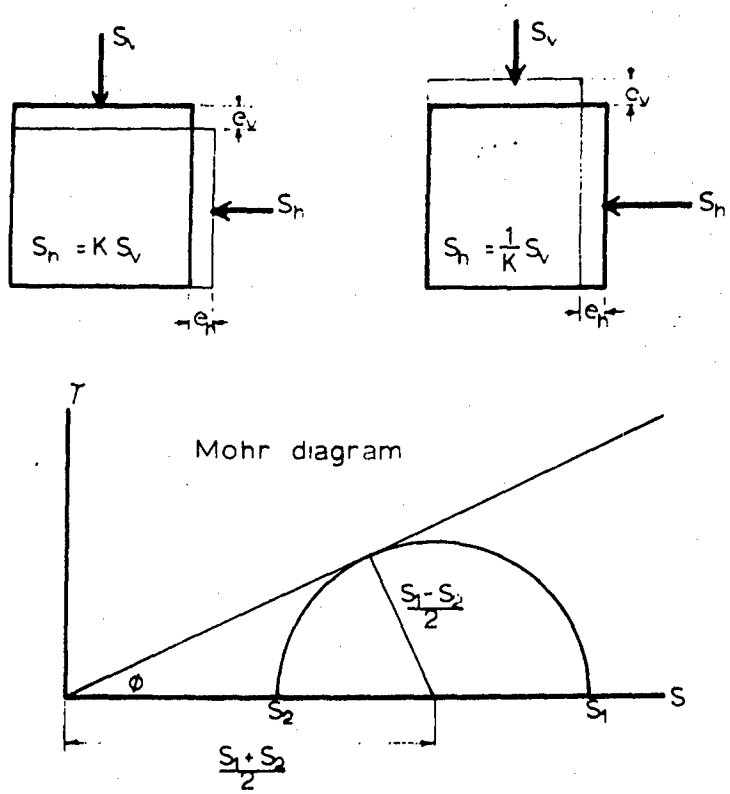

$$K = \frac{S_2}{S_1} = \frac{1 - \sin \phi}{1 + \sin \phi}$$

Figure B-27. Deformation Condition

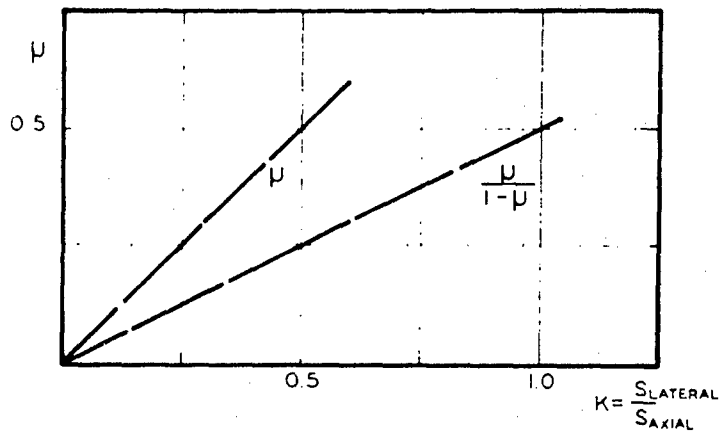

Figure B-28. Two Dimensional vs Three Dimensional Analysis

3. Ground Shock

The subject of ground shock is rather complex and in general not readily approached by a realistic theoretical analysis. The complexity results from the problem of correctly analyzing the source and of predicting the response of the nonhomogeneous, nonelastic, nonisotropic soils material. However, the two sources of ground shock are: the direct transmitted earth shock; and the air blast induced ground shock. The first is applicable only for surface and underground bursts and originates at the center of the explosion. The second results from the high overpressure blast wave as it travels outward from the explosion point subjecting the ground to a large surface pressure. The direct transmitted wave is accompanied by large plastic deformations within a few crater radii and is, therefore, attenuated rapidly with distance. However, the air blast induced ground motion are dependent upon the peak overpressure and, therefore, predominate for a much greater radial distance.

Because many researchers have shown that the probability of survival does not increase much for an increase in design overpressure from 100 to 1000 psi (for a CEP of approximately one mile) and because of the increase in cost which accompanies the higher overpressure designs, the maximum side-on overpressures which we should concern ourselves with are approximately 100 to 200 psi. If this is accepted, then the distances at which these overpressures occur are well outside the range of any significant direct-transmitted ground shock. Then the problem is reduced to an evaluation of air blast induced ground shock. *

Air blast induced ground shock can be best introduced by showing an air blast wave and the resulting seismic wave and stressed soil. Figure B-29 shows this with the soil pressure wave traveling along a soil column perpendicular to the wave front. The distribution of pressure in the soil column varies from zero at the front of the wave to a maximum located some distance (K) behind the wave front to the attenuated overpressure existing at the surface. The variation of pressure from the wave front to the peak to the surface will be assumed to be linear even though it is apparent it will not be such.

The variation in pressure along the stressed soil column is the result of the nonlinearity of the stress strain characteristic of soil. Since, as discussed previously, the velocity of wave propagation is directly proportional to the modulus of elasticity of a material, it is seen that as the stress level of the wave increases the slope of the stress strain curve (the Modulus of Elasticity) decreases. Therefore, the increased stress levels of the pressure wave are propagated at slower velocities, hence, resulting in the pressure peak following the wave front.

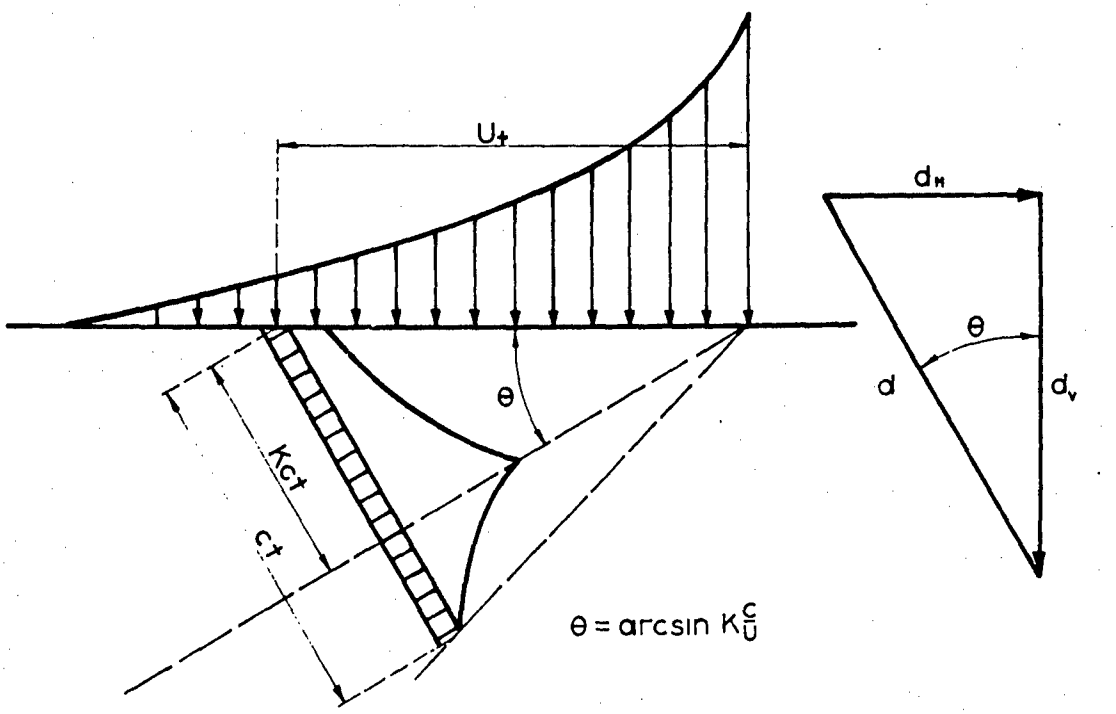

Figure B-29. Stressed Soil Column

Figure B-30 shows the real and linearized stress strain curves for soil and indicates the significance of the non-elasticity of soil. The various values of constrained modulus for the wave front (M_i), the wave peak (Mp), and the uloading cycle (Mr) will be discussed with the derivation and application to soil strains and displacements.

Figure B-31 shows a procedure presented by Wilson and Sibley for the evaluation of the constrained modulus for the determination of ground displacements. This is the same procedure discussed in Chapter 4 of the AFDM.

Once the constrained modulii have been evaluated, they can be rewritten in terms of velocity, and curves similar to those in figure B-32 can be constructed. These curves will be predominate in the evaluation of ground displacement since the determination of the location of the wave front and wave peak will be made from this graph. A step-by-step solution using this figure can be accomplished by dividing an increment of depth by the average value of velocity for the increment and summing the results to find the location of the wave front and wave peak at any time.

An example of this is shown in figure B-33. The location of the wave front and wave peak can be visually indicated by imagining a horizontal line on this figure at any time (i.e. at time 0.02 seconds) which would indicate the location of the wave front and wave peak by the intersection point of the two curves (i.e. Zi = 42 ft and Zp = 20 ft).

The movement of the wave through the soil mass and the effect of the increasing stress between the wave front and the wave peak results in strain values which are defined by the constrained modulus defined as Mp. However, the strain values for decreasing stress levels between the wave peak and the surface depend upon the constrained modulus defining the unloading cycle Mr. This will be discussed later with a discussion of the equations presented in the AFDM.

*Christensen, W. J., CDR,CE ,USN, Atomic Defense Engineering Technical Study #28, Sept., '59 (U)

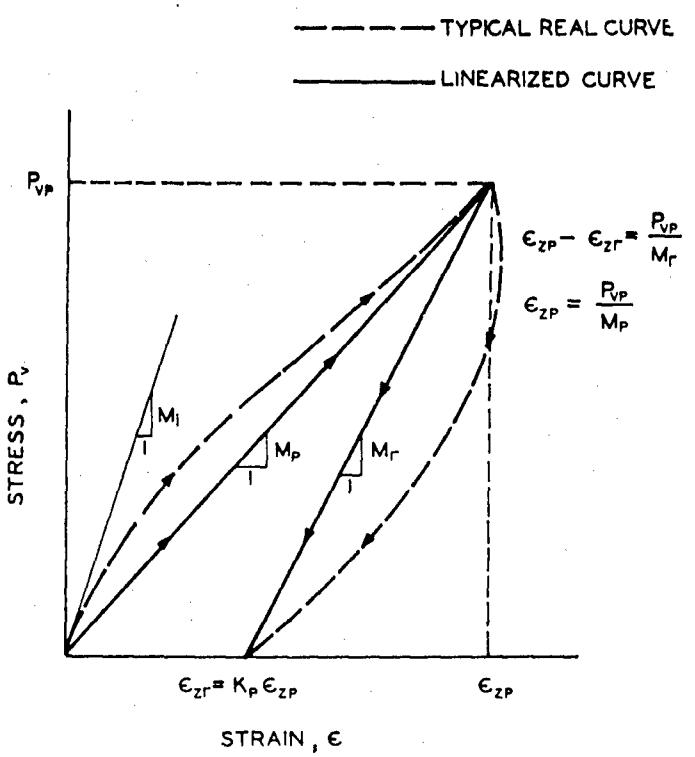

Figure B-30. Real and Linearized Stress-Strain Curves

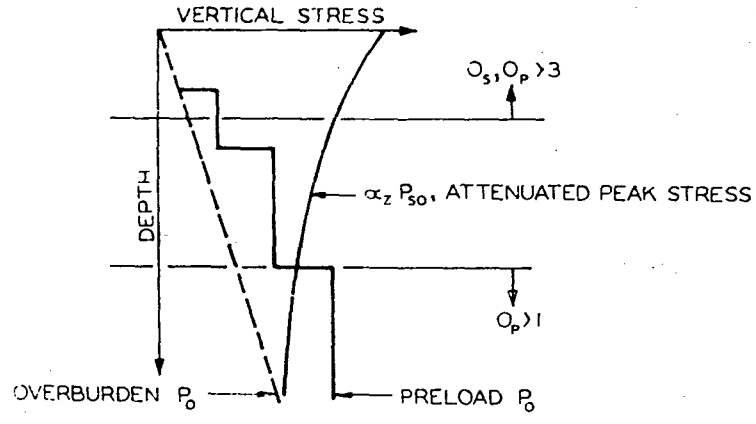

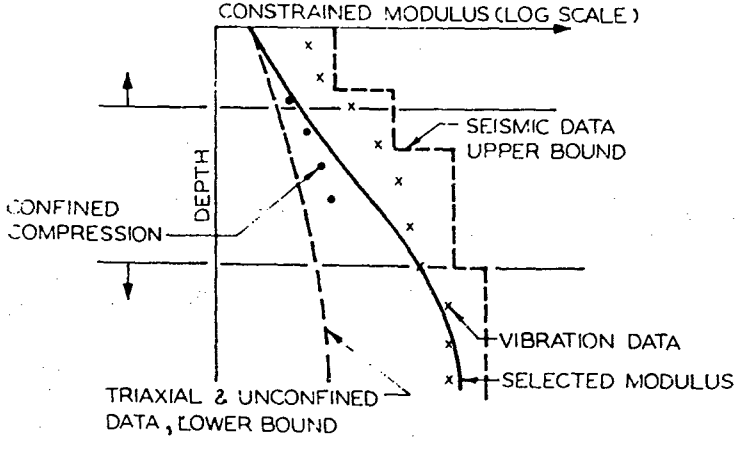

Figure B-31. Selection of Constrained Modulus

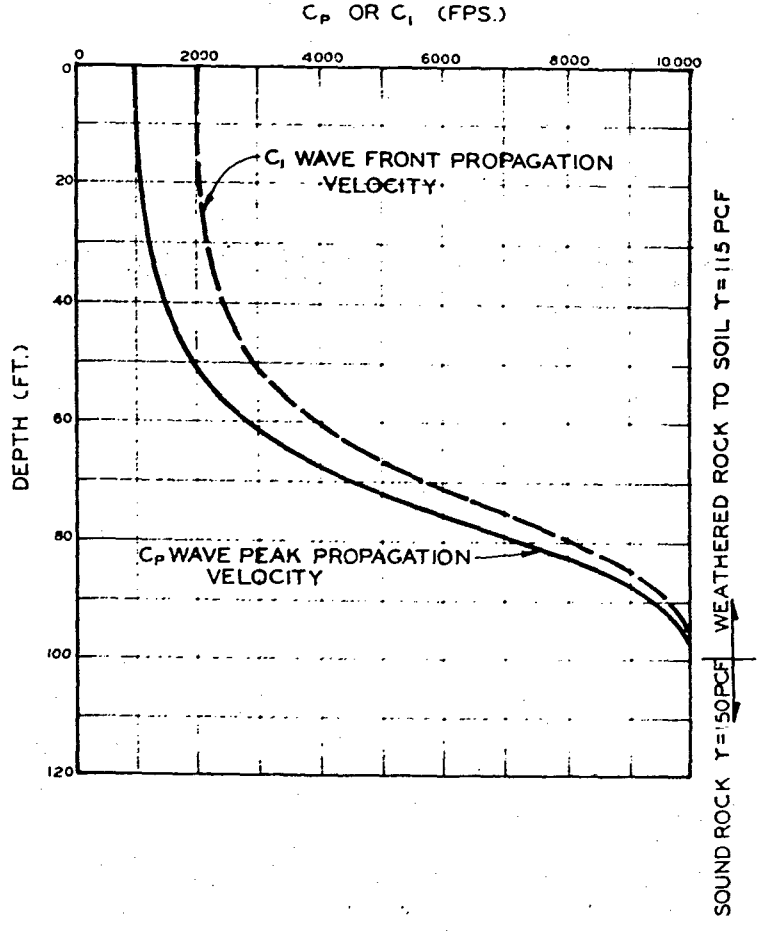

Figure B-32. Soil Parameters

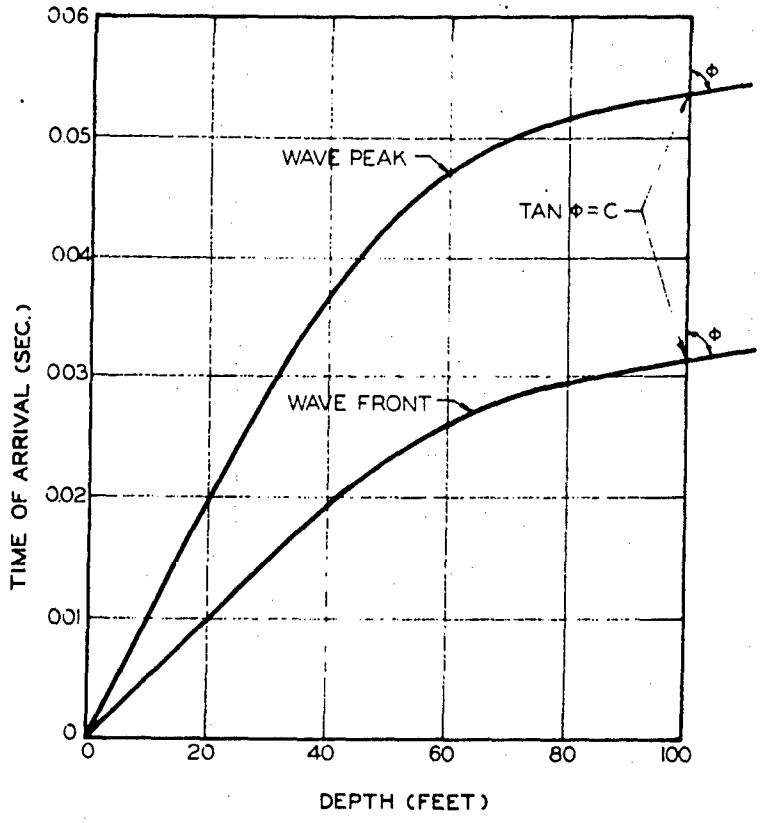

Figure B-33. Wave Form Arrival Time

A closer examination should now be made of the effect of the pressure wave on the soil at any particular depth. Figure B-34 shows graphically the location and configuration of the pressure wave when the wave front has just reached a depth Za. Shown horizontally, is a stress time curve for the depth Za indicating the time during which the pressure rises from zero to its maximum value (referred to in the figure as a rise time). It is during this period of time that the detrimental velocities and accelerations will occur. It is apparent then that the relative location of the wave front and wave peak are important in ground motion study. They in turn, however, are dependent upon the correct evaluation of the stress strain characteristics of the soil.

Because of the nonlinearity of the stress-strain relationship of soil it is apparent that the profile of the stress wave and the profile of the strain wave are not proportional. Figure B-35 shows qualitatively the distribution of stress in the stress waves and the distribution of strain in the strain waves. The envelope of the stress at the wave peak is defined by the attenuation of the pressure with depth. The approach currently being used to evaluate the attenuation of pressure is the spatial attenuation factor:

$$\alpha = \frac{1}{1 + \frac{Z}{Lw}}$$

This evaluates the pressure at any level on the basis of the Boussinesq's equations and the stress isobars resulting from the size of the loaded area. This attenuation factor is conservative since it does not include any loss due to visco-elastic or plastic deformation, which is bound to occur.

The results of this procedure of obtaining soil displacements by using a summation of successive static solutions based on soil parameters for dynamic loadings is shown in figure B-36. The total displacements are shown for the surface and for a depth of 100 ft, and the relative displacement of the two are also shown.

The University of Arizona has created a computer solution using this approach. A comprehensive evaluation of the effect of various relative values of Mp, Mr, and Mi in the evaluation of ground shock has been undertaken. A description of this solution is presented after Soil Structure Interaction.

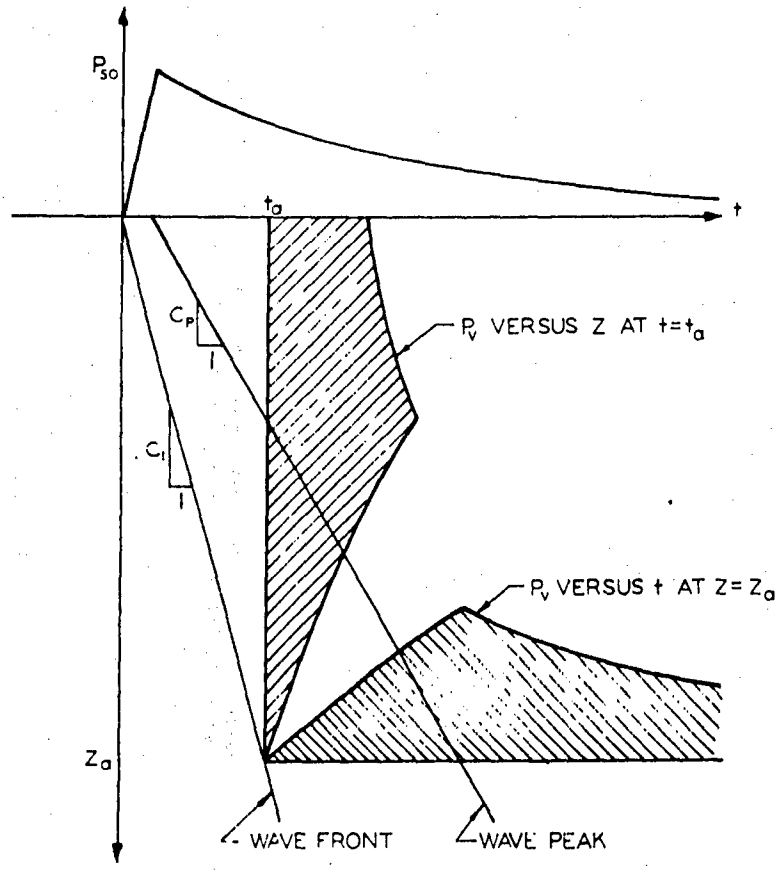

Figure B-34. Change of Wave Form With Depth

4. Soil Structure Interaction

It is well known that flexible thin-wall structures which normally exhibit a very limited load carrying capacity, have a very large load carrying capacity when surrounded by soil. This principle is used in the design of culverts, pipeline casing, and flexible bulkheads for highways and other earth embankments. The "nuclear age" has recently focused new attention on this phenomena because of the problem of underground shelters. Unfortunately, however, not enough is known about this soil-structure interaction to predict the ultimate load carrying capacity of such an underground structure with any degree of accuracy. The Bureau of Yards and Docks has made substantial progress in the area of soil-structure interaction on culverts, but little has been done on structures of other configurations.

The studies undertaken at the University of Arizona as a part of this research project have as an objective the evaluation of the soil structure interaction and, therefore, an evaluation of the load carrying characteristics of the various basic possible shelter configurations. The studies are divided into two parts since the soil can beneficially assist the structure in two basic ways. First, the soil can restrict the deformations of the structure and, therefore, increase the mode of failure and the failure load; or in addition, the soil pressure can redistribute over the structure according to the degree of flexibility of the various parts of the structure and usually increase the ultimate load. Second, the pressure can redistribute around the structure by an "arching action" to the adjacent soil, therefore allowing a greater proportion of the load applied to the soil-structure system to be carried by the soil and less by the structure. These simplifications of the complex problems which involve the composite action of the soil and a structure, constitute the phenomena of "soil-structure interaction."

Because of the expense and time necessary to conduct full scale tests, and because of the valuable knowledge obtained from simple laboratory tests conducted to failure, the studies conducted at the University of Arizona apply the theories of model testing to the evaluation of the basic possible shelter configurations by small simplified models.

The study of soil-structure interaction has been divided for the research into the following two phases:

a. The first phase deals with the structural benefication resulting from the restricted deformation and redistribution of pressures occurring as a result of the soil-structure interaction. This was done by using tension membranes, therefore eliminating the variable of the change in mode of failure, which would isolate the problem of the redistribution of pressure. These tension membranes used in conjunction with the membrane theory allow a very complete evaluation of the way in which the deformation of a structure changes the distribution of soil pressure action against the structure. This is a very important concept, since a vertical pressure acting against the roof of a shelter may be increased by blast overpressure by an amount which exceeds the load carrying capacity of the structure. However, as the roof deflects under the increase in pressure, shear stresses are developed in the soil and the resulting arching causes a portion of the load to be transferred to the edge of

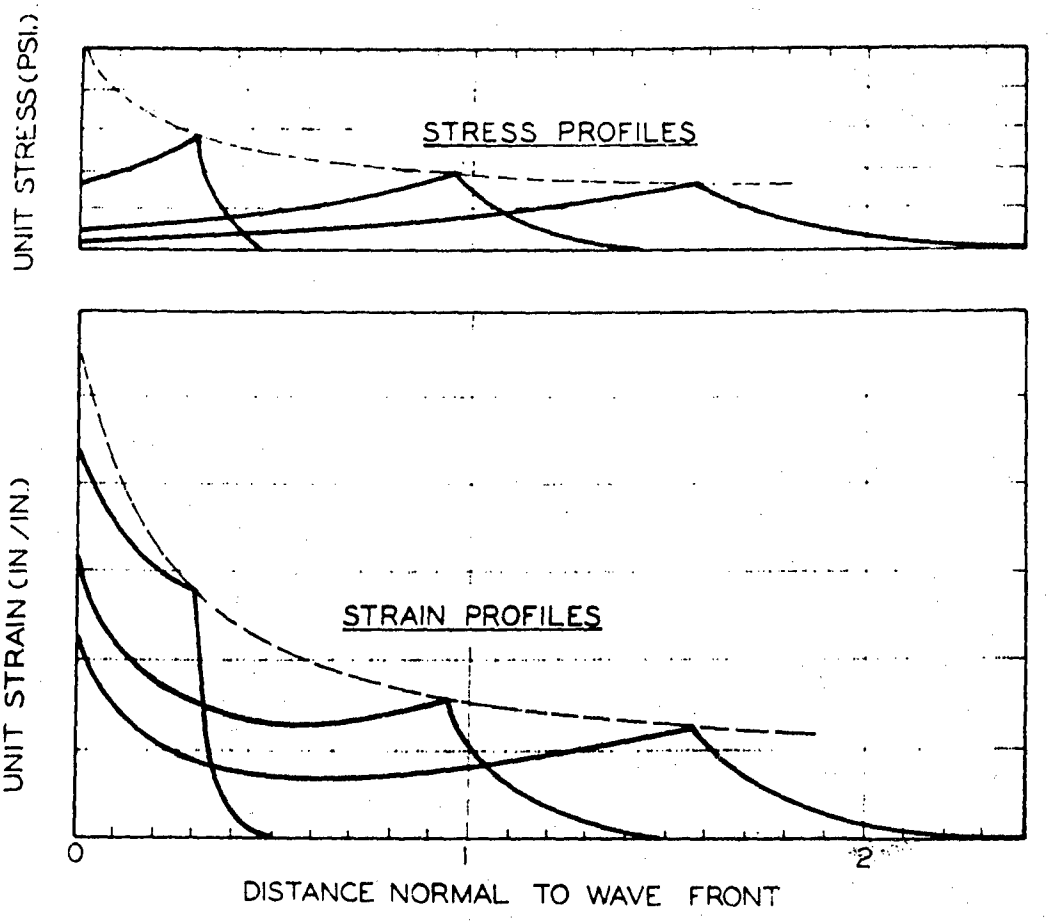

Figure B-35. Stress and Strain Distribution

the roof where it has less detrimental effect. Therefore, although the average earth pressure is greater, due to the blast overpressure, the distribution has been changed so that the stresses in the structure are less than would be expected under normal distribution. This characteristic of soil-structure interaction is evaluated by loading buried flat circular membranes made of a ductile metal with a blast overpressure whose rise time and maximum pressure simulate a nuclear blast. The deformations and principle curvatures of the resulting deflected membranes are then used to evaluate the distribution of pressure on the structure.

b. The second phase is that in which the redistribution of the total load applied to the soil-structure system is evaluated to determine the relative proportion carried by the structure and by the soil. This little known phenomena was pioneered by Marston and Spangler and is still not completely understood even for static loading conditions. Therefore, the research undertaken in this area is based on evaluation of the distribution of load to the soil and the structure for the static condition and an extension of these results to dynamic blast loadings. The same type of circular membrane structure is being used in this phase in order to maintain a closer correlation between the two phases of this study. In this phase, the model structure is buried in a container of soil and the overpressure is applied statically. The evaluation of the distribution of pressure, as discussed later, is then determined by measuring the amount of load transmitted to the structure and to the soil mass.

The two types of soil-structure interaction are shown in figure B-37. The pressures shown on the roof of the structure and at roof level in the surrounding soil are the subject of research presently being conducted at the University of Arizona and represent qualitatively the results obtained thus far.

The redistribution of pressure on the structure is adequately described by the approach presented in the AFDM. The assumptions used in the derivation and the resulting attenuation formulas are described in figure B-38. An arbitrary maximum deflection to span value of 0.02 is used in this approach. This value (0.02) represents a maximum shear strain across the top of the structure of 4%. This agrees well with the results obtained in our laboratories and the results obtained from these equations also correlate well with our experimental results.

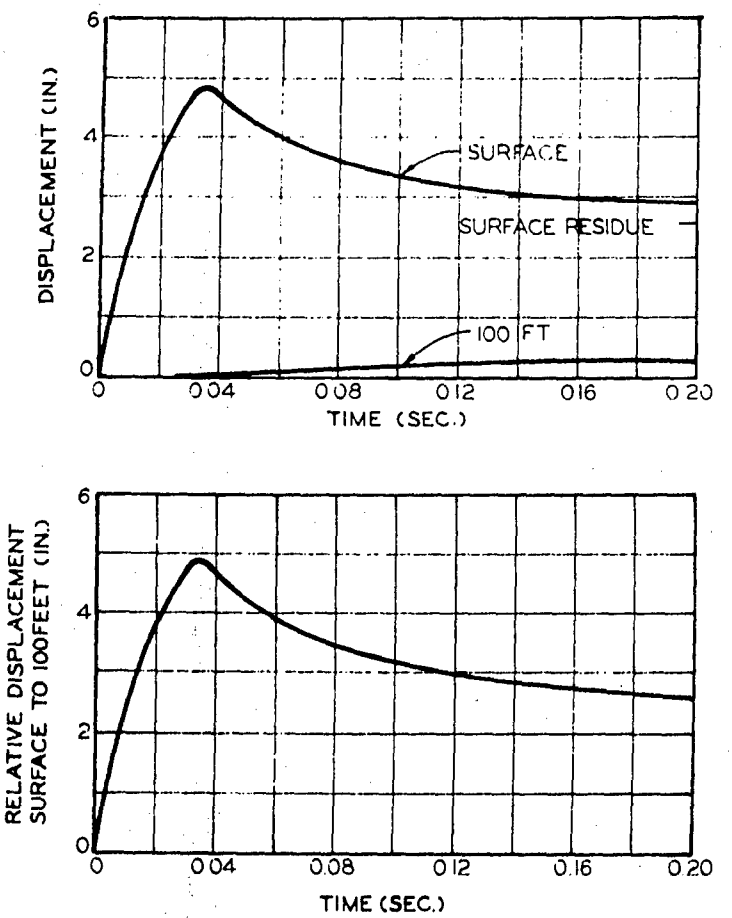

Figure B-36. Displacement - Time Curves

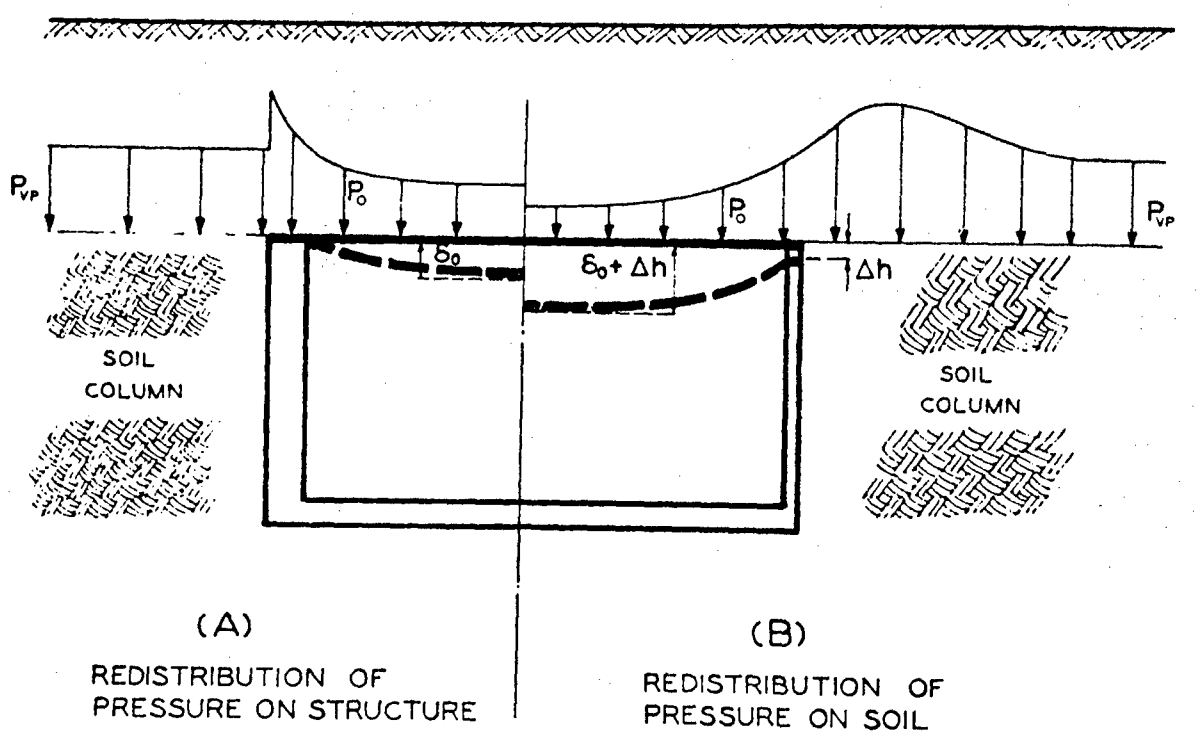

Figure B-37 Soil Structure Redistribution of Pressure

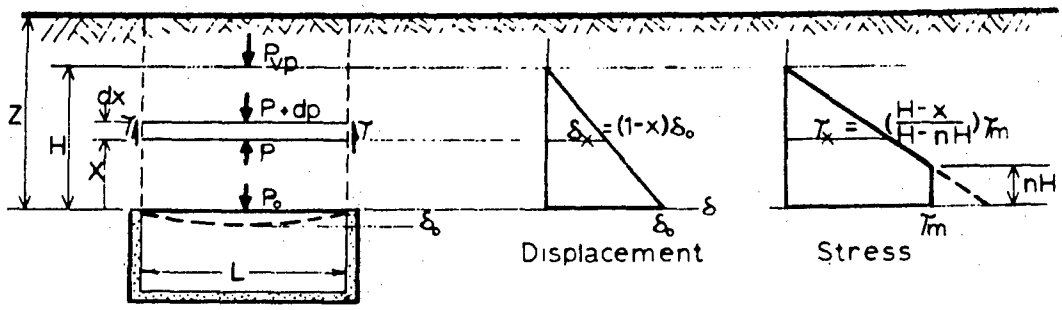

For $n \geq 0$ or $\delta_0 \geq .02L$

$$\gamma = \frac{1+n}{2}\gamma_m \quad \text{and} \quad \frac{P_o}{P_{vp}} = \frac{1 - \frac{1+n}{4}\frac{H}{R} K \tan\phi}{1 + \frac{1+n}{4}\frac{H}{R} K \tan\phi}$$

For $n < 0$ or $\delta_0 < .02L$

$$\gamma = \frac{1}{2}\frac{\delta_0}{.02L}\gamma_m \quad \text{and} \quad \frac{P_o}{P_{vp}} = \frac{1 - \frac{H}{4R}\frac{\delta_0}{.02L} K \tan\phi}{1 + \frac{H}{4R}\frac{\delta_0}{.02L} K \tan\phi}$$

Figure B-38. Soil Arching Design Criteria

A comparison of the equations describing the attenuation of soil pressure due to soil structure interaction and experimental results is indicated in figure B-39.

In this figure: Curves (a) and (b) indicate the correlation for a structural configuration which makes use of passive pressures in the soil-structure interaction; curves (c), (d), (e), and (f) indicate the close correlation for initially flat roofs, between the AFDM procedure (Eq's 5-35 and 5-36) and the experimental results obtained in our laboratories. Curves (c) and (f) are for a total useful depth, and a useful depth of the total minus one-quarter of the span, in computing the attenuation. A useful depth of the total minus one-quarter of the span is suggested by the AFDM and it indicates close but conservative results. Curves (g) and (h) show the correlation between the total load applied to the structure and the "arching" analysis described previously. A close correlation is shown. At present, additional work is being done in this area for various types of soils. Curve (i) shows an experimental evaluation of the blast chamber and indicates the effect of the blast chamber configuration on the structural models tested; this is shown only to indicate the lack of blast chamber effect on the free-field pressure for the depths used in the study.

5. Free Field Ground Displacements

a. Introduction

To obtain order of magnitude of free field ground displacements, a computer program was developed to determine the vertical displacement versus time as a function of soil properties and the weapon parameters. This program was based on one-dimensional wave propagation equations and included nonlinear properties of the soil medium. As a result, residual displacements as well as peak displacements were determined for the surface and at various depths.

The governing equations and the computer flow diagram are presented in the following section.

b. Computer Program

(I) Definitions

The data statement for this program consists of the following parameters:

Engr.	Comp.	Definition
P_{so}	PSO	Peak side-on overpressure (psi)
MT	WYM	Yield (Megatons)
---	B	Slope of the log constrained modulus vs depth curve (log e)
E_i	EMI	Seismic modulus (lbs/ft^2)
---	CK	Intercept of log constrained modulus vs depth curve (lbs/ft^2)
---	ROE	Mass density (lbs. sec^2 /ft^4)
k	SK	$(1 - M_p/M_r)$ or E_{zr}/E_{zp}
z	DZP	Size of depth increments down to the point of peak vertical pressure (Feet)
---	DIV	Any even number
---	COP	Depth at which constrained modulus equals seismic modulus

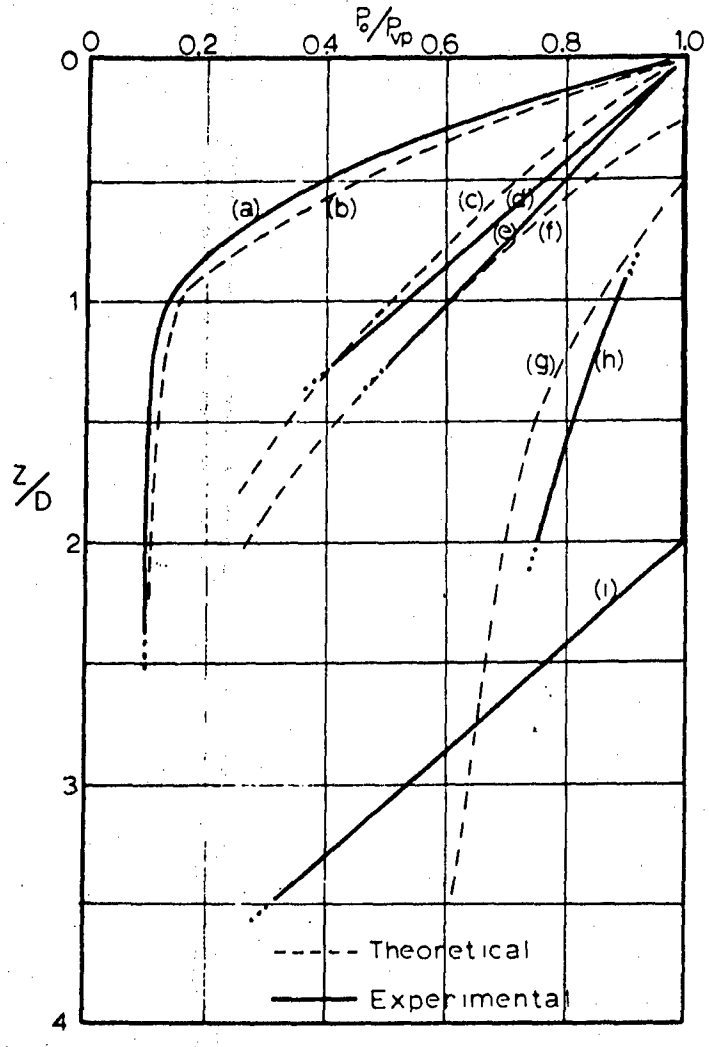

Figure B-39. Results of Soil Arching Studies

These parameters will eventually make the program general enough for use in computing the free field ground displacements at any distance from any size weapon. The only preliminary hand calculation required is that for PSO, the value of which is highly dependent upon the targeting analysis for the area under consideration. The program as it is now set up is applicable only to a PSO of 50 PSI. Work is now underway to further generalize the program to include all PSO ranging from 10 PSI to 2000 PSI.

(2) Determination of Variables

Using the results of triaxial compression tests, unconfined compression tests and seismic tests run at the University of Arizona for soil samples typical of the Tucson Valley, the log of the constrained modulus was plotted against equivalent depth. At depths where the ratio of the attenuated peak overpressure to either the overburden soil pressure or the preload pressure was greater than 3, the curve for the constrained modulus was constructed closer to the lower bound (triaxial and unconfined data). At depths where the ratio of the attenuated peak overpressure to the preload pressure was less than 1, the curve for the constrained modulus was constructed closer to the upper bound (seismic data). The interval between these end conditions was approximated by a straight line. This procedure for the determination of the resulting "selected modulus" curve is in accordance with the generally accepted method as outlined in the AFDM. In order to make this selected modulus depth relationship amenable to the computer program, an exponential equation was written to describe the variation of selected modulus with depth. This equation is no longer valid past that depth (COP) at which the selected modulus has in effect become the seismic modulus.

Since the depth COP will be a function of the particular soil type being investigated, the parameter COP has been considered a variable in the computer program. In our case COP = 80 feet (refer to figure B-40). Once the log selected modulus vs depth curve has been determined the parameters B, EMI, and CK as previously defined can be obtained.

With PSO and WYM known from the targeting analysis of the area, the only variables in the program remaining to be determined are ROE, SK, DZP and DIV. The mass density ROE is determined by the standard soil mechanics test procedures. SK is the ratio of residual strain to maximum strain and can be obtained from the stress-strain curve for the soil as predetermined in the laboratory.

DZP is an arbitrary increment of depth used to define the depth at which the attenuated peak vertical stress exists. Finally, DIV is any even number which when divided into the depth interval between the pressure wave front and pressure wave peak will break it up into an even number of increments and thereby make it amenable to Simpson's Rule of Approximate Integration. The same value of DIV is used for the depth between the surface and the attenuated peak vertical stress.

(3) Assumptions

In order to facilitate solving the problem of free field ground displacements certain assumptions were made. These are:

(a) The stress-strain curve for the soil type under consideration was linearized.

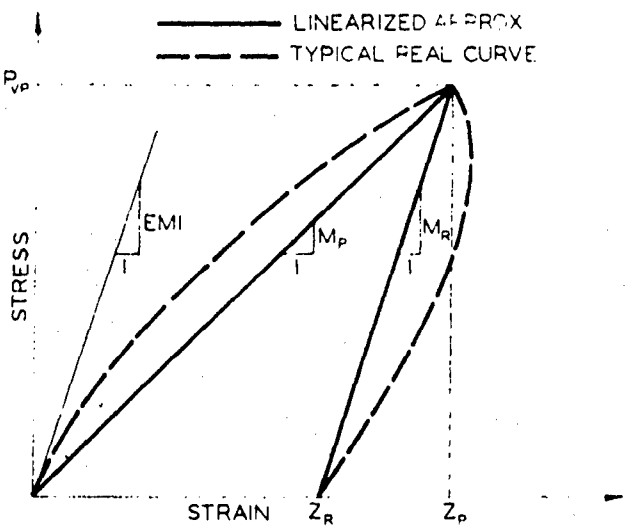

Figure B-40. Linearized Stress-Strain Curves

The consequence of this assumption is to increase the strain slightly for any given stress level on the loading portion of the curve and conversely to decrease the strain slightly for any given stress level on the unload portion of the curve. The assumption will yield conservative values of strain on the loading portion of the curve, and whereas, at first sight, the strains resulting from the linearized approximation on the unload portion of the curve would seem unconservative, we notice that the maximum residual strain of the linearized curve corresponds exactly with that of the real curve. Thus, even with the linearized assumption, the ratio of the residual strain to the peak strain remains the same, and this is the important factor in determining unloading strains.

(b) The stresses and motions are assumed to result from a one-dimensional dilatational wave. Thus, we will concern ourselves only with vertical strain.

(c) As a result of previous assumptions, the time dependent loading function must be considered as acting uniformly over a surface of infinite extent. Thus, shearing stresses do not enter into the analysis.

(d) Surface loads are considered as instantaneous static loads. This enables the subsurface stress to be computed by "freezing" the stress pattern at successive times as the stress front and stress peak progress downwards through the soil.

(e) Only spatial attenuation of the peak surface overpressure is considered in the determination of the peak vertical stress at depth. In effect this assumes that, upon loading to a peak value, the soil acts as an elastic, homogeneous, isotropic medium, for otherwise the inelastic behavior of the soil would have to be considered as an energy dissipator. By assuming only spatial attenuation with depth, the peak vertical pressure values determined should be conservative.

(f) A linear variation of the stress profile is assumed between the stress front and stress peak and between the stress peak and the surface overpressure. This can be represented as follows:

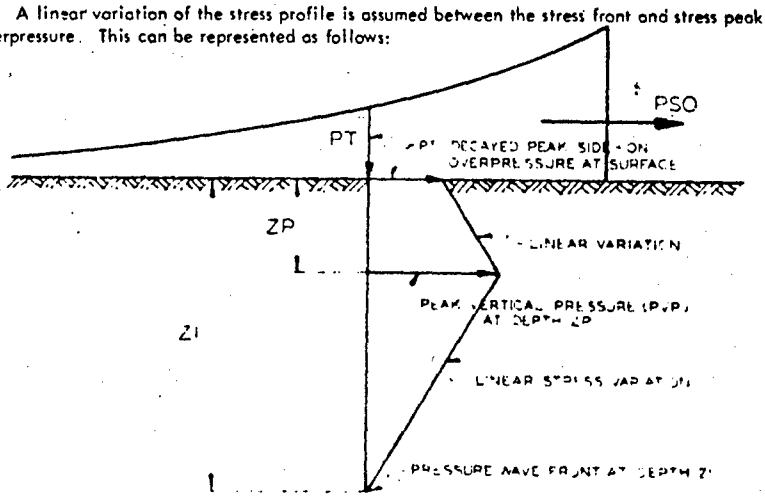

Figure B-41. Front and Stress Peak Variation

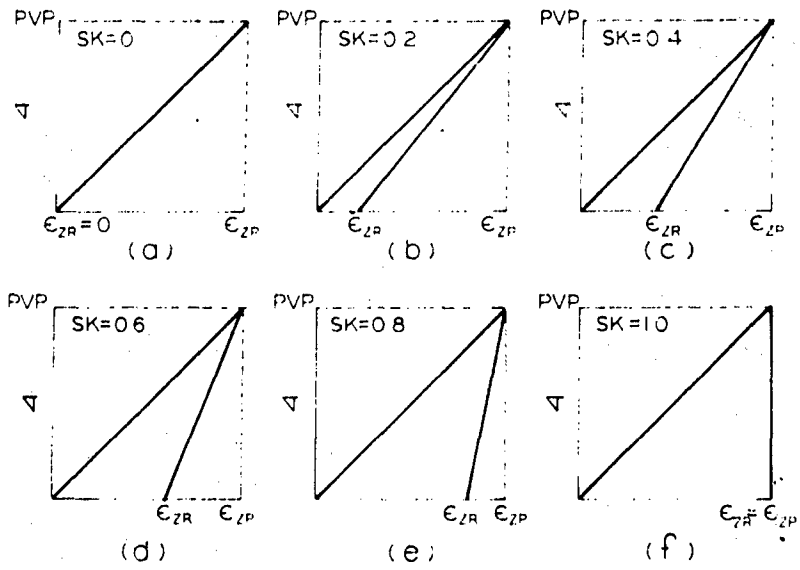

Figure B-42. Linearized Curves used in Study

Figure B-42 (a) represents a perfectly elastic material (e.g. steel below the yield point) where stress is proportional to strain both on the loading and unloading portions of the curve. Figures B-42 (b) through B-42 (e) represent various degrees of plasticity so that in each case, upon unloading, there remains a residual strain. This indicates that the constant of proportionality (constrained modulus of deformation M_p) for the loading portion of the curve differs from the constant of proportionality (constrained modulus of deformation M_r) for the unloading portion of the curve. The ratio (SK) of the residual strain to the peak strain is usually selected as the parameter which defines the unloading stress-strain curve of the soil and this ratio is related to the differences in moduli by the expression: $SK = 1 - M_p / M_r$

The effect of this difference is vividly shown in the plot of displacement at the surface vs time after arrival of PSO, shown as figures B-42. Figure B-42 (f) represents the perfectly plastic case wherein there is no decrease of strain with decrease in load.

(g) The seismic modulus is considered a constant since the soil has been assumed to be a homogeneous, isotropic medium. In reality the soil is generally stratified, and this would mean a "stepped" variation of seismic modulus. Such variations in seismic modulus, however, could very easily be included in the program since EMI is already included therein as a variable parameter.

(4) The Program

Although there are many variations, the basic computer program for the determination of free field ground displacements due to a nuclear detonation is as follows.

The constant, $L_W = 230 \left[\frac{100}{PSO}\right]^{1/2} [WYM]^{1/3}$ is computed for the given overpressure and weapon yield. This information is needed later on in the program for the determination of ALP, the spatial attenuation factor from the formula ALP = 1/1+ZP/FLW.

The next step in the program is dependent upon a previous decision as to what depth of peak vertical pressure will have significant effect upon the resulting displacements. This decision requires some degree of judgement since too shallow a depth will not yield the maximum displacement. Thus, in this respect, it seems safe to assign a depth equal to or greater than COP, the depth at which the constrained modulus equals the seismic modulus. In any case, this depth is divided by DZP, the predetermined size of the depth increment down to the point of peak vertical pressure, to define for the computer the number of times it must go through the displacement computation. Thus, if the depth chosen were 80 feet and the size increment by which we wished to progress to 80 feet were chosen as 5 feet, the computer would solve the problem 80/5 or 16 times. In the basic program this statement was the outside "do loop" i.e., the machine was set to do this problem for N = 1 to 16. At N = 1, the depth (ZP) at which the peak vertical pressure occurred was 5 ft, at N = 2, ZP was 10 ft; at N = 3, ZP was 15 ft, and so forth down to 80 ft.

The next step was to determine the arrival time of the peak vertical pressure, PVP, at a given ZP. Here an "if" statement was introduced, i.e., if ZP < COP ft one procedure was followed, if ZP ≥ COP ft, another was followed. For ZP < COP ft, in order to determine the time required for the peak vertical pressure to arrive at the depth ZP, a summation had to be made of the time, DELT, it took for the pressure peak to travel through each DZP down to ZP. However, DELT is inversely proportional to the square root of the selected modulus, M_p. The selected modulus in turn, varies logarithmically with depth so that over an increment DZP the selected modulus could display a significant variation. Thus, an average value for each increment was needed. For example, in considering the time for the pressure peak to travel between the 15 ft and 20 ft depths, the M_p for 17.5 ft was used as long as 20 ft was < COP. A general expression was written that would assure this average value for each increment of depth.

If ZP ≥ COP, the selected modulus no longer varied with depth and became in effect, the seismic modulus. Thus, the time required for the pressure peak to travel through an increment DZP at a depth below COP was merely equal to $DZP\left(\frac{ROE}{EMI}\right)^{1/2}$ a constant value for all DZP below COP.

With the time for PVP to travel to a depth ZP now known, the next step was to determine the location of the pressure wave front. This depth ZI was easily derived from the expression:

$$ZI = \sum DELT \left(\frac{EMI}{ROE}\right)^{1/2}$$

The interval between ZI and ZP was then divided into DIV increments of size DZL where DZL = (ZI - ZP)/DIV. Starting at ZI where the vertical stress equals zero, the computer proceeded to calculate the stress at various consecutive depths DZL feet less than the previous depth until it reached depth ZP where the stress was the peak vertical attenuated stress PVP. Figure B-43 illustrates the procedure.

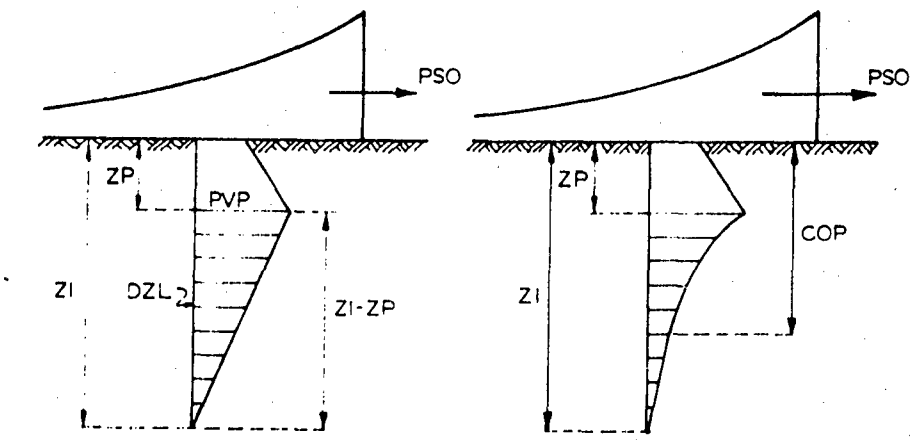

Figure B-43. Notation for One-Dimensional Wave Propagation (Loading)

In order to take into account the fact that M_p becomes EMI at a certain depth COP, an "if" statement had to be introduced before the strains corresponding to the calculated stresses could be determined. This statement set the computer so that if the depth under consideration was less than COP, the value of M_p was to be computed for that particular depth, since above COP the selected modulus itself is a function of depth. The strain at this depth was then determined using the equation for strain for the loading portion of the stress-strain curve.

If the depth under consideration was greater than COP, EMI was used in the strain computation. The value of EMI was assumed constant with depth and was given as part of the original data. Refer to figure B-43.

With the strains below ZP now computed, Simpon's Rule for Approximate Integration was employed to sum the area beneath the strain curve and thereby arrive at a value for the lower displacement DISPL. Although the stresses were assumed to vary linearly with depth, Simpson's Rule had to be used in order to account for the nonlinearity of the strain profile above depth COP due to the nonlinear variation of M_p with depth above COP.

With the lower displacement now computed for a particular ZP, the calculation of the upper displacement was the next logical step. The upper displacement refers to that which takes place between the surface and depth ZP. The same procedure was adopted here as was used to determine the lower displacement, i.e., first to determine the stress at depth ZP and the stress at the surface, and then, assuming a linear variation of stress between these two points, to compute the corresponding strains at various depths along the interval. Since the stress at ZP was already known from previous computations (PVP = ALP x PSO), all that was needed was the value of the surface stress. This stress PT (refer to figure B-43) was found to be the time dependent decay of the peak side-on overpressure. Unfortunately, equations for the variation of PT with time were not available, so an approximate expression had to be derived from the curves found in the AFDM. An equation relating PT to PSO, TIME and WYM was finally obtained, but its use is limited to a PSO of about 50 PSI. Work is now underway to extend the expression for PT to include all PSO from 10 to 2000 PSI and thereby further generalize the program.

With the stresses at the surface (PT) and at depth ZP (PVP) known, the interval ZP was divided by DIV to break it up into an equal number of increments of size ZP/DIV feet. Then, starting at depth ZP and proceeding upward in increments of ZP/DIV feet, the stress was computed at each depth. In this way the linear stress profile was obtained as illustrated in figure B-43. Before proceeding to the strain computation an "if" statement had to be introduced to assure a proper value of selected modulus.

As before, if the depth under consideration were less than COP, then the value of the selected modulus had to be computed. If the depth under consideration were greater than or equal to COP, then the value of the selected modulus merely became the value for the seismic modulus EMI. With this distinction made, the strain at each level of the previously computed stresses was calculated (see figure B-44), and the area under the resulting strain curve again summed by Simpson's Rule to yield the upper displacement, DISPU. The equations for strain in the upper interval differed radically from the equations for strain in the lower interval since the former were computing strains on the unload portion of the curve where the effects of residual strain had to be taken into account. The total displacement was obtained by summing the upper and lower displacements.

The print-out of this computer program included the following items:

(1) Time in seconds after the arrival of the peak side-on overpressure.
(2) ZP - the corresponding depths to which the pressure wave peak had descended. (Feet)
(3) ZI - the corresponding depths to which the pressure wave front had descended. (Feet)
(4) PT - the value of the surface pressure corresponding to the times given above. (Psi)
(5) DISPL - the corresponding lower displacement in feet.
(6) DISPU - the corresponding upper displacement in feet.
(7) DISP - the sum of the corresponding DISPL and DISPU or the total displacement for the times given above. (Feet)

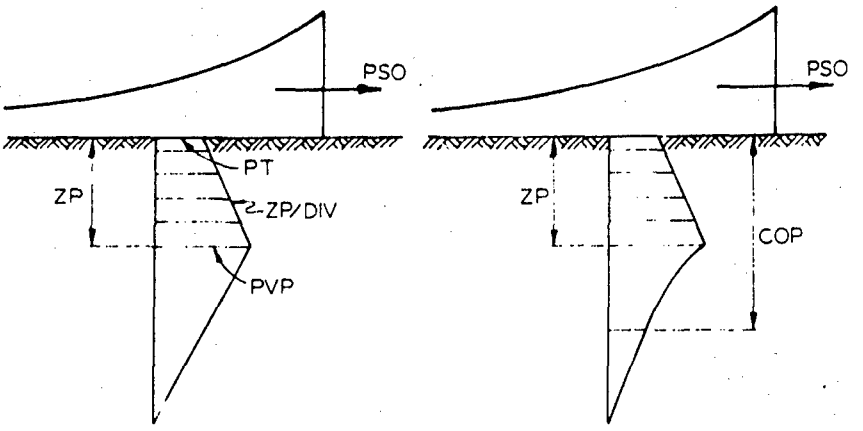

Figure B-44. Notation for One-Dimensional Wave Propagation (Unloading)

(5) Results

Since the stress-strain relationship for even what may be called a "typical soil" is of an extremely complex nature,(h) it seemed advisable to generalize our investigation of a given soil by prescinding from the stress-strain curve obtained in the laboratory. Thus, we undertook to investigate the effect of each of the following six linearized stress-strain relationships upon the surface displacement due to a 50 psi overpressure from a nuclear air-burst. See figures B-45 through B-47.

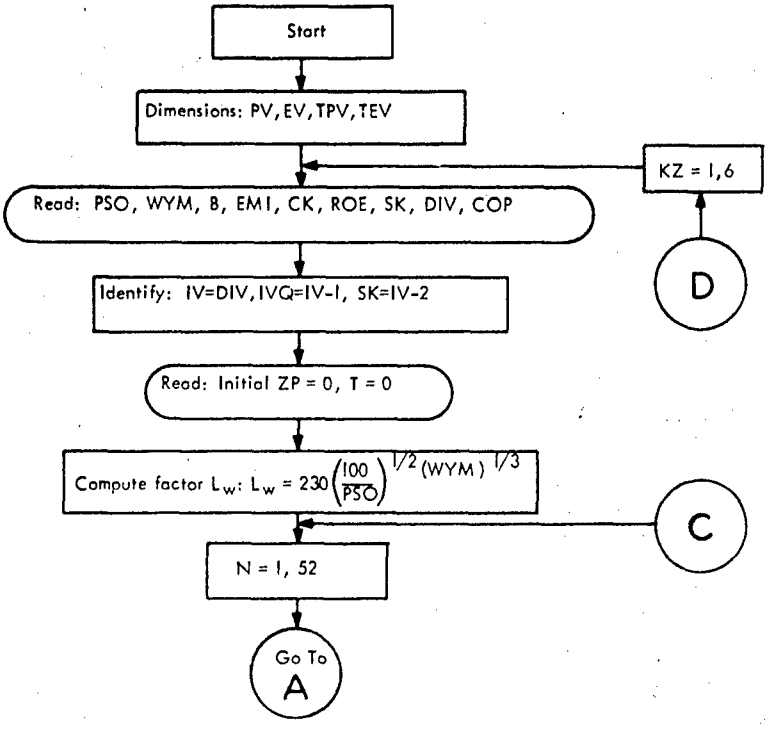

Figure B-45. Flow Diagram, Chart I

(h) "Inelastic Wave Propagation in Soil Columns", by Werner Heierli, Journal of Soil Mechanics and Foundations Division, Proc. ASCE, Vol. 88, No. SM6, Dec. 1962, p. 38. Also, "The Behavior of Soils Under Dynamic Loading," by R. V. Whitman et.al. Massachusetts Institute of Technology, August 1954. ASTIA-AD64-32, pp. 104-121.

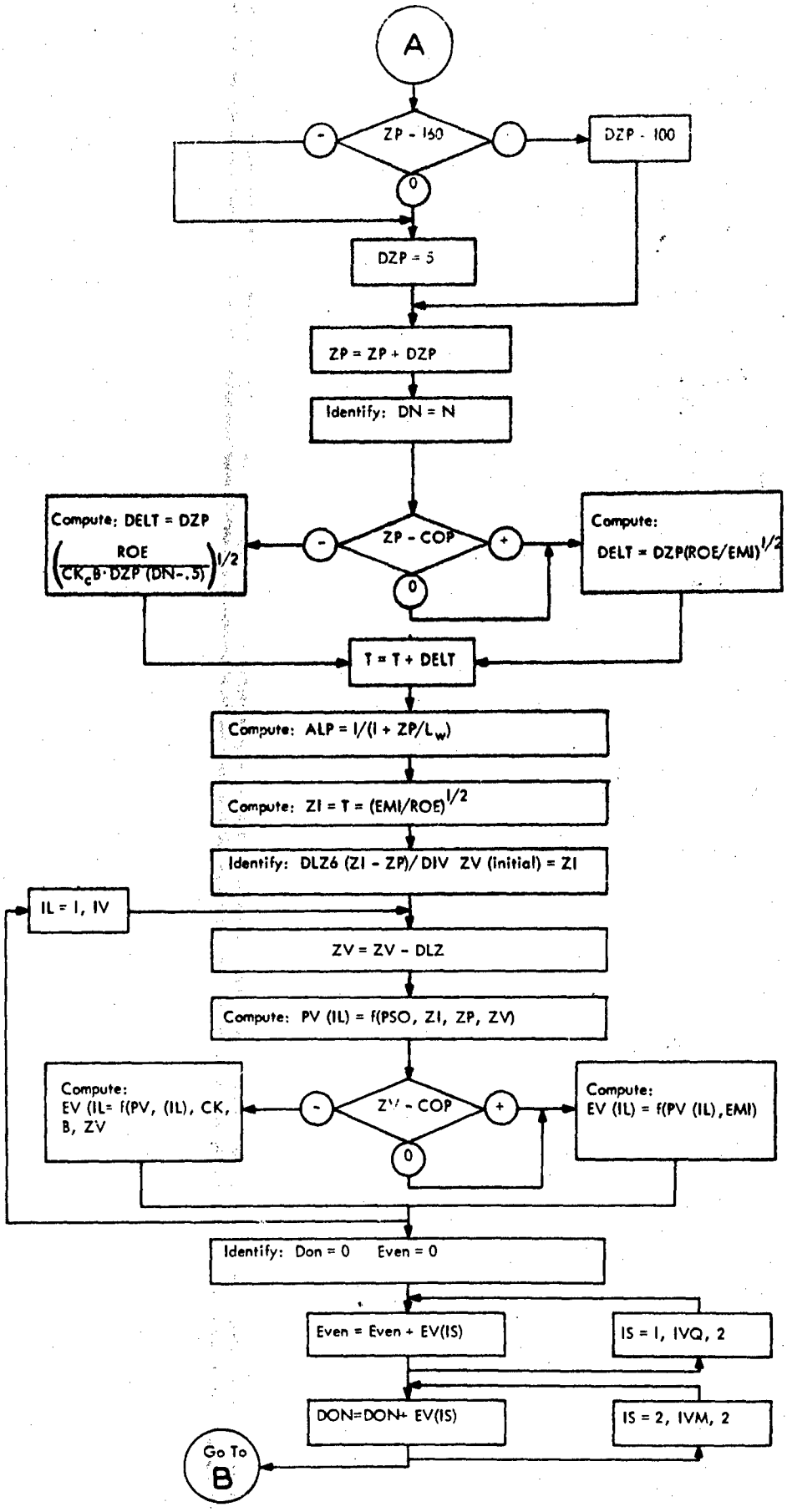

Figure B-46. Flow Diagram, Chart 2

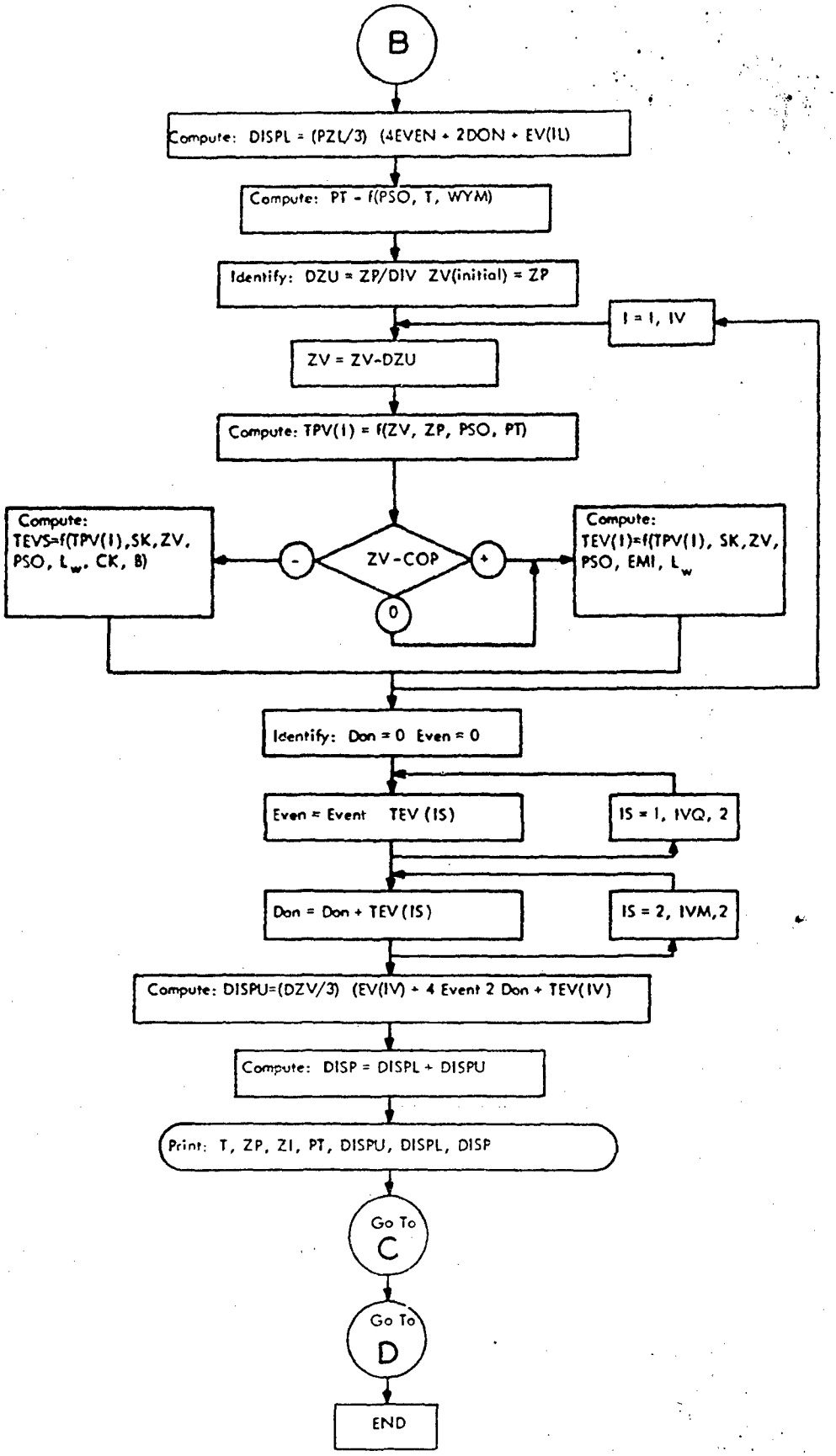

Figure B-47. Flow Diagram, Chart 3

D. Prediction of Initial Radiation

1. Introduction

One of the special features of a nuclear explosion is the fact that it is accompanied by the emission of nuclear radiation. This radiation, which is quite different from thermal radiation, consists of gamma rays, neutrons, beta particles, and a small proportion of alpha particles. Most of the neutrons and part of the gamma rays are emitted in the actual fission process, that is to say, simultaneously with the event. The remainder of the gamma rays are produced in various secondary nuclear processes, including decay of the fission products. The beta particles are also emitted as the fission products decay. Some of the alpha particles result from the normal radioactive decay of the uranium or plutonium which has escaped fission in the weapon, and others (helium nuclei) are formed in hydrogen fusion reactions.

Because of the nature of the phenomena associated with a nuclear explosion, either in the air or near the surface, it is convenient (for practical purposes) to consider the nuclear radiations as being divided into two categories--initial and residual. The line of demarcation is somewhat arbitrary, but it may be taken as about 1 minute after the explosion. The initial nuclear radiation, with which this division will be concerned, refers to the radiation emitted within 1 minute of the detonation. For underground or underwater explosions, it is less meaningful to separate the initial from the residual nuclear radiation, although the distinction may be made if desired.

The ranges of alpha and beta particles are comparatively short and they cannot reach the surface of the earth from a high altitude air burst. Even when the fireball touches the ground, the alpha and beta particles are not very important. The initial nuclear radiation may thus be regarded as consisting only of the gamma rays and neutrons produced during the first minute of the nuclear event. Both of these nuclear radiations, although different in character, can travel considerable distances through the air. Further, both gamma rays and neutrons can produce harmful effects in living organisms. It is the highly injurious nature of these nuclear radiations, combined with their long range, that makes them so significant. Although the energy of the initial gamma rays and neutrons is only about 3 percent of the total energy, compared with some 35 percent appearing as thermal radiation in an air burst, the nuclear radiations can cause a considerable proportion of the casualties.

Most of the gamma rays accompanying the actual fission process are absorbed by the weapon materials and are thereby converted into other forms of energy. Thus, only a small proportion (about 1 percent) of this gamma radiation succeeds in penetrating any great distance from the exploding weapon; but, as will be seen shortly, there are several other sources of gamma radiation that contribute to the initial nuclear radiation. Similarly, the neutrons produced in fission are to a great extent slowed down and captured by the weapon residues or by the air through which they travel. Nevertheless, a sufficient number of fast (fission) neutrons escape from the fireball region to represent a significant hazard at considerable distances.

Although shielding from thermal radiation at distances close-in to the burst point is a fairly simple matter, this is not true for gamma rays and neutrons. For example, at a distance of 1 mile from a 1-megaton explosion, the initial nuclear radiation would probably prove fatal to a large proportion of exposed human beings even if they were shielded by 24 inches of concrete. A much lighter shield would provide complete protection from thermal radiation at the same location. The problems of shielding from thermal and nuclear radiations are thus quite distinct.

The effective injury ranges of these two kinds of nuclear weapon radiations may also differ widely. For explosions of moderate and large energy yields, thermal radiation can have harmful consequences at appreciably greater distances than can the initial nuclear radiation. Beyond about 1-1/4 miles, the initial nuclear radiation from a 20-kiloton air burst, for instance, would not cause observable injury even without protective shielding. However, exposure to thermal radiation at this distance could produce serious skin burns. On the other hand, when the energy of the nuclear explosion is relatively small, for example, a kiloton or less, the initial nuclear radiation has the greater effective range.

In the discussion of the characteristics of the initial nuclear radiation, it is desirable to consider the neutrons and the gamma rays separately. Although their ultimate effects on living organisms are much the same, the two kinds of nuclear radiations differ in many respects. The subject of gamma rays will be considered in the section which follows, and neutrons will be discussed later.

2. Sources of Gamma Rays

In addition to the gamma rays which actually accompany the fission process, contributions to the initial nuclear radiations are made by gamma rays from other sources. Of the neutrons produced in fission, some serve to sustain the fission chain reaction, others escape, and a large number are inevitably captured by non-fissionable nuclei. As a result of neutron capture, the nucleus is converted into a new species known as a "compound nucleus," which is in a high energy (or excited) state. The excess energy may then be emitted almost instantaneously, as gamma radiations. These are called "caputure gamma rays," because they are the result of the capture of a neutron by a nucleus. The process is correspondingly referred to as "radiative capture."

Neutrons produced in fission can undergo radiative capture reactions with the nuclei of various materials present in the weapon as well as with those of nitrogen in the surrounding atmosphere. These reactions are accompanied by gamma rays which form part of the initial nuclear radiation. The interaction with nitrogen nuclei is of particular importance since some of the gamma rays thereby produced have very high energies and are, consequently, much less easily attenuated than the other components of the initial gamma radiation.

The interaction of fission neutrons with certain atomic nuclei, particularly heavy nuclei, provides another source of gamma rays. When a "fast neutron," for example one having a large amount of kinetic energy, collides with such a nucleus, the neutron may transfer some of its energy to the nucleus; leaving the latter in an excited (high-energy) state. The excited nucleus can then return to its normal energy (or ground) state by the emission of the excess energy as gamma rays. This type of interaction of a fast neutron with a nucleus is called "inelastic scattering" and the accompanying radiations are referred to as "inelastic scattering gamma rays."

The gamma rays produced in fission and as a result of other neutron reactions and nuclear excitation of the weapon materials all appear within a second (or less) after the nuclear explosion. For this reason, the radiations from these sources are known as the "prompt" or "instantaneous" gamma rays.

The fission fragments and many of their decay products are radioactive isotopes which emit gamma radiations. The half-lives of these radioactive species range from a fraction of a second to many years. Nevertheless, since the decay of the fission fragments commences at the instant of fission; and because in fact their rate of decay is greatest at the beginning, there will be an appreciable liberation of gamma radiation from these radioisotopes during the first minute after the explosion. In other words, the gamma rays emitted by the fission products make a significant contribution to the initial nuclear radiation. However, since the radioactive decay process is a continuing (or gradual) one, spread over a period of time which is long compared to that in which the instantaneous radiation is produced, the resulting gamma radiations are referred to as the "delayed" gamma rays.

The instantaneous gamma rays and the portion of the delayed gamma rays which are included in the initial radiation are nearly equal in amount, but they are by no means equal fractions of the initial nuclear radiation transmitted from the exploding weapon. The instantaneous gamma rays are produced almost entirely before the weapon has completely blown apart. They are, therefore, strongly absorbed by the dense weapon materials, and only a small proportion actually emerges. The delayed gamma rays, on the other hand, are mostly emitted at a later stage in the explosion; after the weapon materials have vaporized and expanded to form a tenuous gas. These radiations thus suffer little or no absorption before emerging into the air. The net result is that the delayed gamma rays, together with those produced by the radiative capture of neutrons by the nitrogen in the atmosphere, contribute about a hundred times more than the prompt gamma rays to the total nuclear radiation received at a distance from an air (or surface) burst during the first minute after detonation.

There is another possible source of gamma rays which may be mentioned. If a nuclear explosion occurs near the earth's surface, the emitted neutrons can cause what is called "induced radioactivity" accompanied by the emission of gamma rays which will commence at the time of the explosion and will continue thereafter. However, except near ground zero, where the intensity of gamma rays from other sources is very high in any event, the contribution of induced radioactivity to the initial gamma radiation is small. Consequently, the radioactivity induced in the earth's surface by neutrons will be treated later as an aspect of the residual or fallout nuclear radiation.

3. Measurement of Gamma Radiation

Thermal radiation from a nuclear explosion can be felt (as heat), and the portion in the visible region of the spectrum can be seen. The human senses, however, do not respond to nuclear radiations except at very high intensities (or dose rates), when itching and tingling of the skin are experienced. Special instrumentation methods, based on the interaction of these radiations with matter, have therefore been developed for the detection and measurement of various nuclear radiations.

When gamma rays pass through any material, either solid, liquid, or gas, they interact with the atoms in a number of different ways. From the viewpoint of gamma-ray dose measurement, two ultimate consequences of these interactions are important. One result is that an electron is expelled from many atoms. Because the electron carries a negative electrical charge, the residual part of the atom is positively charged, that is it becomes a positive ion. This process is referred to as "ionization," and the separated electrons and positive ions are called "ion pairs."

The second consequence of gamma ray interaction occurs readily in certain solids and liquids, as well as in gases. Instead of the electron being removed completely from the atom, as is the case in ionization, it acquires an additional amount of energy. As a result, the atom is converted into a high-energy (or excited) electronic state. This phenomenon is called "excitation."

Both ionization and excitation have been used for the detection or the measurement of gamma rays, as well as of other nuclear radiations. Normally a gas will not conduct electricity to any appreciable extent; but as a result of the formation of ion pairs, by the passage of nuclear radiations, the gas becomes a reasonably good conductor. Several types of instruments, for example the Geiger counter and the pocket chamber (or dosimeter), for the measurement of gamma (and other) radiations, are based on the formation of electrically charged ion pairs in a gas and its consequent ability to conduct electricity.

Operation of a scintillation counter, on the other hand, depends upon excitation. When an atom or molecule becomes electronically excited, it will generally give off the excess energy within about one millionth of a second. Certain materials, usually in the solid or liquid state, are able to lose their electronic excitation energy in the form of visible flashes of light or scintillations. These scintillations can be counted by means of a photomultiplier tube and associated electrical devices.

In addition to the direct effects of ionization and excitation, there are indirect consequences, notably chemical changes. One example is the blackening or fogging of photographic film which appears after it is developed.

Although some special instruments will record both the total radiation dose and the dose rate, most radiation measuring devices are designed to indicate one or the other. However, the ability to measure both dose rate and total dose is important for the initial nuclear radiation as well as for the delayed radiation to be discussed later.

4. Gamma-Ray Dose-Distance Relationship

The gamma-ray exposure dose at a particular location, resulting from a nuclear explosion, is decreased as distance increases from the point of burst. The relationship of the radiation dose to the distance is dependent upon two factors, analogous to those which apply to thermal radiation. First is the general decrease due to the spread of the radiation over larger and larger areas as it travels away from the burst point. As with thermal radiation, the dose received is inversely proportional to the square of the distance from the explosion, so that it is said to be governed by the "inverse square" law. Second is an attenuation factor which allows for decrease in intensity due to absorption and scattering of gamma rays by the intervening atmosphere.

The gamma-radiation exposure doses at known distances from explosions of different energy yields have been measured at a number of nuclear test explosions. The results obtained for air bursts are summarized in the form of two graphs: the first (figure B-48) shows the dependence of the initial gamma-ray dose on the actual distance (or slant range) from a 1-kiloton explosion; the second (figure B-49) gives the scaling factor to be used to determine the dose at the same slant distance from an explosion of any specific energy yield up to 20 megatons. The data are based on the assumption that the average density of the air in the transmission path, between the burst point and the target, is 0!9 of the normal sea-level density. Because of variations in weapons design and the different characteristics of the gamma rays associated with fission and fusion, as well as for other reasons, the gamma-ray doses calculated from figures B-48 and B-49 cannot be exact. For yields from about 1 to 100 kilotons TNT equivalent they are reliable within a factor of about two; from 100 kilotons to 1 megaton, within a factor of about 5; and above 1 megaton, within a factor of about 10.

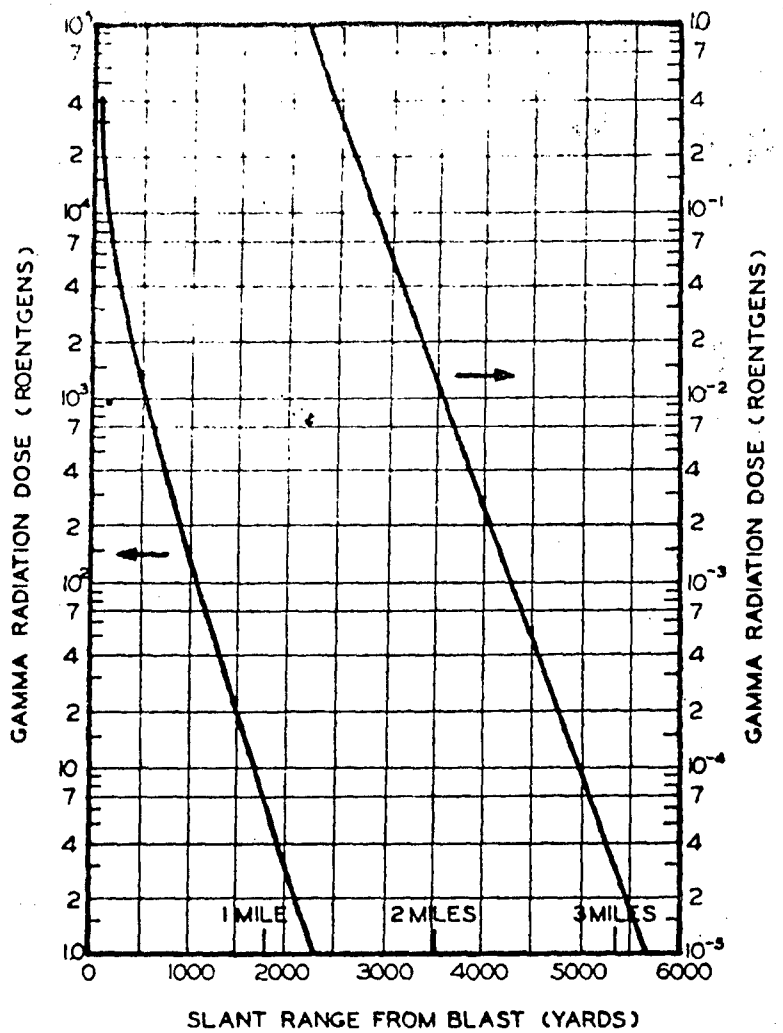

Initial gamma-radiation dose as a function of slant range from burst for 1-kiloton air burst, based on 0.9 sea-level air density

Figure B-48. Slant Range From Burst (Yards)

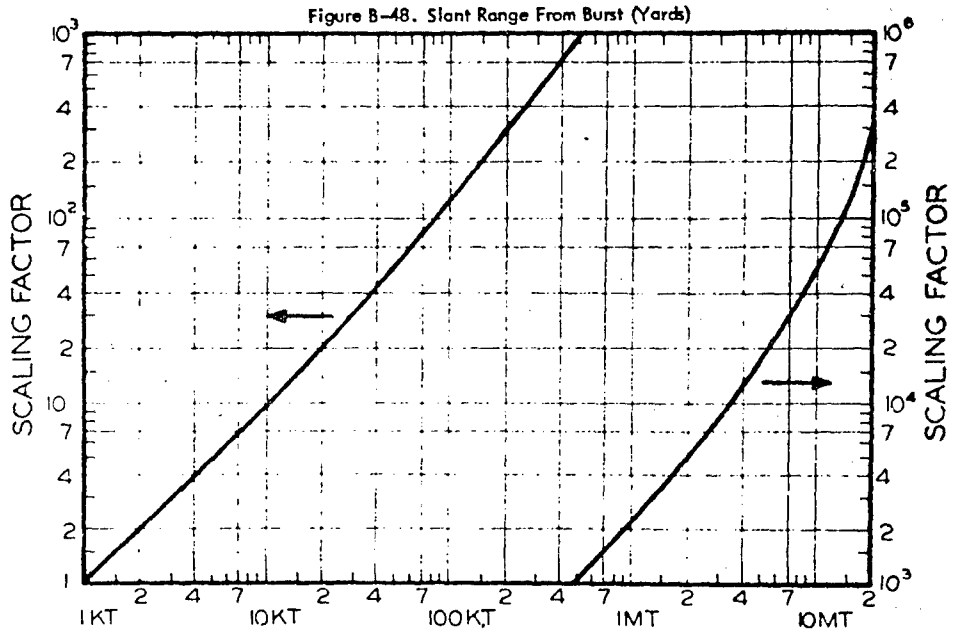

Scaling factor for initial gamma-radiation dose

Figure B-49. Explosion Yield

The method of using the curves in figures B-48 and B-49 may be illustrated by determining from them the initial gamma-radiation dose received at a distance of 1,700 yards from a 100-kiloton air burst. From figure B-48, the exposure dose at this distance from a 1-kiloton air burst is 10 roentgens. The scaling factor for 100 kilotons is found from figure B-48 to be 120. Hence, the gamma-ray dose in the case specified is 10 × 120 = 1,200 roentgens.

The values in figure B-48 are somewhat dependent upon the density of the air between the center of the explosion and the point on the ground at which the radiation is received. This is so because the air absorbs some of the gamma radiation in the course of its transmission, the dense air near the earth's surface absorbing more than the less dense air at higher altitudes. The results in the figure are based upon an average air density in the transmission path of 0.9 of the sea-level value. If the actual density is higher or lower, the gamma-ray dose will be decreased or increased, respectively.

It will be noted from figure B-49 that, in the higher energy range, the scaling factor increases more rapidly than does the energy of the burst. For example, for a 100-kiloton explosion the scaling factor is about 120, and for a 1,000-kiloton (1-megaton) yield it is roughly 2,100. The reason for this increase is the sustained low air density, following the passage of the positive phase of the shock wave, especially for explosions of high energy yield. As a result, there is less attenuation of the (delayed) gamma rays from the fission products.

The gamma-ray doses to be expected from explosions of various energies can be expressed in another form, as in figure B-50. The slant ranges from the explosion, at which certain specified doses of initial gamma radiation would be received, for air bursts in the energy range from 1 kiloton to 10 megatons, can be read off directly. For intermediate doses, the corresponding slant distances can be estimated by interpolation.

Strictly speaking, the foregoing data and conclusions are applicable only to air bursts. In a surface burst, the presence of dust and debris produced by the explosion will cause a reduction in the exposure dose at any given distance (slant range) from the point of burst. Consequently, the dose-distance relationships may be expected to vary with the height of burst, especially if the detonation occurs not too far above the earth's surface. It is generally suggested that the initial gamma-radiation dose from a surface burst be taken as two-thirds that from an air burst at the same slant distance. However, the errors inherent in the available data, are such that the variations arising from the proximity of the burst to the surface are usually not significant.

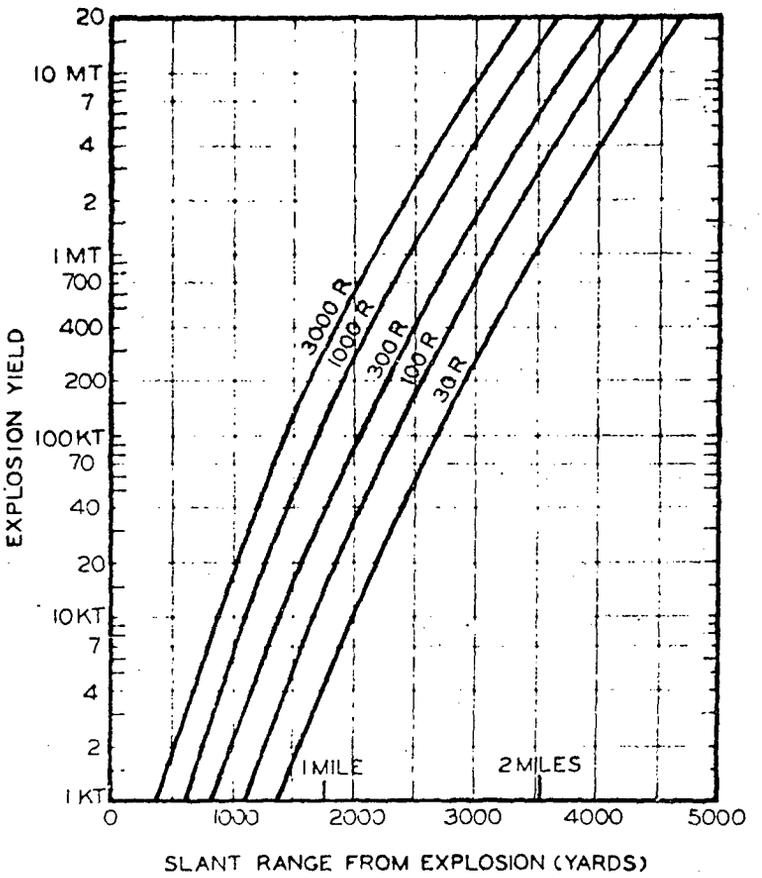

Figure B-50. Initial Radiation Attenuation Curves

5. Rate of Delivery of Initial Gamma Rays

Radiation dose calculations based on figures B-48 and B-49 involve the assumption that the exposure lasts for the whole minute which was somewhat arbitrarily set as the period in which the initial nuclear radiation is emitted. It is important to know, however, something about the rate at which the radiation is delivered from the weapon. If this information is available, it is possible to obtain some idea of the dose that would be received if part of the radiation could be avoided, for example, by taking shelter within a second or two of observing the luminous flash of the explosion.

The rate of delivery of the initial gamma rays depends upon a number of circumstances, the most significant of which are the energy yield of the explosion and the distance from the point of burst. The percentage of the total dose received up to various times for two different cases is shown in figure B-51.

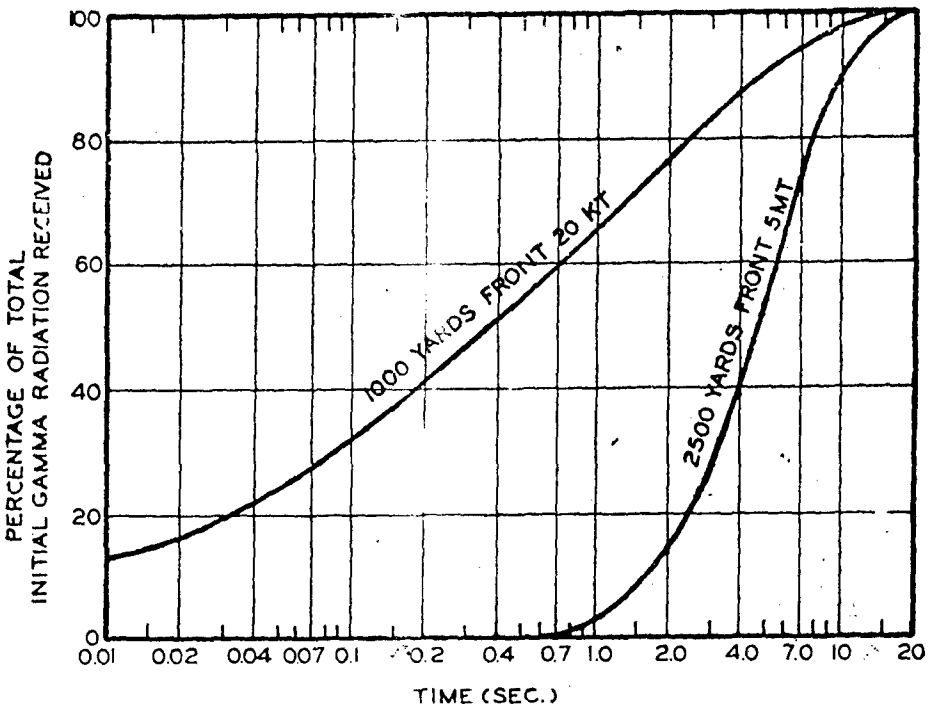

Figure B-51. Initial Gamma Ray Attenuation

One curve represents the rate of delivery at a distance of 1,000 yards from a 20-kiloton air burst and the other at 2,500 yards from a 5-megaton explosion. It is apparent that in the former case about 65% and in the latter case about 5% of the total initial gamma radiation dose is received during the first second after the detonation.

If some shelter could be obtained (by falling prone behind a substantial object) within a second of observing the explosion flash; in certain circumstances it might make the difference between life and death. The curves in figure B-51 show that for a weapon of high energy the gamma radiation may be emitted more slowly, especially in the early stages immediately following the explosion, than for one of lower energy. Avoidance of part of the initial gamma-ray dose would appear to be more practicable for higher energy bursts.

6. Sources of Neutrons

Although neutrons are nuclear particles of appreciable mass, whereas gamma rays are electromagnetic waves (analogous to X-rays), their harmful effects on the body are similar in character. As with gamma rays, only very large doses of neutrons may be detected by the human senses. Neutrons can penetrate a considerable distance through the air and constitute a hazard that is greater than might be expected from the fact that they are only a small fraction (about 0.025 to 1%) of the total yield.

Essentially all the neutrons accompanying a nuclear explosion are released either in the fission of fusion process. All of the neutrons from the latter source and over 99% of the fission neutrons are produced almost immediately; probably within less than a millionth of a second of the initiation of the explosion. These are referred to as the "prompt" neutrons.

In addition, somewhat less than 1% of the fission neutrons, called the "delayed" neutrons, are emitted subsequently. Since the majority of these "delayed" neutrons are released within the first minute, however, they constitute part of the initial nuclear radiation. Some neutrons are also produced by the action of gamma rays of high energy on the weapon materials. These make a very minor contribution and so can be ignored.

The neutrons produced in the fission process have a range of energies, but they are virtually all in the region of high energy. Such high-energy neutrons are the fast neutrons referred to previously, their energy being kinetic in nature. In the course of the scattering collisions between the fast neutrons and atomic nuclei, there is an exchange of energy between the neutrons and nuclei. Within the weapon itself, where heavy nuclei (e.g., of uranium) are present, some of the neutrons lose energy as a result of inelastic scattering; the energy removed being emitted in the form of gamma radiation.

In other collisions, there is a simple transfer of kinetic energy from the fast neutron to the struck nucleus; these are called "elastic collisions" and are not accompanied by gamma radiation. Because of the variety of collisions which occur with different nuclei, the neutrons leaving the region of the explosion have speeds (or energies) covering a wide range; from fast, through intermediate, to slow. The neutrons of slowest speed are often called "thermal neutrons" because they are in thermal (or temperature) equilibrium with their surroundings.

The occurrence of an equilibrium spectrum is related to a combination of circumstances which arise during passage of the neutrons through the air. The loss of the slower neutrons by capture (by nitrogen nuclei) is just compensated by the slowing down of fast neutrons. Consequently, the proportion (or fraction) of neutrons present in any particular energy range appears to be essentially constant at all distances of interest. The total number of neutrons, however, received per unit area at a given location is less the farther that point is from the explosion; because, in addition to being spread over a large area, some of the neutrons are removed by capture.

E. Prediction of Fallout Radiation

1. Introduction

It is convenient to consider the fallout in two parts--early and delayed. Early fallout is defined as that which reaches the ground during the first twenty-four hours following a nuclear explosion. It is the early fallout from surface, subsurface,or low air bursts that is capable of producing radioactive contamination over large areas with an intensity great enough to represent an immediate biological hazard. Delayed fallout, which is that arriving after the first day, consists of very fine particles which settle in low concentrations over a considerable portion of the earth's surface. In later stages, this delayed fallout is referred to as "world-wide" fallout. Because of radioactive decay during the relatively long time which the particles are suspended in the atmosphere and the large areas which it is spread over, the delayed fallout poses no immediate biological hazard although it may be a long-term hazard.

In the case of an air burst, particularly when the fireball is well above the earth's surface, a fairly sharp distinciton can be made between the initial nuclear radiation, considered previously, and the residual radiation. The reason is that, by the end of a minute, essentially all of the weapon residues will have risen to such a height that the nuclear radiations no longer reach the ground in significant amounts. Subsequently, these fine particles are widely dispersed in the atmosphere and descend to earth very slowly.

In the case of surface, especially subsurface explosions, the demarcation between initial and residual radiation is not as definite. Some of the radiations from the weapon residues will be within range of the earth's surface at all times, so that the initial and residual categories merge. For very deep underground and underwater bursts the initial gamma rays and neutrons produced in the fission process may be ignored since they are absorbed by the surrounding medium. The residual radiations, from fission products and from radioactive species produced by neutron interaction, are then the only kinds of nuclear radiations that need be considered. In the case of a surface burst, both initial and residual nuclear radiations must be taken into account.

2. Distribution of Early Fallout

There are two main ways in which the earth's surface can become contaminated with radioactive material. One is by induced activity following the capture of neutrons by various elements present in the soil (or sea); and the other is by fallout, that is, by the descent of radioactive particles from the column and the resulting cloud. The amount of contamination and its distribution over the earth's surface are principally dependent upon the energy yield, height of burst, nature of the surface over (or on) which the detonation occurs, and the meteorological conditions.

An air burst, by definition, is one taking place at such a height above the earth that no appreciable quantities of surface materials are taken up into the fireball. The radioactive residues of the weapon then condense into extremely small particles which remain suspended in the atmosphere for a long time. Hence, except under special meteorological conditions, there will be no early (or local) fallout. However, depending on the characteristics of the weapon, the height of burst, and the nature of the surface there will be more or less contamination in the general vicinity of ground zero as a result of radioactivity induced by neutron capture. The contamination which might arise in this manner is variable; but it is probable that, apart from strong underground structures, the area would be completely devastated by blast and fire.

As the height of the burst decreases, and soil and debris from the earth's surface are taken up into the fireball, an increasing proportion of the fission products condense into particles of appreciable size. These contaminated particles range in diameter from less than 1 micron to several millimeters; the larger ones begin to fall back to earth even before the radioactive cloud has attained its maximum height, whereas the smallest ones remain suspended in the atmosphere for a long time.

The proportion of the total radioactivity of the weapon residues that is present in the early fallout, sometimes called the "early fallout fraction," appears to vary from test to test. For land surface bursts the early fallout fraction has been estimated to range from 50 to 70%. Values somewhat higher than this are expected from shallow underground bursts, whereas for water surface bursts the value is lower, in the neighborhood of 30%. It will be assumed here that 60% of the total radioactivity of a land surface burst will be in the early fallout.

The spatial distribution within the cloud is not known accurately. It is generally accepted that the mushroom head from a land surface burst contains about 90% of the total radioactivity and the remaining 10%is in the stem. The highest concentration of radioactivity initially lies in the lower third of the mushroom head. To give some idea of the values involved, the figures B-52 and B-53 show average values of stabilized cloud heights and times of particle fall, respectively.

3. Activity and Decay of Early Fallout

The early fallout consists mainly, but not entirely, of fission products. An indication of the manner in which the dose rate of the actual mixture decreases with time may be obtained from the following approximate rule: for every seven-fold increase in time after the explosion, the dose rate decreased by a factor of ten. For example, if the radiation dose rate of 1 hour after the explosion is taken as the reference point, then at 7 hours after the explosion the dose rate will have decreased to one-tenth; at 7 x 7 = 49 hours (or roughly two days) it will be one-hundredth; and at 7 x 7 x 7 = 343 hours (roughly two weeks) it will be one-thousandth of that at 1 hour after the burst. Another aspect of this rule is that at the end of 1 week (7 days), the radiation dose will be one-tenth the value after 1 day. This rule is within 25 % accuracy up to 2 weeks and within a factor of two up to roughly 6 months after the burst.

Information concerning the decrease of dose rate on the early fallout can be obtained from the continuous curve in figures B-54 and B-55; in which the ratio of the approximate exposure dose rate (in r/hr) at any time after the explosion to a convenient reference value, called the "unit-time reference dose rate," is plotted against time in hours. The use of the reference dose rate simplifies the representation of the results and the calculations based on them, are illustrated by figures B-54 and B-55.

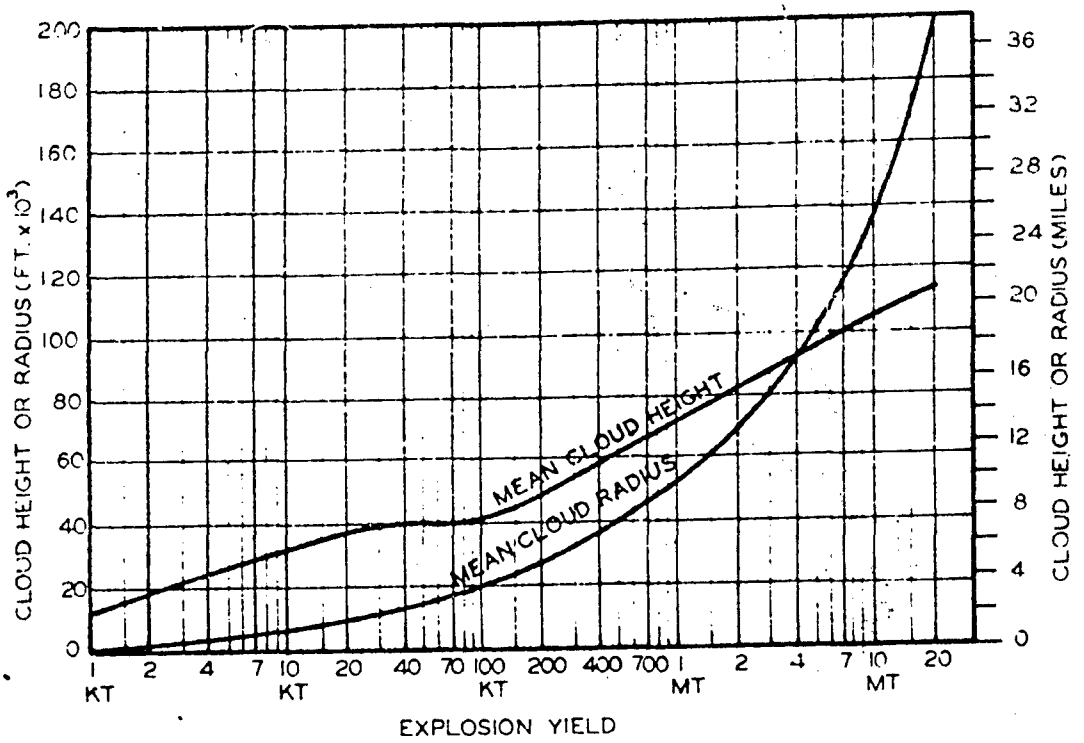

Figure B-52. Average Values of Stabilized Cloud Height

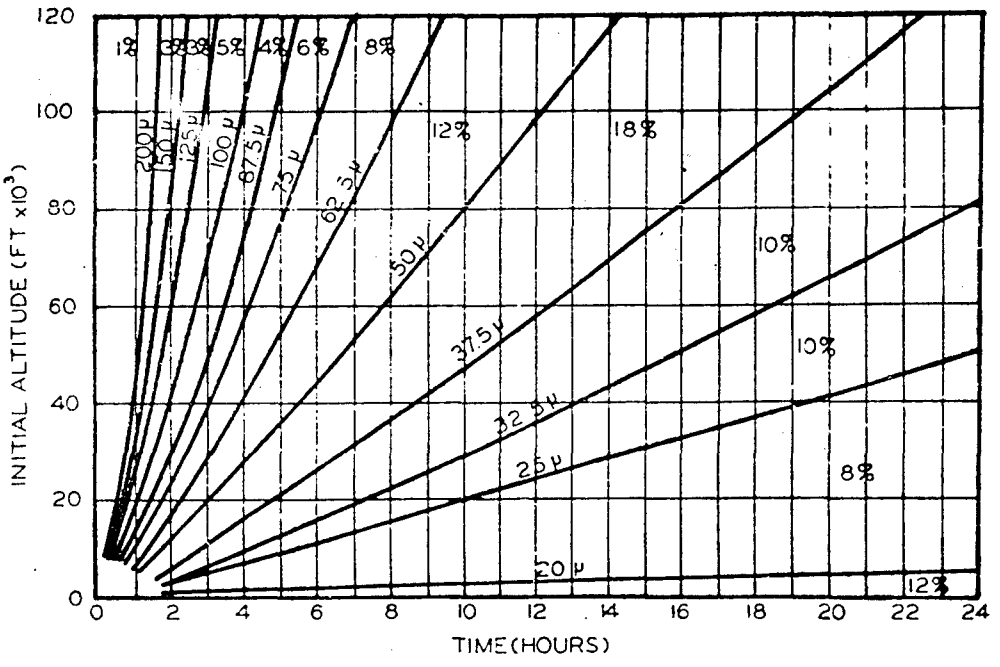

Figure B-53. Time of Fall of Particles and Percentage Of Total Activity Carried

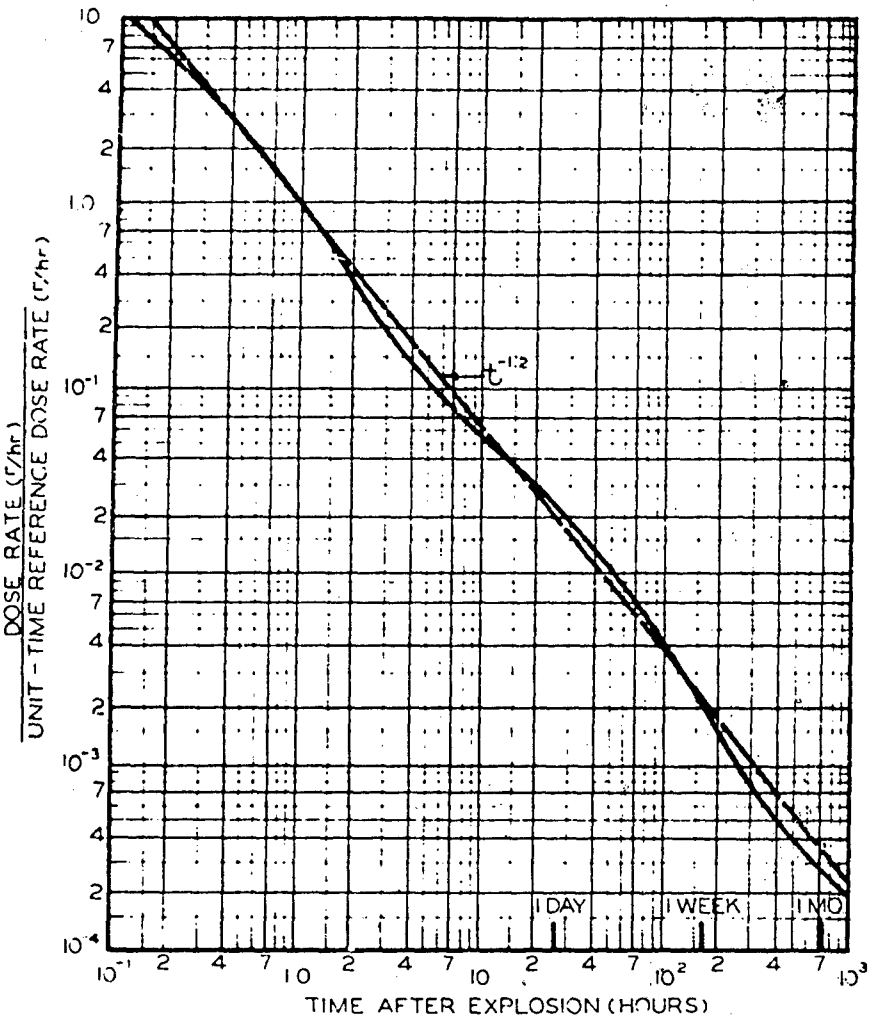

Figure B-54. Dependence of Dose Rate vs Time After Explosion

Suppose, for example, that at a given location the fallout commences at 5 hours after the explosion and that at 15 hours, when the fallout has ceased to descend, the observed dose rate is 4.0 roentgens per hour. From the curve in figure B-54 it is seen that at 15 hours the ratio of the actual dose rate to the reference value is 0.040; hence, the unit-time reference dose rate must be 4.0/0.040=100 roentgens per hour. By means of this reference value and the decay curves, it is possible to estimate the actual dose rate at any time after the fallout is complete. Thus, if the value at 24 hours after the explosion is needed, figure B-54 is entered at the 24 hours point. Move up until the plotted line is reached and read the ratio of dose rate to reference dose rate of 0.023. The required dose is then 0.023x100=2.3 roentgens per hour.

If the dose rate is known at any time by actual measurement, the value at any other time can be estimated. All that is necessary is to compare the ratios (to the unit-time reference dose rate) for the two given times as obtained from figures B-54 and B-55. For example, suppose the dose rate at 3 hours after the explosion is found to be 50 r/hr; what would be the value at 18 hours? The respective ratios are 0.23 and 0.033 respectively. Hence, the dose rate at 18 hours is 50x0.033/0.23=7.2 roentgens per hour.

It should be noted that the figures are to be used to obtain dose rates. In order to determine the actual or total radiation dose received it is necessary to multiply the average dose rate by the exposure time. However, since the dose rate is steadily decreasing during the exposure, appropriate allowance must be made.

The radiation dose rate and dose can be calculated by expressing the curves in figures B-54 and B-55, in equation form. If the exponent of 1.2 is used the equations are valid up to about 6 months as can be seen from figure B-55.

Radiation intensity (dose rate) at any time t is:

$$R_t = R_1 t^{-n} = R_1 t^{-1.2} = \frac{R_1}{t^{1.2}}$$

where: R_1 = unit-time reference dose rate
t = time after the detonation in hours
n = Kaufman exponent assumed to be 1.2 (up to 6 months)
R_t = intensity (dose rate) at time t.

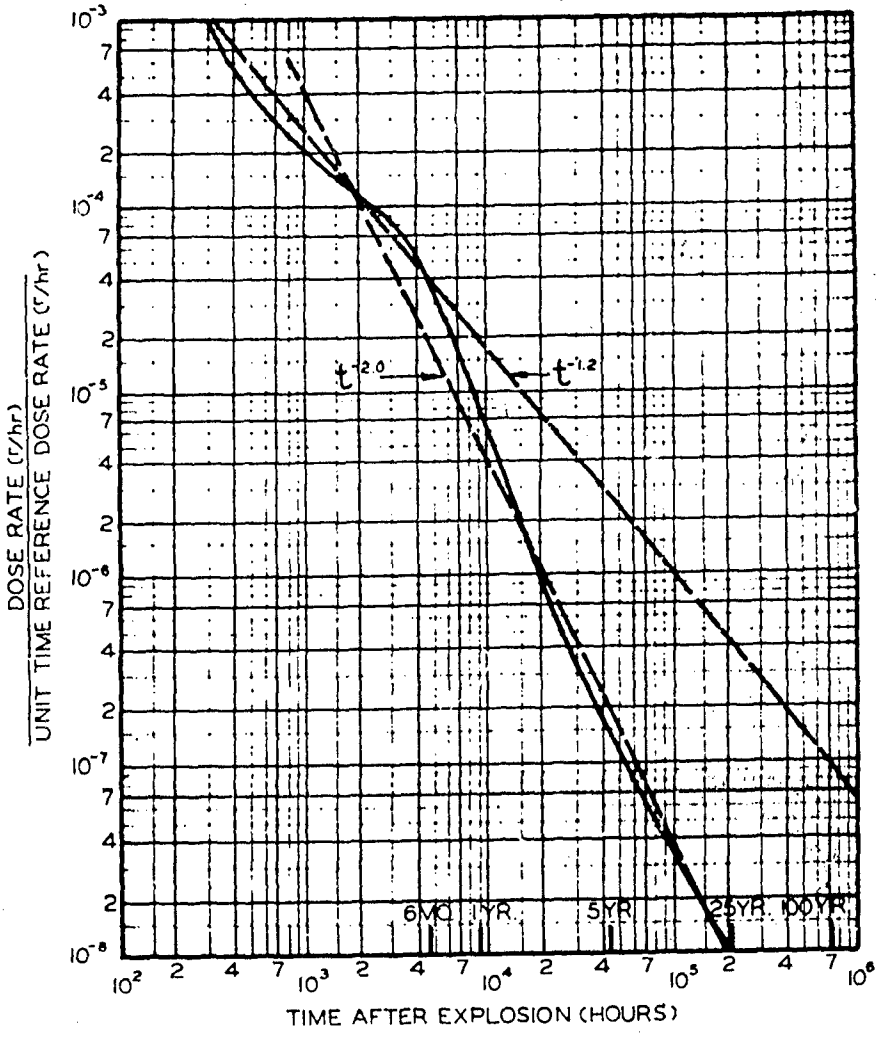

Figure B-55. Dose Rate vs Time After Explosion

the total dose can be expressed as: $D = \frac{R_1}{n-1} t_1^{1-n} - t_2^{1-n} = 5R_1 (t_1^{-.2} - t_2^{-.2})$

where: D = dose in roentgens
t_1 = time of entry in the field, in hours after detonation.
t_2 = time of exit from the field, in hours after detonation.

We will now consider another fallout example. Suppose that at various times after a nuclear explosion a series of readings (figure B-56) were taken as follows:

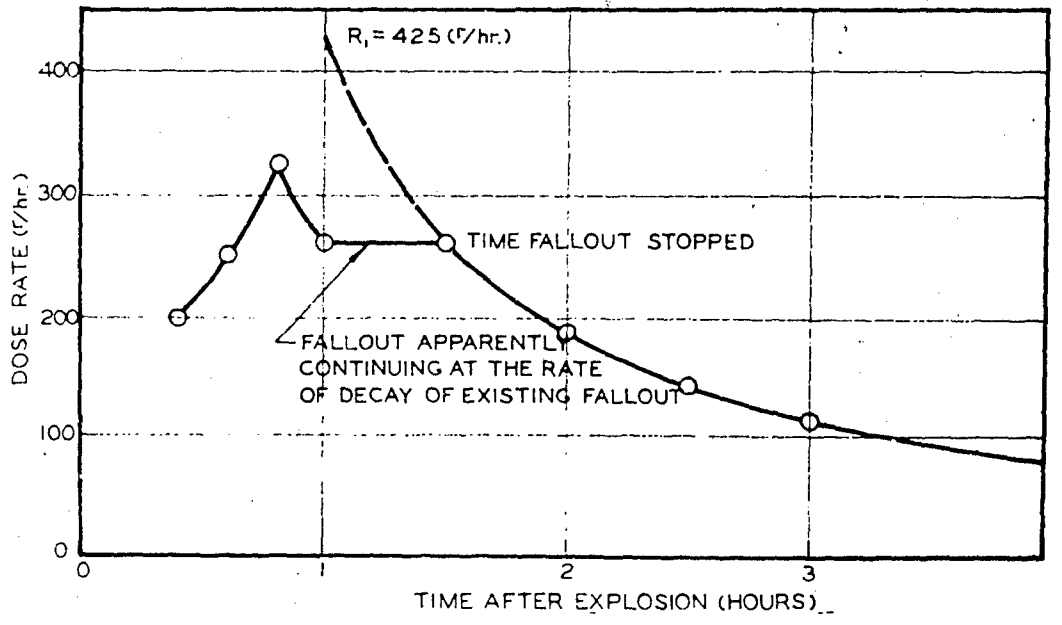

Figure B-56. Fallout Dose Rate vs Time After Explosion

0.4 hours	:	200 r/hr	1.5 hr	:	260 r/hr
0.6 hours	:	250 r/hr	2.0 hr	:	185 r/hr
0.8 hours	:	325 r/hr	2.5 hr	:	141 r/hr
1.0 hours	:	260 r/hr	3.0 hr	:	114 r/hr

(1) When has all the fallout arrived?
(2) What is the unit-time reference dose?
(3) If you were in this radiation field from time $t_1 = 2$ hours to $t_2 = 3$ hours, what dose would you receive?

The solution is: the fallout has all arrived at time t = 1.5 hours. Note that for the portion of the curve between 1 hour and 1.5 hours the curve is flat indicating that the fallout was arriving at the same rate as the rate of decay of the previous fallout.

(b) $R_1 = R_t\, t^{1.2} = R_{2\ hr}\,(2)^{1.2} = 185(2)^{1.2} = 425$ r/hr

(c) $D = 5R_1\,(t_1^{-0.2} - t_2^{-0.2}) = 5(425)\,(2^{-0.2} - 3^{-0.2}) = 5(425)\,(0.871 - 0.803) = 144.5$ roentgens

To consider the problem of target areas with large population concentrations nearby, it is necessary to subdivide the early fallout into two parts: close-in fallout and downwind fallout. This is necessary because the usual methods of obtaining fallout patterns are not valid within 20 to 40 miles of the target. To consider this region close to the target we must use an approach known as "close-in fallout prediction."

For a more complete background in this area refer to "The Effects of Nuclear Weapons" published by the U. S. Atomic Energy Commission. For our purposes here we will outline methods of prediction of fallout but will assume the reader has some knowledge of the effects of nuclear weapons.

4. Prediction of Close-In Fallout

Here, an attempt has been made to determine the unit-time reference dose rates to be used close to ground zero. The available fallout data does not provide values which are useable within 20 to 40 miles of ground zero. The idealized fallout patterns do not take into account the contribution from radioactive particles in the stem. With the aid of figures B-52 and B-53, and an extension of the idealized fallout pattern dose rate, curves in figure B-57 have been obtained. The dose rates may appear to be quite large. However, the values coincide closely with calculations made by J. E. McDonald in his article in the Journal of the Arizona Academy of Science, Vol. 2, (1962).

The width of contamination in close-in fallout is approximately the radius of the radioactive stem from figure B-58, plus a distance factor of 0.10 times the distance in miles downwind. This type of approximation is good only to about 40 miles downwind.

5. Prediction of Downwind Fallout

Several methods have been developed for predicting dose rates and total doses resulting from fallout. The four general categories are: the mathematical fallout model, the idealized fallout pattern, the danger sector forecast, and the analog method. Each of these techniques requires, of course, a knowledge of the total yield and amount of fission in the explosion, the burst height, the windstructure to the top of the radioactive cloud in the vicinity of the burst.

The method we will use to predict downwind fallout is the method of idealized fallout patterns. These patterns represent the average fallout field for a given yield and wind condition. No attempt is made to indicate irregularities which will undoubtedly occur in a real fallout pattern, because the conditions determining such irregularities are highly variable and uncertain. In spite of their limitations, idealized fallout patterns are useful for planning purposes, for example in estimating the overall effect of fallout from a large-scale nuclear attack. Although it will undoubtedly underestimate the fallout in some locations and overestimate in others, the evaluation of the gross fallout problem over the whole area affected should not be greatly in error.

For detailed fallout prediction, the winds from the surface to all levels in the radioactive cloud must be considered. However, for the idealized patterns, the actual complex wind system is replaced by an approximately equivalent "effective wind." This is taken as a mean value of the wind speed and direction from the surface to some representative height in the cloud. The level chosen generally lies between the bottom and the center of the mushroom head, where the concentration of radioactivity is believed to be a maximum.

By assuming little or no wind shear, that is, essentially no change in wind direction at various altitudes, the idealized fallout patterns have a regular cigar-like shape. But if the wind direction changes with altitude, the fallout will spread over a wider angle and the radiation level at a given distance from ground zero will be decreased because the same amount of radioactive material will be spread over a larger area. Lower wind speeds will make the pattern shorter in the downwind direction; this will decrease the level of radiation at some distance from the burst and will increase the dose rates immediately downwind of ground zero. If the wind speed is higher, the contaminated area will be greater, and the radioactivity will be higher at large distances from ground zero and lower immediately downwind of ground zero.

Before considering an idealized fallout pattern, it is important to understand how such a pattern develops over a large area during a period of several hours following a 1-megaton fission-yield surface burst. This may be illustrated in the diagrams of figures B-59 and B-60. The effective wind speed is taken as 15 miles per hour. Figure B-59 shows a number of contours (or "isodose-rate" lines) for certain (arbitrary) round-number values of the dose rate, as would be observed on the ground, at 1, 6, and 18 hours, after the burst.

A series of total (or accumulated) dose contours (or "isodose" lines) for the same times are given in figure B-60. It should be understood, of course, that the various dose rates and doses change gradually from the area one contour to the next. Similarly, the last contour line shown does not represent the limit of the contamination. The dose rate (and, therefore, the dose) will continue to be present, at a diminished value, over a greater distance. The reader should also bear in mind that this is an idealized pattern; and that "hot spots" or areas of high radiation levels form, as drifts of dust forming. The pattern will often be a "dog-leg" shape rather than a more regular cigar-like shape.

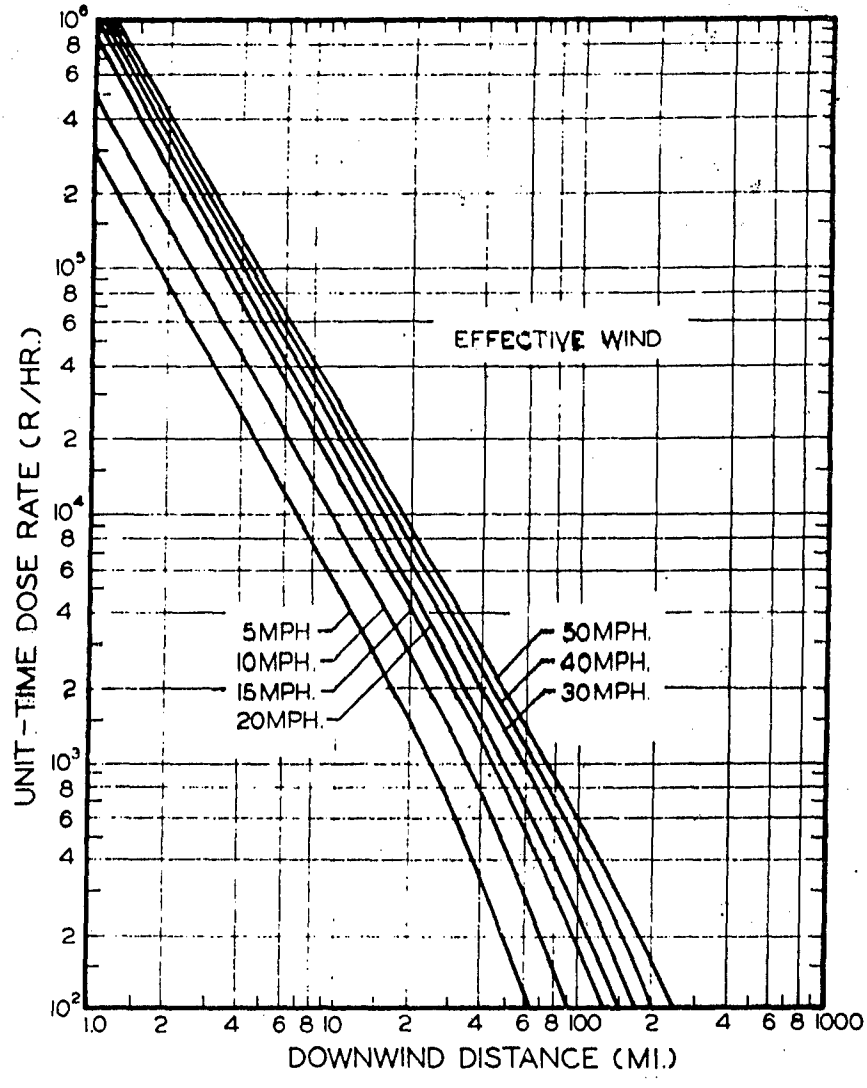

Figure B-57. Close-In Dose Rate Curves

Turning to figure B-59, it is seen that the total radiation dose received at the given location by 1 hour after the explosion is small, because the fallout has only just begun to arrive. By 6 hours, the total dose has reached over 3000 roentgens and by 18 hours a total dose of some 4800 roentgens will have been accumulated. Subsequently, the total dose will continue to increase, toward the value at time infinity, but at a slower rate. (See also figure B-60)

Next, consider a point 100 miles downwind from ground zero. At 1 hour after the explosion the dose rate, as indicated in figure B-59, is zero, since the fallout will not have reached the specified location. At 6 hours, the dose rate is about 1 roentgen per hour; at 18 hours about 5 roentgens per hour. The fallout commences at somewhat less than 6 hours after the detonation and it is essentially complete at 9 hours, although this cannot be determined directly from the contours given. The total accumulated dose from figure B-60 is seen to be zero at 1 hour after the explosion, less than 1 roentgen at 6 hours, and about 80 roentgens at 18 hours. The total (infinity) dose will not be as great as at locations closer to ground zero, because the quantity of fission products reaching the ground decreases with distance from ground zero.

In general, therefore, at any given location, at a distance from a surface burst, some time will elapse between the explosion and the arrival of the fallout. This time will depend on the distance from ground zero and the effective wind velocity. When the fallout begins to arrive, the dose rate will be small, but will increase as more and more fallout descends. After the fallout is complete, radioactive decay of the fission products will cause a steady decrease in the dose rate.

The idealized unit-time reference dose-rate contours for a 1 megaton fission-yield surface burst, with an effective wind speed of 15 miles per hour, are represented in figure B-61. This figure is based partly on test observations and partly on calculations. The maximum downwind distances and widths of the contours for various dose rates, down to 0.1 roentgen per hour, are recorded in the following table. No attempt is made here to express the upwind fallout pattern; this will be treated later.

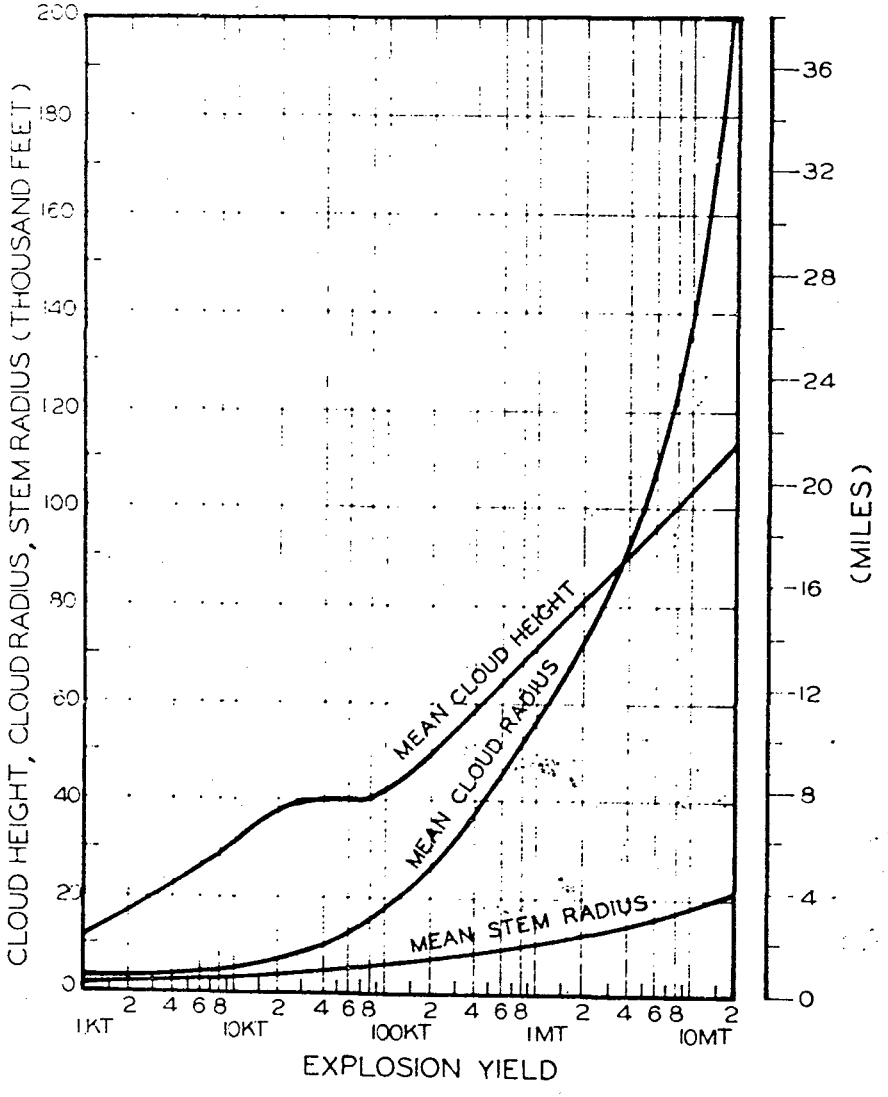

Figure B-58. Cloud Characteristics vs Yield

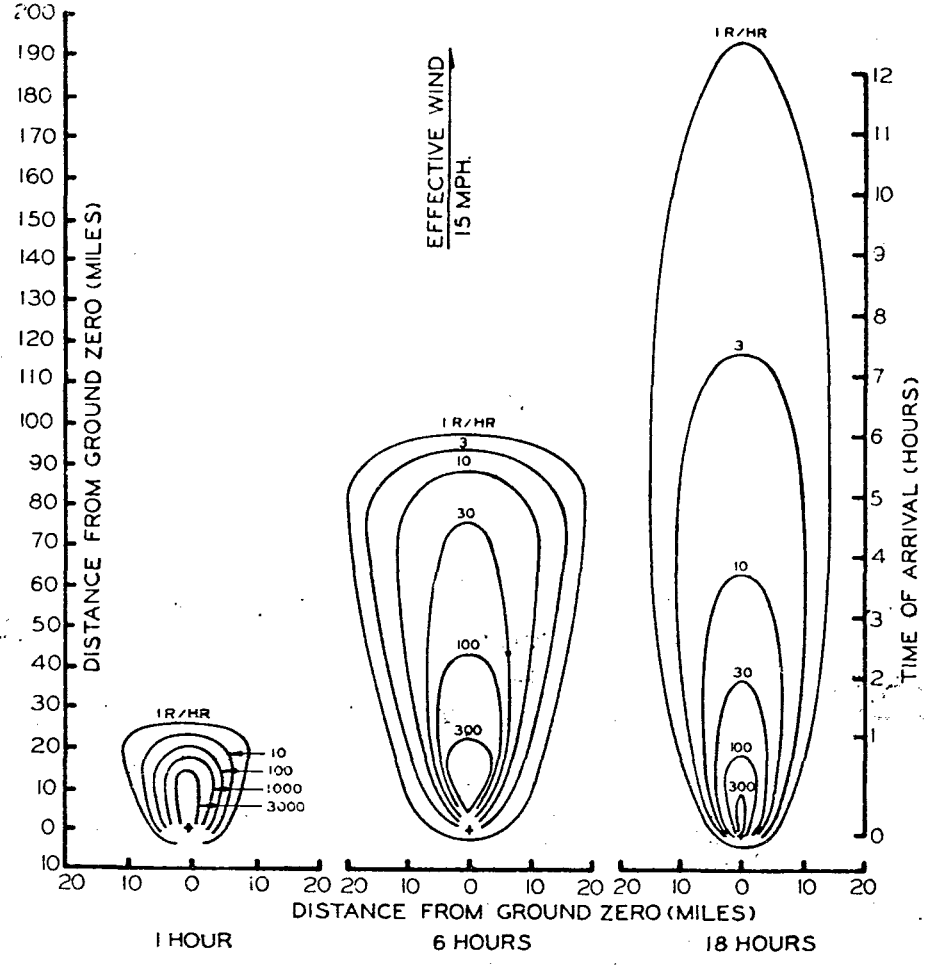

Figure B-59. Dose Rate Contours After A Surface Burst, One Megaton Fission Yield

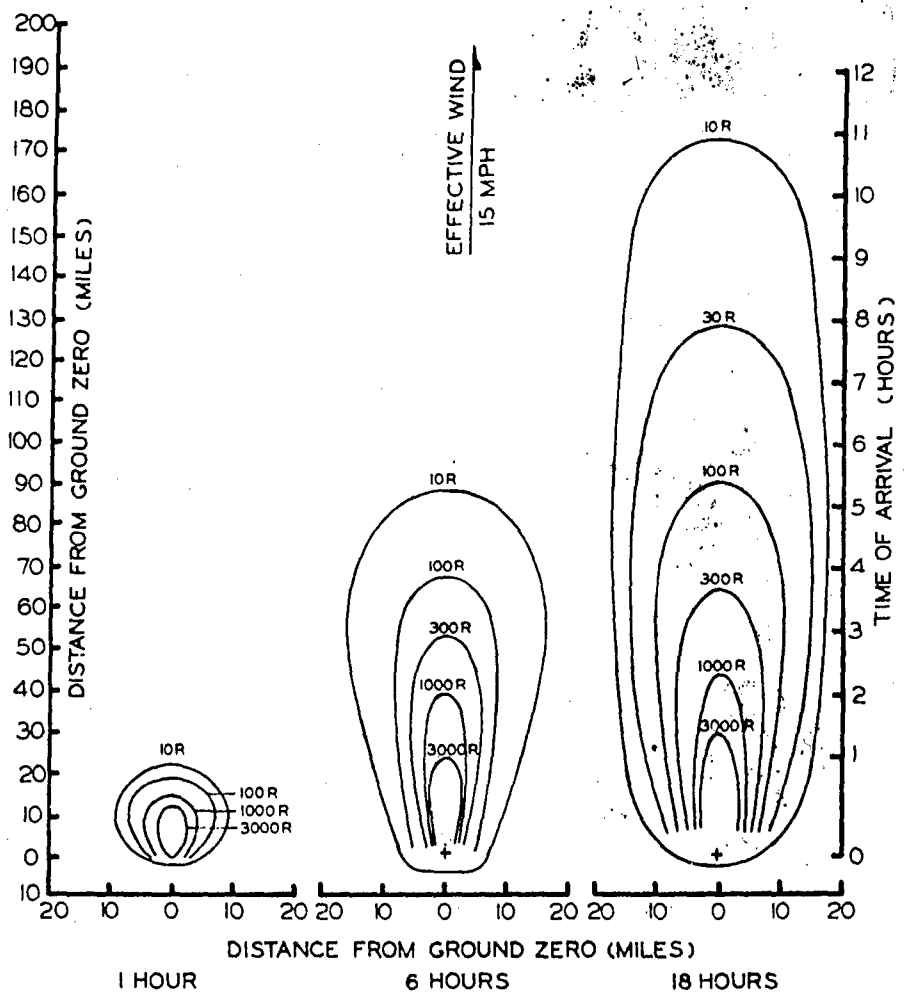

Figure B-60. Time Reference Dose Rate Pattern From 1 Megaton Surface Burst

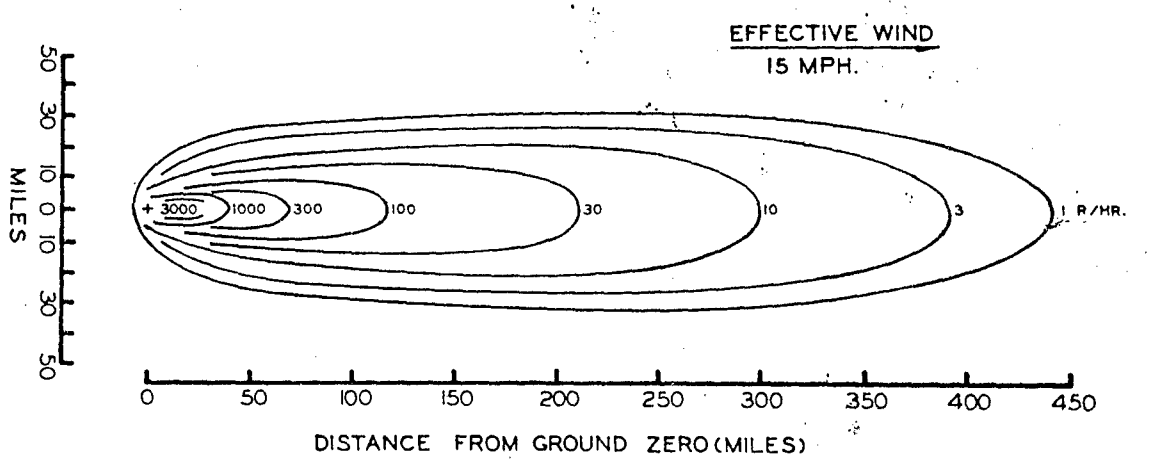

IDEALIZED UNIT-TIME REFERENCE DOSE-RATE PATTERN FOR EARLY FALLOUT FROM A ONE-MEGATON FISSION YIELD SURFACE BURST (15 MPH. EFFECTIVE WIND SPEED)

Figure B-61. Extended Time Reference Dose Rate Pattern

It should be understood that the idealized dose rates and total dose calculations made from figure B-61 would be those indicated by monitor instruments in open country with no shielding. Any type of shelter or shielding would decrease the dose received.

Downwind Extent of Unit-Time Reference Dose-Rate Contours
For 1-Megaton Fission Surface Burst With 15 MPH Wind.

Reference dose rate (roentgens/hour)	Downwind distance (statute miles)	Maximum width (statute miles)
3000	23	6
1000	42	10
300	74	12
100	120	18
30	210	30
10	300	42
3	390	50
1	440	56
0.3	500	60
0.1	530	62

6. Scaling Fallout Patterns

In order to obtain the idealized fallout pattern for a fission yield of F megatons, the values of the various contour lines in figure B-61 may be multiplied by F. Thus, for a weapon having a total yield of M megatons with 50% of the energy derived from fission, the factor would be 0.5 M. This scaling procedure works well for surface bursts from about 100 kilotons to 10 megatons fission yield. However, the higher values of dose rate (and dose) may be overestimated for fission yields in excess of 1 megaton. As the weapon yield increases so also does the initial volume of the radioactive cloud; therefore, the maximum concentration of activity in the cloud does not change at the same rate as the yield. At greater distances downwind the law is more reliable because, as a result of spreading by the wind, the initial cloud volume has relatively little influence on the concentration of fallout on the ground.

It should be noted that the proportional scaling procedure makes no allowance for the effect of the total (fission plus fusion) yield; thus it predicts the same fallout pattern for a 1-megaton all fission detonation as for a 2-megaton 50% fission explosion. Actually the unit-time reference dose rate near ground zero might be somewhat smaller in the latter case because the same amount of radioactivity is spread over a larger volume of the initial cloud. At greater distances downwind from the burst point the effect of the initial cloud concentration is small, as indicated above. Furthermore, at such locations the dilution effect may be compensated for by the fact that the cloud from the 2-megaton explosion will probably rise higher; thus increasing the distances at which particles, from the same relative position in the cloud, reach the ground.

The "effective wind" speed and direction are the mean values from the ground up to a certain level in the radioactive cloud, depending on the total yield of the explosion. As a very rough estimate, the atmosphere layers over which the wind is to be averaged as a function of the weapon yield are:

Total yield	Layer
Less than 1 MT	Surface to 40,000 feet
1 MT to 5 MT	Surface to 60,000 feet
More than 5 MT	Surface to 80,000 feet

These values should be adequate for the rough evaluation of hypothetical fallout situations based on the idealized patterns. More elaborate prediction schemes take into consideration winds at different levels instead of a single average effective wind.

If there is no directional wind shear, then doubling the wind speed would cause the particles of a given size to reach the ground at twice the distance from ground zero, so that they should be spread over roughly twice the area. Based on this conclusion, the following scaling laws may be used in connection with the idealized fallout pattern: the unit-time reference dose-rate value for each contour in the 15 mph wind velocity pattern of figure B-61 is multiplied by 15/v, where v is the actual effective wind velocity in miles per hour; and the downwind distances in figure B-61 are multiplied by v/15. For a 30 mph wind, for example, the contour values would be halved and the distances doubled.

It will be apparent that in scaling for either yield or wind speed the values of the dose-rate contours are changed. The scaled downwind extent for any given contour value may be readily obtained by plotting the scaled dose rates versus the scaled downwind distances on logarithmic graph paper and reading downwind distances corresponding to the desired contour value from the resulting smooth curve; see figure B-62.

7. Upwind Fallout from Megaton-Range Explosion

A technique for predicting the ideal fallout contours in the upwind and crosswind directions has been developed from data obtained in connection with tests of devices in the megaton range at the Eniwetok Proving Grounds. The treatment is based on the expectation that the upwind extent of fallout will depend primarily on three factors: the maximum upwind extent of the radioactive cloud, the minimum time required for particles from the upwind edge of the cloud to reach the ground, and the mean effective wind from the ground up to the altitude of the broadest part of the cloud.

Observations at Eniwetok have indicated that, for megaton-range detonations, the broadest base of the cloud is generally stabilized at almost the altitude of the tropopause which was about 55,000 feet in the test area. The mean arrival time on the ground for upwind fallout was found to be about 30 minutes. In the continental United States, the height of the tropopause is less and the estimated arrival time would be 24 minutes. Hence, while falling particles from the upwind edge of the cloud would be carried downwind back toward ground zero a distance (in miles) equal to 0.4 times the wind speed in the United States.

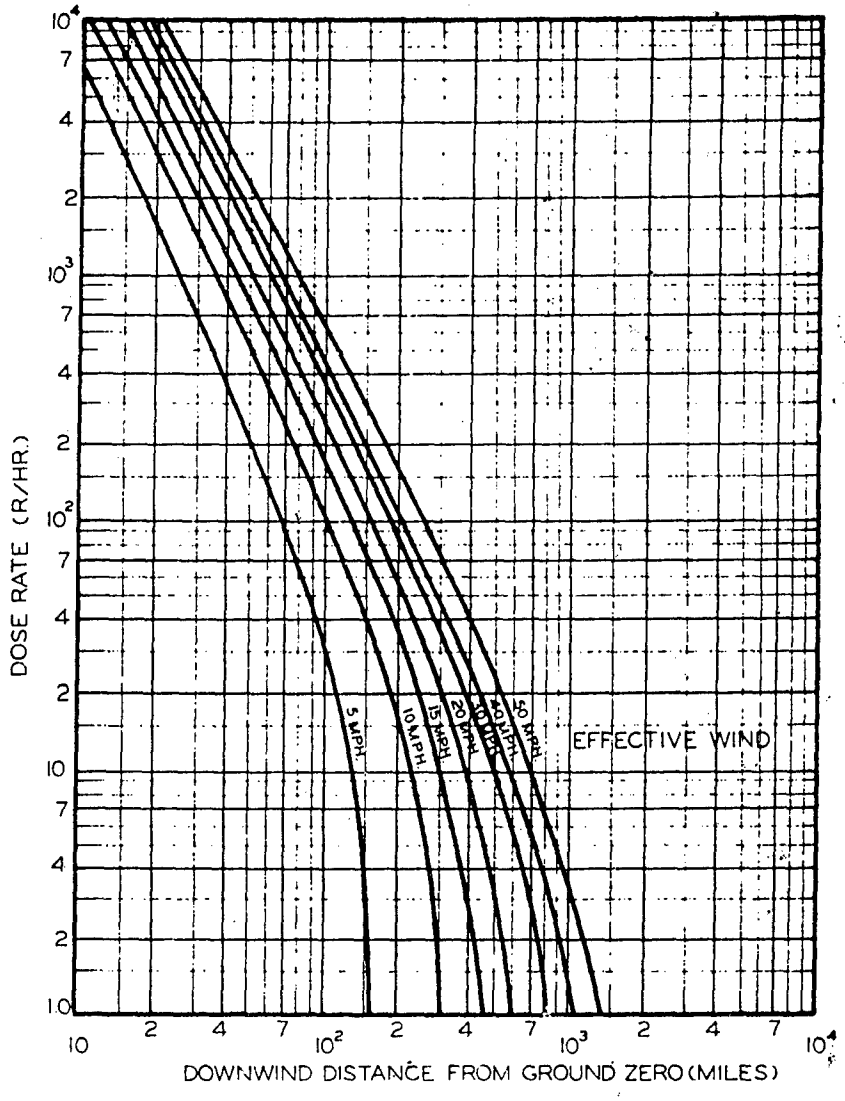

Figure B-62. Downwind Distribution

The same reasoning may be applied to specific dose-rate contours. It may be assumed that if there were no wind the contours would be circles centered at ground zero. The radius of each contour would then be determined only by the total yield and the fission percentage. Presumably, the radius of a contour would not be effected by the wind, but the center of the circles would be displaced in the downwind direction by the same distance the particles are carried downwind from the edge of the cloud.

From the available data on upwind and crosswind fallout in tests made at Eniwetok, contours for unit-time reference dose rates of 1, 10, and 100 roentgens per hour have been derived. These have been adjusted to zero wind speed and the radii of the corresponding circles are shown in figure B-63, as a function of the total yield of the surface burst, assuming 50% fission. If the fission percentage is different from this value, then the indicated dose rates should be multiplied by the ratio of the actual fission percentage to 50%. Figure B-63 also gives the radius for a peak blast overpressure of 7 psi, representing the area of almost total destruction. The dimensions of the visible cloud at 10 minutes after the explosion are also given (being the average time at which the cloud becomes stabilized).

To convert these results into the idealized contours for an actual situation, it is necessary to know the effective wind speed and direction. In view of the uncertainty of the height of the cloud base, it is recommended that the speeds for altitudes of both 40,000 and 60,000 feet be considered and the lesser be taken for the present purpose. The wind direction should also be that for 40,000 feet. Multiplication of the mean wind speed by 0.4 would then give the displacement from ground zero of the centers of the circular contours in the downwind direction. Mean wind speeds and expected direction of fall of particles, for various elevations, can be obtained from UF (Upper-air Fallout) wind data reported regularly by the U. S. Weather Bureau.

For purposes of illustration, consider a 10 megaton surface burst, with a 50% fission yield. Suppose that the mean wind from the surface to 40,000 feet is 25 mph and its downwind direction is 30° east of north, and that the mean wind speed to 60,000 feet is 20 mph. Hence, the effective wind speed to be used in constructing the upwind pattern is 20 mph, with a direction of 30° east of north. The displacement of the center of the contour circles is thus 0.4 x 20 = 8 miles, in the downwind direction.

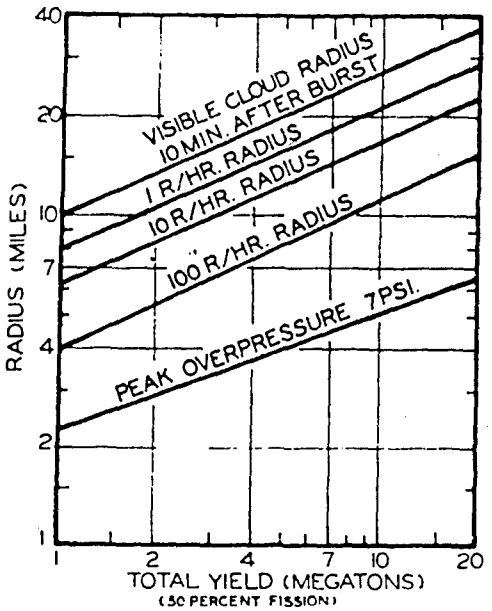

Figure B-63. Radii for Unit-Time Dose Rates from Early Fallout as Function of Total Yield Surface Burst

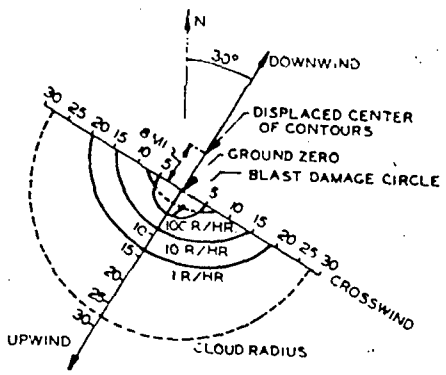

Figure B-64. Illustration of Calculation of Upwind Early Fallout Pattern

From figure B-63 the radii of the unit-time reference dose-rate contours for a 10 megaton burst are:

1 roentgen/hour	:	21 miles
10 roentgen/hour	:	16.5 miles
100 roentgen/hour	:	11 miles

Semi-circles are now drawn having these radii with the center point 8 miles downwind of ground zero, as shown in figure B-64. Any contour, for example the one for 100 roentgens/hour, passing through the circle of severe blast damage (7 psi overpressure), which has a radius of about 5 miles in the present case, may be regarded as uncertain. The area within this blast damage circle may be expected to be heavily contaminated by induced activity, stem fallout, and throw-out, regardless of the wind speed.

8. Tucson Sample Problem:

Close-in Fallout: If the assumed attack level is 10 MT on each of the Titan II sites and an assumed fission yield of 50% then we must choose an effective wind speed and direction. A likely condition would be if the three sites 9, 10, and 11 were depositing close-in fallout on the center of the city and the wind speed were 20 mph. We will take each site separately and add them up.

	Site 9	Site 10	Site 11
Distance from City	36 miles (SW)	28 miles (SW)	20 miles (SW)
Stem Diameter	7.4	7.4	7.4
Dist. Factor 1/10 (D)	3.6	2.8	2.0
Width of Fallout	11.0 miles	10.2 miles	9.4 miles
Unit Time Dose Rate	1600 r/hr/MT	3000 r/hr/MT	5000 r/hr/MT
Dose Rate for 5 MT Fission Yield	8000 r/hr	1500 r/hr	25000 r/hr
Total	48,000 r/hr over the city.		

Of course this does not take into account any interaction effects and it may not be the worst condition. It is possible to consider the interaction of Sites 5, 8, 11, 13, 15, and 18 (with an attack pattern of two 10 megaton explosions at each site) and arrived at a radiation level of 200,000 r/hr.

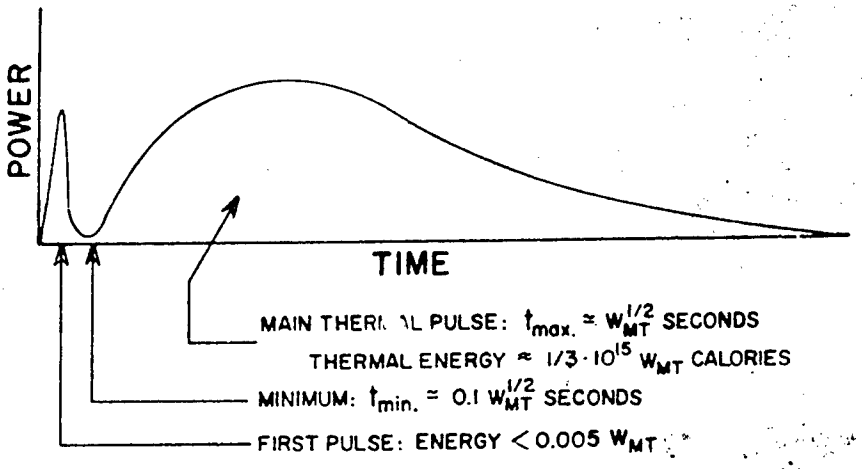

Figure B-65. Thermal Pulse Amplitude and Duration

F. Prediction of Thermal Radiation

1. Introduction

A nuclear detonation releases a relatively large fraction of its energy content in the form of thermal radiation. The reason for this large thermal release is the extremely high temperatures produced when the large energy created (10^{15} calories of heat per megaton) is released in a fraction of a microsecond. These high temperatures of the order tens of millions of degrees then lead to a high rate of energy loss to the surrounding to the surrounding air. Initially, the high temperature of the bomb radiates thermal energy at wavelengths to which the air is opaque. Thus the radiated energy in turn heats the air until its temperature reaches about a million degrees resulting in the formation of a plasma. The plasma is transparent to radiation and radiates to the surroundings.

2. Thermal Pulse

Release of energy in the form of plasma results in the first thermal energy pulse observed in atmospheric explosions. About 10% of the total radiant energy is released in this pulse. It is terminated within a few microseconds by the formation of the shock wave which heats the surrounding air, making the air relatively opaque which shields the fireball from its surroundings. As the shock expands, it weakens, and heats the air less and less. The shock front then becomes more transparent resulting in an increase in the rate of emission of radiant energy as the fireball shine-through. Eventually the energies of the fireball dissipate with the radiant energy release, dropping to zero. A plot of thermal radiation versus time is shown in figure B-65(i).

The first pulse is short because it originates in a small radiating sphere. The energy released is less than one percent of the total explosion energy. The second pulse lasts longer and comes from a larger spherical source and accounts for one-third of the total yield. If the burst occurs at the surface, the injection of dirt into the fireball makes it more opaque, resulting in a decrease in the radiant portion of the yield by something more than a factor of two.

The effects of the atmosphere modify the energy reaching a distant observer rather markedly. The radiating fireball is initially at a very high temperature, emitting energy primarily in the ultraviolet and soft x-ray range. The air will pass energy only in the visible range. The air thus screens the observer until the fireball cools to 5000 K where its emission falls mainly in the visible range. Thus the effect of the air is to delay the final radiant power output until the shock is well expanded.

The energy emitted as visible light is subject to some scattering and absorption. Thus the radiant energy reaching a point is dependent not only on the yield (W) and the distance, but on the visibility or transmittance of the air. An approximate formula for calculating thermal energy intensity is:

$$Q = WT/D^2$$

where, Q is thermal energy intensity in cal/cm^2,
W is yield in kilotons
D is distance in miles, and
T is the transmittance.

A curve of transmittance versus distance is given below:

(i)Brode, Harold L., "Thermal Radiation from Nuclear Explosions," The Rand Corporation, paper P-2745, August 1964.

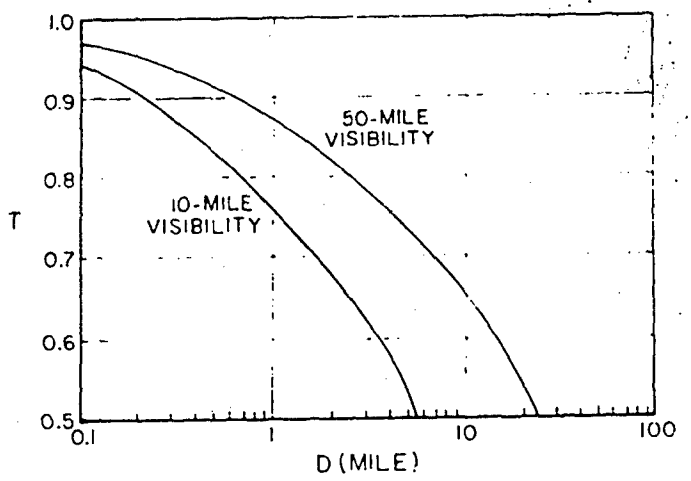

Figure B-66. Thermal Energy Attenuation With Distance

3. Radiant Energy

Based on the available results, the thermal radiant energy as a function of slant range is given in figure B-66 for visible of 10 and 50 miles.

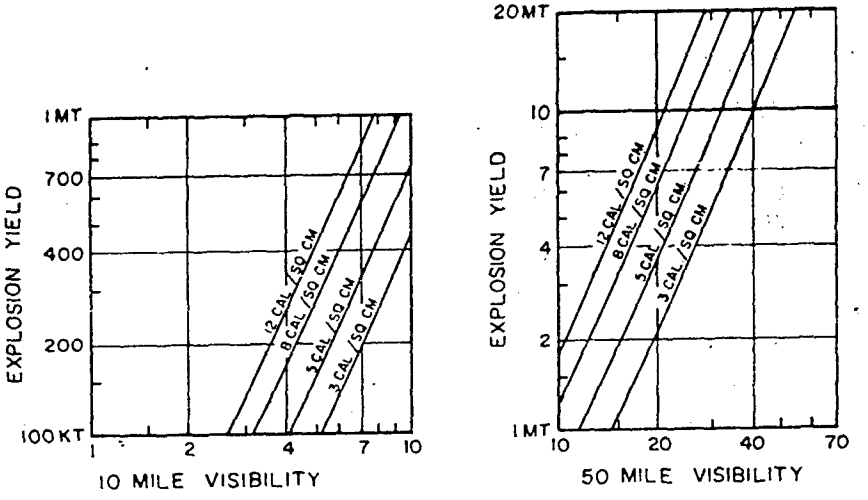

Figure B-67. Thermal Energy Attenuation With Visibility

The 50 mile visibility is more representative of the desert southwest.

The effect of such heat fluxes in igniting materials is dependent not only on the materials, but also on the atmospheric condition at the time and on the rate of delivery of the heat from the source. Haze, smog, low cloud layers, or fog are just as effective in shielding the light from a nuclear explosion as they are as a shield against sunlight. Further, the humidity (or lack of it) in the air may be a very important factor in conditioning materials prior to exposure to the radiant energy from a weapon.

APPENDIX - PART C
ENGINEERING ANALYSIS AND DESIGN

LIST OF ILLUSTRATIONS

PART C

ENGINEERING ANALYSIS AND DESIGN

A. Introduction

When design to resist blast and other close-in nuclear weapons effects is considered, it is only logical to realize that simultaneously large amounts of initial radiation and fallout may be inevitable realities. It is this combination of effects which make buried structures most feasible. The shielding required to meet the radiation requirements and the structural strength required to meet blast requirements both point to these forms of structures as desirable and economical. As a result, it is fitting that information on the design of protective construction should include the analysis and design of buried structures.

Little experience is available on this subject, but this fact is not a sufficient cause to avoid the application of judgement and engineering intuition to develop practical solutions. The economies available in such structures force engineers to develop conservative procedures for design; at the same time test data and research feed the store of knowledge necessary to refine the designs.

B. Soil-Structure Interaction Forces

1. Definition

Soil-Structure interaction forces are those forces which act at the interface between a buried structure and the surrounding soil medium. These are generally considered to be normal pressures, but shearing forces also exist at this interfacial junction.

2. Distinction between types of forces

Normal forces are pressures which act normal to the interfacial surface and are generally in the same order of magnitude as the surface overpressures in the air medium above the ground surface. Shearing forces are those forces which are tangential to the interfacial surface and generally are in the same order of magnitude as the respective shearing forces in the soil under these conditions. In general, the normal forces produce the greater effect or response in the structure and, because of this, we will limit our discussion to the action of structures under this interaction component only.

C. Effective Soil-Structure Interaction Pressures

1. Definition

The effective soil-structure interaction pressure is defined as that normal pressure distribution which at a given instant will produce a static free-field deformation in the structure equal to the deformation of the structure in the soil medium at that same instant. It follows then, if we can neglect the shearing components of interaction forces, that the moments and stresses under this effective pressure will equal those in the confined structure at the same instant.

2. Dependent variables

Effective soil-structure interaction pressures depend upon the characteristics and homogeneity of the soil, the nature of the loading, and the stiffness and geometry of the buried structure, in relationship to the surrounding soil.

D. Types of Buried Structures

Because the type of buried structure has so much to do with the nature of buildup or attenuation of the passing overpressure, it is appropriate to consider these types in some detail. The three basic types, into which categories most buried structures fall, are the rigid, rigid-flexible, and flexible types. See figure C-1.

1. Rigid buried structures

Rigid buried structures are those buried structures which by definition undergo negligible deformation upon loading. As a result of their rigidity, they have certain pecularities of interaction behavior which will be discussed in more detail later.

2. Rigid-flexible buried structures

A rigid-flexible structure is one which be definition exhibits rigid characteristics until some point in the rising loading cycle; at this point it yields or flexes in such a manner so as to reduce its volume or alter its shape considerably.

3. Flexible buried structures

Flexible buried structures are those structures which by definition exhibit yielding or other noticeable structural deformation immediately at the first sign of an overload. They continue this yielding or reduction in volume behavior throughout the rising loading cycle.

E. Settlement ratios

To understand the nature of soil-structure interaction phenomena, it is appropriate to consider three basic types of settlement ratios. These are positive, negative, and zero ratios.

1. The positive settlement ratio

a. Definition

The positive settlement ratio by definition is associated with the change in geometry of the soil mass surrounding a buried structure such that the structure feels a vertical load in excess of the resultant of the dead and live loads immediately overhead.

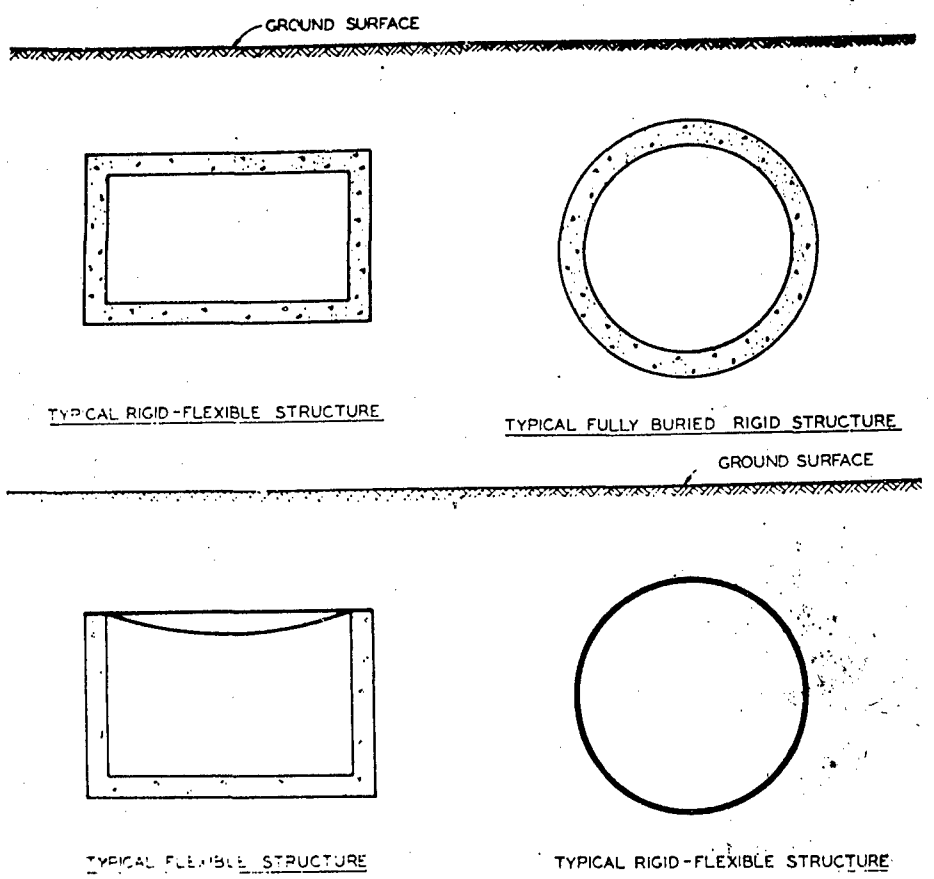

Figure C-1. Types of Buried Structures

b. Visual description

The concept of positive settlement ratio may be described visually by the idealized drawing in figure C-2. It will be observed that the soil mass surrounding the structure deflects more than the vertical column of soil in which the structure is contained. As a result of this idealized geometrical discontinuity, vertical shearing forces are produced which add to the load that is normally experienced. The effective soil-structure interaction pressure for this situation is then larger than that existing in an undisturbed soil at this same depth. To be sure, this sudden discontinuity does not usually exist and more corbeling action may be observed, however the overall effect is the same.

c. Systems conducive to positive settlement ratios

Systems which produce positive settlement ratios are generally those which contain rigid structures. These rigid structures increase the overall stiffness of the vertical column of soil in which they are contained. A simplified version of this result is shown in figure C-3. If we assume a stress-strain relationship such as Hooke's Law to be valid, the left column of soil will deflect an amount ΔL_1, where $\Delta L_1 = \frac{PL}{E}$. The column of soil which contains the rigid structure will deflect an amount, $\Delta L_2 = \frac{P(L-D)}{E}$, where D is the height of the rigid structure. These two displacements differ by an amount, $\frac{PD}{E}$. The first is always greater than the second, all other things being equal. The magnitude of this difference to some extent determines the amount to which the pressure reaching the structure is increased by this geometrical action.

2. The negative settlement ratio

a. Definition

The negative settlement ratio by definition is associated with the change in geometry of the soil mass surrounding a buried structure such that the structure feels a vertical load which is less than the resultant of the dead and live loads immediately overhead.

b. Visual description

The negative settlement ratio is shown visually in figure C-4. It will be observed that the soil mass surrounding the structure deflects less than the vertical column of soil in which the structure is contained. As a result of this idealized geometrical discontinuity, vertical shearing forces are produced which subtract from the load that is normally experienced. The effective soil-structure interaction pressure for this situation is then smaller than that existing in an undisturbed soil at the same depth. As before, the sudden discontinuity does not exist and in reality soil arching takes place but the overall effect is the same.

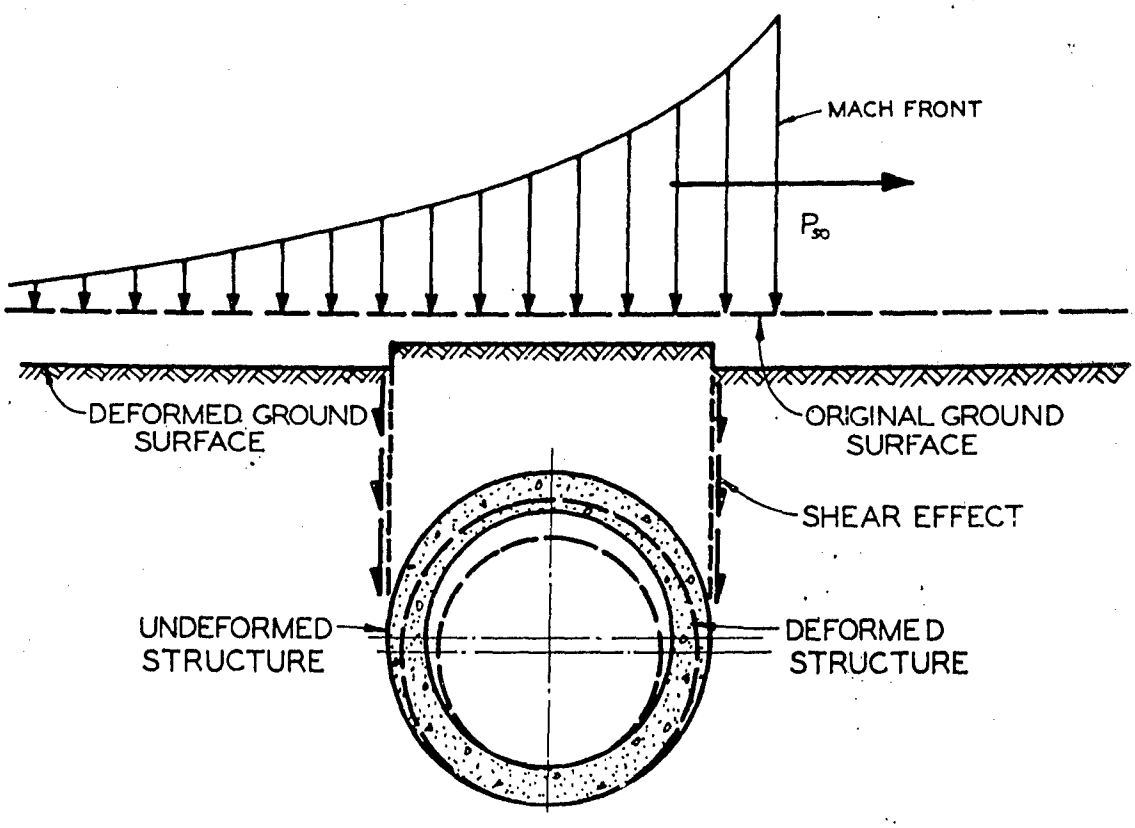

Figure C-2. Idealized Positive Settlement Ratio

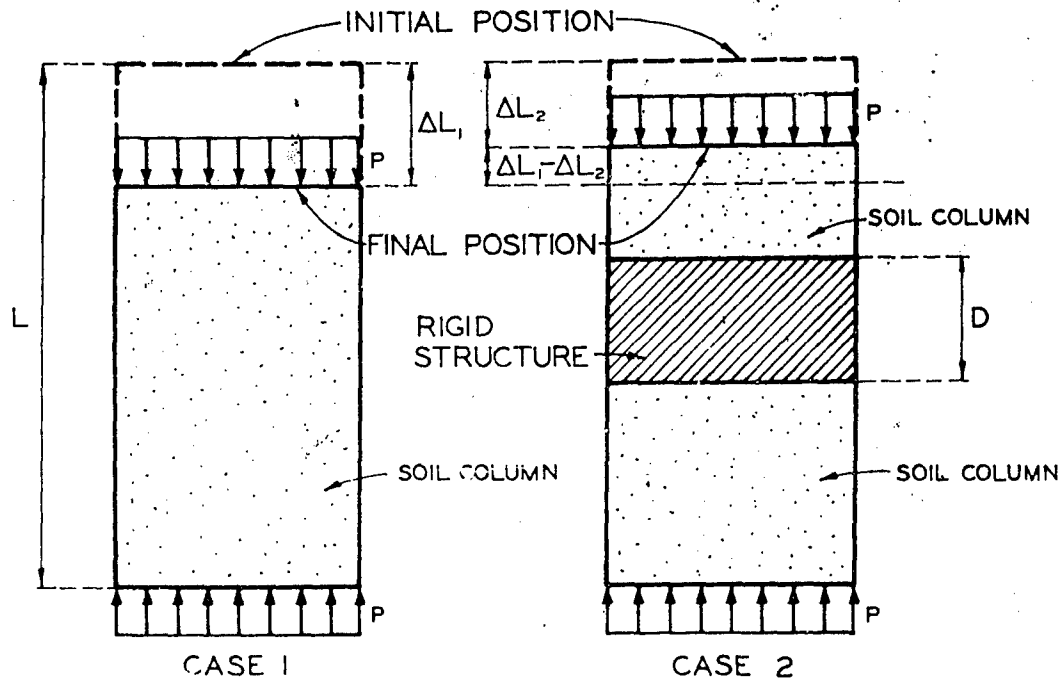

Figure C-3. Positive Settlement Ratio

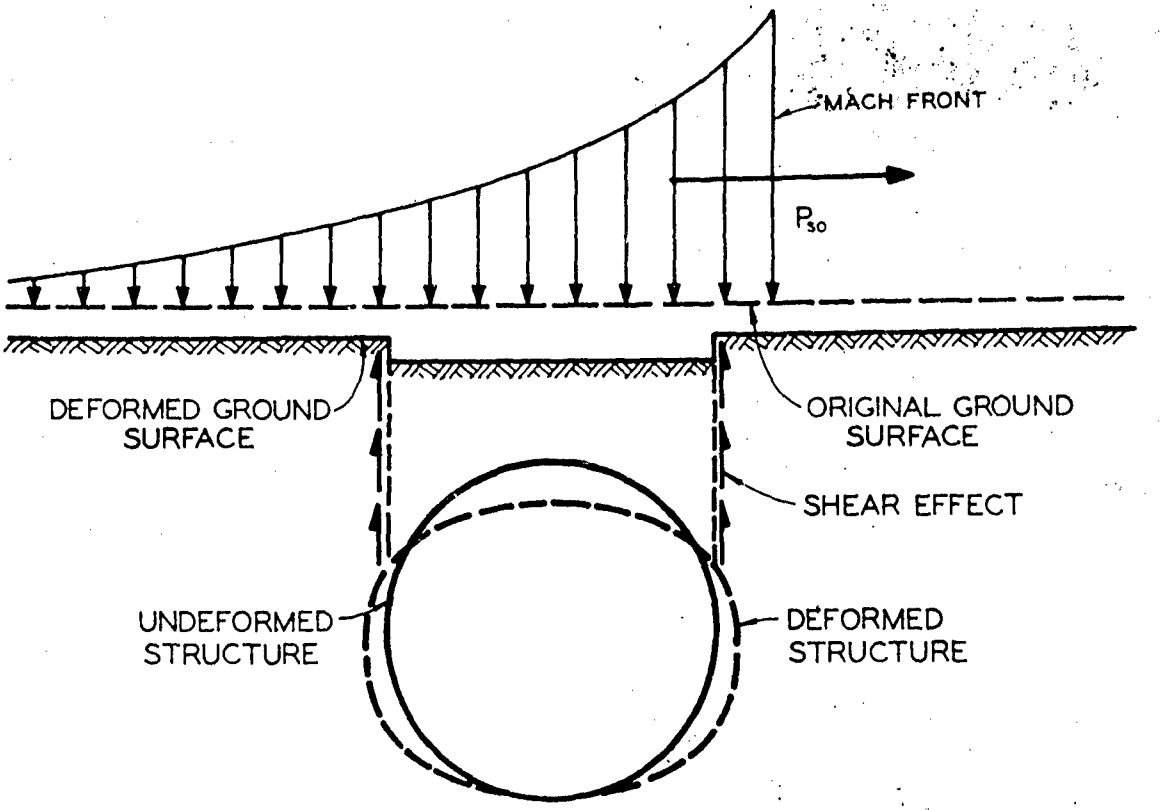

Figure C-4. Idealized Negative Settlement Ratio

c. Systems conducive to negative settlement ratios

Systems which produce negative settlement ratios are generally those which contain flexible structures. These flexible structures reduce the overall stiffness of the vertical column of soil in which they are contained. A simplified version of this result is shown in figure C-5. If the same linear stress-strain relationship is assumed as that previously, the left column of soil will deflect an amount $\Delta L_1 = \frac{PL}{E}$, as before. The column of soil on the right, which contains the flexible structures, will deflect an amount $\Delta L_2 = \frac{P(L-D)}{E} + \Delta D$. If ΔD is greater than $\frac{PD}{E}$, then ΔL_2 will be greater than ΔL_1. ΔD will always be greater than $\frac{PD}{E}$ if the structure is more flexible than the soil mass it replaces. Flexible structures by definition are not as stiff as surrounding soil; therefore, they always produce negative settlement ratios.

3. Zero settlement ratio

a. Definition

A zero settlement ratio is defined as being associated with that condition which exists when the surrounding soil mass and the soil column containing the structure deflect equal amounts. Under such conditions, the effective soil structure interaction pressure is equal to that existing in an undisturbed soil medium at the same point. Figure C-6 shows such a condition.

b. Systems conducive to zero settlement ratios

These systems are those in which the soil and structure possess equal stiffnesses. Certain types of rigid, rigid-flexible, and flexible structures may at some point in their loading cycle exhibit this behavior. In general, such situations rarely happen throughout the entire loading cycle.

F. Soil-structure interactions

1. Rigid fully-buried structures

Rigid fully-buried structures generally produce positive settlement ratio conditions and, as a result, should be designed for pressures in excess of those existing at similar points in undisturbed soils. By definition, a rigid structure is one which undergoes negligible deformation on loading. According to the AFDM definition, a fully-buried structure is one which is buried sufficiently so that transient effects of shock wave loadings may be neglected. Figure C-1 shows a typical rigid buried structure. This arch, if corresponding to the fully-buried definition, can only undergo uniform compressive stress by virtue of its uniform pressure loadings. The only bending that can develop is due to the change in curvature associated with the uniform change in radius that results from this idealized loading.

Qualitative aspects of the behavior of this structure under a traveling pressure wave are shown in figure C-7. At initial contact of the wavefront with the structure, non-uniform pressures are developed. These pressures deform the cylinder immediately with the result that passive earth pressures develop on the sides at right angles to the wavefront. Very rapidly, the situation degenerates or stabilizes into that shown in the later diagrams. Once the pressure is uniform, it then starts to decay in a manner somewhat proportional to the decaying surface wave.

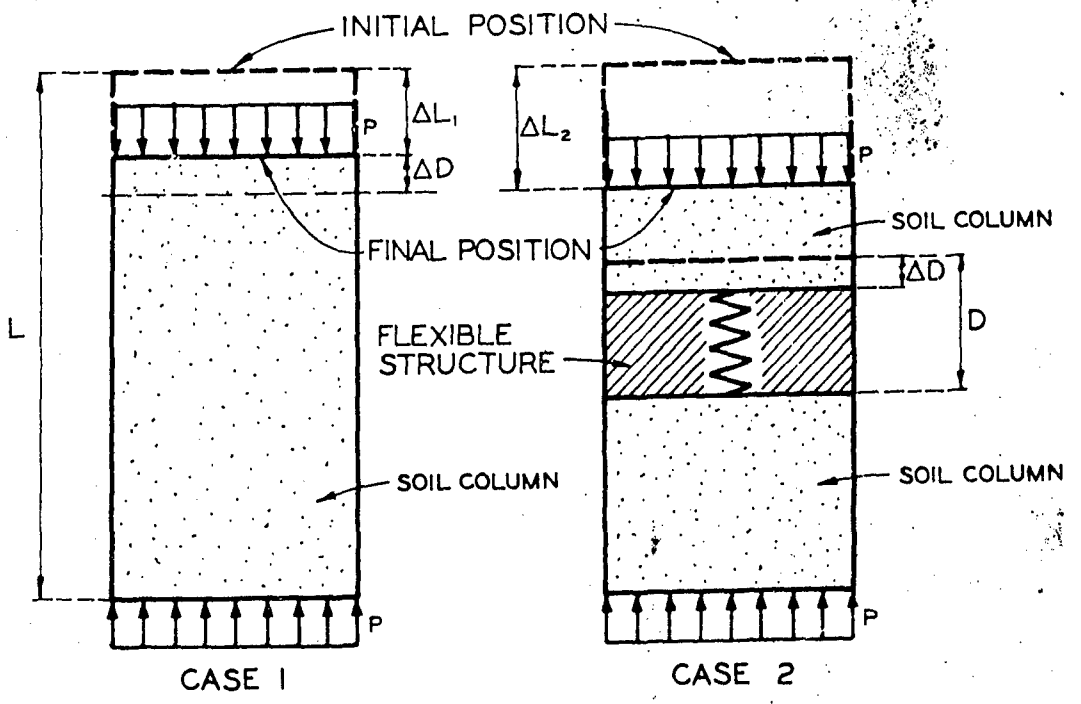

Figure C-5. Negative Settlement Ratio

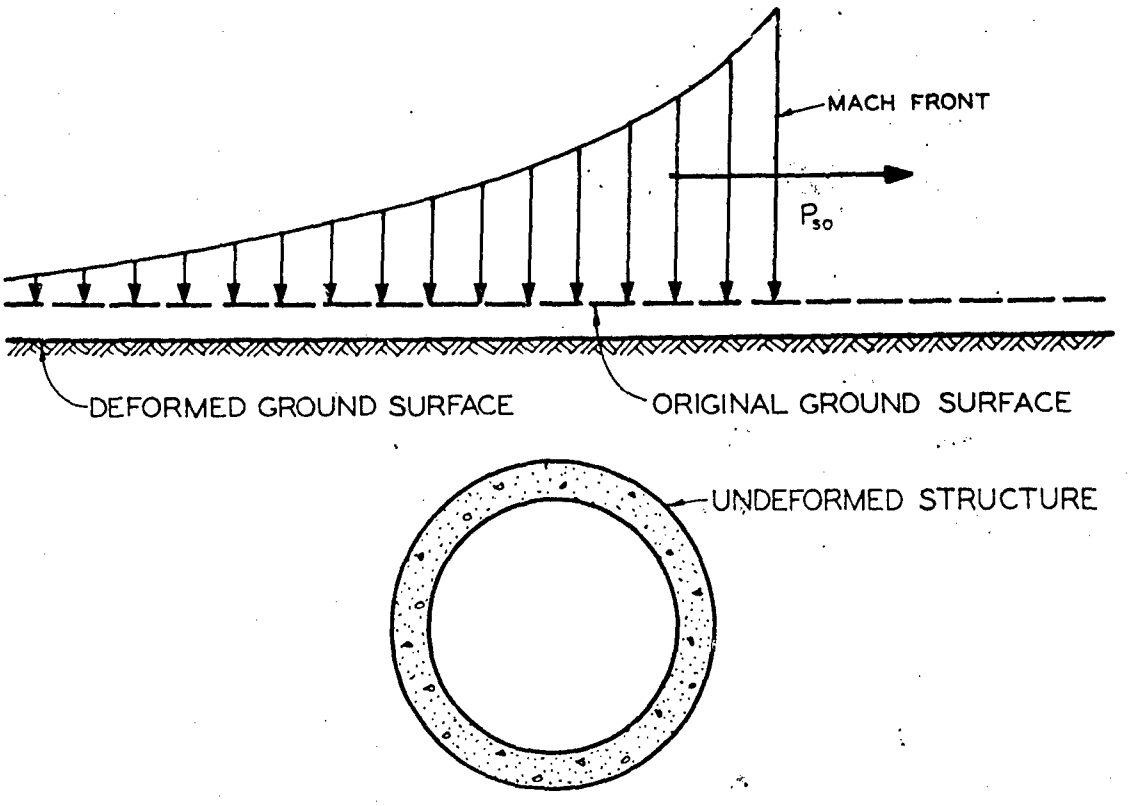

Figure C-6. Zero Settlement Ratio

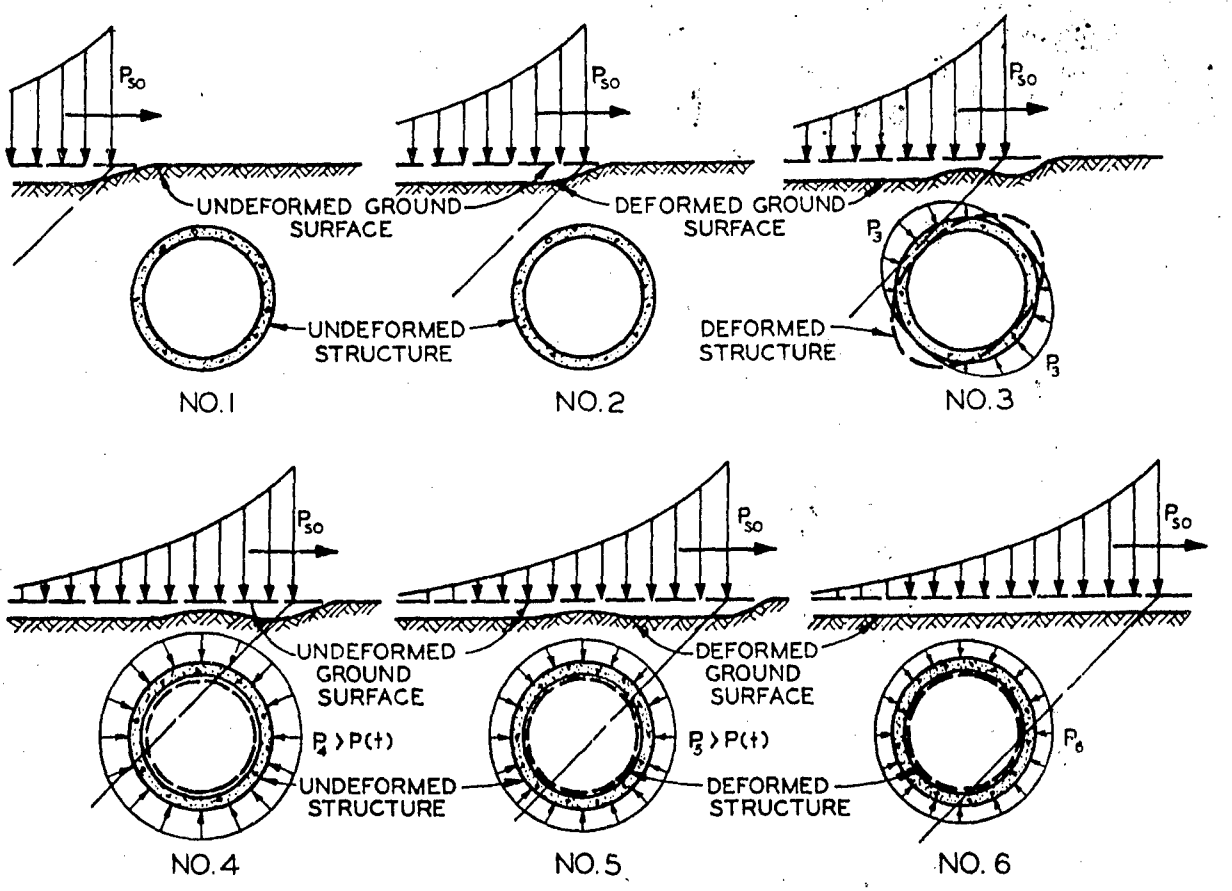

Figure C-7. A Structure Under A Traveling Pressure Wave

2. Flexible buried structures

Flexible buried structures exhibit the opposite behavior to rigid structures. Yielding begins almost instantly with the sign of overpressure and continues until such has been relieved. A typical flexible structure is shown in figure C-1. These structures contain yielding tension membranes as the roof and floor. Such structures will produce negative settlement ratios which rapidly attenuate blast overpressures.

3. Rigid-flexible buried structures

As the name implies, a rigid-flexible buried structure exhibits the qualities of each type during its loading cycle. As might be expected, positive settlement ratios immediately followed by negative ratios may develop. A typical rigid-flexible structure is shown in figure C-1. Another type of popular rigid-flexible structure is the steel culvert which is actually ambidextrous in that it may exhibit rigid, flexible, or rigid-flexible behavior depending on the nature of loading, type of backfill procedure, etc. Generally, however, it is quite rigid until either large elastic deformations or buckling takes over. Either of these latter effects are those of a flexible nature. Figure C-8 shows stable elastic yield of this structure. Figure C-9 shows unstable yield.

4. Summary of effects

The various types of structures, because of their various actions, feel different transmitted pressure waves. These waves, in their different forms, may be seen in figure C-10. Notice the immediate advantages of the rigid-flexible and flexible types.

G. Analysis features

Quantitative predictions of soil-structure interaction loads are most difficult. Here we have a statically indeterminate structural problem of the worst type. Very little quantitative information, of any kind, is available to substantiate reliable magnitude predictions. There is a particularly intense need for more theoretical and experimental data on the soil-structure interaction phenomenon. The recent soil-structure interaction symposium at the University of Arizona was designed to review the current state of the art in this regard.*

H. Design features

The ultimate in structural analysis is to find an answer, such as stress and displacement, given a structure, its supports and its loads. Obviously, for most physical systems there is generally but one answer. The analyst hopes to either find this answer exactly or else deter-

*Soil-Structure Interaction Symposium held at the University of Arizona, June 8-11, 1964, in Tucson, Arizona.

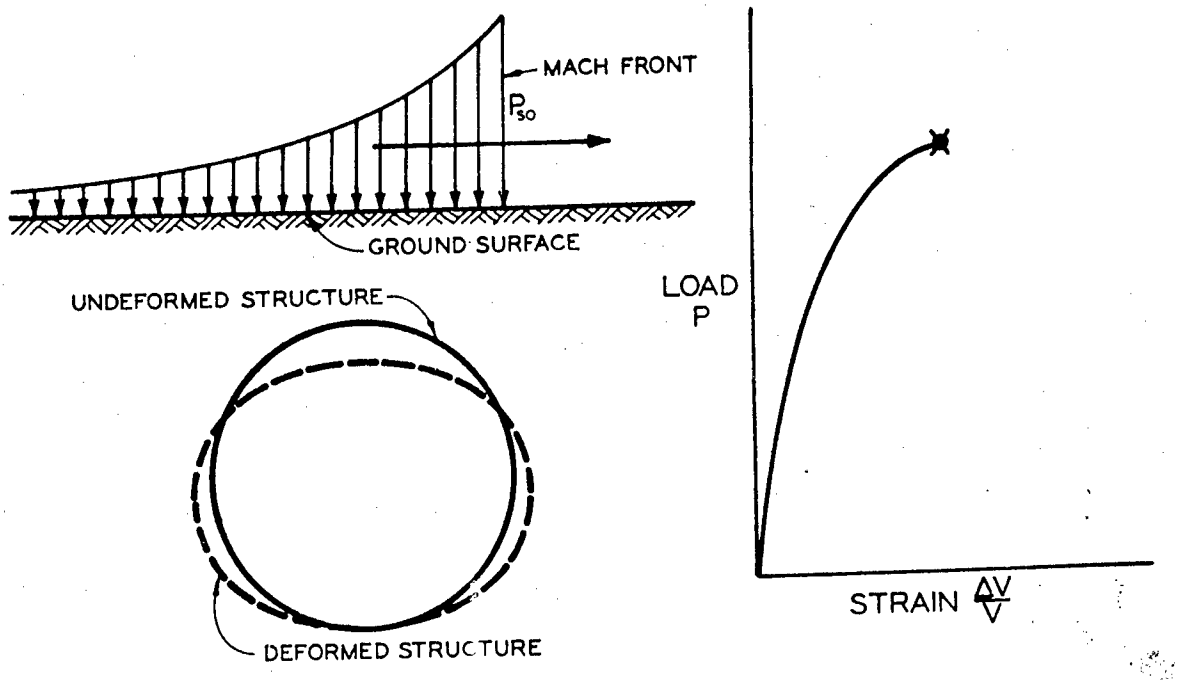

Figure C-8. Stable Yield of Culvert

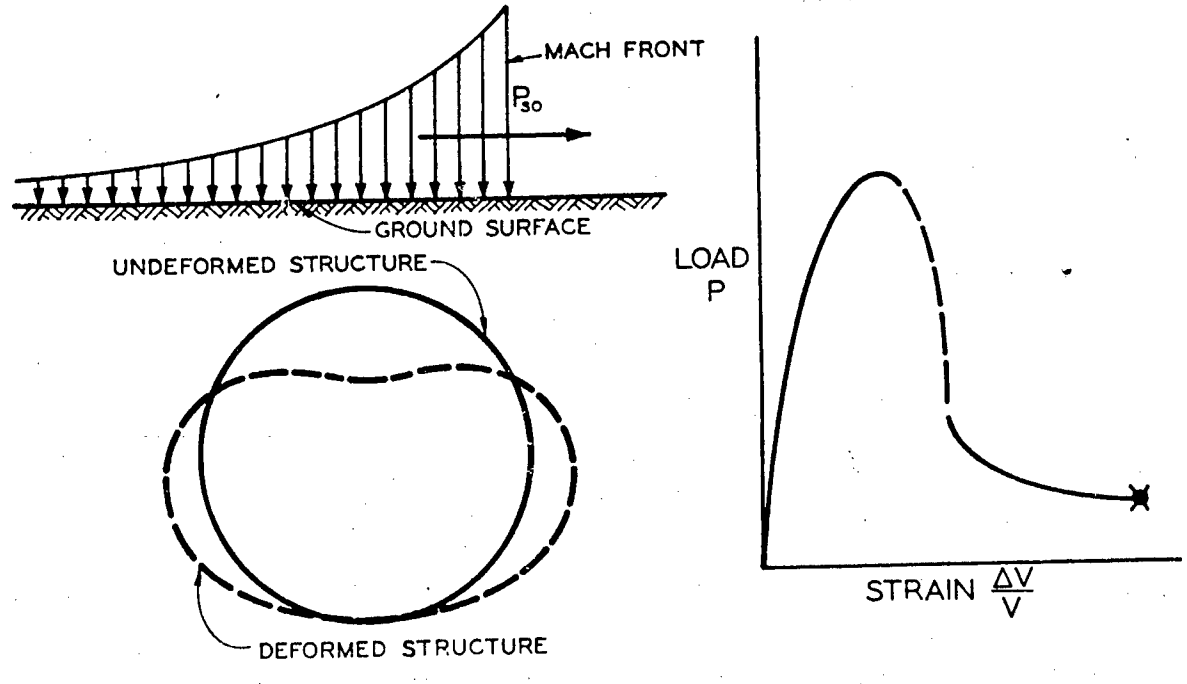

Figure C-9. Unstable Yield of Culvert

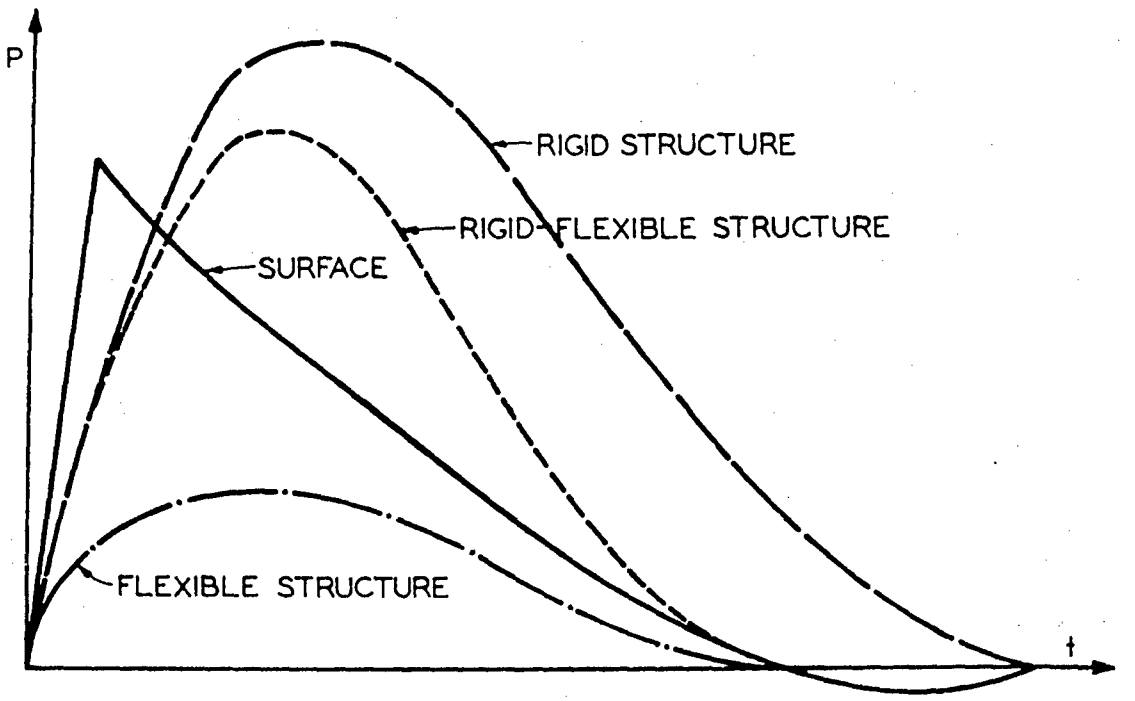

Figure C-10. Pressure Waves on Structures

A qualitative understanding of the general physical behavior of an underground structure, as we have just considered, is not sufficient for analysis. However, such an understanding is sufficient for design. Because so little is known about the quantitative behavior of underground structures, as compared with those above-ground, we unavoidably find that our designs are conservative. This is not altogether bad, however, because the source of conservatism is generally found in the supporting strength offered by the soil. For regions in which blast overpressures are considered, close-in fallout and initial radiation will almostassuredly be such that quite a bit of mass will be required for adequate shielding. There is no more economical mass for shielding than earth and therefore, in such regions, buried structures make sense from the fallout and radiation standpoint, as well as from the blast resistance standpoint.

I. Design of fully-buried structures

1. General

The design of a fully-buried structure, as the design of any structure, depends upon many factors, both quantitative and qualitative. Many decisions which are based on preliminary information must be made before any actual structural design can even be commenced. Among these decisions and respective preliminary information upon which they depend are the following:

a. Overpressures

The magnitude of peak overpressures that may be produced at the point in question due to a near nuclear burst must be estimated. This, of course, is dependent upon many factors such as magnitude of weapons, location of bursts, type of burst, terrain effects, etc. Part A of the appendix discusses this subject in more detail.

b. Duration of positive phase of loading function

The duration of positive phase of the passing pressure wave may be important, if the dynamics of the system are considered. Also associated with this, is the rise time for the respective loading. In general, the negative phase is unimportant for a buried structure.

c. Ground motions

Predictions for the respective ground motions and peak accelerations must be determined. As for the case of overpressures, these depend upon weapon size, location, type and nature of burst. In addition to this, properties of the soil medium play a most important part. Both direct ground shock and air-induced ground shock are important, however, air-induced ground shock covers a wider range of application. Part B of the appendix discusses this subject in more detail. Motions of the buried shelter are assumed to be the same as those of the surrounding soil.

d. Shielding requirements

The depth of soil cover greatly affects the shielding characteristics and resulting protection factors of the enclosed space. The protection factors which must be developed, are based on initial radiation, early fallout, and delayed fallout predictions. Shelter stay times are also closely related to these factors. Five feet of earth is usually sufficient to resist most close-in fallout effects.

e. Probability of survival

The relative importance of the structure and the validity of the loading predictions govern the determination of the desired probability of survival requirement. This requirement affects the selection of structural type, be it rigid, flexible, or rigid-flexible.

f. Functional uses

The function determines the required size or space as well as certain aspects of the shape. Required stay times also affect space requirements because of associated supply storage quantities.

The activities of the personnel and equipment may also impose certain conditions upon the selection and design of the structure.

2. Selection of the structural form

a. The various structural forms which have a capacity for resisting overpressures should be considered in light of the magnitudes of the peak overpressure and duration of the positive phase. Some of the advantages and disadvantages of the various forms follow:

(1) Rigid concrete structures

These structures have an advantage of lack of deformation on loading and lifetime permanence with respect to corrosion, etc. Unfortunately, however, in regions of high overpressure, they may exhibit spalling characteristics and possible brittle failures.

(2) Rigid-flexible metal structures

These structures, such as the steel culvert, have a degree of toughness to overload and shock which makes their use in regions of high overpressure very desirable. They tend to deform excessively under overloads, however, and adequate allowance for this possibility must be made. Also, they may be subject to corrosive action from water. Unpredictable stability problems may develop which require conservative design. Functional planning of space also creates unique problems, unless, of course, mobility capacity is desirable.

(3) Rigid-flexible concrete structures

These structures gain their flexibility by either elastic or inelastic action. Such structures are susceptible to cracking and spalling and, therefore, their use should be questioned in regions of high overpressure. They are relatively simple to form, however, and may find extensive use in situations where such cracking and spalling is unimportant to the desired function.

(4) Flexible metal structures

Structural forms which are flexible and stable and which gain their flexibility by uniform yielding are most desirable forms for use in regions of high overpressure and ground shock. By virtue of their negative settlement ratio behavior, they have an excellent capacity to absorb large overloads. They may be subject to corrosive action, however, and also the change in volume of the structure due to yielding may be significant enough to render these shapes undesirable. Proper conception of these structures can eliminate all possibility of buckling.

3. Design of fully-buried structures

a. Arches

The design of these structures is well presented in the Air Force Design Manual and as a result, this information will not be repeated here. The reader is referred to this source for specific information on recommended design procedures for this type of structure.

b. Domes

Domes may be designed by the same general procedure as cylinders. A fully-buried dome will "feel" a uniform pressure and as the result of this will carry most of this load by direct stress. The membrane theory of shells should be used for the design of these structures, however, a minimum of about 0.4% of steel should be used in each direction. Buckling in doubly-curved shells is not nearly as likely as in the cylindrical types. In general, buckling need not be considered as long as the loads are uniformly distributed. Boundary conditions for domes can be quite serious, however, and because of this special considerations must be made at these points. Consider the elliptical dome. The ellipse may be used, in this case, to eliminate hoop tension at the boundary. The shape has a ratio of major to minor axis of $\sqrt{2}$ which brings about this zero stress condition under uniform pressure. The added functionality offered by the fast rise from the spring line--enables the people to stand close to the wall.

In general, domes are superior to cylinders as structures, but they do not lend themselves functionally to any sort of transportation network. They, like cylinders, are rigid and thus produce positive settlement ratio effects. To offset these effects, domes naturally guide the soil into an arching behavior, but this requires foundation yielding or a similar effect to produce the appropriate negative settlement.

J. Flexible Membranes

1. General

Flexible buried structures, because of yielding characteristics which produce negative settlement ratios, offer the ultimate in economy because of the way in which they force the soil to resist the overload. The most efficient flexible structure is that which simultaneously yields under constant stress at every point in its plane. The behavior of such a structure may be predicted in advance by an inverse solution to the differential equations for stress in shell structures under normal pressure loadings.

The introduction of this approach to design was made by H. P. Harrenstien at the symposium on Shell Research, Delft, The Netherlands, August 30, 1961. The application at that time was directed toward the "Configuration of Shell Structures for Optimum Stress." Basically, the approach involves the initial assignment of a given final stress state, such as that of constant stress. The search is then made for the shell structure which exhibits this final state of stress under a previously assigned normal pressure loading. For the situation at hand, a uniform yield stress may be assumed under a blast pressure loading. The configuration of this yielding membrane under this blast pressure loading is then the desired result.

For an example of the structural efficiency of a system such as this, consider the following design comparisons.

2. Membrane Analysis of a Thin Plate

For a comparison consider the same span as that of a previously designed flat slab.

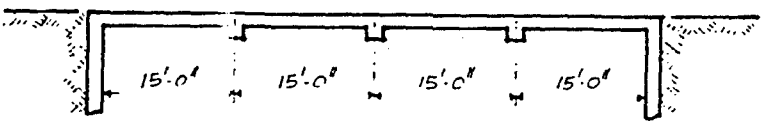

Where under a standard design with p_o = 50 psi the resulting section is as follows:

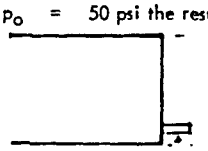

$$A_s = 0.02(17)\ (12)\ \frac{in^2}{ft.} = 4.08\ \frac{in^2}{ft.}$$

Now consider the same span covered with a thin steel plate.

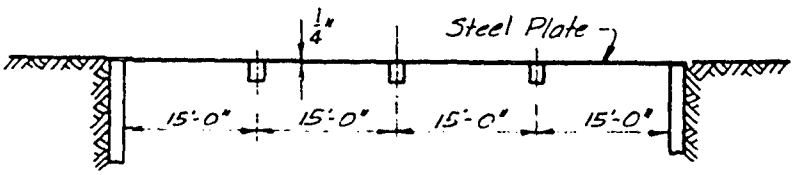

Assume that when the load is applied the plate will yield into a circular arc. Consider a free body of the loaded section:

at yield $T = f_s^t = 40{,}000\ (1/4) = 10{,}000$ lbs/in.

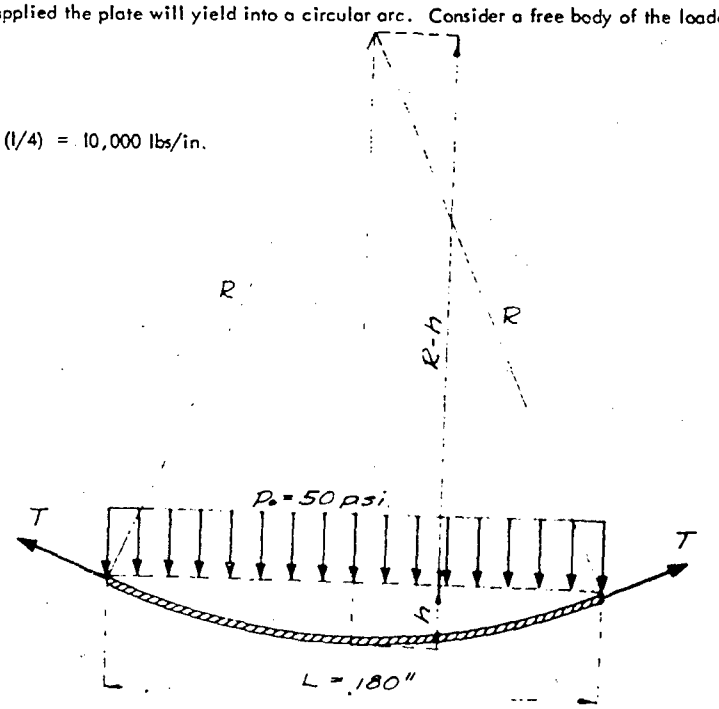

By static equilibrium:

$$\sum F_v = 0$$

$$P_o (L) - 2\left(10{,}000 \frac{L/2}{R}\right) = 0$$

$$P_o = \frac{10{,}000}{R} \quad \text{or} \quad R = \frac{10{,}000}{P_o}$$

This determines the radius as a function of the load only, independent of the length (L). This condition in itself is insufficient since no consideration is given to the percentage elongation.

For this particular case of loading: $P_o = 50$ psi $\quad R = \frac{10{,}000}{50} = 200$ in.

Now consider the equation of the triangle bounded by R and R-h.

$$(R-h)^2 = R^2 - \left(\frac{L}{2}\right)^2$$

$$R - h = \sqrt{R^2 - \left(\frac{L}{2}\right)^2}$$

$$h = R - \sqrt{R^2 - \left(\frac{L}{2}\right)^2}$$

h for this case is given by: $h = 200 - \left[(200)^2 - (90)^2\right]^{1/2} = 200 - 178 = 22"$

Calculation of the percentage of elongation:

$$\%e = \frac{S - L}{L}$$ where S is the arc length of the membrane

$$S = R \alpha = (200)\, 2 \tan^{-1} \frac{90}{178} \frac{\pi}{180} = 187.2"$$

$$\%e = \frac{187.2 - 180}{180} = \frac{7.2}{180} = 0.04 = 4\%$$

3. Two-Way Circular Membrane

Consider a circular plate of diameter L subjected to a load of P_o psi, and clamped around the circumference.

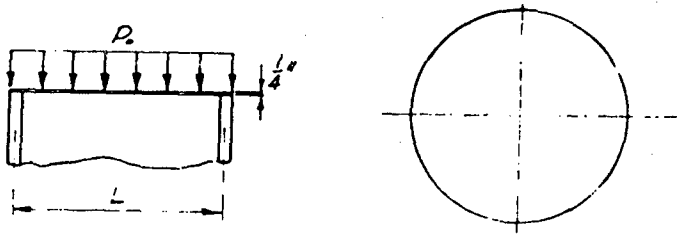

$$T = f_s t = 40{,}000\ (1/4) = 10{,}000 \text{ lb.}$$

From static equilibrium:

$$\sum F_v = 0$$

$$P_o \pi \left(\frac{L}{2}\right)^2 = 10{,}000 \left(\frac{L/2}{R}\right) \pi \left(\frac{L}{2}\right) 2$$

$$P_o = \frac{20{,}000}{R} \quad \text{or} \quad R = \frac{20{,}000}{P_o}$$

For $P_o = 50$ psi, $R = 400$ in.

It must be noted at this point that in order to obtain the membrane state in each of the previous examples the edge conditions must be considered. The lateral force which develops from the membrane forces of the plate, must be resisted by some structural element.

4. Application of the General Membrane Theory

Consider a free-body of an element of a shell:

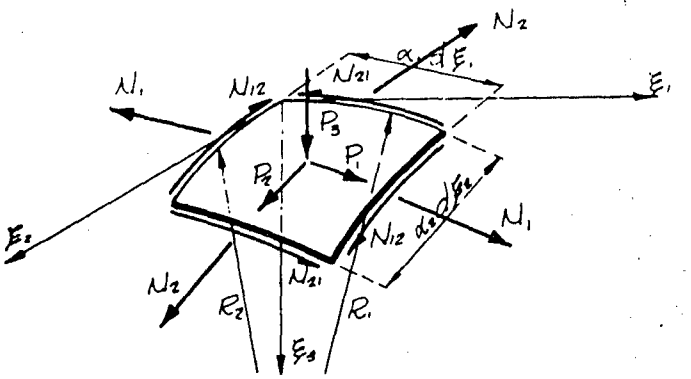

From the equilibrium conditions:

$$\frac{\partial(\alpha_2 N_1)}{\partial \xi_1} + \frac{\partial(\alpha_1 N_{21})}{\partial \xi_2} + N_{12}\frac{\partial \alpha_1}{\partial \xi_2} - N_2 \frac{\partial \alpha_2}{\partial \xi_1} + \alpha_1 \alpha_2 P_1 = 0$$

$$\frac{\partial(\alpha_1 N_2)}{\partial \xi_2} + \frac{\partial(\alpha_2 N_{12})}{\partial \xi_1} + N \frac{\partial \alpha_2}{\partial \xi_1} - N_1 \frac{\partial \alpha_1}{\partial \xi_2} + \alpha_1 \alpha_2 P_2 = 0$$

$$\frac{N_1}{R_1} + \frac{N_2}{R_2} + P = 0$$

For: $N_1 = N_2 = +S$ (constant), and $N_{12} = N_{21} = 0$

$$\frac{1}{R_1} + \frac{1}{R_2} = -\frac{P_3}{S}$$

For an axially symmetrical case, the above equation can be rewritten in the following form:

$$\frac{1}{r\left[1+\left(\frac{dr}{dz}\right)^2\right]^{1/2}} - \frac{\frac{dr}{dz^2}}{\left[1+\left(\frac{dr}{dz}\right)^2\right]^{3/2}} = -\frac{P_3}{S}$$

or

$$\frac{1}{r\left[1+\left(\frac{dz}{dr}\right)^2\right]^{1/2}} + \frac{\frac{d^2z}{dr^2}}{\left[1+\left(\frac{dz}{dr}\right)^2\right]^{3/2}} = -\frac{P_3}{S}$$

For extremely small slopes, an approximate equation can be written as:

$$\frac{1}{r}\frac{dz}{dr} + \frac{d^2z}{dr^2} = -\frac{P_3}{S}$$

For cartesian coordinate systems the equation becomes:

$$\frac{\frac{\partial^2 z}{\partial x^2}}{1+\left(\frac{\partial z}{\partial x}\right)^2} + \frac{\frac{\partial^2 z}{\partial y^2}}{1+\left(\frac{\partial z}{\partial y}\right)^2} = -\frac{P_3}{S}\left[1+\left(\frac{\partial z}{\partial x}\right)^2+\left(\frac{\partial z}{\partial y}\right)^2\right]^{1/2}$$

Again, if the slopes are all small this equation will reduce to the following:

$$\frac{\partial^2 z}{\partial x^2} + \frac{\partial^2 z}{\partial y^2} = -\frac{P_3}{S}$$

Now let us apply the general theory to the two previous examples, the flat one-way plate and the circular plate.

First Example follows: (on next page)

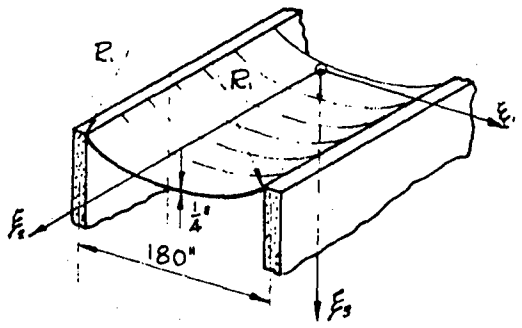

$R_2 = \infty$, $P_3 = P_o$

$S = P$

$\frac{1}{R_1} + \frac{1}{R_2} = \frac{-P_3}{S}$ becomes

$\frac{1}{R_1} + \frac{1}{\infty} = -\frac{P_o}{P}$, $\frac{1}{R_1} = -\frac{P_o}{P}$

$R_1 = \frac{-P}{P_o}$

$R_1 = \frac{-10,000}{50} = -200$ in.

Second Example

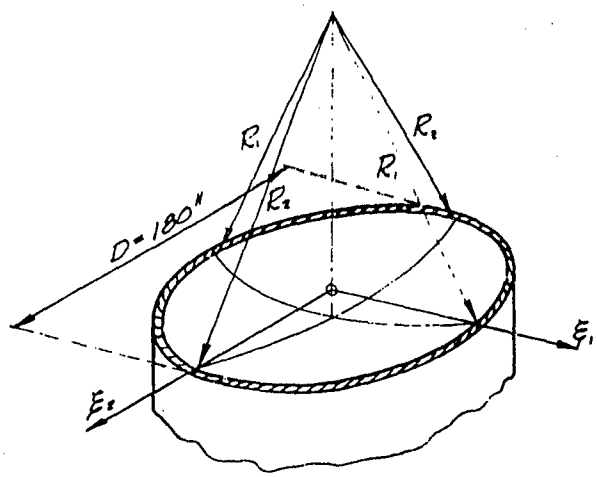

$R_1 = R$, $R_2 = R$

$P_3 = P_o$, $S = P$

$\frac{1}{R_1} + \frac{1}{R_2} = \frac{-P_3}{S}$ becomes

$\frac{1}{R} + \frac{1}{R} = \frac{-P_o}{P}$ $\frac{2}{R} = \frac{-P_o}{P}$

$R = \frac{-2P}{P_o}$

$R = \frac{-2\ (10,000)}{50} + -400$ in.

5. Numerical Solution to Membrane Equations, Axially Symmetrical case:

$$\frac{\frac{dz}{dr}}{r\left[1 + \left(\frac{dz}{dr}\right)^2\right]^{1/2}} + \frac{\frac{d^2z}{dr^2}}{\left[1 + \left(\frac{dz}{dr}\right)^2\right]^{3/2}} = \frac{-P_o\,(r)}{P}$$

The finite difference method of approximation may be used to define the differential equation in terms of a discrete number of finite displacements. This is accomplished by approximating the slope of a curve at a point in terms of the deflection of that particular point and of the surrounding points. For an axially symmetrical case, a generalized curve corresponding to the meridian may be considered.

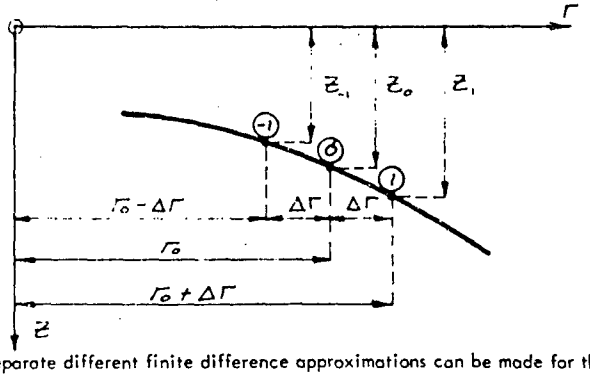

For point 0, three separate different finite difference approximations can be made for the first derivative.

The approximations are:

Forward difference: $\left.\frac{dz}{dr}\right]_o \doteq \frac{z_1 - z_o}{\Delta r}$ Central difference: $\left.\frac{dz}{dr}\right]_o \doteq \frac{z_1 - z_{-1}}{2\,\Delta r}$

Backward difference: $\left.\frac{dz}{dr}\right]_o \doteq \frac{z_o - z_{-1}}{\Delta r}$

In this case, the approximation of the first derivative as the central difference will be used: $\left.\frac{dz}{dr}\right]_o \doteq \frac{z_1 - z_{-1}}{2\,\Delta r}$

The second derivative can be found in the following way:

$$\left.\frac{d^2z}{dr^2}\right]_o \doteq \frac{d}{dr}\left(\frac{dz}{dr}\right) \doteq \frac{\left.\frac{dz}{dr}\right]_1 - \left.\frac{dz}{dr}\right]_o}{\Delta r}$$ using the forward difference, then using the backward difference

for $\left.\frac{\partial z}{\partial r}\right]_1$ and $\left.\frac{\partial z}{\partial r}\right]_o$ the expression becomes: $\left.\frac{d^2z}{dr^2}\right]_o \doteq \frac{\frac{z_1 - z_o}{\Delta r} - \frac{z_o - z_{-1}}{\Delta r}}{\Delta r} = \frac{z_1 - 2z_o + z_{-1}}{(\Delta r)^2}$

This particular combination of differences is used to keep the number of additional unknowns that are involved to a minimum. Other expressions for derivatives could be developed in a similar manner if needed.

Using the developed expressions, the equation of the axially symmetrical case can be written entirely in terms of discrete displacements, (Z_i).

$$\frac{z_1 - z_{-1}}{2r_o\,\Delta r} + \frac{z_1 - 2z_o + z_{-1}}{(\Delta r)^2\left[1 + \left(\frac{z_1 - z_{-1}}{2\,\Delta r}\right)\right]} = \frac{-P_o}{P}\left[1 + \left(\frac{z_1 - z_{-1}}{2\,\Delta r}\right)^2\right]^{1/2}$$

To use this equation, a starting point on the axis of symmetry must be assumed. Successive calculations from the above equation can then be made for each new unknown displacement.

6. Two-Dimensional Case

The general equation for the two-dimensional case in cartesian coordinates is:

$$\frac{\frac{\partial^2 z}{\partial x^2}}{1 + \left(\frac{\partial z}{\partial x}\right)^2} + \frac{\frac{\partial^2 z}{\partial y^2}}{1 + \left(\frac{\partial z}{\partial y}\right)^2} = -\frac{P_3}{S}\left[1 + \left(\frac{\partial z}{\partial x}\right)^2 + \left(\frac{\partial z}{\partial y}\right)^2\right]^{1/2}$$

For this case the finite difference expressions can be written for a surface in a manner similar to that used in the previous one-dimensional case.

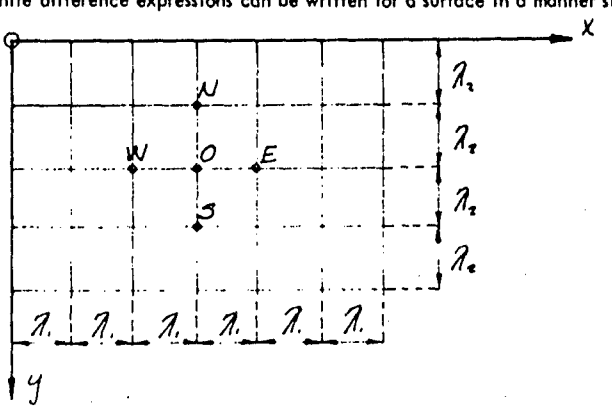

Since the general equation is written using partial derivatives, with respect to x and y, the respective derivatives in these individual directions must be considered separately. For example, consider the curves formed at the intersection of the surface with planes parallel to the x-z and y-z planes respectively which pass through point 0. The resulting curves are then similar to the one-dimensional case and the partial derivatives in this direction can therefore be written in the same way, that is:

$$\frac{\partial z}{\partial x} = \frac{z_e - z_w}{2\,\lambda_1}, \qquad \frac{\partial^2 z}{\partial x^2} = \frac{z_e - 2z_o + z_w}{\lambda_1^{\,2}}$$

$$\frac{\partial z}{\partial y} = \frac{z_s - z_n}{2\,\lambda_2}, \qquad \frac{\partial^2 z}{\partial y^2} = \frac{z_s - 2z_o + z_n}{\lambda_2^{\,2}}$$

These approximations can now be put into the general equation.

$$\frac{\frac{z_e - 2z_o + z_w}{\lambda_1^{\,2}}}{1 + \left(\frac{z_e - z_w}{2\,\lambda_1}\right)^2} + \frac{\frac{z_s - 2z_o + z_n}{\lambda_2^{\,2}}}{1 + \left(\frac{z_s - z_n}{2\,\lambda_2}\right)^2} = -\frac{P_o}{P}\left[1 + \left(\frac{z_e - z_w}{2\,\lambda_1}\right)^2 + \left(\frac{z_s - z_n}{2\,\lambda_2}\right)^2\right]^{1/2}$$

If the slopes are small, the general equation can be linearized by setting: $\left(\frac{\partial z}{\partial x}\right)^2 = 0, \left(\frac{\partial z}{\partial y}\right)^2 = 0$

then the resulting equation is: $\frac{\partial^2 z}{\partial x^2} + \frac{\partial^2 z}{\partial y^2} = -\frac{P_3}{S}$ which is the Poisson equation.

The same finite difference approach can be used for this Poisson equation resulting in the following expression.

$$\frac{z_e - 2z_o + z_w}{\lambda_1^2} + \frac{z_s - 2z_o + z_n}{\lambda_2^2} = -\frac{P_o}{P}$$

For a uniform grid, $\lambda_1 = \lambda_2 = \lambda$; and this equation can be simplified to: $z_e + z_w + z_s + z_n - 4z_o = -\frac{P_o \lambda^2}{P}$

7. Application

The finite difference equations developed earlier may be programmed for solution on a digital computer. If such an approach is used, date sufficient for development of design curves may be generated. Such data are presented as curves in figures C-11 through C-17. Explanation on the use of these curves follows:

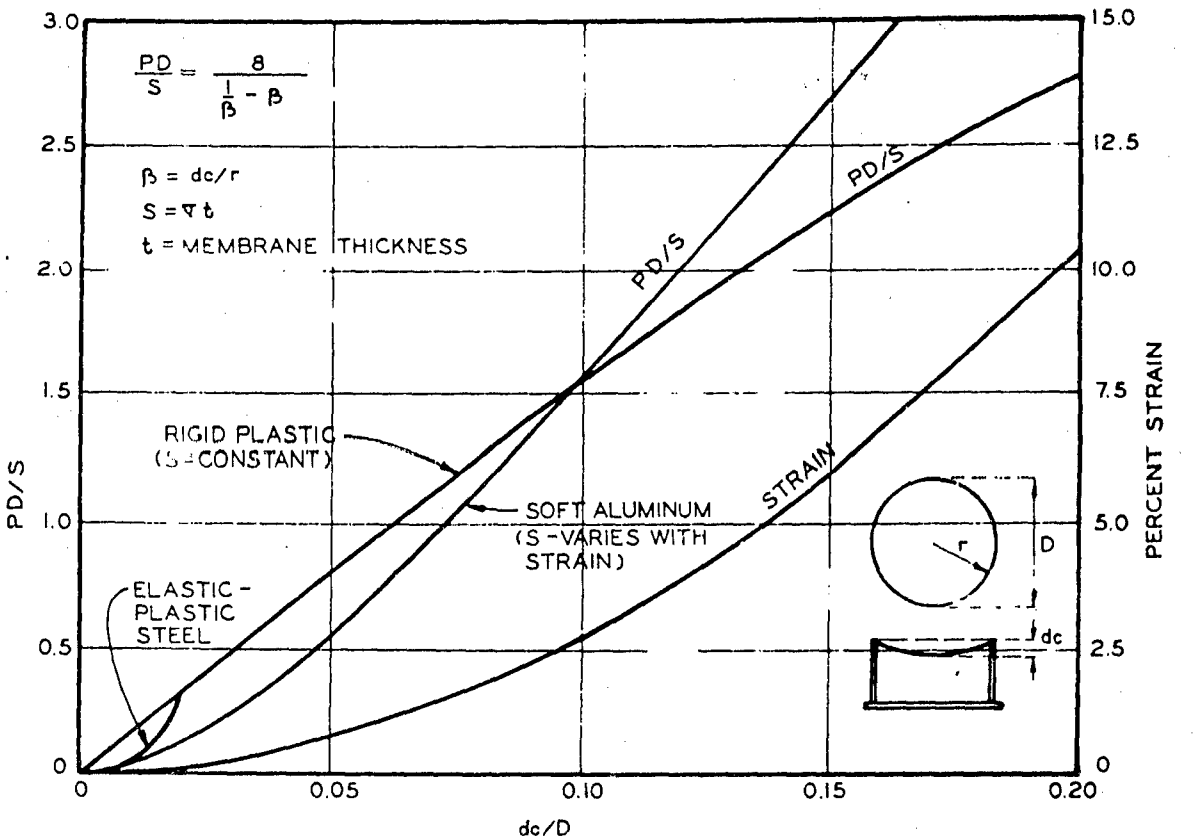

Figure C-11. Circular Membrane

(1) Figure C-11 presents load-strain relationships for circular membranes under uniform pressure. Consider the case of the design of a flat circular steel membrane of 30 ft span for an overpressure of 50 psi. Let us assume that the product of the yield stress and thickness is 10,000 lb per in. as before. Compute the following:

$$\frac{pD}{S} = \frac{(50)(30)(12)}{10,000} = 1.8$$

For this value of the parameter $\frac{pD}{S}$, such a membrane will deflect an amount $\frac{d_c}{D} = 0.113$ if it is soft aluminum and 0.121 if it is mild steel. For these values, the strains are 0.027 and 0.028 respectively. At a yield stress of 40,000 psi, the thickness of the steel would be 1/4 in. Soft aluminum, at a yield stress of 20,000 psi would have to be 1/2 in. thick.

An approach which is somewhat more realistic is to assign a value of limiting strain and then find the required membrane thickness. For example, if we assume 5% strain (a reasonable value for mild steel), we can enter figure C-11 at the 5% strain level and read a corresponding value of 2.05 for $\frac{pD}{S}$. If p = 50 psi and D = 30 ft as before, then: $2.05 = \frac{(50)(30)(12)}{S}$, from which S = 8770 lb per in.

If fy = 40,000 psi, then $t = \frac{8770}{40,000} = 0.219$ in. Thus, we see that a 0.219 in. thick mild steel circular membrane will support a pressure of 50 psi at a $\frac{dc}{D}$ ratio of 0.137. At 10% strain, this same membrane will support a static overpressure corresponding to $\frac{pD}{S} = 2.7$. This value yields an overpressure of: $\frac{(2.7)(8770)}{30(12)} = 66.8$ psi

(2) Figure C-12 is the same as figure C-11, except that it is only for rigid-plastic materials such as steel.

Figure C-13 is similar to figure C-12, only for a square membrane.

Figure C-14 presents design curves for square yielding steel membranes in which the yield stress is assumed to be 36,000 psi. Notice the variation in thickness and strains.

Figure C-15 is similar to figure C-13, only for a rectangular membrane of length equal to 1-1/2 times its width.

Figure C-16 is the same as figure C-15, only for a rectangle whose length is twice its width.

Figure C-17 is the same as figure C-15, only for a rectangle whose length is three times its width.

The design curves presented may be used with confidence provided that proper boundary support is included. Continuous membranes have the advantage of reducing the real boundary problems to those around the periphery of the structure only. The maximum boundary force that can develop is equal to the value of S for the particular membrane in question. In general, it will actually be smaller than this value because of the fact that it really is only the horizontal component of S, that is important.

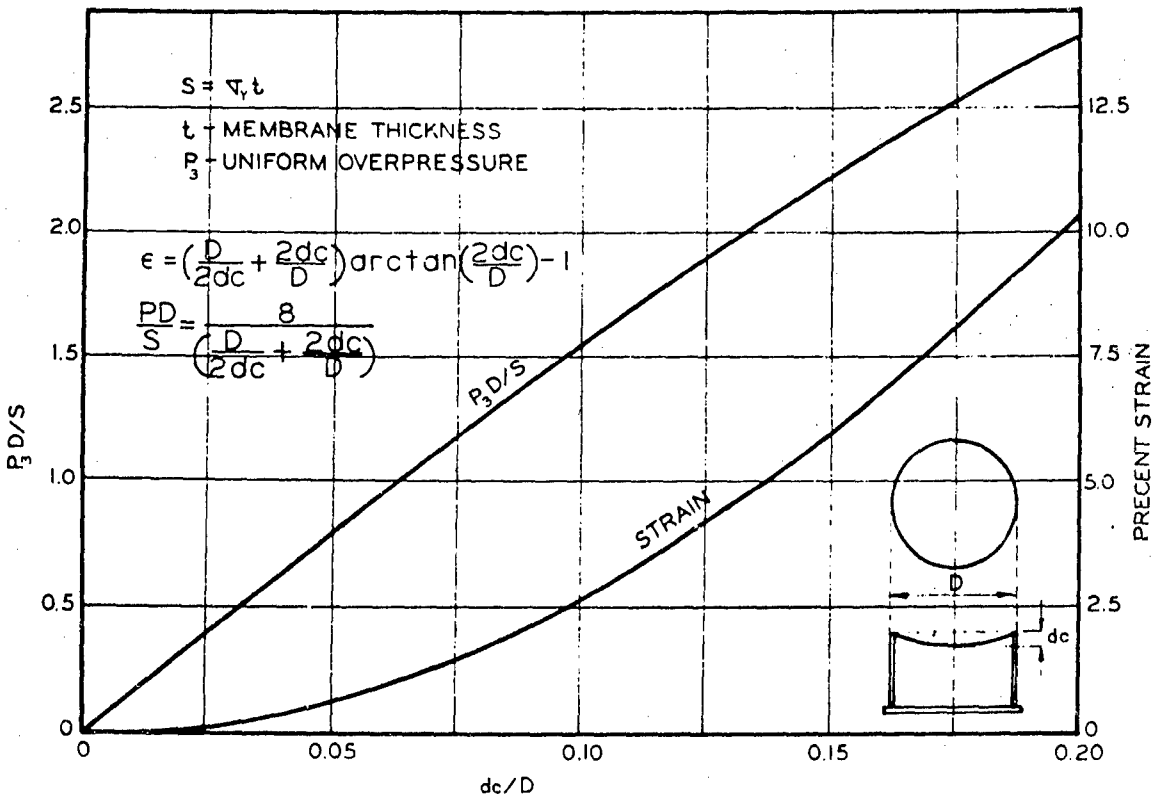

Figure C-12. Circular Steel Membrane

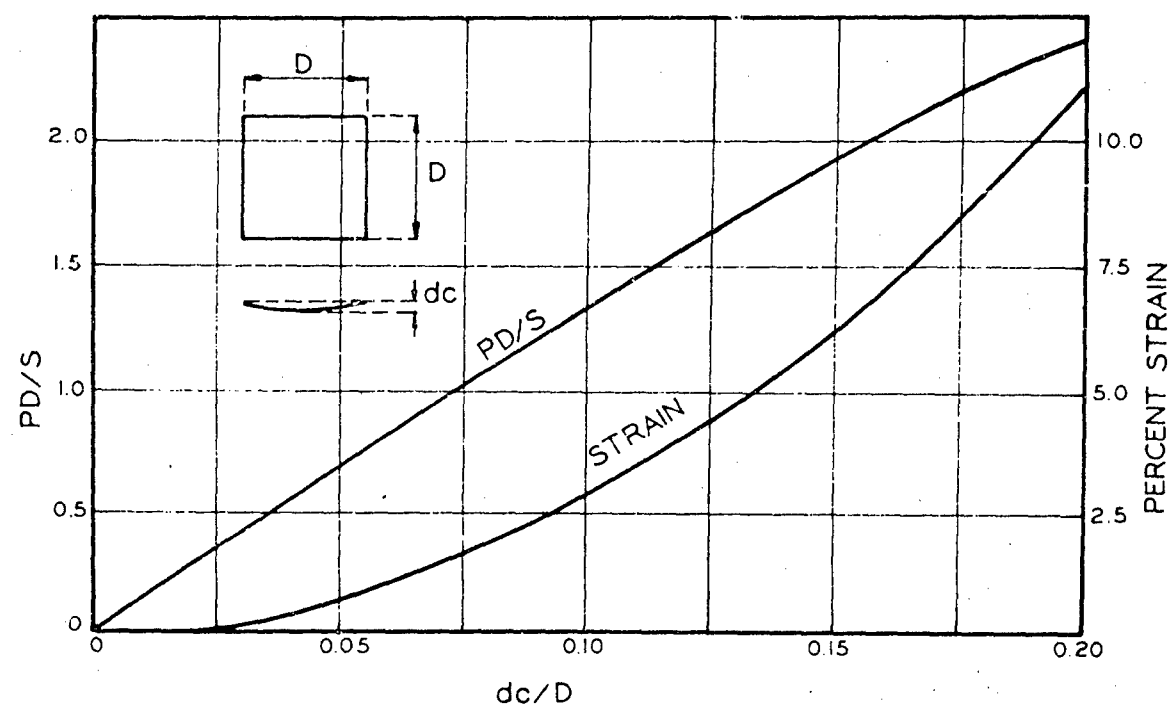

Figure C-13. Square Steel Membrane

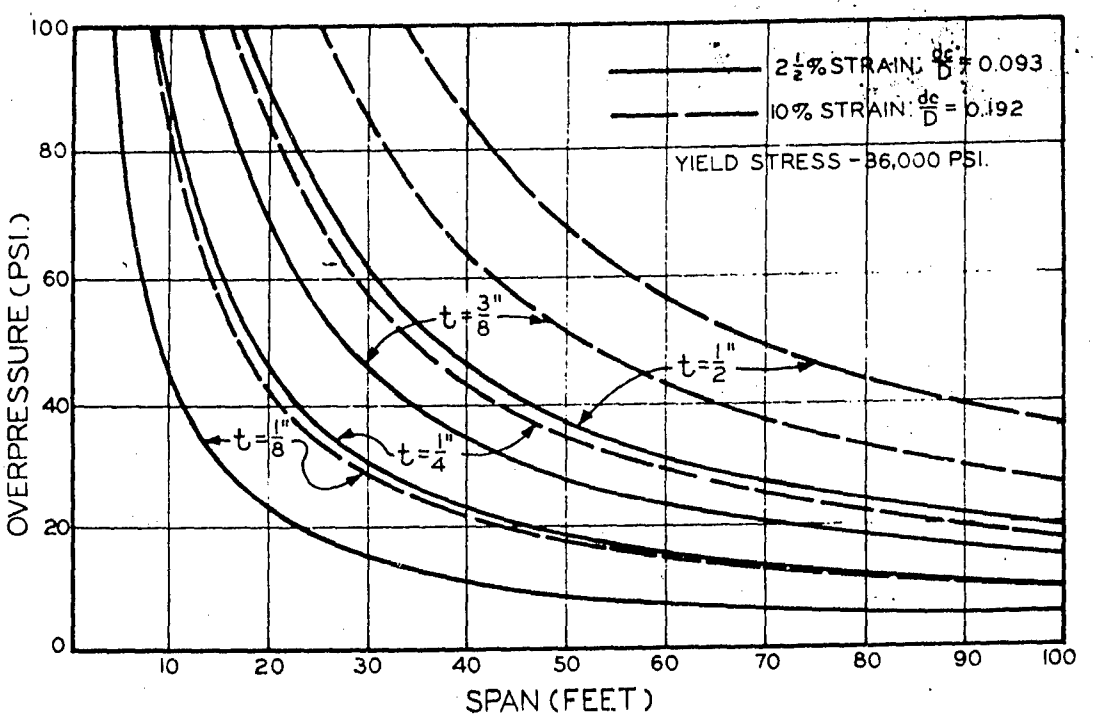

Figure C-14. Square Membrane, Design Curves

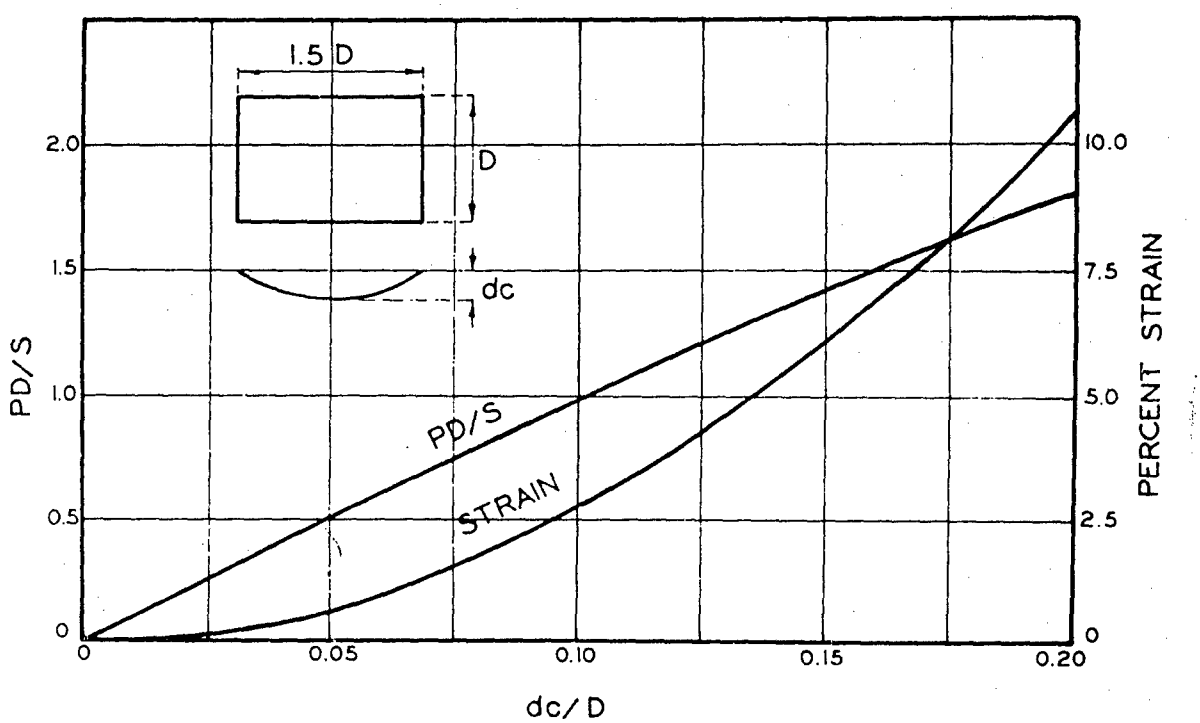

Figure C-15. Rectangular Steel Membrane (D x 1.5D)

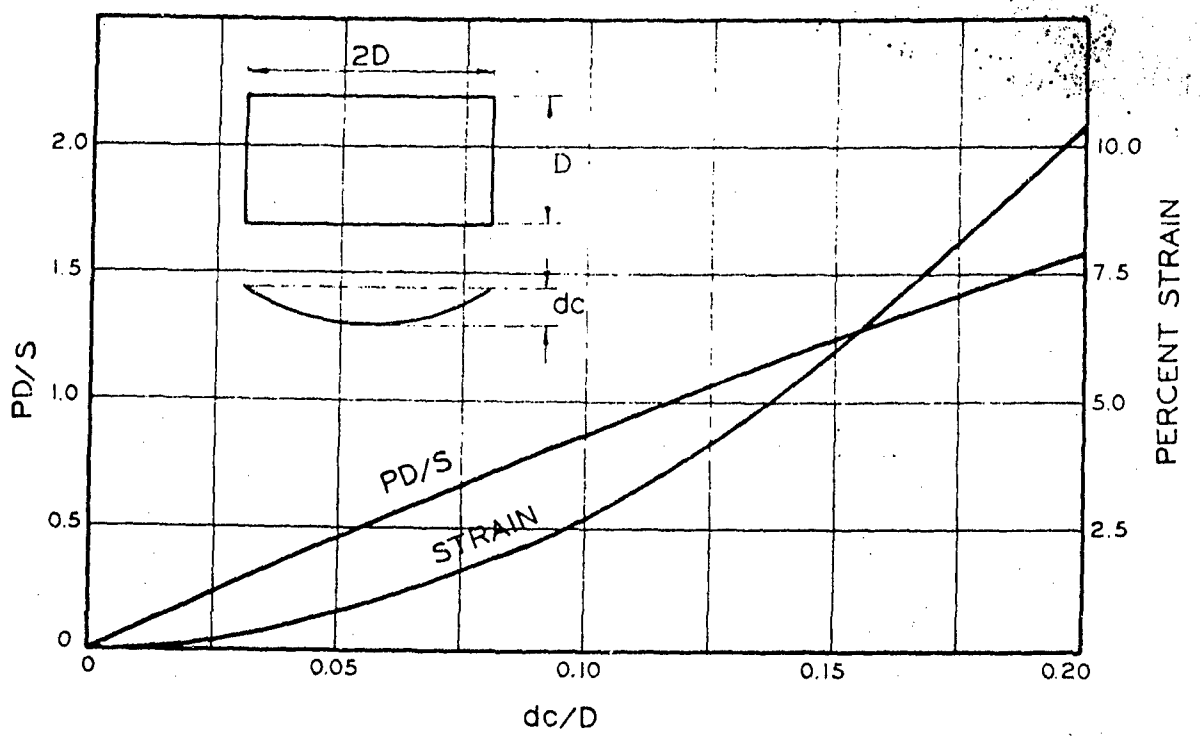

Figure C-16. Rectangular Steel Membrane (D x 2D)

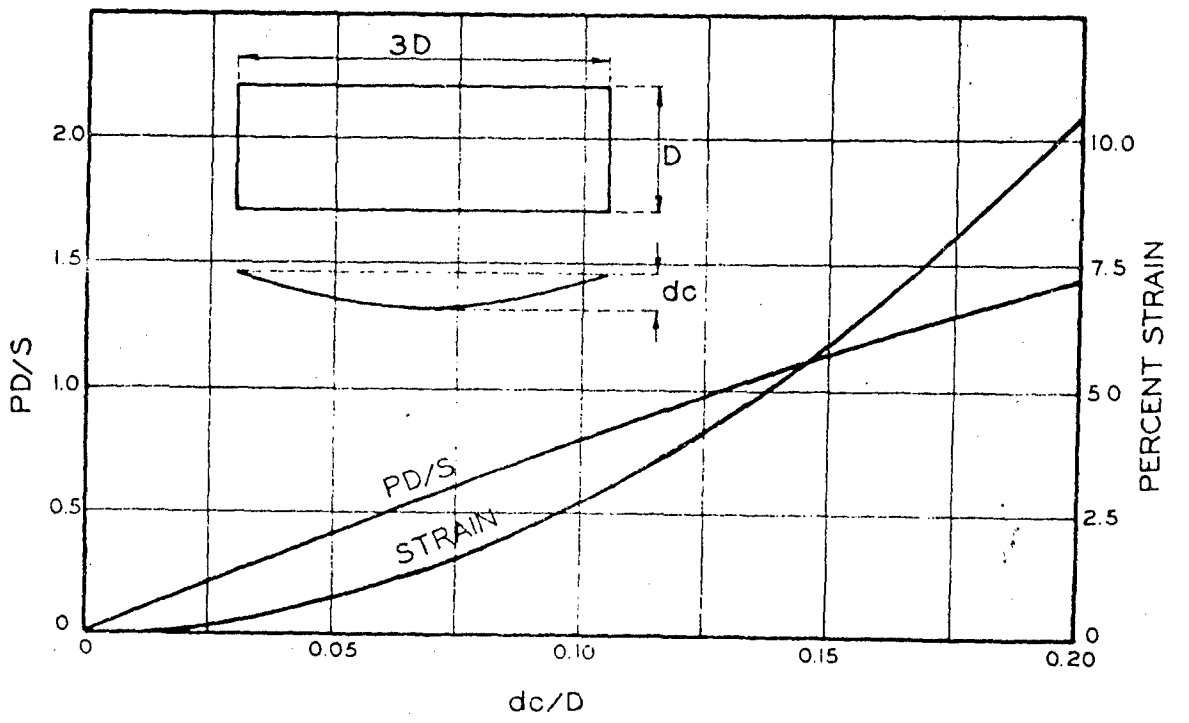

Figure C-17. Rectangular Steel Membrane (D x 3D)

K. Effects of Entrance Configuration on Attenuation of Blast Overpressure

1. Introduction

The most vulnerable component of an underground shelter, to a nuclear weapon, is the entrance. Much research has been directed toward the structural design of blast doors and hatches to resist specific assumed overloads. Less effort has been expended in designing the passageways through which both refugee and blast pressure must traverse to reach the shelter door.

The first phase of a shelter design program must include an evaluation of blast characteristics based on bomb size, detonation altitude, and proximity of shelter to ground zero. The type of occupancy must be considered, and the following classification is possible:

a. Long-time operational shelters for the protection of active military personnel, important governmental and civil service agencies, and perhaps some essential industries. These shelters would be occupied during crucial international situations and would not change significantly during an actual attack. They would be large, elaborate, and costly. There would be ample power provided for the operation of utilities, and heavy blast doors could be power operated and automatically controlled.

b. Short-time protective shelters which would be occupied by individuals, families or communities only in the event of imminent attack. The majority of shelters would fall into this classification. The extent of protection would be limited due to economic considerations. Entrances would pose several important design problems here. Blast doors should be light enough to permit hand operation by an individual. Tunnels and doors must provide passage for all occupants in a brief period of time. Protection should be provided to those already in the shelter if a nuclear explosion occurs during the period of entry.

2. Notation

The notation which is used in the following discussion is defined below:

A	$A = 60° - 1/2\ \alpha$
B	$B = 40° + 1/2\ \beta$
A + B	Pressure Numbers (Prandtl-Busemann)
a	Velocity of sound in air
a*	Critical velocity of sound (when q = a)
C_L	Left-running characteristic curve
C_R	Right-running characteristic curve
M	Mach Number (M = q/a)
M*	Critical Mach Number (M* = q/a*)
P	Static Pressure
P_x	dp/dx
P_1, P_2, P_3, etc.	Static pressure in region 1, 2, 3, etc.
P_o	Free stream stagnation pressure
q	Flow velocity
u, v	Velocity components of q
u_x, v_x, u_y, v_y	Derivatives of u and v with respect to x and y
α (alpha)	Angle to right-running epicycloid
β (beta)	Angle to left-running epicycloid
γ (gamma)	Ratio of specific heats
θ (theta)	Angle of flow direction
μ (Mu)	Mach angle
ν (Nu)	Angular displacement of epicycloid cusp
ρ (Rho)	Fluid density
δ (delta)	Flow turning angle

3. Blast and Overpressure Origin

When a nuclear explosion occurs in the air, the shock front moves out radially from the burst center until it strikes the ground surface and is reflected. The reflected wave overtakes and fuses with the incident wave to form a Mach front which moves outward along the ground surface. The region outside of the circle of fusion is referred to as the Mach region, and the dynamic pressure is directed nearly horizontal. The total pressure behind the Mach front in the Mach Region is the sum of the overpressure of incident and reflected waves plus the dynamic pressure.

The region inside the circle formed by incident and reflected wave fusion is called the regular region, and the total pressure depends on the angle of incidence of the shock wave with the ground surface. Except for high altitude bursts, the regular region is a small part of the total area subject to blast damage. Furthermore, no regular region would form at all under extremely low air bursts and in the cases of surface and subsurface bursts. Therefore, it is reasonable to assume that the majority of underground shelters will be designed to withstand pressures associated with the Mach region. The magnitude of the peak overpressure in the Mach region depends on weapon size, burst height, distance from ground zero, and terrain features. None of these factors can be reliably predicted in advance. However, if an arbitrary value of overpressure is selected as the design load, the design results can be scaled upward or downward to fit specific design requirements.

When a shock front passes over a tunnel entrance, a pressure wave is propagated into the tunnel and reflected waves are created which interact and build up a flow pattern of ever-increasing complexity. A direct theoretical approach to the solution of this three-dimensional supersonic flow problem is not available. However, approximate relationships can be obtained by assuming two-dimensional steady, isentropic flow and applying a graphical method developed by Busemann. This "Characteristic Method" has been used extensively to design supersonic wind tunnels and nozzles. The method consists of a step by step construction of the flow pattern based on the geometric relations between incident waves, reflected waves, and boundary configurations.

The assumption of isentropic flow which is necessary for the development of the Characteristics Method precludes its application from flows involving strong shock waves. However, the method will give correct results for expansion waves and nearly correct results when applied to flows involving weak shocks or small turning angles. It is probable that the speed of propagation of the blast wave front in the Mach region will dimish rapidly to velocities just above the sonic velocity. In this case, the anthrophy change across a shock wave may be neglected and isentropic flow is implied.

4. Development of the Characteristic Theory

A two-dimensional steady isentropic flow can be described mathematically by two equations of motion and the equation of continuity.

$$\rho(u\,u_x + v\,u_y) = P_x \tag{1}$$

$$\rho(u\,v_x + v\,v_y) = P_y \tag{2}$$

$$(\rho u)_x + (\rho v)_y = 0 \tag{3}$$

Where u and v are velocity components in the x and y directions, ρ is the mass density, p is the pressure, and the subscripts x and y designate the partial derivatives with respect to the directions x and y. The speed of sound or sonic velocity, a, is related to the changing rate of pressure with respect to density by:

$$a^2 = \frac{dP}{d\rho} \tag{4}$$

Substituting (4) into (1) and (2) gives:

$$u\,u_x + v\,u_y = a^2\ \rho_x\ \rho^{-1} \tag{5}$$

$$u\,v_x + v\,v_y = a^2\ \rho_y\ \rho^{-1} \tag{6}$$

Combining (5) and (6) by addition gives: $u^2 u_x + uv\,(u_y + v_x) + v^2 v_y = -a^2\ \rho^{-1}(u\ \rho_x + v\ \rho_y)$ (7)

Equation (3) can be written: $\rho_x u + \rho u_x + \rho_y v + \rho v_y = 0$ (3a)

or $\rho^{-1}(u\ \rho_x + v\ \rho_y) + u_x + v_y = 0$ (3b)

Combining (3b) with (7) gives: $(a^2 - u^2)\,u_x - uv(u_y + v_x) + (a^2 - v^2)\,v_y = 0$ (8)

Restricting the flow to an irrotational condition requires that: $u_y - v_x = 0$ (9)

In 1929, Busemann developed a graphical method for solving equations (8) and (9) for specific isentropic irrotational flow problems. In application, the distribution of velocities at the starting point in the flow problem are known. These initial values determine certain curves, called characteristics, which can be used to predict the subsequent flow pattern. The characteristic curve of equations (8) and (9) is defined as the curve along which a solution of (8) and (9) may have discontinuities in the derivatives of the velocity components, although all fluid properties are continuous functions of x and y in the region where the characteristic curve exists. If u and v are continuous functions of x and y, the variations of the velocity components u and v along the characteristic curve can be expresses as:

$$du = u_x dx + u_y dy \tag{10}$$

$$dv = v_x dx + v_y dy \tag{11}$$

Writing (8) and (9) as a single equation and grouping with (10) and (11) gives a system of three equations in three unknowns (u_x, u_y, v_y).

$$\begin{aligned} &(a^2 - u^2)\ u_x - 2uvu_y + (a^2 - v^2)\ v_y = 0 \\ &d_x u_x + d_y u_y = du \\ &d_x u_y + d_y v_y = dv \end{aligned} \tag{12}$$

In general, one would expect equations (12) to define a unique set of values of the three partial derivatives. According to the definition of the characteristic curve, however, the discontinuity condition requires that there be at least two distinct sets of values of these derivatives. A theorem from algebra states that if the solution of a system of linear algebraic equations is expressed as the quotient of determinants, then more than one set of solutions exist only when all numerators and the denominator vanish. In fact, it can be shown that if the denominator and one of the numerators vanish, then all numerators vanish. Expressing the solution for u_y in determinant notation:

$$u_y = \begin{vmatrix} a^2 - u^2 & 0 & a^2 - v^2 \\ d_x & du & 0 \\ 0 & dv & d_y \end{vmatrix} \div \begin{vmatrix} a^2 - u^2 & -2uv & a^2 - v^2 \\ d_x & d_y & 0 \\ 0 & d_x & d_y \end{vmatrix} \tag{13}$$

For the existence of characteristics:

$$(a^2 - u^2)\,\frac{du}{dx} + (a^2 - v^2)\,\frac{dv}{dy} = 0 \tag{14}$$

$$(a^2 - u^2)\left(\frac{dy}{dx}\right)^2 + 2uv\,\frac{dy}{dx} + (a^2 - v^2) = 0 \tag{15}$$

The derivative $\frac{dy}{dx}$ can be constructed in the xy plane which is referred to as the physical plane. Solving (15) for $\frac{dy}{dx}$ produces two roots:

$$\left(\frac{dy}{dx}\right)_L = \frac{uv + a\,(u^2 + v^2 - a^2)^{1/2}}{u^2 - a^2}$$

$$\left(\frac{dy}{dx}\right)_C = \frac{uv - a\,(u^2 + v^2 - a^2)^{1/2}}{u^2 - a^2} \tag{16}$$

These two families of characteristics are designated as C_L and C_R corresponding to the plus and minus signs in (16). In order to construct the characteristics in the physical plane, it is necessary to determine the variation of u and v along the characteristics. This is accomplished by finding the equation of the characteristics in the uv plane which is called the hodograph plane. Equation (14) can be written as:

$$\frac{dv}{du} = -\frac{a^2 - u^2}{a^2 - v^2}\,\frac{d_y}{dx} \qquad (14a)$$

Substituting (16) into (14a) produces two equations for the slopes of the two families of characteristics (C^+, C^-) in the hodograph plane.

$$\left(\frac{dv}{du}\right)_L = \frac{uv + a\,(u^2 + v^2 - a^2)^{1/2}}{a^2 - v^2}$$

$$\left(\frac{dv}{du}\right)_R = \frac{uv - a\,(u^2 + v^2 - a^2)^{1/2}}{a^2 - v^2} \qquad (17)$$

If the u and v axes of the hodograph plane are taken parallel to the x and y axes of the physical plane, the following relations are a consequence of equations (16) and (17).

$$\left(\frac{dy}{dx}\right)_L \left(\frac{dv}{du}\right)_R = -1$$

$$\left(\frac{dy}{dx}\right)_R \left(\frac{dv}{du}\right)_L = -1 \qquad (18)$$

Equations (18) are the orthogonality relations of two curves as expresses in analytic geometry. The physical characteristic of one family is orthogonal to the hodograph characteristic of the opposite family. This relation has practical significance in the graphical construction of characteristic nets, and is illustrated in figure C-18 for the characteristics of the velocity q in the uv plane.

5. Geometrical Relations of the Characteristic Curves

a. Characteristics in the physical plane.

In the study of supersonic flow, curves which everywhere make an angle μ with the direction of the stream lines are called Mach lines. By definition,

$$\sin \mu = M^{-1} \qquad (19)$$

In a uniform, parallel flow, the Mach lines consist of two families of straight lines making the angle 2μ with each other. This is illustrated in the physical plane of figure C-18 where the characteristics are drawn as Mach lines. In any flow, the angle between the Mach lines at a point is bisected by the streamline through the point.

Since M, the Mach Number, is defined as q/a, then: $a = q \sin\mu$ (20)

and from figure C-18, $u = q \cos\theta$

$v = q \sin\theta$ (21)

Substituting (20) and (21) into (16) gives for the slopes of the physical characteristics:

$$\left(\frac{dy}{dx}\right)_L = \frac{\cos\theta \sin\theta + \sin\mu \cos\mu}{\cos^2\theta - \sin^2\mu}$$

$$\left(\frac{dy}{dx}\right)_R = \frac{\cos\theta \sin\theta - \sin\mu \cos\mu}{\cos^2\theta - \sin^2\mu} \qquad (22)$$

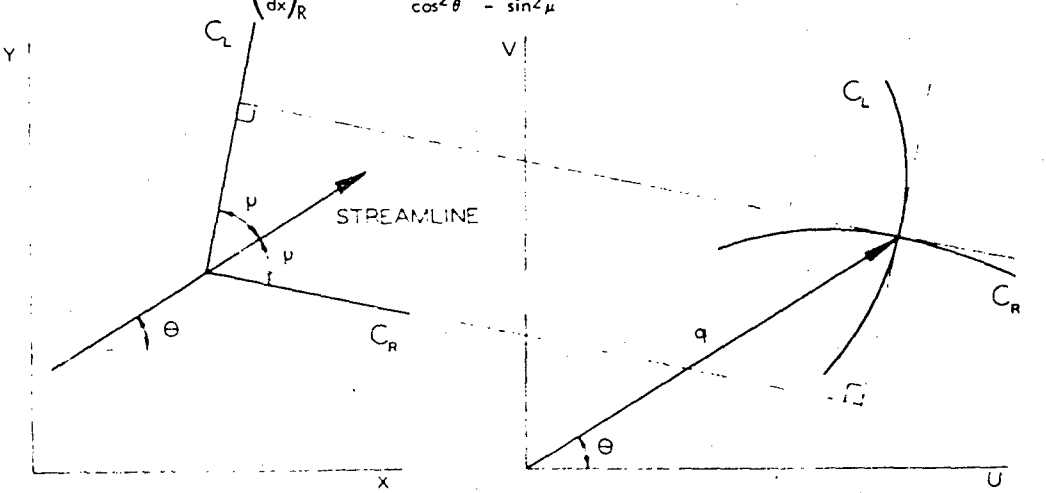

Figure C-18. Characteristics of the Velocity q in the uv Plane

By use of trigonometric identities, (22) can be reduced to:

$$\left(\frac{dy}{dx}\right)_L = \tan(\theta + \mu)$$

$$\left(\frac{dy}{dx}\right)_R = \tan(\theta - \mu) \qquad (23)$$

Referring again to figure C-18, the characteristics in the physical plane as defined by (23) are identical to the Mach lines as defined by (19). Equation (20) shows that the component of velocity normal to the physical characteristic (Mach line) is always equal to the speed of sound.

b. Characteristics in the hodograph plane.

A hodograph is a graph in polar coordinates in the velocity plane. In order to construct the hodograph characteristics, the velocity components u and v are expressed as in (21) and differentiated to find the velocity variations along the characteristic curves.

$$du = q \sin\theta \, d\theta + \cos\theta \, dq$$

$$dv = q \cos\theta \, d\theta + \sin\theta \, dq \qquad (24)$$

Substituting (21) and (24) into (17) produces:

$$d\theta = \pm (M^2 - 1)^{1/2} \frac{dq}{q} \qquad (25)$$

In order to plot the characteristics with reference to θ, the direction angle of the velocity q, it is necessary to integrate (25). This cannot be done directly since M is a variable; however, the integration can be accomplished by introducting the critical Mach Number M* which is defined as:

$$M^* = \frac{q}{a^*} \qquad (26)$$

where a^* is the critical velocity. The critical velocity is defined as that for which $q = a$. The advantage of introducing M^* lies in the fact that is is proportional to q since a^* is constant, whereas M varies inversely with a. The relation between M and M^* is such that:

$$(M^2 - 1)^{1/2} = b \left(\frac{M^{*2} - 1}{b^2 - M^{*2}}\right)^{1/2} \qquad (27)$$

where $b = \left(\frac{\gamma+1}{\gamma-1}\right)^{1/2}$, and γ is the ratio of specific heat at constant pressure to specific heat at constant volume. For air γ is 1.4 and b is 2.45. By applying equation (27), equation (25) becomes: $d\theta = \pm b \left(\frac{M^{*2} - 1}{b^2 - M^{*2}}\right)^{1/2} \frac{dq}{q}$ (25a)

Integrating (25a) gives: $\pm (\theta - \theta_1) = b \tan^{-1}\left(\frac{M^{*2} - 1}{b^2 - M^{*2}}\right)^{1/2} - \tan^{-1}\left(\frac{M^{*2} - 1}{b^2 - M^{*2}}\right)^{1/2} b$ (28)

where θ is the value of θ corresponding to $M^* = 1$. The two equations in (28) are the equations of a pair of epicycloids in polar coordinates. These are plotted in figure C-19 in the hodograph plane with M^* measured radially from the center and the angle of flow direction θ measured counterclockwise from the u axis. The epicycloids, which are the characteristics, can be constructed graphically by the following procedure:

(1) Construct two concentric circles of radius $M^* = 1$ and radius $M^* = 2.45$.
(2) Turn the angle θ from the u axis and plot the point P_o on the inner circle ($M^* = 1$).
(3) Construct a circle of diameter 1.45 tangent to the inner circle at P_o. This circle is also tangent to the outer circle ($M^* = 2.45$).
(4) As this circle of diameter 1.45 rolls counterclockwise around the inner circle, the point P traces a locus known as the left-running epicycloid or characteristic $C_{L\theta}$, where the subscript θ denotes the starting point of P at P_o on the inner circle.
(5) As the rolling circle moves, the locus of P gives the complete epicycloid $C_{L\theta}$ which finally is tangent to the outer circle at $\theta - \theta_1 = \frac{\pi}{2}(b-1) = 0.725\pi$. If the rolling circle turns clockwise from P_o, the right-running characteristic $C_{R\theta}$ is traced. For each value of θ_1, a pair of characteristics can be plotted.

The hodograph characteristics are illustrated in a different manner in figure C-20. The right-running characteristic starts on the unit circle ($M^*=1$) at $\theta_1 = \alpha$, and this characteristic curve is designated as $C_{R\alpha}$. Similarly, the left-running characteristic which starts at $\theta_1 = \beta$ is designated as $C_{L\beta}$. Each point P in the hodograph plane can be determined by a pair of intersecting characteristics $C_{R\alpha}$ abd $C_{L\beta}$.

Figure C-20 shows that the velocity magnitude at P is a function of the difference $\alpha - \beta$, i.e., $M^* = F(\alpha - \beta)$; and the velocity direction is expressed by $\theta = (\alpha + \beta)/2$. Thus, the velocity vector at point P is completely specified by the values of α and β.

c. Graphical construction of the characteristics diagram.

A useful tool for constructing the characteristics diagram is a polar diagram of critical Mach number versus Mach angle. Combining equations (19) and (27), one can obtain:

$$M^{*2} \sin^2\mu + \frac{M^{*2} \cos^2\mu}{b^2} = 1 \qquad (29)$$

in which $b = 2.45$. Equation (29) can be plotted in polar coordinates (M^*, μ) as an ellipse with minor semi-axis equal one and major semi-axis equal b. This is shown in figure C-21. If the ellipse is plotted to the same scale as the hodograph, then it can be superposed on the hodograph with center coinciding with that of the unit circle and $P(M^*, \mu)$ coinciding with $P(M^*, \theta)$. This superposition is shown in figure C-22. As previously mentioned, the Mach lines in the physical plane are perpendicular to the characteristics in the

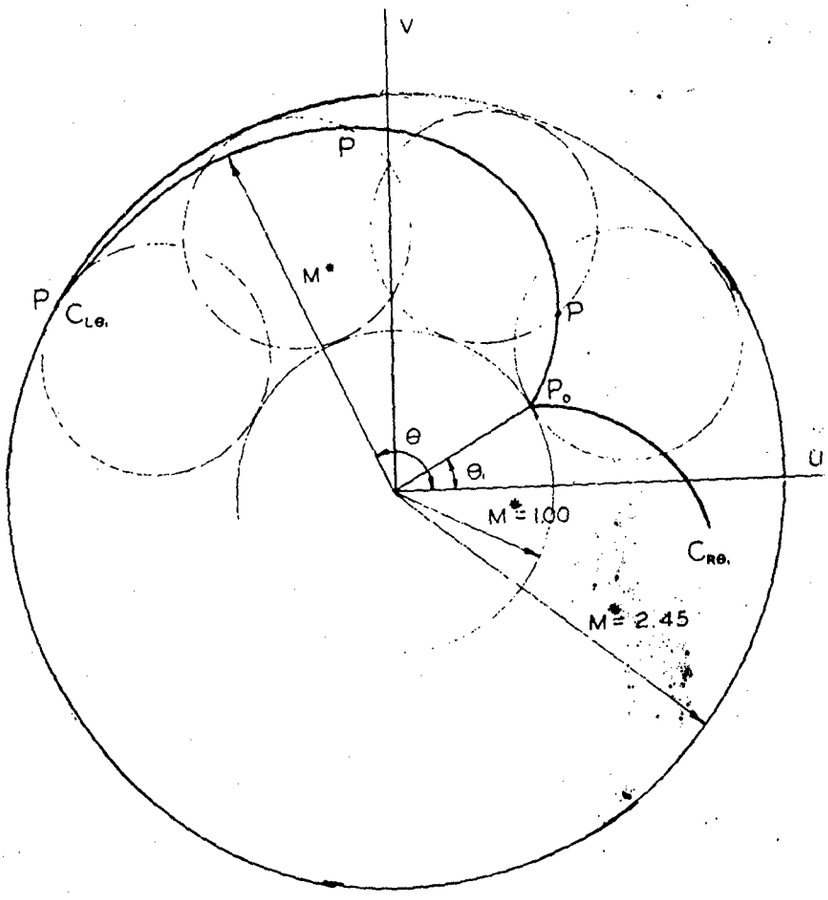

Figure C-19. Pair of Epicycloids in Polar Coordinates

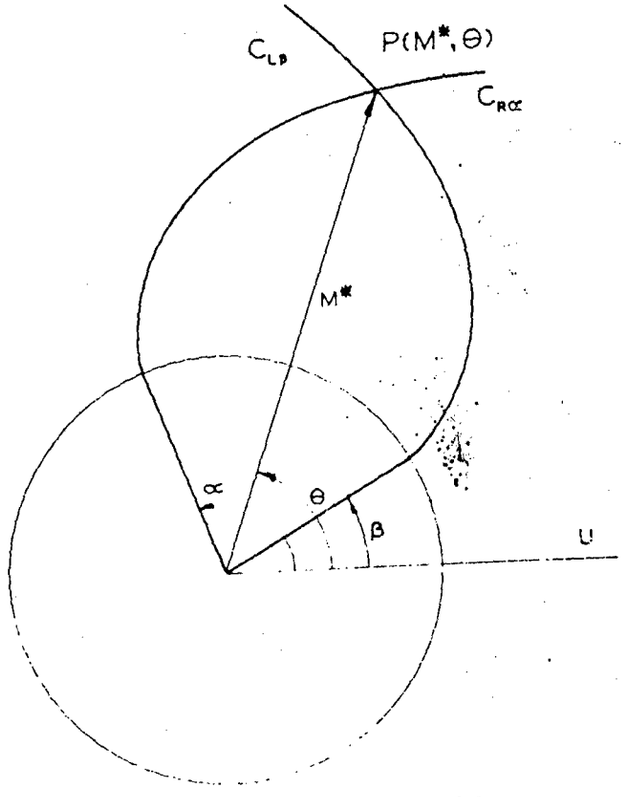

Figure C-20. Hodograph Characteristics

hodograph plane. The major axis of the ellipse is a Mach line (according to the definition of a Mach line) and therefore must be perpendicular to the tangent to the characteristic which passes through P(M*, θ). For this reason, the ellipse can be used to determine the local direction of the hodograph characteristics at any point in the diagram. This superposition is facilitated by the use of figures C-23 and C-24. Figure C-24 is known as a characteristics diagram and plots the two families of epicycloids as a finite number of curves determined by equal increments of α and β (see figure C-19). The angle ν is the angular displacement from the cusp to the point P(M*, θ), i.e., $\nu = \theta - \beta$ or $\alpha - \theta$. Maximum $\nu = 0.725\pi$ is the maximum value of $\theta - \theta_1$, (see figure), therefore maximum = 130.45 degrees. The significance of the numbers on the characteristics diagram in figure C-24 will be explained later.

d. Construction of supersonic flow past convex boundaries.

Consider an initial uniform flow with Mach number M_1* and a convex boundary with a right-turning angle δ . With M_1* and δ known, it is required to determine the Mach number M_2* which exists beyond the turn as shown in figure C-25. Since M_1* and its direction in the physical flow are given, we can locate M_1* in the hodograph plane and draw the right-running hodograph characteristic, $C_{R\alpha}$, by tracing a characteristics diagram such as figure C-24. This is shown in figure C-26. Now the left-running characteristic, C_{L1}, can be drawn in the physical plane (figure C-25) by using the hodograph ellipse. When the ellipse is superimposed on the hodograph, the major axis is parallel to the physical characteristic, C_{L1}, which originates at the corner on the boundary. It may be recalled that the characteristics in the physical plane are Mach lines and therefore lines of constant velocity. Next, M_2* is drawn in the hodograph plane at an angle δ from M_1* and extending from the origin to the epicycloid, $C_{R\alpha}$. By again superposing the ellipse on the hodograph, the second Mach line, C_{L2}, can be constructed in the physical plane.

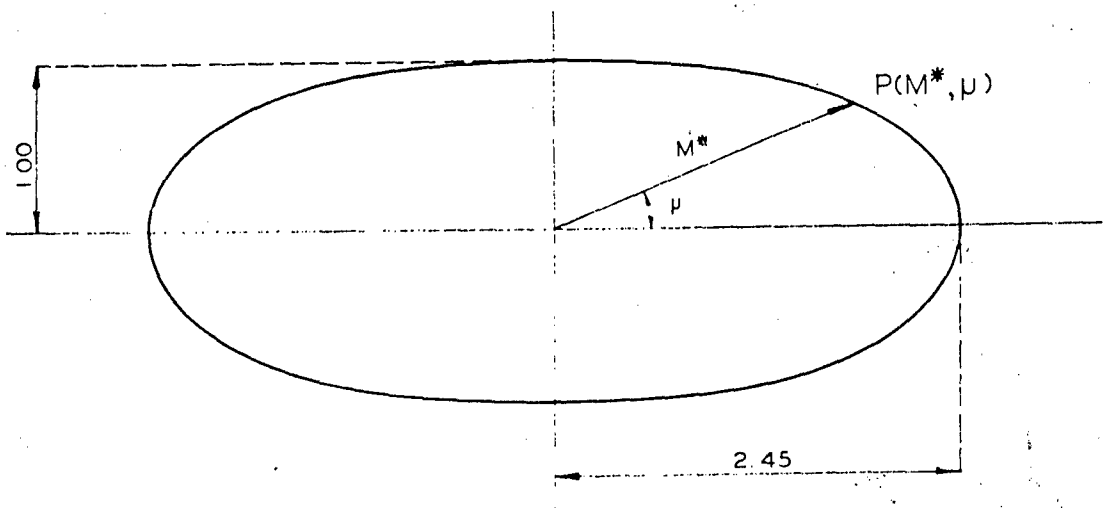

Figure C-21. Polar Coordinates (M*, μ) As An Ellipse

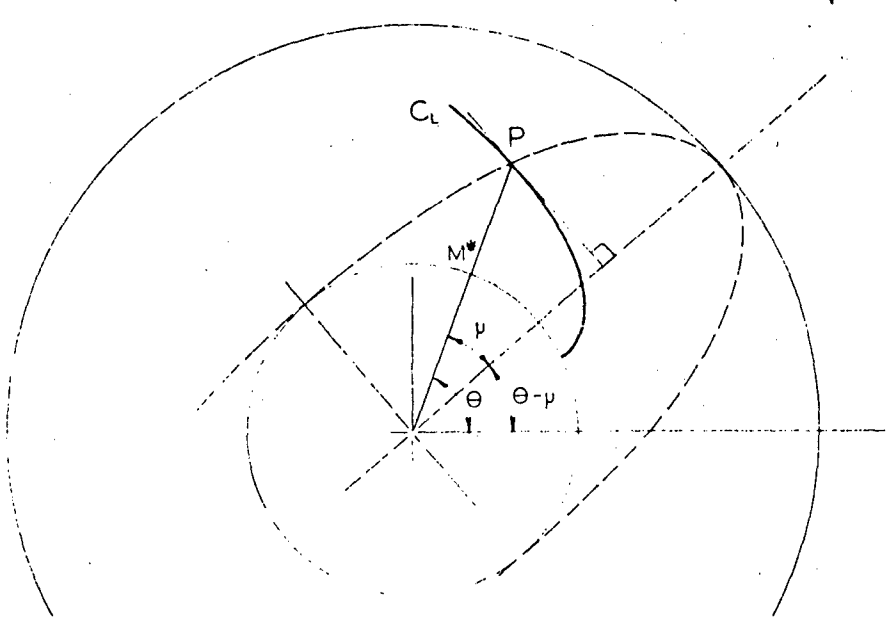

Figure C-22. Elipse Superimposed on A Hodograph

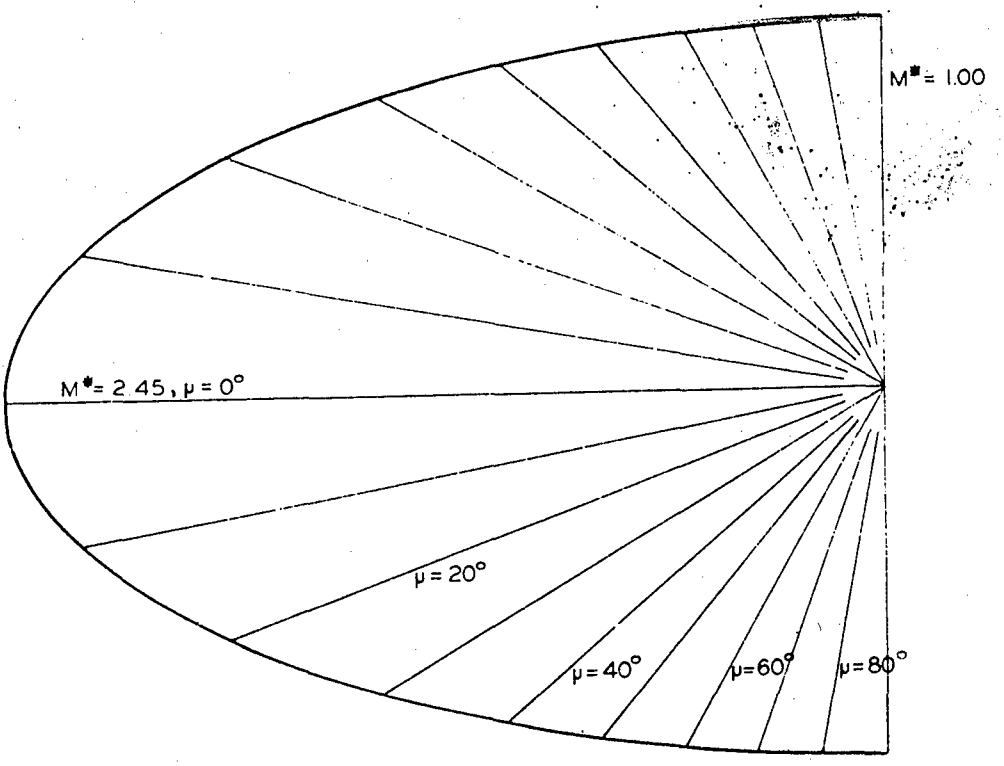

Figure C-23. Epicycloid Elipse

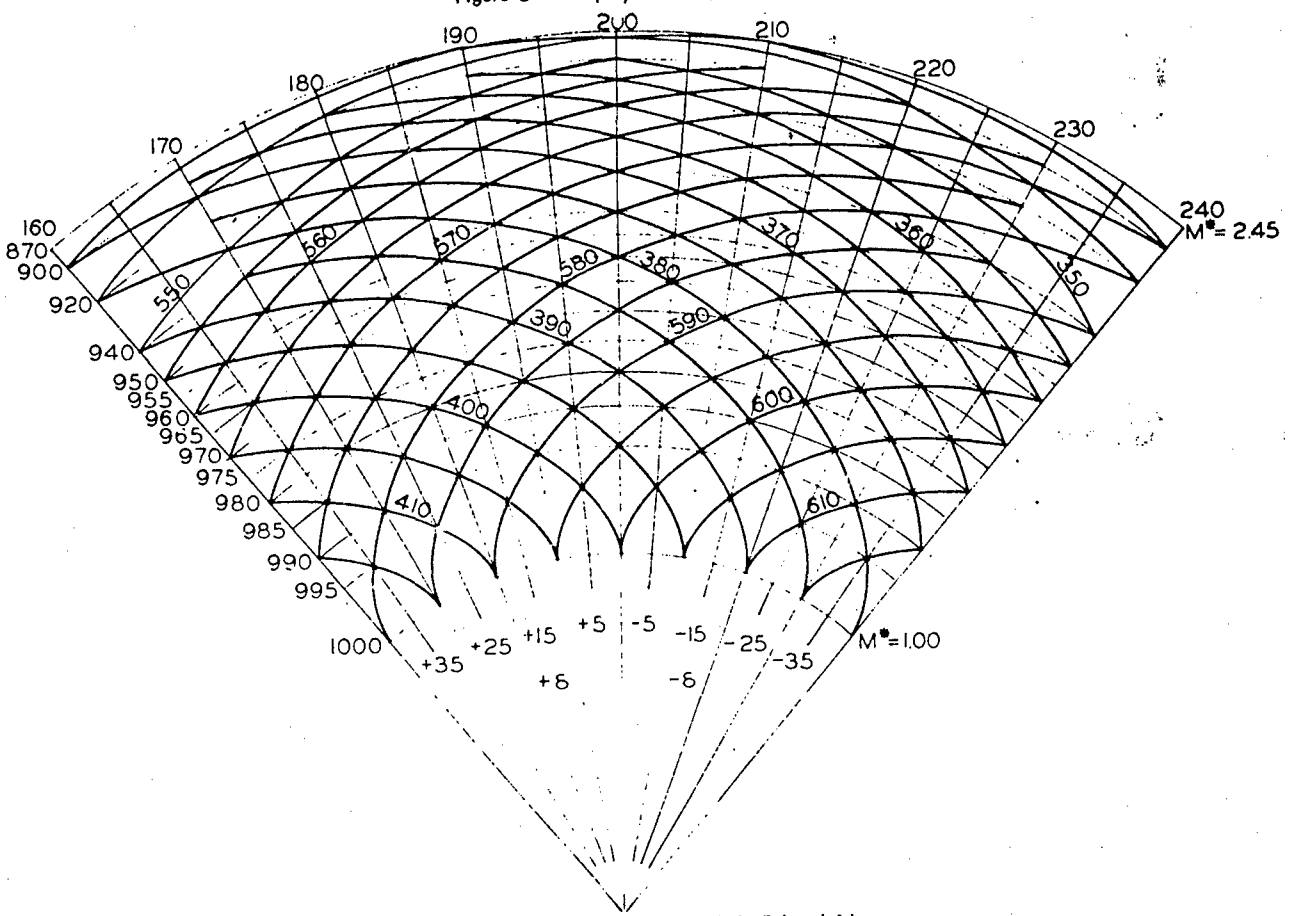

Figure C-24. Characteristic Epicycloids

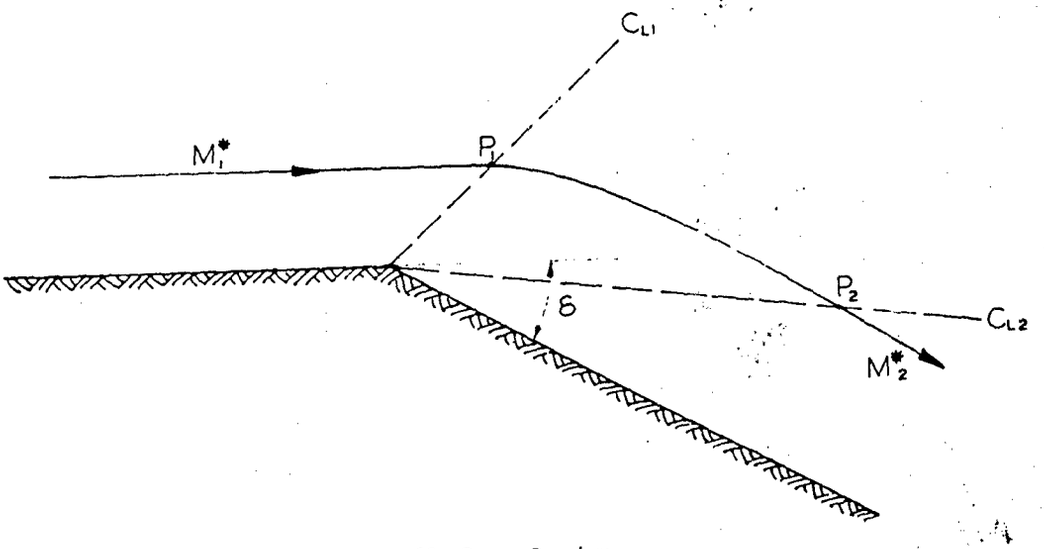

Figure C-25. Convex Boundary

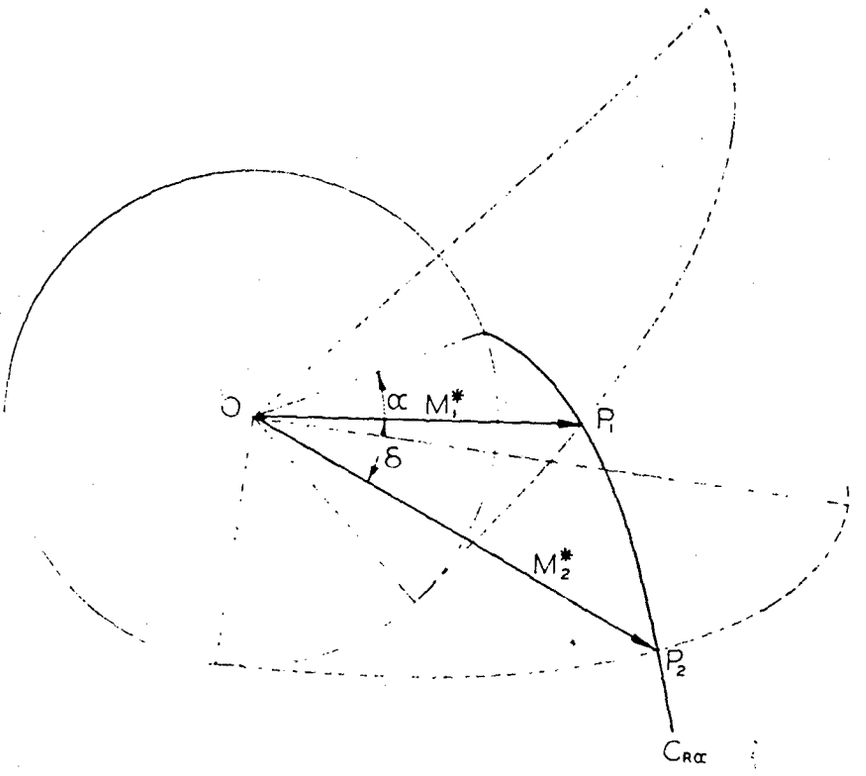

Figure C-26. Right-Running Hodograph Characteristics

For a curved convex boundary, the flow field can be constructed by replacing the curved boundary by straight segments each turning a small increment $\Delta\delta$ of the total turning angle δ. Since the physical characteristics are normal to the hodograph characteristics of the opposite family, it is convenient to draw a mean physical characteristic for each increment $\Delta\delta$ and plot these normal to the segment of epicycloid subtended by $\Delta\delta$. This construction is shown in figure C-27.

e. Construction of supersonic flow past concave boundaries.

If supersonic flow turns a concave finite corner, an oblique shock wave occurs. For small angles and high supersonic flow, the flow behind the shock remains supersonic and the resulting shock is weak with negligible change in entropy. Thus, the flow is approximately isentropic and the characteristics method may be used. When a concave curved boundary is encountered by supersonic flow, the velocity decreases, and at some distance away from the boundary the compression Mach lines or waves focus together to form a finite shock. However, if the flow field is bounded on both sides such that the focal point is outside of the field, the compression Mach waves cannot form a shock and isentropic flow again results. An example of supersonic flow past a curved concave boundary is shown in figure C-28. In this example, the lower convex boundary is shaped such that no reflection waves are produced. In describing supersonic flow in the physical plane, the term Mach wave or merely the word wave--is used in place of the terms Mach line or characteristic.

f. Reflection of mach waves from solid boundaries.

When Mach waves reach a boundary, they are reflected as waves of the opposite characteristic family. The incident and reflected Mach waves divide the flow field into regions in which the flow direction is parallel to the adjacent boundary, and the Mach number for each region is a function of intersecting right-running and left-running hodograph characteristics. Figure C-29 illustrates the development of reflected waves in a two-dimensional tunnel with a concave turning angle in the lower boundary. The flow in region 1 is parallel to both boundaries and M_1^* is a function of the hodograph characteristics α and β as shown in the hodograph. Point 1 in the hodograph represents region 1 in the physical flow. The flow in region 2 is parallel to the lower boundary, and the flow direction has turned through angle δ. Since the flow cannot be parallel to the upper boundary as well, the incident wave $C_1\ (\beta + 2\delta)$ reflects to form the reflected wave $C_R\ (\alpha - 2\delta)$ which isolates region 2 from the upper boundary. As the flow moves into region 3, it again parallels the upper boundary and a second reflection of the Mach wave occurs on the lower boundary. This build-up of flow regions continues throughout the length of the tunnel. In figure C-29, the incident and reflected waves are compression waves. If the incident wave is an expansion wave, then the reflected wave is also an expansion wave.

The application of the characteristics diagram is simplified by the use of two parameters introduced by Prandtl and Busemann. These parameters provide a system of numbering the epicycloids. The left-running epicycloids are identified by $B = 400 + 1/2\ \alpha$ while the right-running epicycloids are denoted by $A = 600 - 1/2\ \beta$. Since each vertex of the net is defined by the angular displacements from the left and right cusps, $\nu = \theta - \beta$ and $-\nu = \theta - \alpha$, the parameters can be related to ν & θ. See figure C-20.

$$A + B = 1000 - \nu$$
$$A - B = 200 - \theta$$

A + B is called the pressure number and A - B is called the direction number. These numbers are polar coordinates of points in the characteristics diagram. All angles are measured in degrees. Referring to figure C-25, the radii are designated by direction numbers, and the concentric circles are assigned pressure numbers. A numerical example will illustrate the use of these parameters. Consider a two-dimensional tunnel with a straight upper boundary and a convex turning angle in the lower boundary. Suppose that the initial critical Mach number is $M_1^* = 1.52$, and the turning angle is 10 degrees. A tabulation of critical Mach number and pressure ratio as functions of the pressure number is given in the following table:

A + B	M*	M	P/P_o
1000	1.00	1.00	0.528
995	1.20	1.26	0.383
990	1.32	1.43	0.299
985	1.43	1.61	0.234
980	1.52	1.77	0.181
975	1.61	1.95	0.138
970	1.69	2.13	0.104
965	1.77	2.34	0.076
960	1.84	2.54	0.055
955	1.90	2.75	0.039
950	1.97	3.03	0.027
940	2.08	3.60	0.011
920	2.26	5.35	0.001
900	2.38	9.19	0.000
870	2.45	∞	0.000

The pressure ratio is the static pressure associated with M* divided by the free-stream stagnation pressure. As shown in figure C-30, the initial flow direction is taken as $\theta = 0$. Region 1 is defined by the pressure number 980 and the direction number 200. This corresponds to epicycloid numbers of 590 and 390. In moving into region 2, the flow turns clockwise 10 degrees. The corresponding direction number on the characteristics diagram is 210. The epicycloid numbers become 590 and 380. This gives a pressure number of 970 for region 2, and the associated M* in the table above is 1.69. The flow in region 3 is again at $\theta = 0$ with direction number 200. The epicycloid numbers are 580 and 380 with pressure number equal to 960. Therefore, $M_3^* = 1.84$. The static pressure in region 3 is 0.055 times the free-stream stagnation pressure.

g. Attenuation of blast overpressure at tunnel entrances

The formation of the flow field at the entrance to a tunnel or duct is extremely complex and depends on surrounding topography as well as the configuration of the portal opening itself. As the blast wave moves across the opening, vortices form, shed, and move down the tunnel eventually forming a wave front. Shock tube studies indicate that a distance of 6 to 10 tunnel diameters are required for the formation of the wave front.(a) After the wave front forms, the flow field can be constructed approximately by applying the characteristics method. Flow conditions in the entrance prior to formation of the wave front must be estimated from available test data.

(a) "First Information Summary of Blast Patterns in Tunnels and Chambers," Aberdeen Proving Ground, Maryland, DASA Report No. 1171, Ballistic Research Labs, March, 1960.

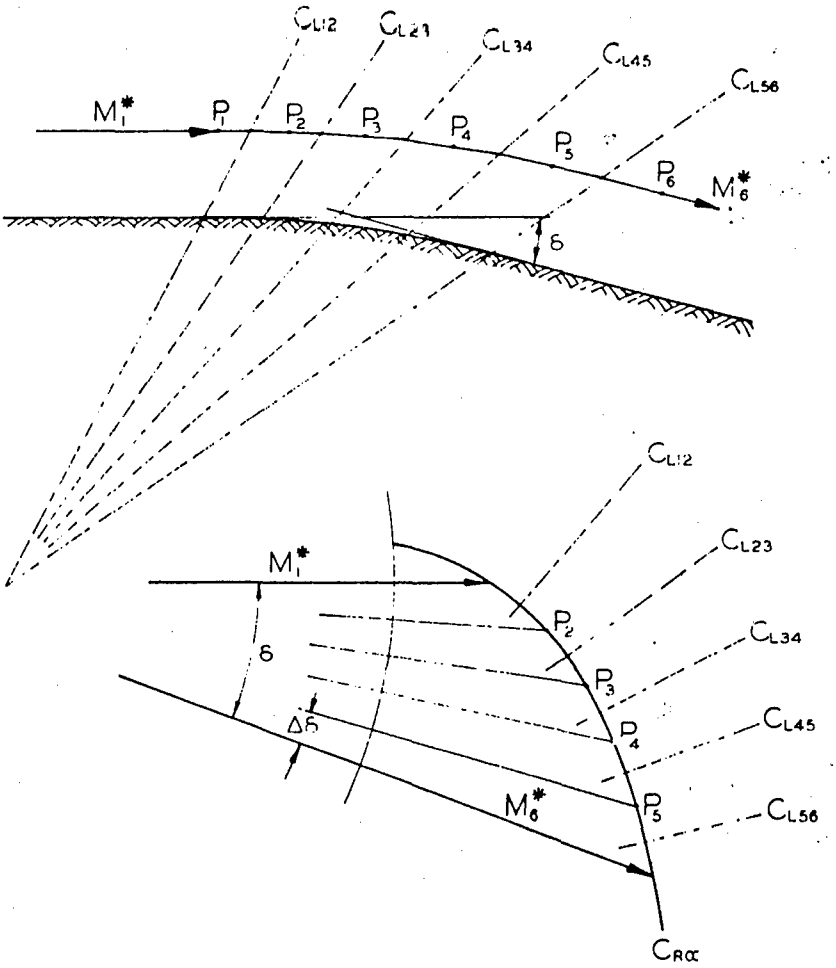

Figure C-27. Incremental Characteristics

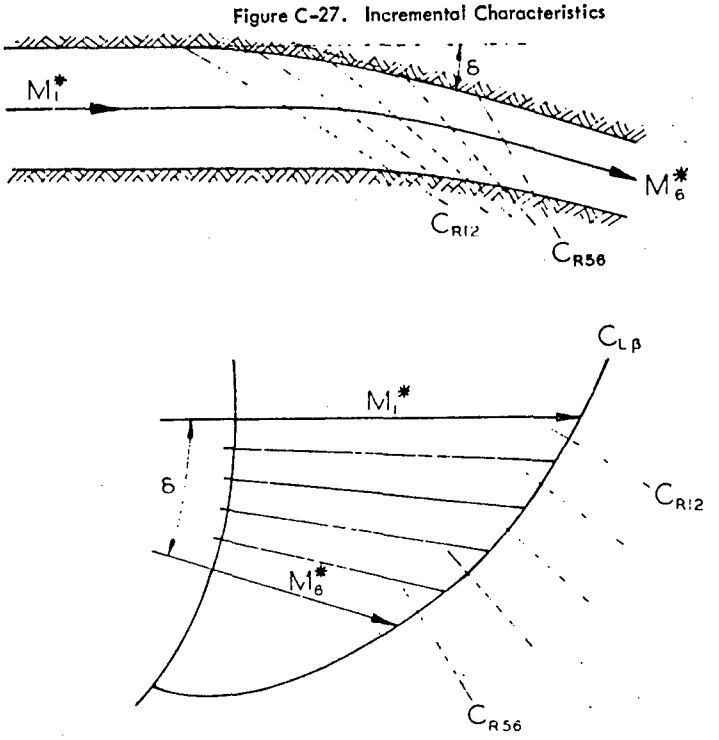

Figure C-28. Supersonic Flow Past Curved Concave Boundary

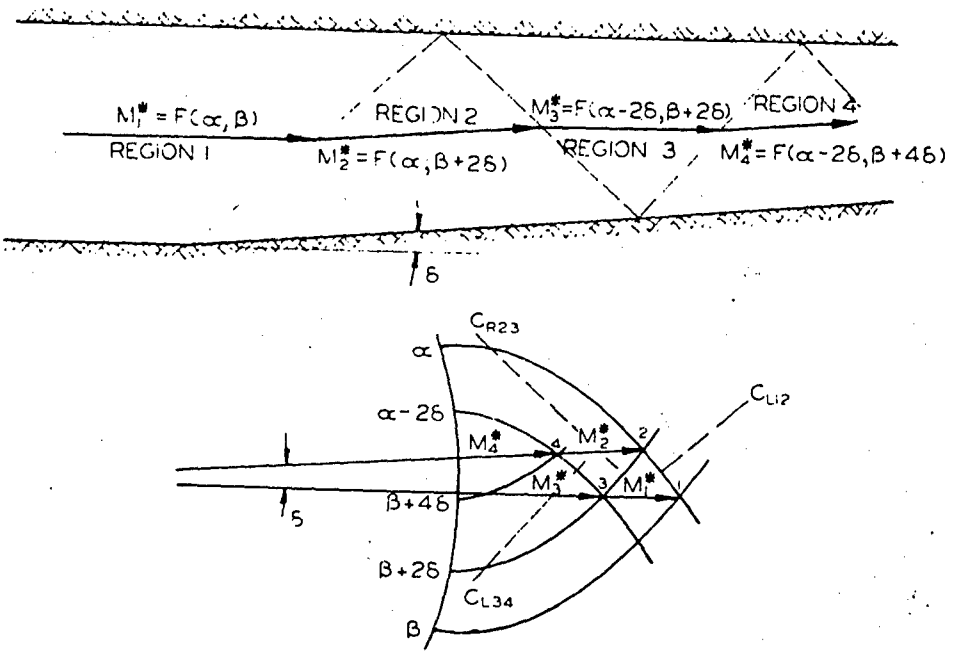

Figure C-29. Incident and Reflected Waves

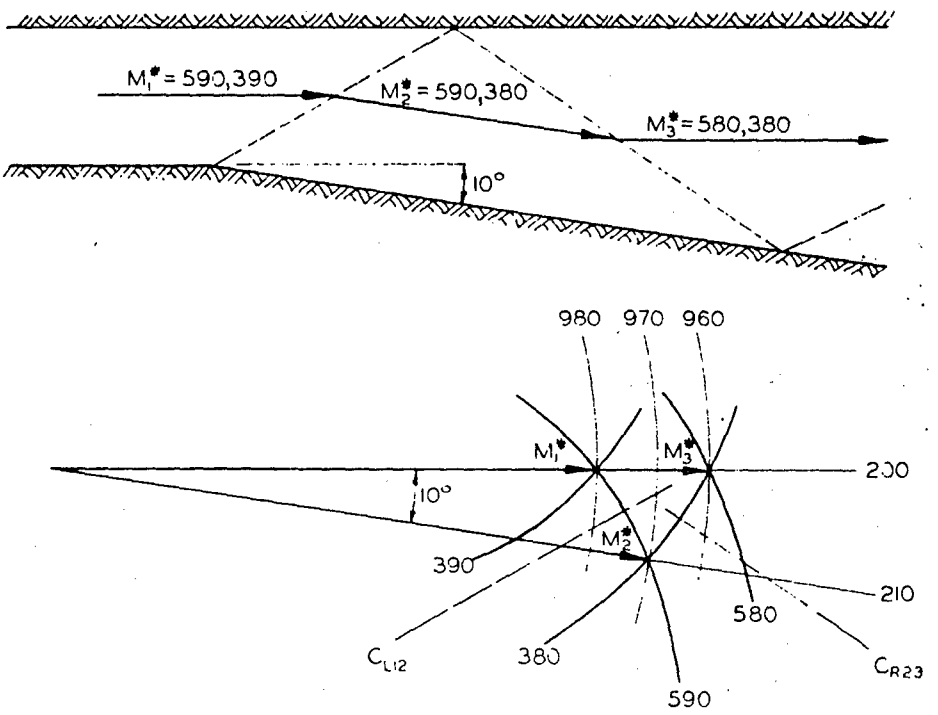

Figure C-30. Static Pressure Over Stagnation Pressure

Figure C-31 shows the relationship between the peak overpressure in the tunnel entrance at the point where the wave front has formed and the peak overpressure at the surface. Three angles of incidence between the tunnel axis and the direction of the surface air blast wave are considered. The models used in these studies were of constant cross-section with smooth walls. The dashed portions of the curves are based on extrapolations beyond the experimental results. The pressure relationship for other angles of incidence can be determined by interpolation between the curves shown.

h. Application of the characteristics method to a typical tunnel section.

To illustrate the application of the characteristics method, the solution of a numerical problem is presented in figures C-32 and C-33. An underground shelter is provided with an entrance tunnel which has the configuration shown in figure C-33. This is a vertical section through the tunnel. The width is assumed to be constant, and the width to height ratio is sufficiently large so that the flow is essentially two-dimensional. The door of the shelter is located in the side wall of the tunnel at the mid-point of its length. The tunnel is open at both ends providing ingress or egress in either direction. From the entrance, the tunnel slopes at 30 degrees for a distance of 10D where D is the height measured normal to the floor. From this point, the tunnel expands to a height of 2D while turning through two 15 degree angles which are spaced 4D apart.

The flow pattern in the tunnel is the result of the blast wave created by a megaton nuclear bomb bursting on the surface 3500 feet from the tunnel entrance. The direction of wave propagation is assumed to be parallel to the longitudinal axis of the tunnel and an overpressure of 100 psi is given. Referring to figure C-31, interpolation between curves 2 and 3 gives a peak overpressure of about 90 psi in the tunnel entrance for an inclination of 30 degrees and a surface peak overpressure of 100 psi. The Mach number associated with the wave front which develops in the entrance can be determined by using the following Rankine-Hugoniot equation for shock waves in standard air:

$$M_1^2 = \frac{1}{7}\left(6\,\frac{P_1}{P_2} + 1\right)$$

Where P_1 and P_2 are the static pressures behind and ahead of the shock. Assuming standard atmospheric pressure ahead of the shock,

$$\frac{P_1}{P_2} = \frac{90}{14.7} = 6.2$$

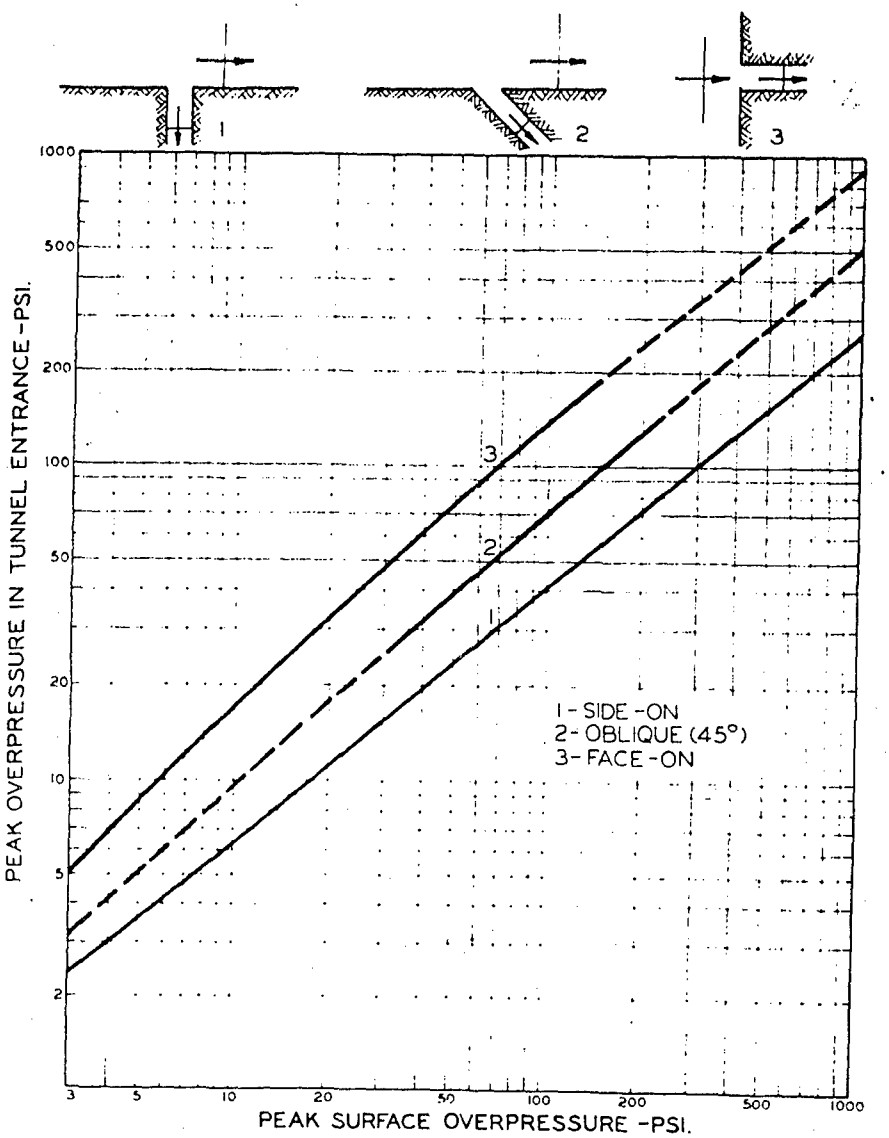

Figure C-31. Surface Overpressure vs Tunnel Entrance Pressure

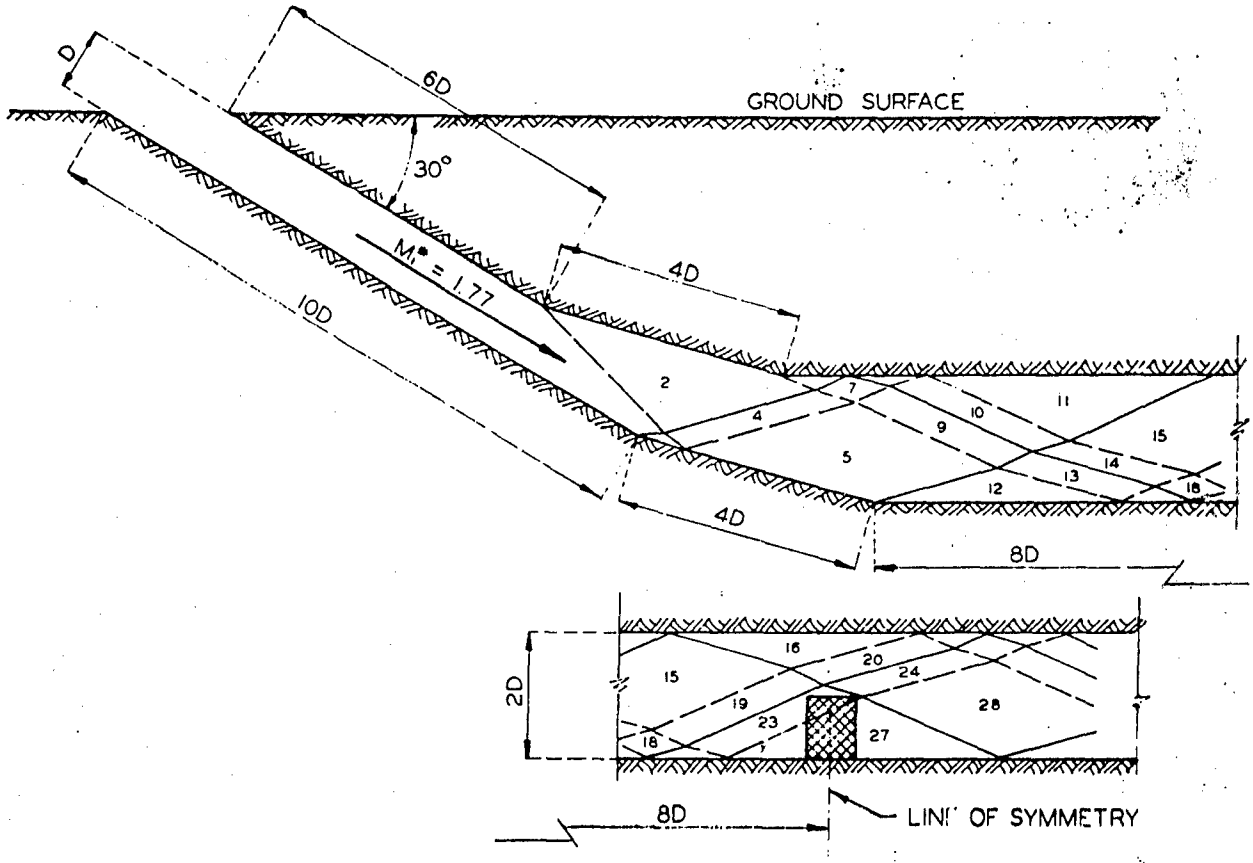

Figure C-32. Solution of Numerical Problem

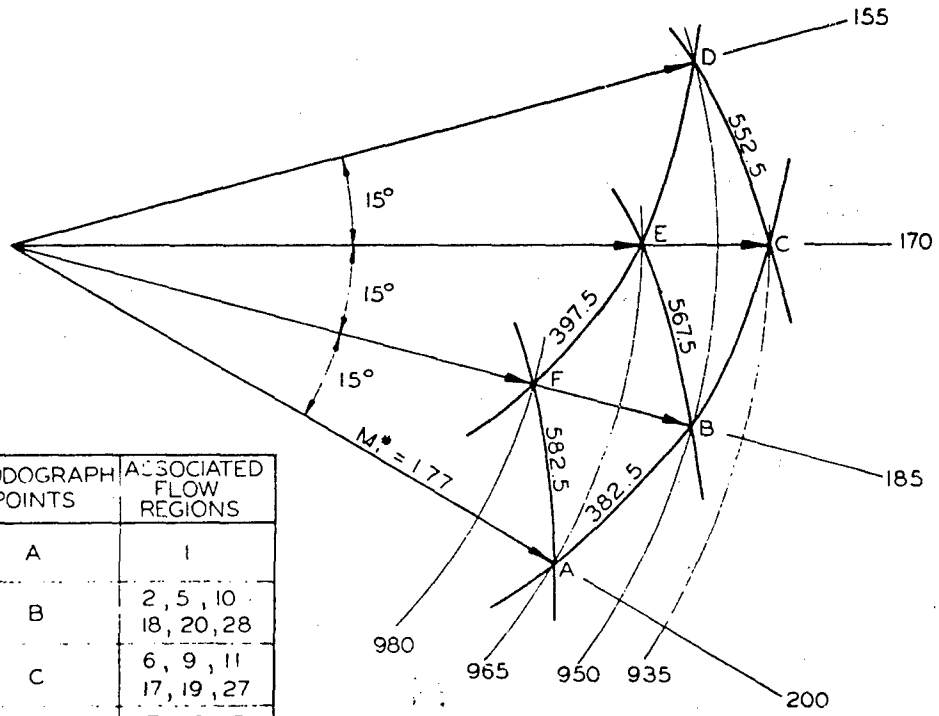

HODOGRAPH POINTS	ASSOCIATED FLOW REGIONS
A	1
B	2, 5, 10 18, 20, 28
C	6, 9, 11 17, 19, 27
D	7, 13, 15 23
E	4, 8, 12, 14 16, 22, 24
F	3

Figure C-33. Vertical Section Through Tunnel

The corresponding Mach number for the initial region of flow is then, $M_1 = 2.34$. Table I gives the critical Mach number, $M_1^* = 1.77$, and the pressure ratio, $P_1 / P_o = 0.076$.

Now that the initial flow conditions are fixed, the characteristics method can be applied to plot the flow pattern. As the flow moves into region 2 it experiences an expansion at the ceiling as a result of the 15 degree convex turning-angle. This produces the expansion wave, shown by the dashed line, which divides region 2 from region 1. At about the same instant, the compression wave, shown by the solid line, is formed at the 15 degrees concave turning-angle in the floor. These waves continue throughout the flow field, reflecting from opposite walls to form the wave pattern shown. Additional waves are produced at the other turning angles. Note that each wave is bent as it crosses a reflected wave from the opposite wall. The direction of these waves is determined from the hodograph shown in figure C-33, which was constructed by use of figure C-24. Each point on the hodograph is defined by pressure number, epicycloid numbers, and direction number, and the associated flow regions in the tunnel are indicated in the tabulation.

The shelter door is located primarily in flow region 27, for which the flow characteristics can be determined by referring to point C on the hodograph. The corresponding pressure number is 935, and by interpolation, Table I gives $M_{27}^* = 2.13$ and $P_{27}/P_o = 0.007$. Since $P_1 = 90$ psi,

$$P_o = \frac{P_1}{0.076} = \frac{90}{0.076} = \frac{P_{27}}{0.007}$$

Therefore $P_{27} = \frac{0.007}{0.076}\ 90 = 8.3$ psi

The top of the door is exposed to region 23 which is associated with pressure number 950, $M_{23}^* = 1.97$, and $P_{23} / P_o = 0.027$. Therefore,

$$P_{23} = \frac{0.027}{0.076}\ 90 = 32 \text{ psi}$$

For purposes of design, the shelter door can be assumed to be exposed to peak overpressure varying from 32 psi at the top to 8 psi at the bottom.

i. Blast resistant doors for underground shelters.

Based on mode of operation, shelter doors can be classified as follows:

1. Power operated, automatic or hand controlled.
2. Gravity operated, automatic or hand controlled.
3. Hand operated.
4. Blast pressure actuated.
5. Fail-safe construction.

There have been many commercial or industrial applications of door construction which fit into the first two classes. This existing means of construction can readily be made applicable to large underground shelters where massiveness is no objection. Pressure-sensing devices can be installed near the tunnel opening, far enough from the door to allow time for closing before the blast wave reaches the door. Reliable, self-sufficient electrical power is necessary for power operation and automatic controls.

Hand operated blast-resistant doors are also commercially available. The shelter can be continuously sealed off from the outside by arranging these doors in pairs with interlock systems which require one door to be closed when the other is open. An important disadvantage in this system is the resulting slow movement of traffic through the interlocked doors. This problem has been solved in commercial buildings by use of the revolving door. With modification, the revolving door can be used as a pressure-lock shelter door. Three problems become evident. First, the revolving door must be properly sealed around the edges and still provide sufficient ease of movement. Second, consideration must be given to the possibility of "wind-milling" due to unsymmetrical distribution of blast pressure. Third, handicapped individuals may become isolated from help in the quadrants formed by the intersecting doors and thus cause the revolving door to become inoperable. It is possible that all three of these problems can be reduced or eliminated by substituting a revolving cylinder for the intersecting revolving doors. This scheme is illustrated in the sketches shown in figure C-34.

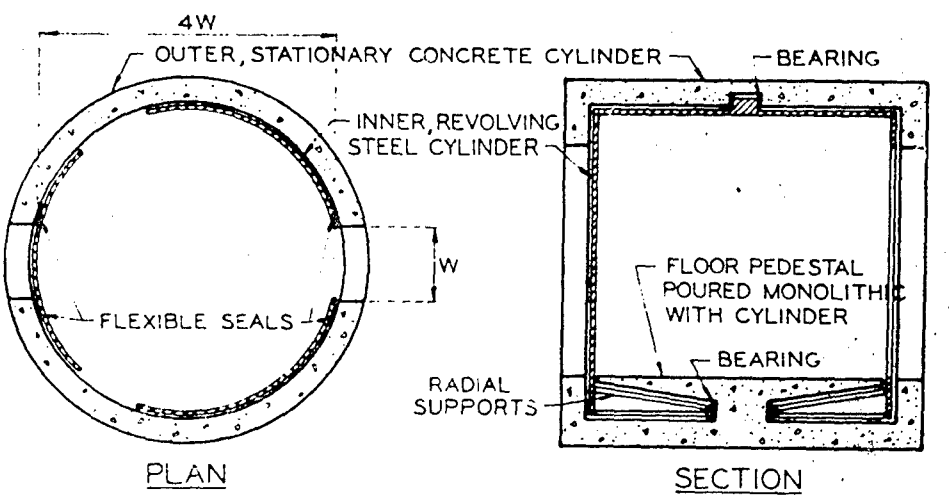

Figure C-34. Intersecting Revolving Doors

The inner revolving cylinder can be designed for an optimum weight-strength ratio by using aircraft-type construction consisting of circumferential wings, longitudinal stringers and stressed skin. The inner cylinder can be provided with hand grips or rails to facilitate revolving.

As previously stated, the overpressure induced by the blast can be detected by pressure-sensing devices which actuate automatic controls for closing the shelter or tunnel doors. In some cases, this overpressure can also be used as a power source for closing a door or a plug in a section of the tunnel ahead of the blast wave. This is shown in figure C-35. The delay loop must be long enough to contain the blast wave until the plug has been forced into place by the overpressure behind the shock. This design requires precise evaluation of wave strength, plug mass, friction force, and wave velocity.

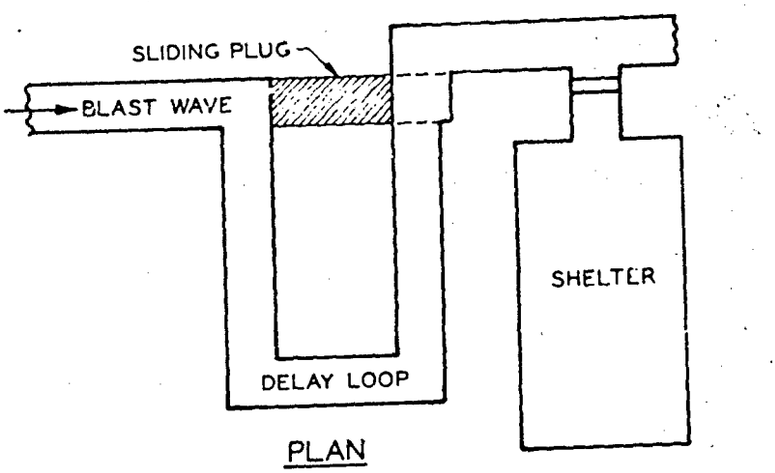

Figure C-35. Fail-Safe Door

In "fail-safe" construction, a section of the tunnel is designed to collapse under an overpressure which would damage the shelter doors. The collapsing tunnel absorbs most of the blast wave energy and plugs the tunnel with debris.

L. Entrance Use, Analogue Analysis

1. Introduction

In heavily populated areas, walking is the only practical and rapid means of moving the population to shelters under emergency conditions. The pedestrian traffic problem arising in this situation must be analyzed to determine the size, number, and location of shelter entrances required. Shelter districts designating the geographical area to be served by each shelter entrance must be established. Then, as the shelter system is constructed, the population of the area must be trained to ensure proper use of available shelter.

2. Constraints

The size, number, and location of entrances and their associated shelter districts depend upon the following constraints:

(a) Population of the area served by a shelter system
(b) Capacity of the shelter served by each entrance
(c) Warning time available to move people into shelters
(d) Arrival rate at each shelter entrance
(e) Entry rate at each shelter entrance
(f) Queuing at each shelter entrance

a. Population

Population of an area determines the shelter capacity required to protect a given proportion of the people in that area at the time a warning is sounded. A detailed analysis of the present and future total population of an area to be served by a shelter system is essential. In addition, an analysis of population distribution on as detailed a geographical scale as practical, including shifts of population concentration during the day and night hours, contributes greatly to the analysis of the pedestrian traffic problem. Once a population analysis is made, intelligent design of the shelter system can commence.

b. Capacity

Capacity of the shelter facilities served by a given shelter entrance places an absolute maximum limit on the number of people using that entrance. Early in the design of the shelter system a decision must be made concerning what portion of the maximum population in a given area will be accommodated by the shelter. In making this decision, consideration must be given to population shifts during the day, to future population increases, and to the possibility that a portion of the shelter system may not be available for use at the time a warning is sounded.

c. Warning time

Warning time is the estimated time that will be available between the instant warning of an attack is sounded and the time the destructive weapons of this attack arrive on a given target. The warning time is thus the period of time available for people to leave their normal daily activities and safely enter a shelter. Warning time is dependent upon military technology which changes constantly. It must be revised as a means of weapons delivery, means of detection of an attack, and the efficiency of the warning system change. However, at any given time a warning is sounded, the warning time available to take shelter is a fixed constant. At present, a warning time of 15 minutes is fairly realistic for a target under intercontinental missile attack. A detailed target analysis should be made to determine the warning time for a specific shelter system under consideration.

The warning time, once determined, may be further divided into three general periods:

Reaction Period
Pedestrian Traffic Period
Safety Margin Period

Reaction period is the period between the instant a warning is sounded and the time people actually start traveling toward shelter. During the day this period will be quite short. At night, in a residential area, the reaction time will be appreciable. Assuming a night attack in a residential district, and assuming a normal distribution of the times people leave their residences, a mean reaction time of 5 minutes with 95% of the population leaving between 3 and 7 minutes after a warning is sounded is a fairly realistic estimate.

Reaction time may also be defined from a slightly different viewpoint. It can be considered to be the time elapsing between sounding a warning and the arrival at the shelter entrance of people in the area immediately adjacent to that entrance. Thus, it is a period just after the warning is sounded when there still is essentially no traffic through the shelter entrance into the shelter.

Pedestrian traffic period is the period during which the population in a given area travel toward and pass through the shelter entrance serving that area. This is the period of primary importance in the analysis of the pedestrian traffic problem. It is the actual time available to move the population from the scene of their daily activities into the shelter.

Safety margin period may or may not exist. It is the remainder of the warning time after the reaction period and the pedestrian traffic period have elapsed, provided the sum of the latter two periods is less than the warning time. If it exists, the safety margin period is a short time when small unexpected contingencies may be handled.

For design work a desired safety margin period may be chosen and the pedestrian traffic problem solved for the remainder of the warning time.

d. Arrival rate

Arrival rate is the rate that people arrive at the entrance as a function of time after a warning is sounded. It may be represented mathematically as:

$$A(t) = \frac{d\,P(t)}{dt}$$

where A(t) is the arrival rate, P(t) is a population segment as a function of the time it takes each segment of the population to reach the shelter entrance, and t is the time after a warning is sounded. The total number of people who have arrived at the shelter entrance at a given time, t, is the integral of the arrival rate:

$$P(t) = \int_0^t A(\tau)\,d\tau$$

The arrival rate is dependent on four factors:

Population Distribution
Walking Speeds
Walking Distances
Congestion of Pedestrian Traffic Routes

Population distribution is the detailed description of the number of people per unit area at every location within a given area. In analysis of the pedestrian traffic problem associated with shelter entrance requirements it is desirable to know the population density for each block of the region served. For still more accurate analysis, population density for each building or lot in the region would be necessary. If none of this data is available then the average population density, determined by dividing the population of a larger region by the area, must be used for an approximation.

Walking speeds are the rates each person travels in movement toward a shelter entrance. Little data is available concerning movement of large groups of people under emergency conditions. Therefore, an assumption must be made that movement to the shelter entrance is disciplined and orderly. To ensure this, proper instruction and training of the population by drills are essential for proper use of shelter system entrances.

Over moderately long distances across level terrain, hikers often use an average speed of 3 miles per hour or an average of 265 feet per minute as a rule of thumb in estimating walking speed. Alexander et al (2) from a distribution of 125 measurements made in downtown Washington, D. C., found in all but a few extreme cases, the walking speeds of pedestrians were between 165 and 360 feet per minute. Schultz (3) determined in tests he conducted that a married couple carrying two small children should be capable of traveling approximately one half mile at an average speed of 350 feet per minute or approximately 4 miles per hour, when they know the time available to reach a shelter is limited.

From this information, an average walking speed of 300 feet per second appears to be a conservative value for use in the absence of more accurate data. This value assumes an orderly population movement by people aware that the time available for them to take shelter is limited. If data giving the distribution of individual walking speeds under emergency conditions is available it should be utilized for analysis of the pedestrian traffic problem.

Walking distances are the distances each person travels following streets and in some cases the halls or passageways of large buildings to reach a shelter entrance. In the cases of large buildings, the walking distances inside the building depend upon its construction. Each one must, therefore, be analyzed individually.

For an area in which streets are layed out in a basically rectangular grid pattern, the boundaries of shelter districts should form squares intersecting the streets at 45° angles. Each shelter entrance should be located near the center of the shelter district. It can then be demonstrated geometrically in figure C-36 that walking distances following the streets are equal from each intersection of the shelter district boundary and a street. The walking distance from the shelter district boundary to the shelter entrance is the maximum walking distance. This distance is equal to one half the diagonal of the square forming the shelter district.

Walking speed and the pedestrian traffic period determine the maximum allowable walking distance and thus, the maximum allowable size of a shelter-entrance district. The maximum allowable walking distance may be calculated by the formula:

$$D_{w\ max\ allow} = S_w T_p$$

where $D_{w\ max\ allow}$ is the maximum allowable walking distance, S_w is the walking speed, and T_p is the pedestrian traffic period.

By simple geometry the length of one side of the shelter district corresponding to a given maximum allowable walking distance is $\sqrt{2}\ D_{w\ max\ allow}$ and the area of the district is $2\,(D_{w\ max\ allow})^2$.

To obtain a most conservative value of the maximum allowable walking distance the slowest expected walking speed should be used. A higher value, such as an average walking speed, can be used to determine roughly the maximum size shelter districts which should be considered for a given warning time.

Congestion of pedestrian traffic routes will obviously slow movement to shelters and it may deny access to shelters. In residential areas and other areas of lower population density the streets are probably adequate to handle all pedestrian traffic without congestion with the exception of the area immediately surrounding the shelter entrance. In large buildings congestion may become acute. On the basis of fire safety studies conducted by the National Bureau of Standards (NBS), (4) a rapid flow rate of persons down stairways is 45 persons per minute for each exit unit (1 exit unit = 22 inches width). Through doorways the NBS flow rate is 60 persons per minute, per exit unit. Based on these flow rates Alexander et al (5) determined that in a tall building meeting the NBS minimum exit requirement for fire safety, (one unit of stairway exit width per 60 persons on each floor), it would be possible to empty only the lower 11 stories in a 15 minute period. This figure assumes that no elevator service is available after the attack warning is sounded. It is apparent that only a portion of the people in a tall building would be able to leave the building and enter an underground shelter during a short warning period. Similarly, congestion of pedestrian traffic routes may occur in densely populated areas with narrow streets which may further be partially blocked by stalled automobiles, trucks, and buses. The NBS standard of 60 persons per minute per 22 inches width may be applied here to indicate whether congestion will occur. Each particular situation of this type requires individual analysis.

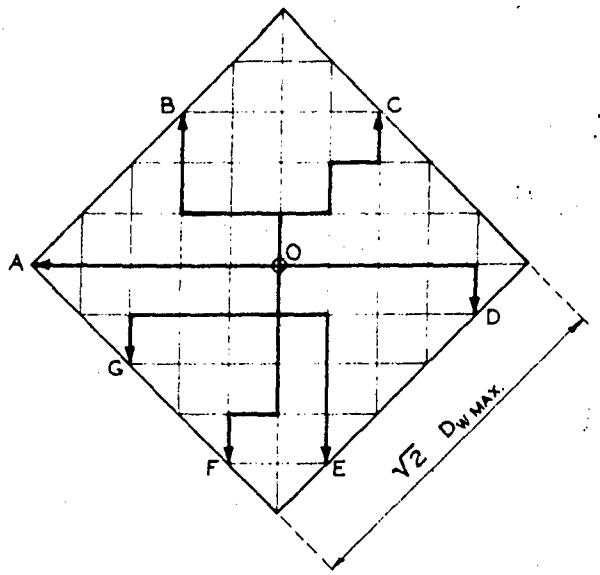

$$D_{W\,MAX.} = \overline{OA} = \overline{OB} = \overline{OC} = \overline{OD} = \overline{OE} = \overline{OF} = \overline{OG}$$

Figure C-36. Walking Distance to Entrance

e. Entry rate

Entry rate is the rate people pass through a shelter entrance into the shelter itself. The maximum entry rate possible at an entrance depends upon the construction and dimensions of the entrance. In many instances structural limitations associated with the design of doors to withstand the expected blast effect will determine the dimensions of an entrance. The NBS standards of 45 persons per minute per 22" width entrance unit on stairways and 60 persons per minute per entrance unit through doorways may be applied to determine maximum entry rate. It is apparent that the use of stairways should be avoided in the design of shelter entrances.

The number of people inside a shelter at time t after a warning is sounded will be the integral of the entry rate,

$$N(t) = \int_0^t E(\tau)\,d\tau$$ where N(t) is number of people in shelter, E(t) is entry rate, = 0 is the time a warning is sounded.

f. Queuing

Queuing at a shelter entrance occurs if the arrival rate exceeds the maximum entry rate. Since structural limitations determine the maximum entry rate it is probable that some queuing will occur either in densly populated areas or in large shelter districts. If queuing does occur time must be available during the pedestrian traffic period to allow those people gathered in the queue to enter the shelter.

The rate at which the queue forms and is dissipated is the difference between the arrival rate and the entry rate. This may be expressed mathematically as:

$$\frac{dQ(t)}{dt} = A(t) - E(t)$$

where: Q(t) is the number of people in the queue at time, t
A(t) is the arrival rate
E(t) is the entry rate

Integrating this equation gives the number of people in the queue at time, t, after a warning is sounded:

$$Q(t) = \int_0^t A(\tau)\,d\tau - \int_0^t E(\tau)\,d\tau = \int_0^t \left[A(\tau) - E(\tau)\right]\,d\tau$$

The formation and dissipation of a queue occurs in distinct phases. During the initial period after the warning is sounded the arrival rate is less than the maximum entry rate. All people arriving at the entrance during this period enter the shelter directly and no queuing occurs. As soon as the arrival rate exceeds the maximum entry rate a queue commences to form. The queue increases until the arrival rate falls below the maximum entry rate. When the arrival rate falls below the maximum entry rate, the flow of people through shelter entrances will continue at the maximum entry rate until the queue is dissipated. When the queue is dissipated the entry rate is again identical to the arrival rate. It should also be noted that the entry rate will obviously become zero at the time the capacity of a shelter is reached or at the time the blast doors are closed. In analyzing the pedestrian traffic problem it is necessary to allow time for the dissipation of the queue during the pedestrian traffic period.

3. Analysis of the Pedestrian Traffic Problem

Analysis of the pedestrian involves basically the following steps. The arrival rate must first be determined for a given shelter district. Then for a given maximum entry rate, the time required for the total population P_{total} of the given shelter district to enter the shelter is determined. This is done by determining the time, t, after the warning is sounded that the integral of the entry rate equals the total population, that is:

$$P_{total} = \int_0^t E(\tau)\,d\tau$$

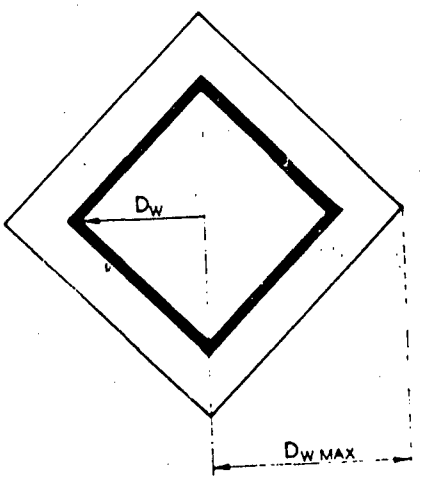

Figure C-37. Incremental Square Ring Concept

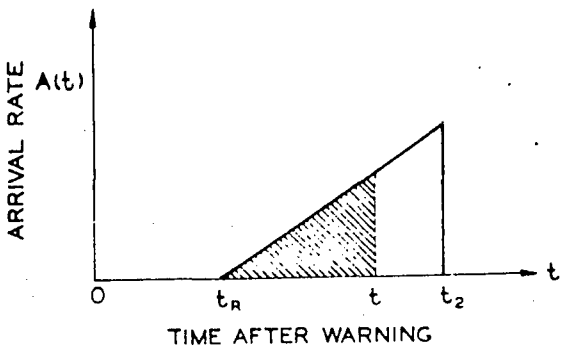

Figure C-38. Arrival Rate vs Time

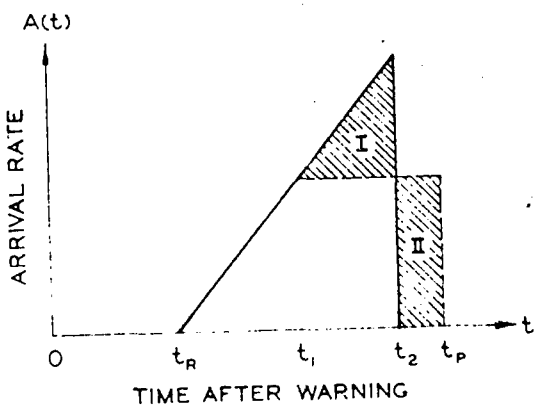

Figure C-39. Arrival Rate vs Elapsed Warning Time

The time, t, required for the total population to enter the shelter is then compared with the time available to take shelter. If time, t, is less than the time available, the combination of shelter district size and maximum entry rate of the entrance are acceptable. When time, t, is equal to the time available, the minimum acceptable combination exists. If the time required to enter the shelter is greater than the time available, either the size of the shelter district must be decreased or the maximum entry rate of the shelter increased in order to offer protection to the entire population of the shelter district.

Arrival rate is the most difficult factor to predict accurately in analyzing the pedestrian traffic problem and determining shelter entrance requirements. The accuracy depends upon the amount and detail of data available and the analytical procedures used.

A rough approximation of arrival rate can be made by assuming a uniform population density throughout a shelter district and using average values of walking speed and reaction period. Walking distances are assumed to be along streets laid out in a rectangular grid with shelter district boundaries intersecting there at 45° angles as developed later. These approximations lead to a simple straight line graphical solution of the pedestrian traffic problem.

During the reaction period from time zero to time, t_r, it is assumed that nobody arrives at the shelter entrance, thus:

$$A(t) = 0 \qquad 0 \le t \le t_r$$

At time t_r, the reaction period ends, the people leave the locale of their daily activities, and those in the immediately adjacent area arrive at the shelter entrance. Thus at time, t_r, the pedestrian traffic period begins.

Since an average value of walking speed S_w is assumed, the time required for all people at walking distance, D_w, to travel that distance to the shelter entrance is:

$$t - t_r = D_w / S_w \qquad t_r \le t \le t_2$$

The time, t_2, denotes the time that the last segment of the population in the shelter district reaches the shelter entrance. It is related to the maximum walking distance $D_{w\,max}$ by the equation:

$$t_2 - t_r = \frac{D_{w\,max}}{S_w}$$

The area ( ) within a given walking distance, D_w, is given by: $= 2 D_w^2$

Since a uniform population density is assumed, the population in this area is: $P(D_w) = 2P_d D_w^2$

Differentiating this quantity gives the number of people in an incremental square ring (figure C-37) who must travel a walking distance to the entrance:

$$\frac{d\,P(D_w)}{d\,D_w} = 4\,P_d\,D_w$$

The number of people arriving at the entrance at time, t, between t_r and t_2 is identical to the number of people traveling the corresponding walking distance D_w.

Changing the independent variable from D_w to t yields the arrival rate: $A(t) = \frac{d\,P(t)}{dt} = 4\,P_d S_w^2\,(t - t_r) \qquad t_r \le t \le t_2$

It is noted this is a linear equation of the form: $A(t) = C(t - t_r)$

At time t_2 the last group of people arrive at the entrance after traveling the maximum walking distance, D_w. After time t_r the arrival rate is assumed to be zero, $A(t) = 0 \qquad t > t_2$

The arrival rate A(t) can easily be plotted versus time, t, in this simplified analysis, as shown in figure C-38.

The integral of A(t) is the total number of people in the shelter district who have reached the shelter entrance at time t. In this linear case, the triangular area under the A(t) curve between times t_r and t_2 (shown shaded in figure C-38) gives this value quite readily. At time t_2 the area under the vurve between t_r and t_2 represents the total population of the district if the shelter capacity is greater than the total population. Since, in this straight line model, the maximum arrival rate A_{max} occurs at time t_2, this value is related directly to the total population, P_{total}, of the district:

$$A_{max} = \frac{2}{t_2 - t_r} \times 100\% = \frac{2\,S_w}{D_w} \times 100\%$$

It can be seen from this equation that for a short pedestrian traffic period in heavily populated areas the maximum arrival rate is quite large. It is likely that the arrival rate will exceed the maximum entry rate and queuing will occur. If this is the case, it is necessary to determine the time required to dissipate the queue. The linear representation of arrival rate lends itself readily to a graphical solution of the problem.

The first step of this solution is to superimpose the entry rate curve upon the plot of arrival rate versus time as shown in figure C-39. These two curves coincide until the arrival rate reaches the maximum entry rate at time t_1. At this point the entry rate will remain constant at E_{max} until time t_r when the queue is dissipated. At time t_p everyone has entered the shelter, the pedestrian traffic period is completed, and the entry rate becomes zero again. Entry rate thus can be expressed mathematically, as follows:

$$E(t) = \begin{cases} A(t) & 0 \le t \le t_1 \\ E_{max} & t_1 \le t \le t_p \\ 0 & t > t_p \end{cases}$$

Since the arrival rate is assumed to drop to zero at time, t_2, while the entry rate continues at E_{max} until time t_p, the integral E_{max} from time t_2 to time t_p, is equal to the number of people that were in the queue at time t_2. Therefore, the following relationship exists in this special case:

$$Q(t_2) = \int_{t_1}^{t_2} \left[A(t) - E_{max} \right] dt = \int_{t_2}^{t_p} E_{max}\, dt$$

These two integrals are represented by the two shaded areas I and II of figure C-39 . The length of time required to dissipate the queue is thus given by:

$$t_p - t_2 = \frac{(t_2 - t_1)\ (A_{max} - E_{max})}{2\ E_{max}}$$

The length of the pedestrian traffic period T_p is now just the sum of the arrival period $t_2 - t_r$ and the queue dissipation period $t_p - t_2$, therefore:

$$T_p = (t_2 - t_r) + (t_p - t_2) = t_p - t_r$$

In situations where queuing occurs, it is now possible to plot a family of curves of the maximum entry rate required versus the length of the pedestrian walking period for various arrival periods $(t_2 - t_r)$. This is done in figure C-40. If a value of walking speed S_w is assumed, then each arrival period $(t_2 - t_r)$ curve corresponds to a maximum walking distance $D_{w\ max}$. The upper end of each curve terminates at the maximum arrival rate for that arrival period.

The curves of figure C-40 may now be used to determine roughly the entrance requirements of a given region. This can be illustrated by an example. Assume that a region has a uniform population distribution of 6000 persons per square mile. Taking the case of a night attack on a residential area, let the average reaction period be 5 minutes and allow a 1 minute safety margin. For a 15 minute warning this leaves a pedestrian traffic period of 9 minutes. Assume an average walking speed of 3 miles per hour or 265 feet per minute. Entrances to the shelter system are to be 8" diameter culverts with butterfly type blast doors mounted on a center post. Each entrance will thus have a maximum entry rate of approximately 120 persons per minute (2 entrance units) dictated by its structure. It is desired to determine the number of entrances required and the size of the shelter districts they will serve.

Going to figure C-40 , maximum walking distances of shelter districts can be assigned to each $t_2 - t_r$ curve since an average walking speed of S_w = 265 feet per minute is assumed. These are tabulated in the following table. The areas of each shelter district, $a = 2(D_{w\ max})^2$ and the population of each shelter district, $p_d a$, are then calculated and listed in this table. Using the values of E_{max} required for each walking distance with a 9 minute pedestrian traffic period as taken from figure C-40, the required entry rates for each size shelter district are caluclated and added to the table. It can be seen that for a maximum entry rate of 120 persons/min dictated by the entrance structure, the largest shelter district in an area of the given population density has a maximum walking distance of a little more than 1/4 mile and an area slightly greater than 1/8 square mile.

$t_2 - t_r$ (min)	$D_{w\ max}$ (ft.)	(mi)	$a=2\ D_{w\ max}^2$ (mi.^{2})	$P(D_w)=P_d a$ (people/shelter district)	Required E_{max} for T_p=9 min (people/min)
3	795	.15	.045	270	30
4	1060	.20	.080	480	55
5	1325	.25	.125	750	90
6	1590	.30	.180	1080	140
7	1855	.35	.245	1470	200
8	2120	.40	.320	1920	300
9	2385	.45	.405	2430	540

Since through streets are laid out every quarter mile in many cities, a system of shelter districts with maximum walking distances of 1/4 mile would be a reasonable choice in this example. In general, it is more desirable to have a large number of small entrances serving small dispersed shelter districts than to have a small number of large entrances serving large shelter districts. For this reason multiple culvert entrances at a single location are not considered.

If the 1/8 square mile shelter districts are chosen the length of the pedestrian traffic period can be taken from figure C-40, for the 120 person/min = E_{max}. For the 6000 persons per square mile population density the pedestrian traffic period is 7.3 minutes. If the population of this area should increase to 8000 persons per square mile the pedestrian traffic period for the entrance would be 9 minutes.

The major weakness of this rough analysis is the use of average values of walking speeds and reaction time. No allowance is made for individual variations of these two quantities. If these variations are taken into account in some manner, the arrival rate as a function of time will not be a straight line relationship, and analysis of the problem becomes more involved.

One approach to the problem of determining arrival rate more accurately is the assumption of statistical distributions of walking speeds and of reaction times. In this approach a uniform population density is still assumed throughout a shelter district of a given size. The shelter district is broken up into finite square rings corresponding to given finite increments of walking distance. Individual walking speeds and reaction times are each taken to fit a normal distribution about a mean value with 95% of the distribution falling between specified upper and lower limits. Using the distribution of walking speeds, the walking distance, and the population of each square ring, a distribution of the number of people versus the time required to travel that walking distance is compiled for each ring. These distributions are then added to get a distribution of population of the shelter district versus the time spent traveling to the shelter entrance. This distribution is finally combined with the distribution of reaction times to obtain the arrival rate as a function of time.

Alexander et al (6) used this procedure to evaluate a shelter district with 1350 ft maximum walking distance in a residential area under night attack. They assumed a 15 minute warning time, of which 1 minute was allowed as a safety margin period. A mean walking speed of 225 ft/min with 95% of the population on a normal distribution between 180 and 330 ft/min was used. Reaction times were assumed to be a normal distribution with a mean value of 5 minutes and 95% of the cases between 3 and 7 minutes. Using the procedure outlined above they obtained the distribution of arrival rate as a function of time shown in figure C-41.

Using this approach, the maximum arrival rate obtained was 23.3% of the shelter district population per minute occurring 9 minutes after the warning is sounded. This is appreciably less than the corresponding values of 35% occurring at 10.3 minutes after the warning is sounded as taken from figure C-40, and assuming a 5 minute reaction time, a maximum walking distance of 1350 ft, and a 255 ft/min walking speed yielding $t_p - t_2$ = 5.3 minutes. This points out that the maximum arrival rate predicted by the straight line arrival rate curve will be higher than should actually be expected.

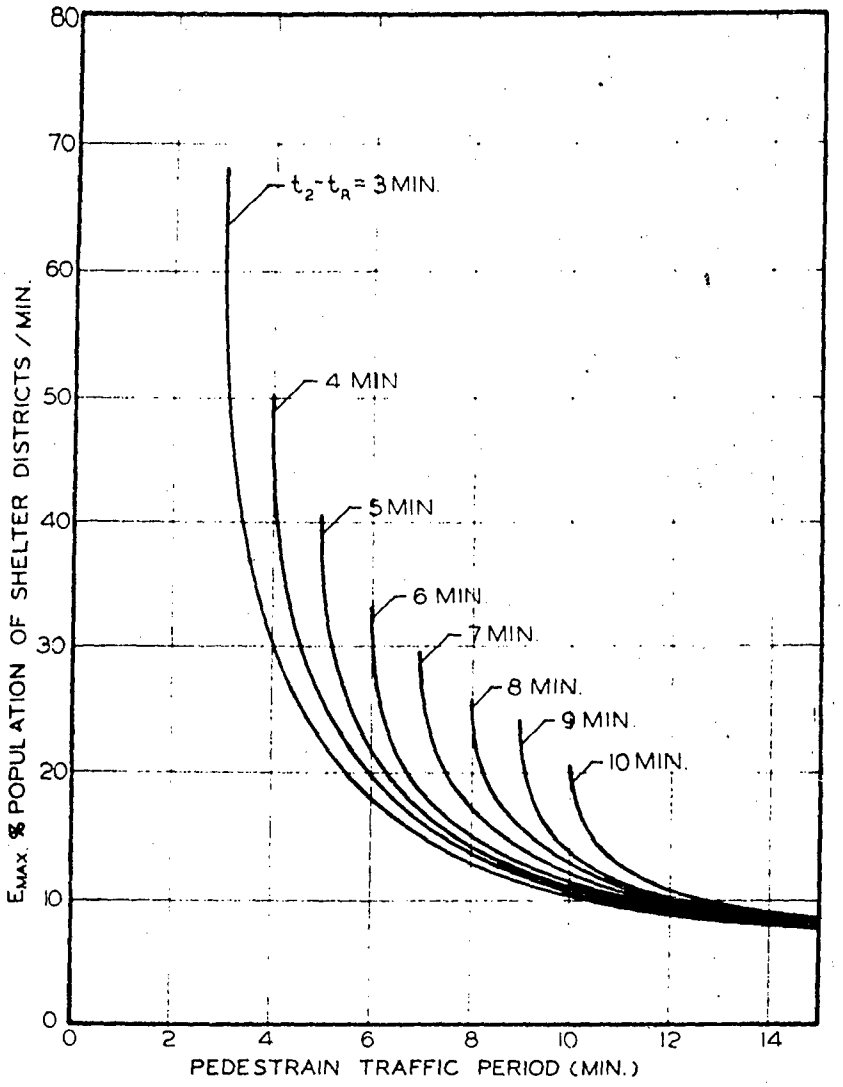

Figure C-40. Walking Period vs Population

The time required for everyone to enter a shelter with various maximum rates can be approached in a manner similar to that used for the straight line arrival rate. However, the actual analysis is a little more involved since the areas being compared are not regular triangles and rectangles. Three major methods of analysis are available in this case:

Graphical analysis using a planimeter or counting squares
Experimental analysis using a physical analogy
Analog computer analysis

Graphical analysis uses exactly the same method as used with the straight line arrival rate curve. The entry rate is superimposed on the arrival rate plot as shown for the preceeding example in figure C-42. The area under the arrival rate curve and above the maximum entry rate curve between t_1 and t_2 is determined either by counting squares or by use of a planimeter, (shaded area I in figure C-42). This area represents the number of people in the queue. The area under the maximum entry rate and above the arrival rate curve, (shaded area II in figure C-42) is determined such that at time, t_3, it is equal to the area I. The queue is dissipated at time, t_3. In the example shown in figures C-41 and C-42 the maximum entry rate required for everyone to enter the shelter entrance in 14 minutes after the warning is sounded is 11.5% of the shelter district population per minute. (7) The corresponding required maximum entry rate, 11.2% of the population/min, interpolated from figure C-40 for the straight line arrival rate model compares quite favorably with that obtained by this more sophisticated approach.

If the above process is repeated for various maximum entry rates, a plot of maximum entry rate versus the time required for the total population to enter the shelter could be made. It would be similar to a single curve of figure C-40. Going through this entire process for various sizes of shelter districts would yield a family of curves similar to figure C-40, but taking into account variations in reaction times and walking speeds.

Experimental analysis using a physical analogy employs physical quantitites to simulate the movement of people to the entrance, the flow of people through the entrance, and the formation and dissipation of a queue.

One physical analogy which might be used is a water tank shown schematically in figure C-43. Flow of water into the tank is regulated by a calibrated valve. This flow into the tank is varied in proportion to the arrival rate. Flow out of the tank is regulated by another valve set at a value proportional to the maximum entry rate. The accumulation of water in the tank then represents the number of people in a queue at the shelter entrance. The time required for the tank to drain is proportional to the time required for the total population to enter the shelter. Repeated experiments for various outlet flow rate settings will enable plotting maximum entry rate required versus the time required for the population to enter the shelter. The main disadvantages to this physical analog analysis are difficulty in constructing the apparatus required to produce accurate results, and the relatively long time required to run a series of experiments.

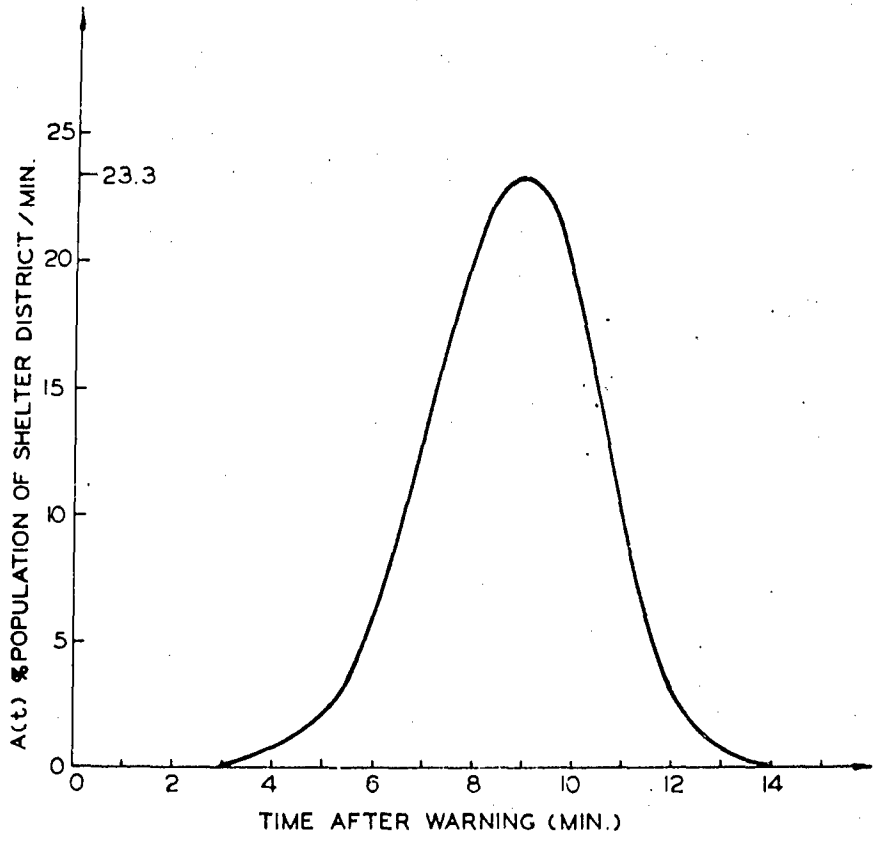

Figure C-41. Time After Warning vs A(t) % Population

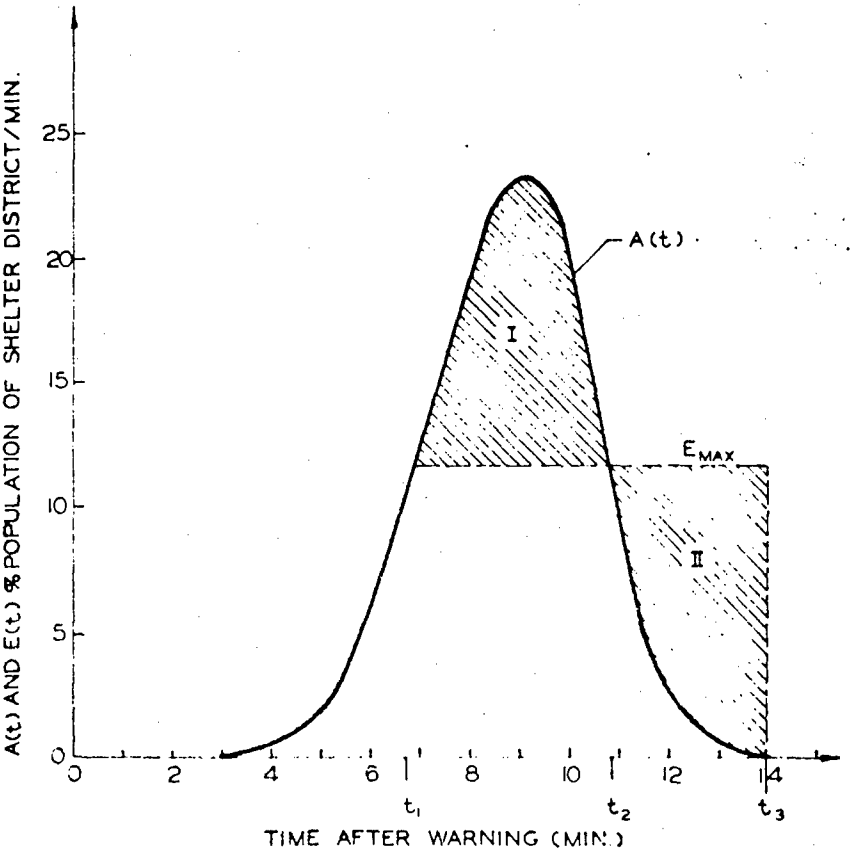

Figure C-42. Time After Warning vs A(t) and E(t) % Population

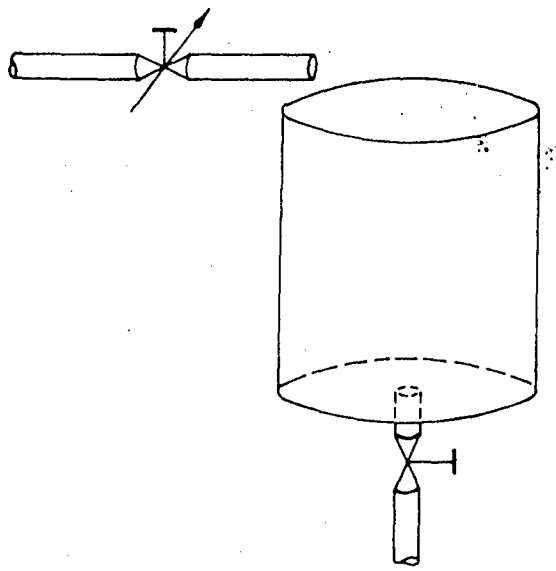

Figure C-43. Entrance Analogy to Water Tank Valve

Analog computer analysis may be used to obtain the same type of information obtained from a physical analogy. The analog computer uses electrical voltages instead of physical substances to represent the movement of people into shelters. In general, solutions can be obtained more rapidly and more accurately with the analog computer once it is set up to simulate a problem.

The application of an analog computer in the solution of the pedestrian traffic problem depends primarily upon the integrators found in modern analog computers and upon the function generating capabilities of the particular computer used.

An analog computer integrator is designated by the symbol:

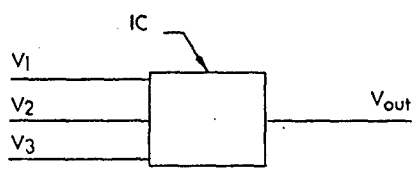

With time of integrator operation proportional to the independent variable of a problem, the output voltage V_{out} is the negative of the initial condition voltage, IC, plus the integral of the total input voltages, thus:

$$V_{out} = -\left\{ \int_o^t \left[V_1 + V_2 + V_3 \ldots \ldots \right] d\tau + IC \right\}$$

Note that the output is opposite in sign to the input. This is true for both integrators and for summers of an analog computer.

A summer is designated by the symbol:

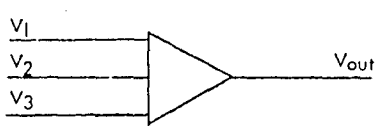

The output voltage of a summer is the negative of the instantaneous sum of the input voltages, thus:

$$V_{out} = -\left[V_1 + V_2 + V_3 \ldots \ldots \right]$$

The outputs of analog computer components which represent significant physical quantities or problem solutions are usually displayed graphically. Oscilloscopes, recording galvanometer strip charts, and X-Y plotters are the most commonly used recording instruments used with analog computers.

If the input voltages of an integrator represent the arrival rate, A(t), and the negative of the entry rate, -E(t), the output voltage of the integrator will be:

$$V_{out} = -\int_o^t \left[A(\tau) - E(\tau) \right] d\tau = -Q(t)$$

As developed previously, this integral is the number of people in the queue, Q(t). Therefore, either one of the analog computer setups of figure C-44 will give the number of people in the queue as a function of time.

The time that Q(t) reaches zero again after reaching a maximum value is the time, t_3, that the queue is dissipated. This solution gives a graphical display queuing, if it occurs. Repeated runs for various combinations of arrival and entry rate, display the interrelationship between these two variables upon the formation and dissipation of the queue.

When the entry rate E(t) is known, the number of people who have entered the shelter, N(t), can be determined since N(t) is the integral of the entry rate E(t) as shown previously. Thus, the analog computer setups feeding -E(t) into an integrator, figure C-45, produces the solution for N(t).

This setup gives a graphical solution of the number of people in the shelter as a function of time.

It must be remembered that the entry rate E(t) depends upon the arrival rate A(t). Thus, while A(t) does not appear explicitly in the setup of figure C- 44 , it is required in order to generate the entry rate E(t).

The above program was set up on the University of Arizona, Department of Nuclear Engineering, CSE 5800 DYSTAC Analog Computer. The arrival rate of figure C-41, as approximated by a 20 segment Diode Function Generator; was the input used. The effects of variation of maximum entry rate were investigated. Selected results of the analog computer solution are presented in the following table. The size of the queue as a function of time after the warning is sounded, Q(t), is shown in figure C-46 for three values of maximum entry rate, E_{max}. The number of people inside the shelter as a function of time, N(t), are shown for these same maximum entry rates in figure C-47. All of the curves of figures C-46 and C-47 were obtained directly from the analog computer in repetitive operation.

Maximum Entry Rate E_{max} (% population/min)	Time Queue is Dissipated t_3 (min)	Maximum Size of Queue Q_{max} (% population)	Time of Maximum Queue $t_{Q\,max}$ (min)
23.3	----	0	----
22	10.0	2	9.5
20	11.0	5	10.0
17	12.0	12	10.3
15	13.0	18	10.5
12	14.0	28	10.8
10	15.0	33	11.0
0	16.0	38	11.2

It can be seen that the displays available from the analog computer give a much more complete picture of the pedestrian traffic problem than other slower and more involved methods of solution. Once the computer is set up, a rapid analysis of the problem using more realistic values of arrival rate than the crude straight line approximation, used earlier, can be made quite easily. The analog computer analysis is further superior to the graphical analysis, and to the experimental physical analog analysis, in that the speed solutions of moderately good accuracy can be obtained.

In summary it should be emphasized that any solution of the pedestrian traffic problem arising in movement of the population to shelter during a given warning time is extremely dependent on the arrival rate. The validity of the arrival rate, used for analysis of the problem, depends upon how well the actual distributions of population, walking speeds, walking distances, and reaction times correspond with those used in the analysis. Two analytical approaches have been treated in detail on the following page: the straight line model using average values; and the approach using normal distributions of walking speeds, and reaction times, while assuming a rectangular grid street pattern and uniform population density.

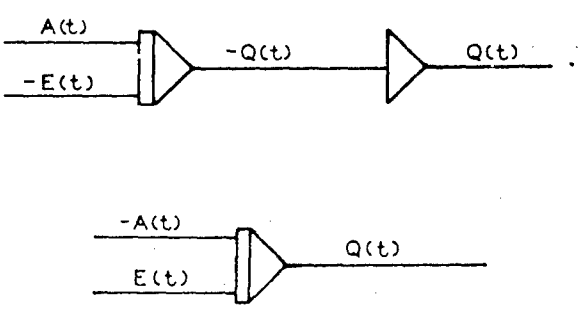

Figure C-44. Configuration to Determine Number in Queue

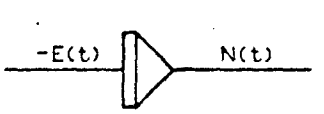

Figure C-45. Solution for N(t)

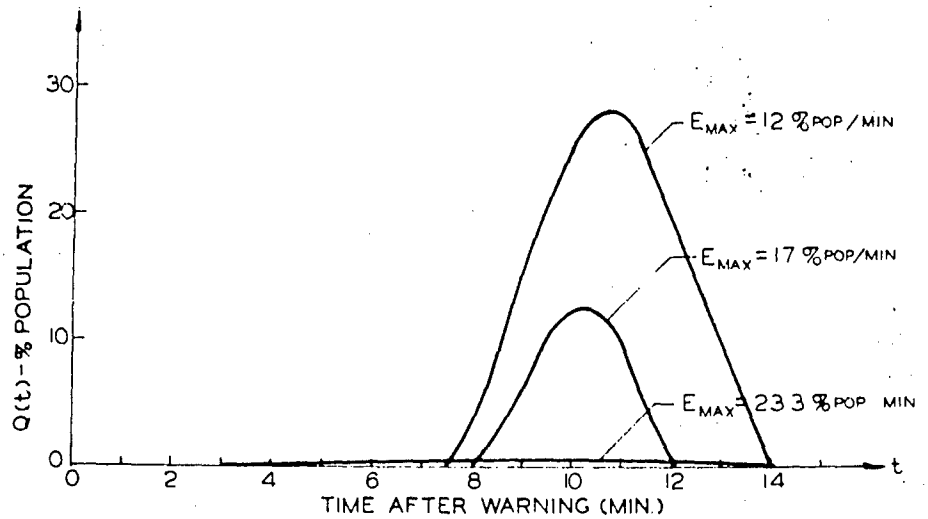

Figure C-46. Number of Persons in Queue

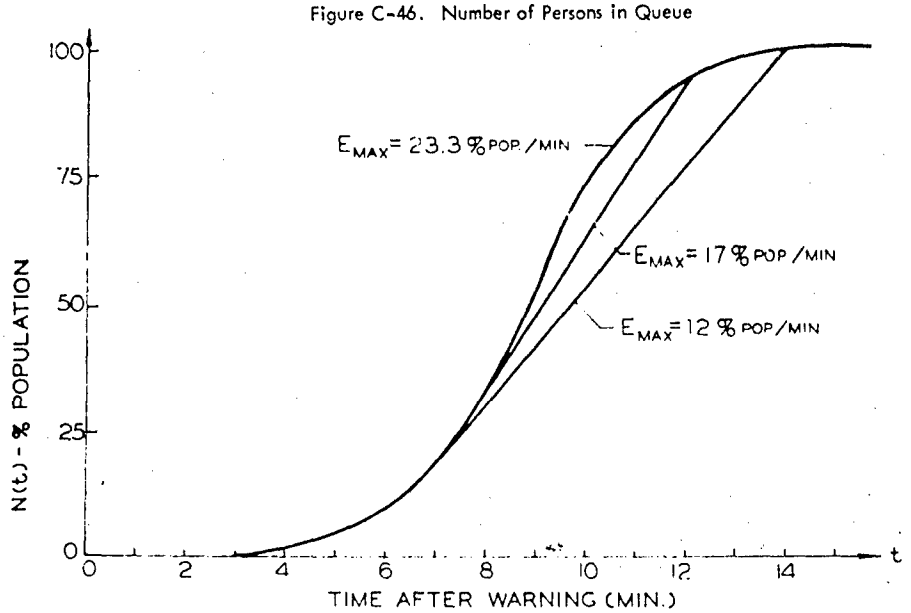

Figure C-47. Number of Persons in Shelter

Other approaches to determinaton of arrivci rate are also available but will not be treated in detail. One other approach may be used where the population distribution is known in minute detail such as for each building or each lot in a district. Here an analysis using an average walking speed for the population of each building or lot, and using actual walking distances to the entrance, might be more valid. This would be especially true in areas where the streets are not laid out in a basically rectangular grid pattern or where the population is very unevenly distributed. Gualtieri and Jensen (8) used an approach similar to this with the aid of a digital computer in their development of shelter assignments for Lincoln, Nebraska.

Ideally, an approach where all factors contributing to the arrival rate were known in detail and used in the analysis would give an exact solution to the problem. Such a detailed analysis is likely to be impractical, especially for design studies.

Once the arrival rate as a function of time has been determined or approximated for a given district, analysis of the pedestrian traffic problem for various entrance sizes can be accomplished by any of the three means developed.

The generation of the arrival rate A(t) depends upon the graphical shape of A(t) and upon the function generating capabilities of the specific analog computer used.

If A(t) can be described by a relatively simple differential or integral equation, it is possible to generate A(t) by performing the mathematical operations satisfying the equation. This approach utilizes the integrators and summers of the analog computer. For example, the straight line ramp function arrival rate used earlier in the simple graphical analysis can be generated quite easily. A constant voltage proportional to the slope of the arrival rate A(t) is fed into an integrator with initial condition set at zero. A suitable switching device is used to cut off the arrival rate at time t_2 and reset the integrator to the zero initial condition. This setup is shown in figure C-48.

The switching device denoted in figure C-48 is a comparator. In this case, it compares the output of the integrator with a fixed input voltage corresponding to the maximum arrival rate A_{max}. When the output of the integrator A(t) is equal to A_{max}. When the output of the integrator A(t) is equal to A_{max}, the comparator resets the integrator to the zero initial condition. The graphical display of this computer setup is shown in figure C-48.

When A(t) is very difficult to describe mathematically, other means of function generation are available on some analog computers. One such device is a Diode Function Generator (DFG) which can be used to approximate a given function using a series

of straight line segments. An independent variable is used as the input to DFG and the straight line segment approximation of a particular dependent variable set up on the DFG is the output.

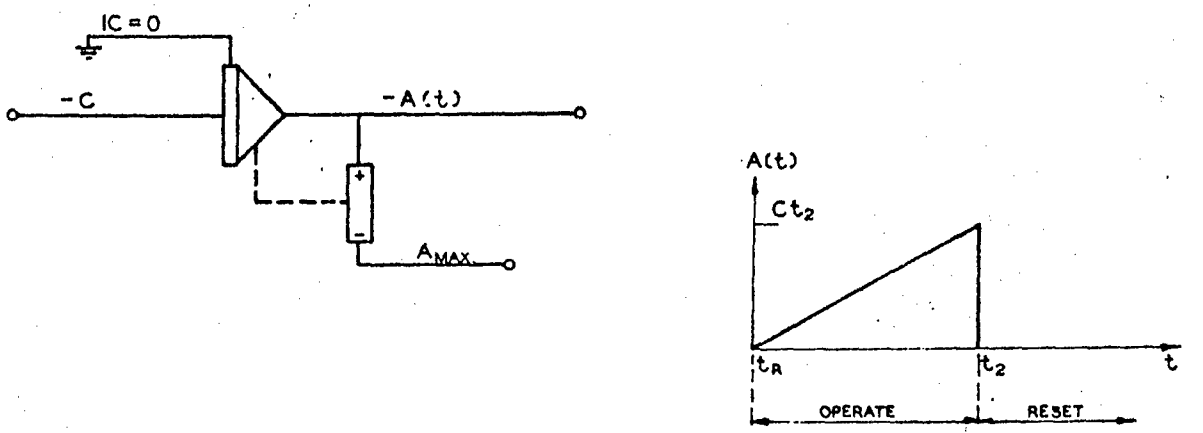

Figure C-48. Comparator and Display

Once the arrival rate A(t) is generated on the computer it must be modified in order to generate the entry rate E(t). One means of performing the necessary operations to obtain E(t) employs a limiter network and an integrator setup in an X-Memory configuration. This network is shown in figure C-49, with the waveforms produced by each stage also shown in figure C-49.

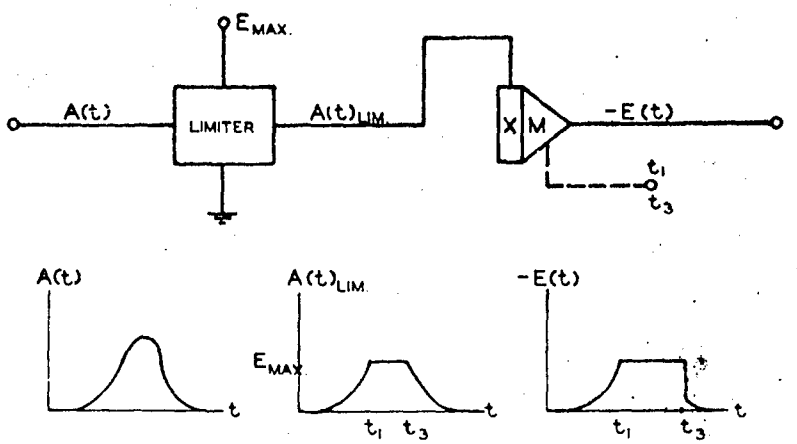

Figure C-49. Limiter Network and Display

The arrival rate, A(t), is fed into a limiter which limits this voltage at the maximum entry rate E(t). This produces the waveform denoted $A(t)_{lim}$ in the cases where the maximum entry rate is less than the maximum arrival rate. When A(t) exceeds E_{max}, queuing begins at time t_1. When A(t) drops below E_{max} at time t_2 the queue commences to dissipate. In order to hold the entry rate at E_{max} until the queue is dissipated the X-Memory is used. The X-Memory follows $A(t)_{lim}$ from time zero to time t_1. At time t_1, the X-Memory is switched, storing the value of $A(t)_{lim}$, which is E_{max}, until time t_3. When the queue is dissipated at time t_3 the X-Memory is switched to follow $A(t)_{lim}$ again. This produces a step drop in the X-Memory output at time t_3. Thus the X-Memory output, taking into account the change of sign in its operation, is the entry rate E(t).

These basic analog computer setups can be combined to produce a complete solution to the pedestrian traffic problem. The complete problem setup is diagrammed in figure C-50. Note that the integrator output Q(t) is fed into a comparator to produce the proper switching of the X-Memory at times t_1 and t_3. Voltages corresponding to all of the variables of interest in this problem are available in this analog computer setup.

A repetitive analog computer provides the optimum utilization of the above program. With a repetitive computer a complete solution of this problem is generated repeatedly many times each second. An oscilloscope is synchronized to the frequency of the computer operation to produce a static display of the desired dependent variable. Then as a parameter of the problem such as the maximum entry rate E_{max} or the arrival rate A(t) is varied in some manner, the effect of this variation is displayed instantly upon the oscilloscope. The computer operator can thus determine visually the effect of variation of a parameter upon the different variables of the problem. This greatly facilitates an optimization of the problem solution to desired criteria such as warning time, maximum queue, or a given portion of the population within the shelter in a given time.

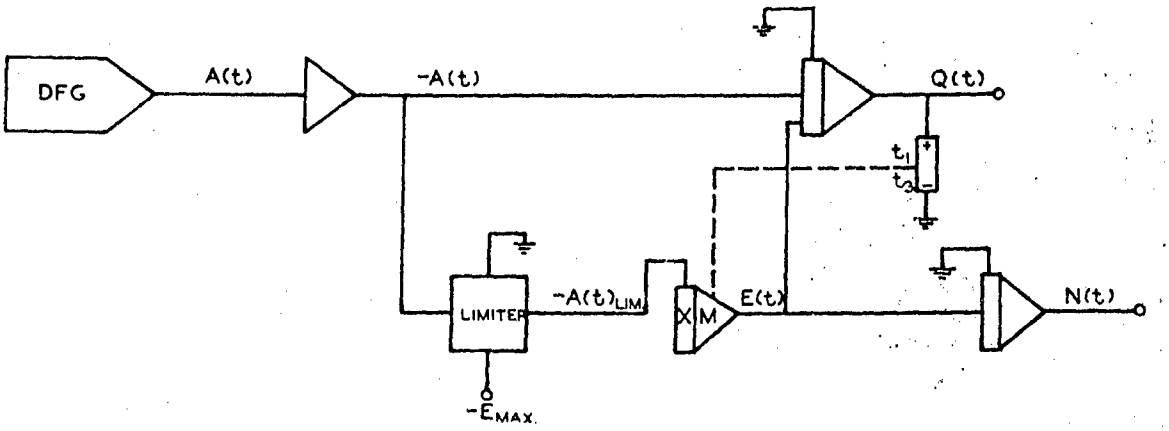

Figure C-50. Combined Logic Diagram

References:

1. Alexander, Michael N. and others. "Effect of Population Mobility on the Location of Communal Shelters." October, 1957, ASTIA-AD204090, p. II.
2. Ibid. p.7
3. Schultz, Sterling E., "Civilian Shelter Against Nuclear Attack, A Study of the Requirements for Tucson, Arizona." Unpublished. Thesis in partial fulfillment of requirements of Master of Science degree at the University of Arizona. Tucson, Arizona. May, 1962, p.118.
4. National Bureau of Standards, Design and Construction of Building Exits, USGPO, Washington, D.C., 1935, p. 40.
5. Alexander, Op Cit, p. 17.
6. Ibid. p.25.
7. Ibid. p.27.
8. Angelo Gualtieri and Gordon F. Jensen, Lincoln Shelter Utilization Study, Volume II, April 1963, OAD RM 106, Stanford Research Institute, Menlo Park, California.